OPTIMAL POWER FLOW MANAGEMENT USING UNIFIED POWER FLOW CONTROLLER

by

Muhammad Sarmad Tariq

A dissertation submitted to the faculty of
The University of North Carolina at Charlotte
in partial fulfillment of the requirements
for the degree of Doctor of Philosophy in
Electrical Engineering

Charlotte

2024

Approved by:

_____
Dr. Sukumar Kamalasadan

_____
Dr.Badrul Chowdhury

_____
Dr.Valentina Cecchi

_____
Dr.Churlzu Lim

ABSTRACT

MUHAMMAD SARMAD TARIQ. Optimal Power Flow Management using Unified Power Flow Controller . (Under the direction of DR. SUKUMAR KAMALASADAN)

With regards to optimal power flow models of FACTs devices, several models have been published. These encompass both DCOPF and ACOPF models incorporating Series as well as Shunt devices. Finding a feasible solution is of utmost importance with respect to OPF solutions. Feasibility not only encompasses feasibility with regards to voltage limits and line flows limits but it includes any constraints related to power flow control devices installed in the power system. These include FACTs devices. Several models have been published where the constraints have been included in non-Linear ACOPF models. However, few exist where the power rating constraints have been incorporated in a Linear ACOPF model.

An LPOPF model is proposed for line loading managment of a power system without any change in real and reactive generation output. The proposed LPOPF model aims to minimze congestion. The accuracy of the proposed model is improved by adjusting the control variables depending on the feasibility and accuracy of linearization of each LPOPF iteration. Furthermore, in order to obtain larger reduction in line loading, the solution space of LPOPF is updated at every iteration regardless of if the solution of the current LPOPF model is feasible or infeasible. This enlarges the solution space of LPOPF and hence helps in obtaining a feasible solution which is more optimal. Morevoer, an LPOPF formulation has been proposed which combines UPFC control along generation control. The co-optimization of the two controls can be used to effectively manage the line loading of the power system. Generation control considered is of three categories which are real generation control, reactive generation control and the combined used of real and reactive generation control. By doing so, the degree of effectiveness of a UPFC can be highlighted in the presence

of generation control. Furthermore, for optimal location of UPFC, a computationally efficient algorithm,namely the teaching learning based optimization(TLBO) has been applied. This method is easy to implement relative to other population based algorithms like particle swarm optimization. The algorithm has been adapted and modified to obtain the optimal combination of UPFC placements on a power system. The discrete version of TLBO has been used which is called DTLBO. The DTBLO has been modified further in order to take into account the combinatorial optimization for the placement of 2 UPFCs. Further modifications have been made for the given DTLBO placement algorithm to improve convergence using steps used in the continuous TLBO algorithm. To the best of authors knowledge, an easy to implement algorithm such as the DTLBO has not been used previously to determine the optimal location of UPFC for line loading management. Lastly, an algorithm is introduced to find the optimal rating of the UPFC considering three generation control scenarios: No generation control, real generation control only and reactive generation control only. A cost-benefit analysis is shown to discuss the trade off between cost of UPFC and degree of control over line loading of the power system.

ACKNOWLEDGEMENTS

I will acknowledge the assistance and guidance from Dr.Sukumar Kamalasadan(PhD Advisor) particularly in the initial conceptual stages of the PhD dissertation. I will acknowledge the comments of the committee members which help cover some unanswered questions in the PhD dissertation. I will acknowledge the UNCC Graduate School for providing the Graduate Assistance Support Plan which helps the student financially. I will acknowledge various instructors in my undergraduate period and my instructors in A/O Levels who helped make foundations in engineering subjects.

TABLE OF CONTENTS

LIST OF TABLES

LIST OF FIGURES

LIST OF ABBREVIATIONS

F Vector of UPFC System State Equations

H Vector of UPFC Power Rating Equations

MVA_{ij} Apparent Power Flowing in the line connecting bus i and bus j

MVA_{se} Apparent Power Rating of Series Voltage Source

MVA_{sh} Apparent Power Rating of Shunt Voltage Source

N Number of buses in the system

P_{des} Real Power Flow reference

P_{se} Real Power consumed/Absorbed by the Series Voltage Source

P_{sh} Real Power consumed/Absorbed by the Shunt Voltage Source

Q_{des} Reactive Power Flow reference

Q_{se} Reactive Power consumed/Absorbed by the Series Voltage Source

Q_{sh} Reactive Power consumed/Absorbed by the Shunt Voltage Source

V_{des} Voltage reference for the PV bus of the UPFC model

Z_{se} Impedance of the UPFC Series Voltage Source

Z_{sh} Impedance of the UPFC Shunt Voltage Source

Δx Change in Power System State Vectors

δ_i Angle at bus i

δ_{se} Angle of Series Voltage Source

δ_{sh} Angle of Shunt Voltage Source

nl number of lines

x_p Vector of System State Variables

x_{upfc} Vector of UPFC State Variables

C_i Cost of Generation

MVA_{max} Maximum Apparent Power Flow Limit of the Line

P Real Power Injection at a bus

P_g Real Power Generation at a bus

Q Reactive Power Injection at a bus

Q_g Reactive Power Generation at a bus

V_i Voltage at bus i

V_{se} Voltage of Series Voltage Source

V_{sh} Voltage of Shunt Voltage Source

X_{tcsc} Reactance of the TCSC

Y_i, Y_{ij} System admittance matrices

i, j Bus index

CHAPTER 1: INTRODUCTION

1.1 Transmission Congestion and Costs Associated with it

Congestion Costs are incurred on an electric grid when theire is insuffucient capacity to deliver low cost generation to load buses. Since the load has to be satisfied, high cost generation is dispatched instead increasing the total generation cost. There are various measures to manage congestion but the congestion cost is paid by the consumer in the end. Recnetly, there has been an increase in renewable deployment which has outpaced the the transmission expanison resulting in an increased congestion. This can be seen in Table.1.1 and Table.1.2 where a large increase in congestion costs can be seen in the year 2020-2021.

The best way to reduce transmission congestion is to increase transmission capacity however upgrading the transmission infrastructure is an expensive process. With the increase in wind and solar PV resources, further there is a need to invest more in the transmission system to enable greater renewable energy interconnection.

Table 1.1: Nationwide Congestion Costs(Millions of Dollars)

2016	$ 6501
2017	$ 7266
2018	$ 8776
2019	$ 6379
2020	$ 6686
2021	$ 13353

Table 1.2: Nationwide Congestion Costs for RTOs(Millions of Dollars)

RTO	2016	2017	2018	2019	2020	2021
ERCOT	497	976	1260	1260	1400	2100
ISO-NE	39	41	65	33	29	50
MISO	1402	1518	1409	934	1181	2849
NYISO	529	481	596	433	297	551
PJM	1024	698	1310	583	529	995
SPP	280	500	450	457	442	1200
TOTAL	3771	4214	5090	3700	3878	7745

1.2 Flexible AC Transmission System Devices

Flexible AC Transmission System (FACTS) is a concept using the help of power electronic switching converters and dynamic controllers to increase the power transfer capability and hence system utilization of the transmission system. It can also be used to increase the stability, security and reliability of AC power system. The class of FACTS includes many devices such as thyristor-based controllers, phase shifters, advanced static VAR compensator, Unified power flow controllers, Interline Power Flow Controllers and other recently introduced modular devices. The need for FACTs is ever increasing due to the high cost of constructing new transmission lines and generation facilities. This has increased the need for better utilization of existing transmission assets. The FACTs can change the transmission line network parameters such as the impedance, current and voltage magnitude and hence by doing so they are able to achieve the above objectives. The FACTs devices are able to change these system parameters in a fast and effective manner.

The types of FACTs devices can be classified as shown in Table.2.1. They are divided according to if they are installed in series and shunt across the transmission line and their control targets. The Shunt controllers are normally used for voltage

Table 1.3: Classification of FACTs Devices

Classification	**Control Targets**	**FACTs Devices**
Shunt Controller	Voltage Regulation	SVC,STATCOM
Series Controller	Real Power Flow Control	TCSC,TCPS,PST, Distributed SSSCs
Combined Series and Shunt Controller	Real and Reactive Power Flow Control,Voltage Regulation	Unified Power Flow Controller

regulation on buses by exchanging reactive power to the bus it is installed across. The series Controllers are used for controlling the flow of real power in the line it is attached to. This is done by injecting a voltage either leading or lagging with respect to the current flowing through the line and thus either a capacitive or inductive impedance is injected into the line. This results in a decrease or an increase in the real power flow in the line the series controller is installed in. The combined series and shunt controllers allow maximum control as they allow control of real and reactive power flow in the line as well as voltage regulation. The UPFC has two voltage sources, a series and a shunt voltage source. Real Power is exchanged between the series and shunt voltage source however the UPFC does not consume any real power. The shunt voltage source exchanges reactive power with the bus to control the voltage. There exist other subsets of control modes for the UPFC but which are less frequently utilized. For example, the UPFC can act as a phase shifting transformer if only real power flow reference is specified. However, the advantage of the UPFC in this control mode as compared to a phase shifting transformer is that the UPFC also allows voltage control to the local bus it is installed to. Moreover, another control mode of the UPFC allows the series injected voltage magnitude and angle to be specified. Thus, there can exist multiple control modes with other specified references with two degrees of freedom.

tabularx

1.3 Current Research Gap,Proposed Research and Main Contributions

With regards to optimal power flow models of FACTs devices, several models have been published. These encompass both DCOPF and ACOPF models incorporating Series as well as Shunt devices. Finding a feasible solution is of utmost importance with respect to OPF solutions. Feasibility not only encompasses feasibility with regards to voltage limits and line flows limits but it includes any constraints related to power flow control devices installed in the power system. These include FACTs devices. Several models have been published where the constraints have been included in non-Linear ACOPF models. However, few exist where the power rating constraints have been incorporated in a Linear ACOPF model. Ref. [1] modesl the UPFC power rating and voltage rating constraints in an LPOPF format. However, modifications can be introduced in this model and enhacements can be made to maximize the benefit of UPFC in line loading management of a power system.

Based on the literature review, the gaps in the Optimal power flow models of FACTs devices are summarised below:

- There exists a lack of Linear-programming based ACOPF models which incorporate the physical constraints of the FACTs devices. To be specific, the physical constraints are determined by the charactersitics of the series and shunt voltage sources comprising the device.

- To extend the previous point, the co-optimization of FACTs and generation control in a computationally efficient OPF with the objective of line loading management needs to be explored.

- Optimization of Allocation of UPFC devices is an area which can be explored further. Several techniques have been used in the past. The recent introduction of Teaching Learning Based Optimization is something which can be applied to UPFC allocation as well.

- The optimal sizing of the UPFC with regards to line loading management can be explored. The consideration of the cost of the UPFC is important as it is an expensive device.

Based on the research gaps discussed above, the summary and contribution of each chapter is discussed below:

- Chapter 2 provides a literature review of the optimal power flow models of FACTs devices.

- Chapter 3 provides a background of the existing newton raphson power models of FACTs devices. Results have been verified and tested for series as well shunt FACTs devices. This will serve as a basis of the UPFC bus injection model used in the following chapters.

- In chapter 4, an LPOPF model is proposed for line loading managment of a power system without any change in real and reactive generation output. Compared to Ref. [1], the proposed LPOPF model aims to minimze congestion by improving the model in Ref. [1]. The accuracy of the proposed model is improved by adjusting the control variables depending on the feasibility and accuracy of linearization of each LPOPF iteration. Furthermore, in order to obtain larger reduction in line loading, the solution space of LPOPF is updated at every iteration regardless of if the solution of the current LPOPF model is feasible or infeasible. This enlarges the solution space of LPOPF and hence helps in obtaining a feasible solution which is more optimal.

- In chapter 5, an LPOPF formulation has been proposed which combines UPFC control along generation control. The co-optimization of the two controls can be used to effectively manage the line loading of the power system. Generation control considered is of three categories which are real generation control, reactive generation control and the combined used of real and reactive generation

control. By doing so, the degree of effectiveness of a UPFC can be highlighted in the presence of generation control.

- In chapter 6, for optimal location of UPFC, a computationally efficient algorithm,namely the teaching learning based optimization(TLBO) has been applied. This method is easy to implement relative to other population based algorithms like particle swarm optimization. The algorithm has been adapted and modified to obtain the optimal combination of UPFC placements on a power system. The discrete version of TLBO has been used which is called DTLBO. The DTBLO has been modified further in order to take into account the combinatorial optimization for the placement of 2 UPFCs. Further modifications have been made for the given DTLBO placement algorithm to improve convergence using steps used in the continuous TLBO algorithm. To the best of authors knowledge, an easy to implement algorithm such as the DTLBO has not been used previously to determine the optimal location of UPFC for line loading management.

- In chapter 7, an algorithm is introduced to find the optimal rating of the UPFC considering three generation control scenarios: No generation control, real generation control only and reactive generation control only. A cost-benefit analysis is shown to discuss the trade off between cost of UPFC and degree of control over line loading of the power system.

CHAPTER 2: LITERATURE REVIEW

2.1 Introduction

Flexible AC Transmission System (FACTS) is a concept using the help of power electronic switching converters and dynamic controllers to increase the power transfer capability and hence system utilization of the transmission system. It can also be used to increase the stability, security and reliability of AC power system. The class of FACTS includes many devices such as thyristor-based controllers, phase shifters, advanced static VAR compensator, Unified power flow controllers, Interline Power Flow Controllers and other recently introduced modular devices. The need for FACTs is ever increasing due to the high cost of constructing new transmission lines and generation facilities. This has increased the need for better utilization of existing transmission assets. The FACTs can change the transmission line network parameters such as the impedance, current and voltage magnitude and hence by doing so they are able to achieve the above objectives. The FACTs devices are able to change these system parameters in a fast and effective manner. A summary of the comparison of a power system with and without FACTs is shown in Fig.2.1.

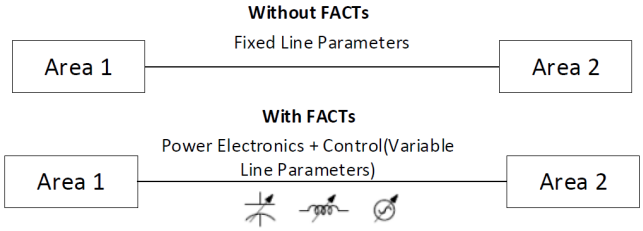

Figure 2.1: Comparison of Power System with and without FACTs

The key benefits of FACTs devices are listed below:

- Improve power transfer capability.
- Increase penetration of renewable energy
- Balance power between parallel transmission paths to prevent overloading /underloading.
- Improve stability margins of existing grid
- Prevent loop flows
- Achieve fast dynamic voltage regulation and frequency control

The locations where the FACTs devices can be installed in a power system are shown in Fig.2.2. As can be seen, they can be used in a wide variety of locations depending on the requirements hence there is a great deal of flexibility in the application of FACTs devices and how you want to tailor it to the system requirements.

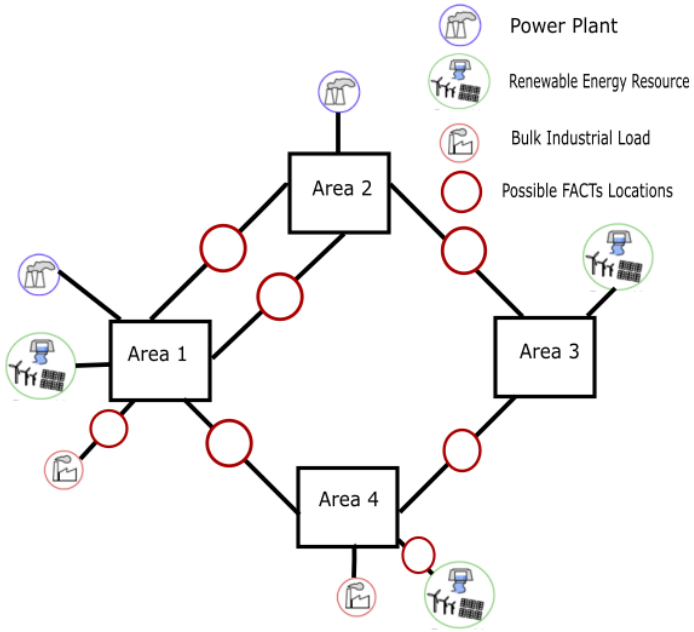

Figure 2.2: Possible Application Locations of FACTs

2.2 Types of FACTs Devices and their applications

The types of FACTs devices can be classified as shown in Table.2.1. They are divided according to if they are installed in series and shunt across the transmission line and their control targets. The Shunt controllers are normally used for voltage regulation on buses by exchanging reactive power to the bus it is installed across. The series Controllers are used for controlling the flow of real power in the line it is attached to. This is done by injecting a voltage either leading or lagging with respect to the current flowing through the line and thus either a capacitive or inductive impedance is injected into the line. This results in a decrease or an increase in the real power flow in the line the series controller is installed in. The combined series and shunt controllers allow maximum control as they allow control of real and reactive power flow in the line as well as voltage regulation. The UPFC has two voltage sources, a series and a shunt voltage source. Real Power is exchanged between the series and shunt voltage source however the UPFC does not consume any real power. The shunt voltage source exchanges reactive power with the bus to control the voltage. There exist other subsets of control modes for the UPFC but which are less frequently utilized. For example, the UPFC can act as a phase shifting transformer if only real power flow reference is specified. However, the advantage of the UPFC in this control mode as compared to a phase shifting transformer is that the UPFC also allows voltage control to the local bus it is installed to. Moreover, another control mode of the UPFC allows the series injected voltage magnitude and angle to be specified. Thus, there can exist multiple control modes with other specified references with two degrees of freedom.

tabularx

Table 2.1: Classification of FACTs Devices

Classification	**Control Targets**	**FACTs Devices**
Shunt Controller	Voltage Regulation	SVC,STATCOM
Series Controller	Real Power Flow Control	TCSC,TCPS,PST,SSSC, Distributed SSSCs
Combined Series and Shunt Controller	Real and Reactive Power Flow Control,Voltage Regulation	Unified Power Flow Controller

2.2.1 Series Controllers

The Series Controllers include devices such as the SSSC, TCSC, PST and the recently introduced Distributed SSSCs. They are normally used to control the real power flow in the transmission line by injecting a voltage in series with the transmission line which changes the impedance of the line. However they have various other control modes which will be discussed later. The circuit diagram of a series controller is shown in Fig.3.1.

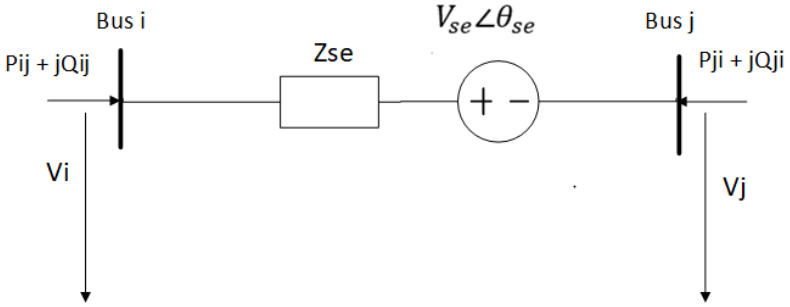

Figure 2.3: Series Voltage Model

Other power flow models which can effectively simulate the series controllers include the Bus Injection Model and the Variable reactance model. These are particularly applicable to TCSC devices. They will be discussed in detail in the next chapters however a brief introduction is provided here.

2.2.1.1 Variable Reactance Model

The variable reactance model is shown in Fig.2.4.

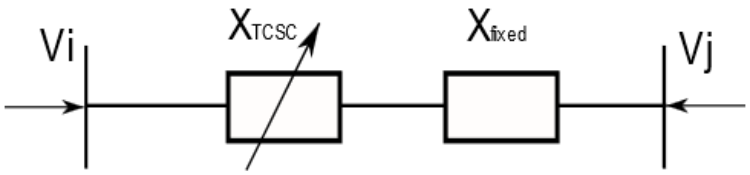

Figure 2.4: Variable Reactance Model

The impedance of the line between bus i and bus j is given by Eq. 2.1.

$$z_k = r_k + j(x_k + x_{tcsc}) = \frac{1}{g_k + b_k} \tag{2.1}$$

2.2.1.2 Bus Injection Model

The Bus Injection Model is shown in Fig.2.5. It models the TCSC as extra buses in the form of a decoupled power flow. Since a series controller is usually used to control the flow of real power thus an extra bus i' is added to the real power flow jacobian matrix. The Reactive power flow jacobian is not affected.

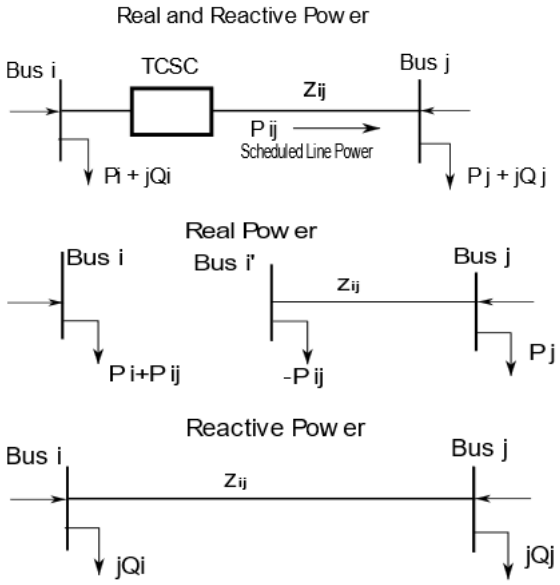

Figure 2.5: TCSC Bus Injection Model

A brief comparison is provided between the three different models in Table.2.2. The control modes of a SSSC device are listed below:

Table 2.2: Comparison between Models of Series Controllers

	Advantages
Series Reactance Model	This models the TCSC as a variable reactance directly which seems intuitive.
Series Voltage Model	-The voltage model allows the existing NR code to be used and only adds an extra separate block to it.
Bus Injection Model	-The convergence of the modified NR flow is not affected.
	Limitations
Series Reactance Model	The change in reactance appears as a non-linear term which may affect convergence.
Series Voltage Model	The convergence is dependent on the initial values of $V_{se} \quad and \quad \delta_{se}$.
Bus Injection Model	Fictitious bus model is not how TCSC controls real and reactive power.

- Active Power Flow Control.
- Reactive Power Flow Control.
- Bus Voltage Control.
- Impedance Control.

tabularx

2.2.1.3 Distributed FACTs

Recently, a new class of devices called Distributed FACTs or Smart Valves has been introduced which are modular devices used to control real power flow. They are similar to conventional TCSC devices in their function however the scale of operation of DFACT devices is very different from the TCSC devices. The power system model for a DFACT device is derived from a company called Smart Wires which has its patent. The smart valve module is shown in Fig.2.6. Fig.2.7 shows the location of DFACT modules attached to a tranmission line. As can be seen, as compared to a

single TCSC device, there are multiple DFACT units installed on a transmission line.

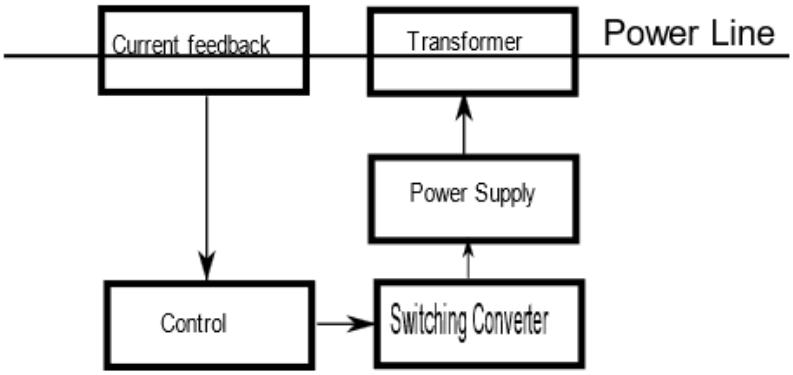

Figure 2.6: Distributed FACT Module

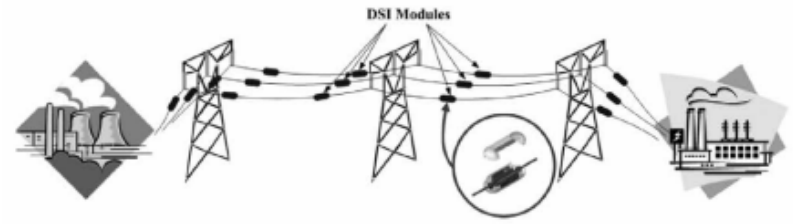

Figure 2.7: Multiple DFACTs installed on a Transmission System

The DFACT module harvest current from the line, transforms it from AC to DC and then injects its back in the form of an AC voltage waveform of the specified frequency. A DFACT module can be operated in three control modes which are listed as: a) Reactance Mode b) Current Mode c) Voltage Mode. In the reactance mode, a DFACT module is set to output a fixed reactance. Thus, the injected voltage will vary to keep the reactance fixed as the current in the line changes. In the current mode, the objective is to keep the line current within a certain range. Thus, if the current is above a threshold value, the DFACT module can increase its inductive injection. Likewise, if the current is below a threshold value, the DFACT module can increase its capacitive injection to increase the current in the line. In the voltage mode, the DFACT module is set to output a fixed voltage. Thus, the injected reactance will vary as the line current changes. Since DFACT device injects a voltage in series with

the line which is either 90 degrees leading or lagging with the current thus leading to either a capacitive or inductive reactance, there are two ways to model it in a power flow, which are either as a variable reactance or as an ideal voltage source in series. Both models effectively model the same device well however normally in AC power flow models, both a voltage source in series and a variable reactance can be modelled while in DC power flow models, a variable reactance is the only way to model a DFACT module. The reactance mode of a DFACT module is modelled in Fig .2.8. It must be emphasized that the DFACT module should not be modelled as a fixed reactance or fixed voltage source. However, it should be modelled as a dynamic line component which responds to power system states and its control objectives.

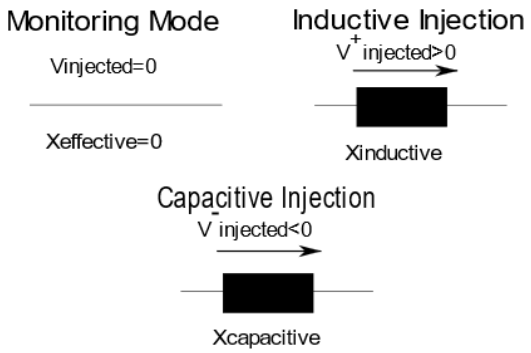

Figure 2.8: Distributed FACTs Control Modes

2.2.2 Shunt Controllers

A STATCOM is usually used to control transmission voltage by reactive power shunt compensation. In ideal steady state analysis, no active power is exchanged between the AC system and the STATCOM. Only reactive power can be exchanged between them. The STATCOM may be used to control one of the following parameters:

- Voltage magnitude of the bus to which STATCOM is connected.
- Reactive Power Injection to the bus to which STATCOM is connected.

- Impedance of the STATCOM.
- Reactive Power Flow.
- Current magnitude of the STATCOM where the current through the STATCOM leads the voltage injection of the STATCOM by 90 degrees.
- Current magnitude of the STATCOM where the current through the STATCOM lags the voltage injection of the STATCOM by 90 degrees.

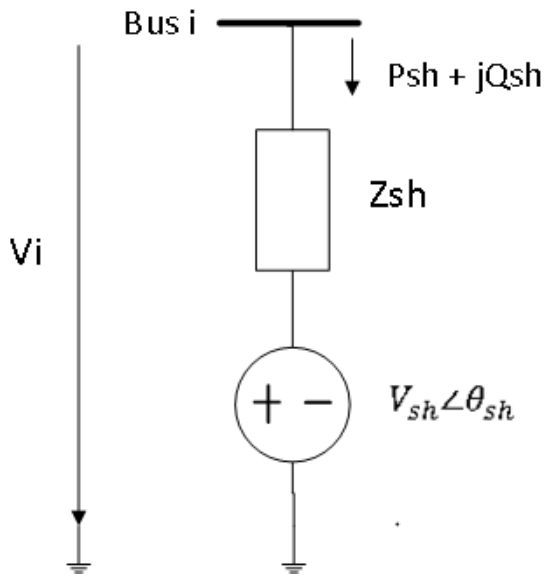

Figure 2.9: STATCOM Model

The two new state variables added in the Jacobian Matrix are the magnitude and anlge of the shunt voltage source. The two new mismatch equations will be the mismatch in the control reference and the real power consumed by the STATCOM.

2.2.3 Unified Power Flow Controller

The Unified Power Flow Controller consists of two converters. The two converters are connected via a common DC link. One of the converters is connected with the transmission line via a series transformer while the shunt inverter is connected to the the bus i via a shunt connected transformer. The shunt voltage source can generate

and consume reactive power. It can also provide active power to the series converter to satisfy the control mode requirements. The circuit diagram of the UPFC is shown in Fig.2.10.

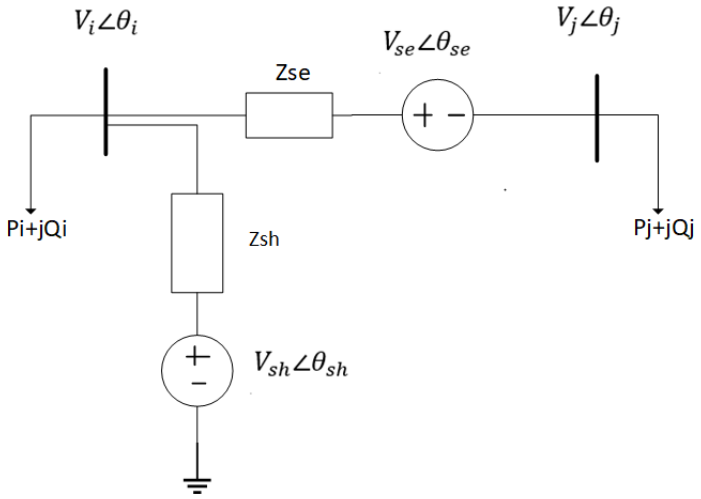

Figure 2.10: UPFC Model

The UPFC unlike the Series and Shunt Controllers has two degrees of freedom. The control modes of the UPFC are listed below:

- Active and Reactive Power Flow Control.
- Power Flow Control by Voltage Shifting.
- General Direct Voltage Injection.
- Direct Voltage Injection with Vse in phase with Vi.
- Direct Voltage Injection with Vse in Quadrature with Vi(lead).
- Direct Voltage Injection with Vse in Quadrature with Vi(lag).
- Direct Voltage Injection with Vse in Quadrature with Iij(lead).
- Direct Voltage Injection with Vse in Quadrature with Iij(lag).

- Voltage Regulation with Vse in Phase with Vi.
- Phase Shifting Regulation.
- Phase Shifting and Quadrature Regulation(lead).
- Phase Shifting and Quadrature Regulation(lag).
- Line Impedance Compensation.

2.3 Power Flow

The power flow solves for a deterministic solution to the power flow equation given by Eq.2.2 and Eq.2.3.

$$S = (V) \times I \tag{2.2}$$

$$S = (V) \times (YV)^* \tag{2.3}$$

V is an N-dimensional vector $V = (V_1, ..., V_N)$ of phasor voltages at each system bus. I is an N-dimensional vector $I = (I_1, ..., I_N)$ of phasor currents injected into the network at each system bus.

Y denotes the bus admittance matrix given by Eq .2.4.

$$Y = \begin{pmatrix} Y_{11} & ... & Y_{1N} \\ . & . & . \\ . & . & . \\ Y_{N1} & ... & Y_{NN} \end{pmatrix} \tag{2.4}$$

S denotes the vector of complex power injections at each bus given by P+jQ. At each bus i, the total injected power is the difference between the generation and the load.

$$S_i = S_i^G - S_i^L \tag{2.5}$$

$$P_i + jQ_i = (P_i^G - P_i^L) + j(Q_i^G - Q_i^L) \tag{2.6}$$

V represents the voltages that characterize the system power flow for a given admittance matrix Y. Conventional Power Flow does not solve for any objective function but instead it is a feasibility problem. This means that the objective is to compute the bus voltages and angles for given bus injections(generation except the slack bus and load). It is an exactly determined problem. The equations which are solved in a power flow are given by Eq.2.7 and Eq.2.8.

$$P_i(V,\delta) = (P_i^G) - (P_i^L) \quad \forall i \in N \tag{2.7}$$

$$Q_i(V,\delta) = (Q_i^G) - (Q_i^L) \quad \forall i \in N \tag{2.8}$$

To reach a deterministic solution, two out of the four unknown variables for each bus have fixed values. The four unknown variables for each bus are net real power injection, net reactive power injection, voltage magnitude and voltage angle. The variables are fixed according to the bus type which are slack bus, load bus and voltage-controlled bus. The classification of the buses are shown in Table.2.3.

Table 2.3: Power System Bus types for conventional power flow

Bus Type	Slack	PQ	PV
Known Quantities	δ, V	P,Q	P,V
Unknown Quantities	P,Q	δ, V	δ, Q
Number of Equations in PF	0	2	1

At the slack bus, the voltage magnitude and angle are fixed to normally 1 V and 0 degrees to provide a reference for the whole power system. The power injections are not fixed so that the losses are covered by the slack bus. For the load bus, the power injections are given but the voltage and angle needs to be calculated. For the PV buses, the real power injection and voltage magnitude are fixed while the reactive power injection and the voltage angle needs to be calculated in the power flow.

2.4 Optimal Power Flow

The Optimal Power Flow solves for an objective function subject to satisfying the power flow equations. The presence of the power flow equations is the distinguishing feature between the optimal power flow and other classes of power system problems such as unit commitment and economic dispatch. The Optimal power flow formulation is described in the following equations:

$$\text{Min} \quad \Sigma C_i(P_i^G) \tag{2.9}$$

$$P_i(V,\delta) = (P_i^G) - (P_i^L) \quad \forall i \in N \tag{2.10}$$

$$Q_i(V,\delta) = (Q_i^G) - (Q_i^L) \quad \forall i \in N \tag{2.11}$$

$$(P_i^{G,min}) \leq (P_i^G) \leq (P_i^{G,max}) \quad \forall i \in G \tag{2.12}$$

$$(Q_i^{G,min}) \leq (Q_i^G) \leq (Q_i^{G,max}) \quad \forall i \in G \tag{2.13}$$

$$(V_i^{min}) \leq (V_i) \leq (V_i^{max}) \quad \forall i \in N \tag{2.14}$$

$$(\delta_i^{min}) \leq (\delta_i) \leq (\delta_i^{max}) \quad \forall i \in N \tag{2.15}$$

The power system modelled in the above formulation has N buses connected by a set of branches L with generators located at a subset $G \subseteq N$ of the system buses. The operating cost of the generator is a function of its real output power $C_i(P_i^G)$. There can be other objective functions as well for the optimal power flow problem some of which are listed below:

- Total generation cost.
- Total Network Loss
- Active/Reactive power loss.

- Power Transfer Capability.
- Optimal Voltage Profile.
- System Loadability.
- Load Shedding.
- Environment Impact.

Furthermore, control variables can include variables other than real and reactive generation. The control variables can be discrete or continuous. Some of the control variables are listed below:

- Real/Reactive generation.
- Regulated Bus Voltage Magnitude.
- Transformer Tap Settings.
- Load Shed
- FACTs Control.
- Line Switching.
- Generator Voltage Control Settings.
- Switched Shunt Reactive Devices.

Optimal power flow problems are also classified according to the solution methods. Different OPF formulations have different selection of variables, objectives and constraints which lead to different solution method design. The types of OPF formulations are Non-Linear programming, Linear programming, Quadratic Programming, Mixed integer linear programming and Mixed integer nonlinear programming. It must also be kept in mind that an OPF solution method needs to satisfy some requirements

as the algorithms are becoming more and more complex. The OPF algorithm will be better if it has the following features:

- Higher Computational Speed.
- Reliability of Solution.
- Robustness of Solution.
- Simple to understand.
- Incorporation of Security Constraints.
- Incorporation of Multiple Objectives.

2.5 Existing Power Flow and Optimal Power Flow Formulations incorporating FACTS devices

2.5.1 Power Flow Modelling of DFACT devices

The initial literature published on distributed facts is focused on its power system modelling and incorporation into the power flow since the main objective of DFACTs is power flow control and congestion management. Ref [2] has published a DCOPF based formulation incorporating distributed facts as a variable impedance series facts devices. The DCOPF formulation is feasible from industry perspective as the day-ahead and real-time markets use DCOPF-based formulation. Another formulation published in Reference [3] is the Shift-factor formulation. This has the advantage of being more computationally efficient as compared to the DCOPF-based formulation as only the congested lines need to be part of the PTDF formulation. Other formulations incorporating distributed facts are based on sensitivity-based gradients. Reference [4, 5] has published such formulation. Linearized sensitivities are calculated for change in power system state variable with respect to a change in line

impedance using the Jacobian matrix and impedance matrix. Sensitivity of different functions can then be calculated with respect to system state variable such as angle and voltages. Such functions can be power flow on lines, power losses and other functions of interest. Steepest descent method is then used to reach an optimal solution for a non-linear optimization problem. This is useful given the fact that unlike the DCOPF and PTDF based formulation, sensitivity-based method is based on AC power flow modelling of DFACTs. The steepest descent runs an ACPF power flow on each step. Another approach presented uses bilinear optimization framework incorporating facts [6]. The approach does not require any knowledge of line flow directions. The formulation (SCED DC Load flow) is based on the day-ahead market since mostly day-ahead dispatch does not include facts optimization hence it is useful in the sense that generation scheduling, and facts can be co-optimized. A mixed integer quadratic(cost function is quadratic) programming formulation has also been presented considering flexible transmission line impedance [7]. This model is pretty similar to Reference [2] in its formulation however the quadratic programming formulation is solved using branch and bound method unlike the LP approach. Another formulation has been published based on linearized transmission system model [8]. This is based on creating a linearized model by creating a perturbation and looking for a proportional relationship between the system operating point perturbations and the injected reactance. Unlike the sensitivity-based method [4], this formulation is based on the DSSCâs physical characteristics in the way that it is formulated as compared to mathematical changes in the reactance of the line. This is due to the way that the coefficients relating the power system state variables to the change in impedance of DSSCs are calculated from the power balance equations. Do note that this model will have increasing errors for large changes in the DSSC reactance and thus this is only practical for small reactance injected by DSSCs. The paper is limited in its application of the formulation in the sense that it does not apply it to very large

systems as it requires computation of a very large set of coefficients. Application of the linearized model is only limited to generator reactive power reduction, voltage correction and line current reduction. DFACTs are mainly useful to line current reduction or increase and it does not address this application in detail. Furthermore, line efficacy (a single figure of merit) is introduced which gives an approximate indication of how effective a DFACTs can be. It is calculated only from the line current magnitudes and hence is easy to compute, however it is not too useful for very large systems. Another formulation presented in the earlier stages of DFACTs is based on steepest descent using DCPF formulation [9]. The method is not efficient as it involves steepest descent and may not be useful to large systems. Since DFACTs have shown some potential to be used in stressed loading conditions for post-contingency correction, an ACPF model of DFACTs under such conditions will be of benefit in power system modelling. Reference [10] has published a linearised ACPF formulation with linearized TSCS and SVC models under stressed loading conditions. The formulation is an ACPF model and divided into two stages. The first stage of the ACPF model outputs the base generation. In the second stage, after a stressed loading condition is introduced and this part of the optimization stage involves power adjustments of generators. It is to be noted that the models of the TSCS devices are also linearized. As of yet, this model is the closest to Linearised ACPF modelling of TCSC devices and is very beneficial to model facts under stressed loading conditions. As DFACTs can be used to increase the total transfer capacity of existing transmission network, formulation which can calculate the total transfer capacity using DFACTs will be useful. In [11], a repeated power flow formulation has been presented which shows how to maximize the power transfer using facts placed using sensitivity factors. A disadvantage of this approach lies for its application to large systems where it is hard to judge how the power flow may be affected by changing the reactance of one line. Furthermore, in meshed networks, the power flow is not directly dependent on the

reactance of the line.

2.5.1.1 Applications of DFACT devices

Applications of DFACTs include mainly congestion management, renewable energy curtailment and phase balancing. The application of DFACTs to reduce wind curtailment has been studied [12]. A stochastic model is used to evaluate various wind scenarios thus providing a solid basis on the impact of DFACTs on cost savings. Another study based on ACPF modelling of TCSC devices with the objective of minimizing wind power spillage has been performed []. It is a two-stage stochastic model. The first stage involves the dispatch of generation without considering any wind scenarios as is the case in the day-ahead market. The second stage takes into account any uncertainty related to wind scenarios and incorporates TCSC devices in the ACPF. Since DFACTs are modular in nature, hence they can be deployed in different lines according to specific requirements. DFACTs can be deployed in some phases in a higher number as compared to another, which we name as unsymmetrical deployment. This is to overcome the phase unbalancing caused due to unbalanced load. Furthermore, multiple high voltage lines operating in parallel will be congested when the first line, often the lowest voltage line, becomes overloaded [13]. Thus, DFACTs can be used to push power away from the low voltage line to the high voltage lightly loaded line [13]. Voltage balancing is another application of DFACTs however it has found limited use thus far. Further study has also been performed in [14] regarding deployment of DFACTs with respect to distributed and lumped line model. Different deployment plans such as deploying DFACTs at the start of the line, in a distributed manner or at the end of the line has been performed and it is explored which deployment is the most suitable. Detailed study of voltage balancing performed by DFACTs is performed in [15]. It is seen that DFACTs placed unsymmetrically can be used to improve voltage balance. Other applications of DFACTs which are studied are post-contingency analysis. Though only studied on a system

level, stability with respect to post-contingency actions of DFACTs is not addressed in any publications yet. During day-ahead market unit commitment run, the operator usually checks for a list of contingencies and sees if there any violations(load shedding or generator over production) In this SCUC, DFACTs are considered in this formulation as an additional flexibility option in order to increase the deliverability of reserves and reduce the contingency violations [16]. In this respect, facts have shown that they can reduce the contingency violation by a considerable percentage. As with any other grid-enhancing technology, a major question is the deployment and implementation of such technologies. Any grid-enhancing technology incurs a cost and hence the number of such devices must be optimized. Various allocation methods with respect to different objective functions have been implemented for distributed facts. One of the paper focused on the deployment of DFACTs tries to deploy DFACTs considering in mind two objective functions, system reliability and system load ability [17]. Because these two functions are conflicting in nature, thus a pareto front fuzzy decision-making approach is used to find an optimal solution. A pareto front is generated to get a solution which satisfies two objectives. Another allocation algorithm has been presented in [18]. This is an MILP formulation. It basically is the only allocation formulation for DFACTs published till yet. The objective function is generation cost reduction. The allocation is solved as part of the dcopf problem. It considers variable impedance DFACTs devices and optimizes the transmission line reactance adjustment range. The model has not been tested for a very large power system such as the 118 bus system because there will be a lot of variables however the formulation can be implemented logically for a large system. Moreover, it has been shown that DFACTs be reallocated letâs say in future years based on changing fuel prices, retirement of old generators and bringing in new renewable energy resources.

Table 2.4: Summary of FACTs Models

Method	**Description**	**Limitation**	**Ref**
Direct Current OPF	Models the tcsc in a dcopf format with shorter computational time	The direction of line flow is assumed to be remain same in TCSC lines for all OPF solutions.	[2]
Shift Factor Structure	Models the FACTs as additional injections in the shift factor structure format, Quick in terms of computational burden	Limited to DCOPF modelling only so it may not accurately model the power flow solution in terms of ac volts and angles	[3]
DCOPF Modelling	The model incorporates variable series reactance in a DCOPF model. The model is an MIQP model.	The model assumes the direction of power flow flowing in positive or negative direction.	[7]
Linearized ACOPF	Incorporates the TCSC in a linearized ACOPF formulations using sensitivities derived from perturbations in system states.	This may not be able to accurately model large-scale systems where relatively large changes in reactance will be needed for power flow control.	[8]

Continuation of Table 2.4

Newton Raphson Power Flow	Newton raphson power flow model of UPFC, TCSC and STATCOM with extra state variables added	Jacobian Matrix needs to be modified.	[19]
Newton Raphson Power Flow	Newton raphson power flow model with facts devices	Jacobian Matrix needs to be modified.	[20]
Bus Injection Model	Models the UPFC,TCSC and STATCOM in terms of bus injections which are modelled as additional buses(PV or PQ Bus) depending on FACTs type.	FACTs device do not control the power flow in terms of bus injections thus it does not accurately represent the FACTS devices physically.	[21]

Continuation of Table 2.4

Steepest Descent	Uses the Linear sensitivities with respect to a change in system impedance matrix to optimize an objective function(e.g. power losses, voltage control) using steepest descent method	Linear sensitivity method may not be suitable for very large systems where there can be multiple TCSC and coordinated control will be hard to achieve using steepest descent.	[5]
Repeated Power Flow Method	Calculate total transfer capability using repeated power flow method and Linear Sensitivity Factors	Inefficient as the reactance of each TCSC line needs to be changed seperately in an iterative fashion and thus coordinated control is hard to achieve	[11]
Steepest Descent Optimization	This formulation models the variable series reactance in terms of a DCOPF formulation with a non-linear objective function(congestion) solved using steepest descent.	Computationally burdensome as it is using steepest descent assuming objective function is convex.	[9]

Continuation of Table 2.4

LPOPF(Dr. Vittal's paper)	Models the UPFC in terms of Bus Injection Model for an LPOPF model solved to increase the system security under contingencies.	The methodology can be made more robust to further minimize the objective function. Multiple FACTs devices can be included rather than only one FACTs device for larger systems.	[1]
MILP Based Optimal Power	Models TCSC devices in the form an MILP with Piecewise Linearisation in a Linearised ACOPF under stressed loading conditions		[10]
Non Linear ACOPF Optimization	This formulation models the TCSC in NLP formulation for a non-convex objective function in an ACPF representation.	The formulation is non-linear and needs a suitable initial point as the objective function is non-convex.	[22]

Continuation of Table 2.4			
Non-Liner Interior Point OPF Method	Models the UPFC and TCSC devices in a non-linear OPF formulation solved using Interior Point Method	The formulation is non-linear.	[23]
Multi-Stage Optimisation(sequential quadratic programming)	Uses the UPFC to solve for minimizing power losses and increasing TTC in a two-stage OPF under contingency conditions	Only focused on TTC reduction of a particular path.So TTC reduction for some paths results in TTC reduction for other paths.	[24]
Linaerised ACOPF Model	Models the UPFC in terms of additional bus injections in a Jacobian matrix format and minimizing the power losses	The optimization is done in an iterative manner which is inefficient.	[25]
End of Table			

2.6 Possible Research Gaps

There are a few research gaps which are worth exploring in the area of modelling the FACTs devices in optimal power flow:

2.6.1 Possible Gap in Linearised ACOPF Modelling of FACTs devices

Linearised power flow modelling of FACTs devices has been explored before in either DC power flow format or in AC power flow. Power flow modelling using DC power flow equations is thoroughly studied as it is easier to model FACTs devices in a linear format. AC power flow modelling of FACTs devices has also been studied before in both non-linear and linear format. Talking specifically of Linearised ACPF modelling of FACTs devices, achieving a feasible solution is important if one is to achieve the maximum benefit of the ACPF solution. In order to achieve a feasible solution, physical constraints of the FACTs devices, which include the ratings of the device, must be included in the mathematical formulation. Not including the physical limits of the FACTs device will lead to solutions which are not practically implementable. Such formulation, which includes the physical constraints of the FACTs devices in a linearised ACOPF format, has been applied to transmission systems in the context of using FACTs devices to correct overloads in [1]. The objective in this case was to reduce line loading for highly loaded lines. However, this formulation can be made more beneficial by modifying the algorithm as it does not maximize the reduction in line loading. The modified algorithm will be able to maximize the utilization of FACTs devices by trying to achieve a larger reduction in line loading as is possible. Moreover, the effects of operating real and reactive generation in combination with FACTs devices can also be explored in this setting. This can be useful in the context of day-ahead markets where real and reactive generations settings can be changed.

2.6.2 Possible Gap in Distributed FACTs Modelling

Power system models which model either a variable reactance or a lumped voltage source in an ACPF exist however the maximum utilization of DFACTs will only be possible if DFACTs are modelled as multiple distributed modules which are able to vary the reactance by a certain percentage. The equivalency of DFACTs as a single

lumped variable reactance like the series conventional devices limit the potential of DFACTs. Each DFACT module should be independently controllable. As is shown in Table.2.5 , there do exist many similarities between TCSC and DFACT devices which further emphasizes the importance of an ACPF model with DFACTs . However the allocation, cost and deployment of these devices is different as shown in Table .2.6. The same comparison can be drawn between TCSC and DFACT devices as can be drawn between centralized energy resources and distributed energy resources. Though both are aimed for the same purpose, their scale of implementation is very different. DERs or DFACTs are aimed to affect the power system on a much smaller scale as compared to centralized energy resources or TCSC devices. Thus, a separate model of DFACTs is required for the ACPF modelling.

Table 2.5: Similarities between DFACTs and TCSC

Similarities between DFACTs and TCSCs
1. Control Real Power Flow
2. Series Devices
3. Power consumed by the device is zero.
4.Changes the line impedance
5.Modelled as a series voltage source
6.Injects voltage leading or lagging(90 deg) with the current
7.Connected to the line by a series transformer

tabularx

With a larger number of unknown variables (reactance) as is expected in the case of DFACT modelling, convergence of ACPF is an expected problem. From experience, DCOPF modelling of DFACT devices with large scale systems such as the Polish 23283 bus system required a large computational time(e.g. 5 mins in Matlab). Thus,

Table 2.6: Differences between DFACTs and TCSC

TCSC	**DFACTs**
Allocated on a very few lines(e.g. 2-3 devices on a IEEE 57 bus system)	Intended to be allocated on multiple line(e.g. 20-30 percent of the lines on a IEEE 57 bus system)
Lumped Device	Modular device
High one-time capital cost	Smaller incremental costs per module
Range of reactance change is high	Range of reactance per module is smaller as multiple modules have to be added to the line
Redeployment is difficult due to its large size	Can be redeployed as it is containerized module
Large installation time	Installation time can be as low as 1 day per module

this will also be an expected problem with a larger number of unknowns in case of distributed devices.

CHAPTER 3: FACTS MODELS AND SIMULATION

3.1 Introduction

This chapter applies the various models of FACTs devices to a modified Newton Raphson power flow. As shown in the previous chapter, the models of the devices are dependent on if the device is a shunt controller, series controller or a combined series and shunt controller. The series controllers are usually modelled either as a variable reactance or a series voltage source. The shunt controllers and combined series and shunt controllers can also be modelled by voltage sources as shown in the previous chapter. In this chapter, these models are incorporated in a Newton Rapshon power flow. Each power flow is given an input which is the control reference of the FACTs device. The control reference can be either one or two states depending on the type of device. The output of the power flow also includes the additional states introduced as a result of the FACTs device. These include the voltage and angle of the respective voltage source used to model the FACTs device.

3.2 Series Voltage Model for the TCSC

The series voltage model for the TCSC is shown in Fig.3.1.

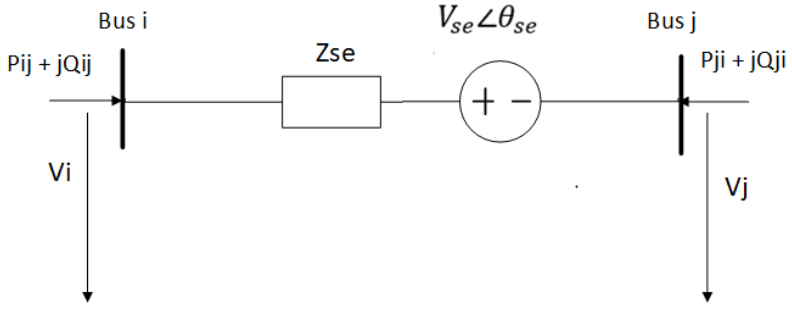

Figure 3.1: Series Voltage Model

The voltage Vse injects a capacitive or inductive voltage with respect to the line current. Two unknowns variables are introduced which are the voltage magnitude Vse and the voltage angle thetase. Two new mismatch equations are introduced to the resulting jacobian matrix. The first mismatch equation is the power flow reference through the line given by Eq.3.1 and Eq.3.2. The second mismatch equation is the power consumed by the source which is 0 as the TCSC device is lossless given by Eq.3.3 and Eq.3.4.

$$P_{ij} = [V_i]^2 g_{ii} - V_i V_j Y_{ij} cos(\delta i - \delta j - \phi ij) - V_i V_{se} Y_i j cos(\delta i - \delta j - \phi ij) \tag{3.1}$$

$$\Delta P(x) = P_{ij} - P_{ref} \tag{3.2}$$

$$PE = -V_i V_{se}(g_{ij} cos(\delta i - \delta se) - b_{ij} sin(\delta i - \delta se)$$

$$+ V_j V_{se}(g_{ij} cos(\delta j - \delta se) - b_{ij} sin(\delta j - \delta se)) = 0 \tag{3.3}$$

$$\Delta PE(x) = PE - PE_{ref} \tag{3.4}$$

The jacobian matrix is modified as shown Eq.3.5.

J1,J2,J3 and J4 are given by Eq.3.41,Eq.3.42,Eq.3.43 and Eq.3.44.

$$\begin{bmatrix} \Delta F \\ \Delta PE \\ .... \\ \Delta Pi \\ \Delta Qi \\ \Delta Pj \\ \Delta Qj \end{bmatrix} = \begin{bmatrix} J1 & J2 \\ J3 & J4 \end{bmatrix} \begin{bmatrix} \Delta \delta se \\ \Delta Vse \\ .... \\ \Delta \delta i \\ \Delta Vi \\ \Delta \delta j \\ \Delta Vj \end{bmatrix} \tag{3.5}$$

$$J1 = \begin{bmatrix} \frac{\partial F}{\partial \delta se} & \frac{\partial F}{\partial V se} \\ \frac{\partial PE}{\partial \delta se} & \frac{\partial PE}{\partial V se} \end{bmatrix} \tag{3.6}$$

$$J2 = \begin{bmatrix} \frac{\partial F}{\partial \delta i} & \frac{\partial F}{\partial V i} & \frac{\partial F}{\partial \delta j} & \frac{\partial F}{\partial V j} \\ \frac{\partial PE}{\partial \delta i} & \frac{\partial PE}{\partial V i} & \frac{\partial PE}{\partial \delta j} & \frac{\partial PE}{\partial V j} \end{bmatrix} \tag{3.7}$$

$$J3 = \begin{bmatrix} \frac{\partial Pi}{\partial \delta se} & \frac{\partial Pi}{\partial V se} \\ \frac{\partial Qi}{\partial \delta se} & \frac{\partial Qi}{\partial V se} \\ \frac{\partial Pj}{\partial \delta se} & \frac{\partial Pj}{\partial V se} \\ \frac{\partial Qj}{\partial \delta se} & \frac{\partial Qj}{\partial V se} \end{bmatrix} \tag{3.8}$$

$$J4 = \begin{bmatrix} \frac{\partial Pi}{\partial \delta i} & \frac{\partial Pi}{\partial V i} & \frac{\partial Pi}{\partial \delta j} & \frac{\partial Pi}{\partial V j} \\ \frac{\partial Qi}{\partial \delta i} & \frac{\partial Qi}{\partial V i} & \frac{\partial Qi}{\partial \delta j} & \frac{\partial Qi}{\partial V j} \\ \frac{\partial Pj}{\partial \delta i} & \frac{\partial Pj}{\partial V i} & \frac{\partial Pj}{\partial \delta j} & \frac{\partial Pj}{\partial V j} \\ \frac{\partial Qj}{\partial \delta i} & \frac{\partial Qj}{\partial V i} & \frac{\partial Qj}{\partial \delta j} & \frac{\partial Qj}{\partial V j} \end{bmatrix} \tag{3.9}$$

3.2.1 Methodology

Base Case

A power flow was run with constant impedance in all lines of the system shown in Fig.3.2.

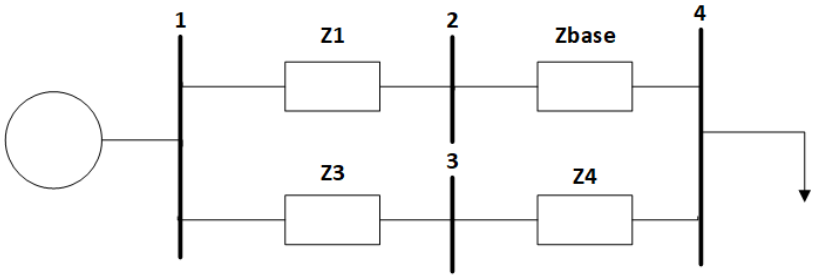

Figure 3.2: Fixed Impedance Model

The power flow in the prospective TCSC line is noted down. For example the real

power flow in line 2-4 is recorded.(i.e.Pref). The power system is then modified to include the series voltage model in the Line 2-4 as shown in Fig.3.3.

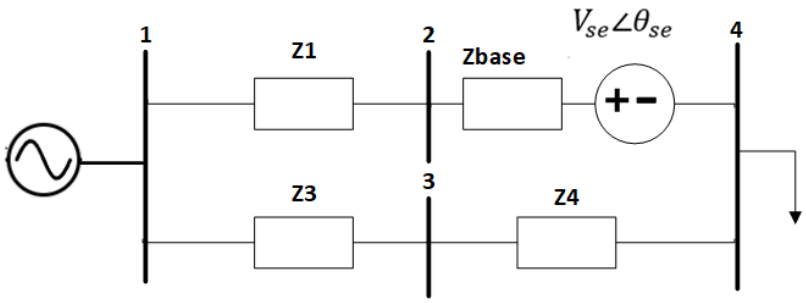

Figure 3.3: Fixed Impedance Model with a series voltage source

The power flow reference in the line 2-4 is set as Pref. The Newton Raphson formulation with the voltage series model is run. Expected Solution is Vse=0 and thetase= - 90 degrees. This is because the Pref here is the same as the base case above. Thus there is no need of a change in impedance for the power flow reference to be satisfied.

Capacitive Case

Another power flow is run with constant impedances in all line of the system but with reduced impedance in the TCSC line. This is shown in Fig.3.4.

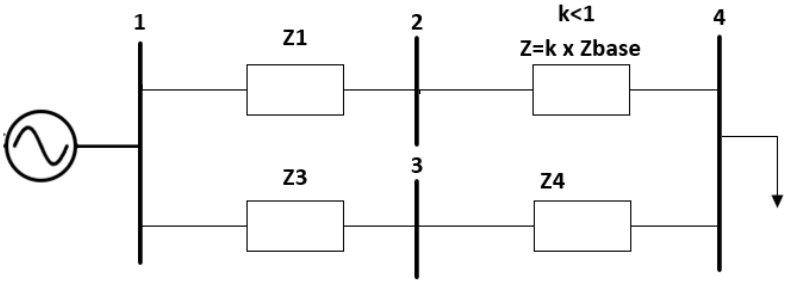

Figure 3.4: Fixed Impedance Model with Capacitive Control

In the system above, the impedance in the TCSC line is set to a value which is lower than the base impedance. The power flow in the TCSC line is recorded. The

power system below is run with the series voltage model included in the line. This is shown in Fig.3.5.

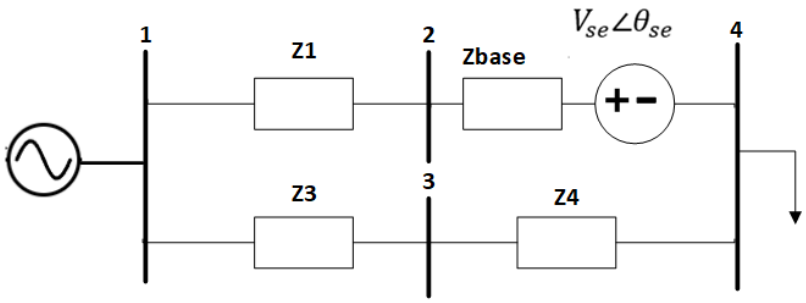

Figure 3.5: Fixed Impedance Model with a series voltage model-Capacitive Control

The expected solution is that the magnitude Vse will be a non-zero and thetase will be approximately equal to -90 degrees. This is because the modified NR power flow needs to satisfy the power reference where the impedance in the line was k * Z base. However, in the second system, the constant impedance in the line is Zbase. Thus there needs to be an impedance change/reduction of (Zbase â k*Zbase) for the power reference to be satisfied. That change in impedance is a result of capacitive voltage injection by the series voltage source.

Calculation of Impedance Injected by Voltage Source

Vi,Vj and Vse is obtained from the solution of the NR power flow.Z Fixed is the base impedance of the line, which is equal to Zbase as mentioned in the diagram above.

$$I_{se} = \frac{Vi - Vj - Vse}{Z_{fixed}} \tag{3.10}$$

$$Z_{se} = \frac{Vse}{I_{se}} \tag{3.11}$$

$$Z_{net} = Z_{se} + Z_{fixed} \tag{3.12}$$

Inductive Control

Another power flow is run with constant impedances in all line of the system but with a higher impedance in the TCSC line.This is shown in Fig.3.6.

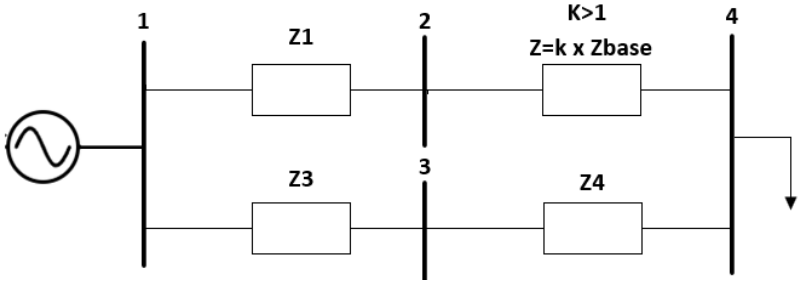

Figure 3.6: Fixed Impedance Model with Inductive Control

In the system above, the impedance in the TCSC line is set to a value which is higher than the base impedance. The power flow in the TCSC line is recorded. The power system below is run with the series voltage model included in the line. This is shown in Fig.3.7.

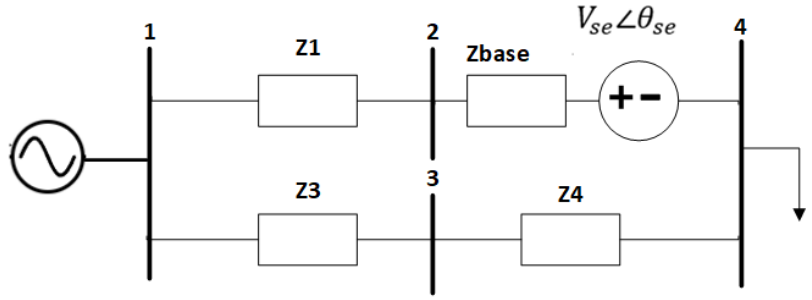

Figure 3.7: Fixed Impedance Model with a series voltage model-Inductive Control

The expected solution is that the magnitude Vse will be a non-zero and thetase will be approximately equal to + 90 degrees. This is because the modified NR power flow needs to satisfy the power reference where the impedance in the line was k * Z base. However, in the second system, the constant impedance in the line is Zbase. Thus there needs to be an impedance change/increase of (k* Zbase â Zbase) for the power reference to be satisfied. That change in impedance is a result of inductive

voltage injection by the series voltage source. For all the systems above, the voltage and angle of the power flow solution of the system with constant impedances will be approximately equal to that of the power flow solution of the system where the series voltage model is included.

3.2.2 5 bus system results

The Series Voltage model is applied on a 5 Bus system shown in Fig.3.8.

Base Case

In the base case, the power reference in the TCSC line is the same as the power flowing in the 5 bus system without any TCSC. Thus, since the power flow is the same as the default 5 bus system, thus TCSC does not inject any voltage. The results for the base case are shown in Table.3.1 and Table.3.2.

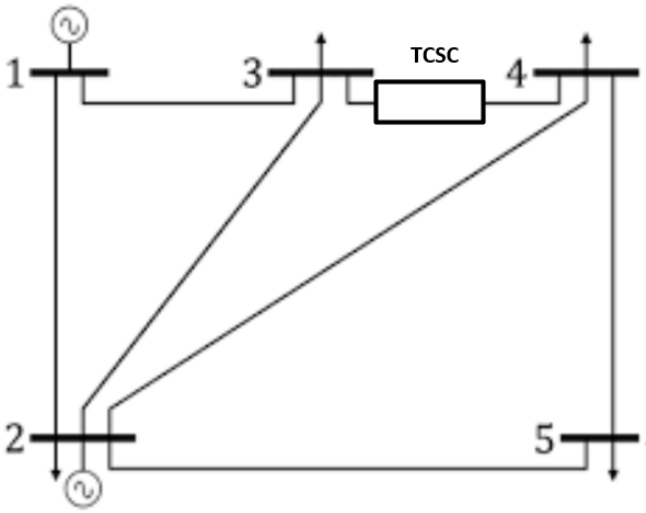

Figure 3.8: 5 Bus System Diagram Base Case

Capacitive Case

The power flow reference in the capacitive case is higher as compared to the power flow in the 5 bus system without any TCSC. Since Zactual and Znet are approximately the same, this shows that the newton raphson algorithm is accurate.In the capacitive

Table 3.1: 5 Bus System Base Case Power Flow Solution

Bus No	Voltage(Volts)	Angle(Degrees)
1	1	0
2	1	-2.6596
3	0.9865	-2.4850
4	0.9834	-3.5035
5	0.9793	-4.0521

Table 3.2: 5 Bus System Base Case TCSC Parameters

Vse	0
δ_{se}	-76 deg
TCSC line	3-4
TCSC Impedance	0.03+0.06i

case, the angle of voltage source injection is around -90 degrees since the injection is capacitive. The results are shown in Table.3.3 and Table.3.4.

Table 3.3: 5 Bus System Capacitive Case Power Flow Solution

Bus No	Voltage(Volts)	Angle(Degrees)
1.	1	0
2.	1	-2.6366
3.	0.9867	-2.5115
4.	0.9832	-3.4288
5.	0.9792	-4.0031

Table 3.4: 5 Bus System Capacitive Case TCSC parameters

Vse.	0.0032
δ_{se}	-78.93 degs
TCSC Impedance.	0.03 + 0.06* 0.8 j
Z actual.	0.030 + 0.0480i
Znet.	0.029 +0.0489i

Inductive Case

The power flow reference in the inductive case is lower than the the power flow in the 5 bus system without any TCSC. In the inductive case, the angle of voltage source injection is around +90 degrees since the injection is inductive. Since Zactual and Znet are approximately the same, this shows that the newton raphson algorithm is accurate. The results are shown in Table.3.5 and Table.3.6.

Table 3.5: 5 Bus System Inductive Case Power Flow Solution

Bus No	Voltage(Volts)	Angle(Degrees)
1.	1	0
2.	1	-2.6797
3.	0.9863	-2.4564
4.	0.9837	-3.5732
5.	0.9794	-4.0961

Table 3.6: 5 Bus System Inductive Case TCSC parameters

Vse.	0.0032
δ_{se}	106 degs
TCSC Impedance.	0.03 + 0.06* 1.2 j
Z actual.	0.0289 + 0.0729i
Znet.	0.03 +0.072i

3.2.3 9 bus system

The 9 bus system diagram with the TCSC connected in line4-5 is shown in Fig.3.9.

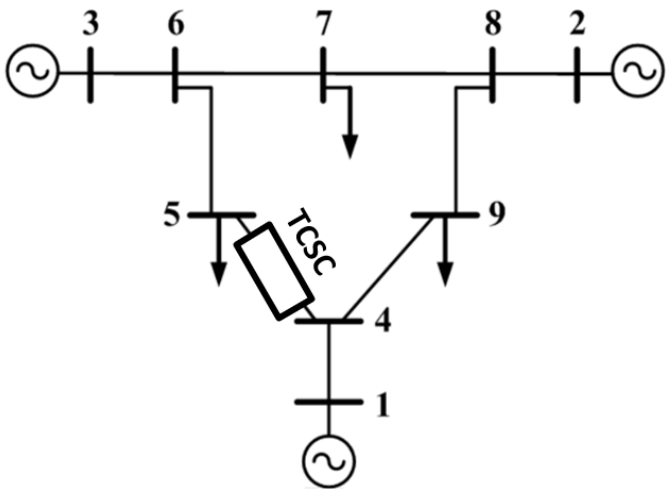

Figure 3.9: 9 Bus System Diagram Base Case

Base Case

In the base case, as the was the case for the 5 bus system, the power reference is equal to power flowing in the 9 bus system without any TCSC. The voltage source magnitude is very close to zero. The results are shown in Table.3.7 and Table.3.8.

Table 3.7: 9 Bus System Base Case Power Flow Solution

Bus No	Voltage(Volts)	Angle(Degrees)
1.	1.04	0
2.	1.025	5.6998
3.	1.025	0.6521
4.	0.9721	-1.7670
5.	0.9302	-2.515
6.	0.9468	-2.972
7.	0.9624	0.5699
8.	0.9384	-1.9696
9.	0.96973	-1.37259

Table 3.8: 9 Bus System Base Case TCSC parameters

Vse.	0.0032
δ_{se}	-139 degs
TCSC line	4-5
TCSC Impedance.	0.03 + 0.06
Pref	43 MW

Capacitive Case

In the capacitive case, the power reference(45 MW) is higher than the power flowing the base case(43 MW). The series voltage magnitude is around 3 times the series voltage magnitude of the base case. The angle is around -90 degrees as the injection is capacitive. The results are shown in Table.3.9 and Table.3.10.

Table 3.9: 9 Bus System Capacitive Case Power Flow Solution

Bus No	Voltage(Volts)	Angle(Degrees)
1.	1.04	0
2.	1.025	6.016
3.	1.025	0.8117
4.	0.9710	-1.7415
5.	0.9334	-2.186
6.	0.9463	-2.881
7.	0.9637	0.857
8.	0.939	-1.7447
9.	0.9697	-1.214

Table 3.10: 9 Bus System Capacitive Case TCSC parameters

Vse.	0.0086
δ_{se}	-143 degs
TCSC line	4-5
TCSC Impedance.	0.03 + 0.06*0.8i
Pref	45 MW
Zactual.	0.03+0.048i
Znet.	0.0289+0.0473i

Inductive Case

In the inductive case, the power reference(41.3 MW) is higher than the power flowing the base case(43 MW). The series voltage magnitude is around 3 times the series voltage magnitude of the base case. The angle is around +90 degrees as the injection is inductive. The results are shown in Table.3.11 and Table.3.12.

Table 3.11: 9 Bus System Inductive Case Power Flow Solution

Bus No	Voltage(Volts)	Angle(Degrees)
1.	1.04	0
2.	1.025	5.4046
3.	1.025	0.5039
4.	0.973	-1.792
5.	0.9272	-2.822
6.	0.9473	-3.057
7.	0.9612	0.302
8.	0.9377	-2.179
9.	0.9697	-1.520

Table 3.12: 9 Bus System Inductive Case TCSC parameters

Vse.	0.0072
δ_{se}	-315 or 45 degs degs
TCSC line	4-5
TCSC Impedance.	0.03 + 0.06*0.8i
Pref	41.3 MW
Zactual.	0.03+0.072i
Znet.	0.0291+0.0713i

3.2.4 30 bus system

The TCSC installed in the 30 bus system is shown in Fig.3.10. The TCSC is installed between a bus 5 which is a PV bus and bus 7 which is a PQ bus. In the base case, the voltage source magnitude is zero. In the capacitive case, the net impedance after the voltage source injection is lower than the base impedance of the base case(i.e. 0.0928i is less than 0.1160i). In the inductive case, the net impedance is larger than the base impedance(i.e. 0.1369i is larger than 0.1160i). In this case, the voltage source magnitude for the inductive and capacitive case is negative as the direction of the voltage source is in the opposite direction. The results for the base case, capacitive case and inductive case are shown in Table.3.13,Table.3.14 and Table.3.15 respectively.

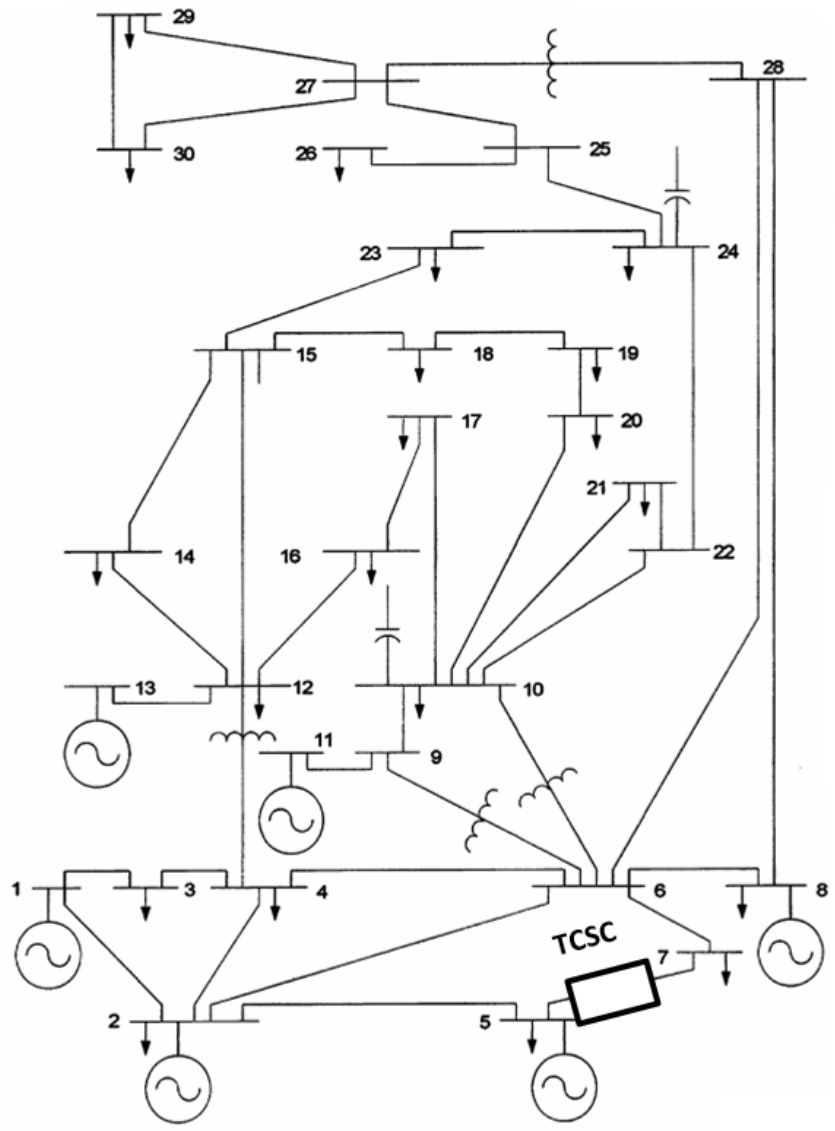

Figure 3.10: 30 Bus System Diagram Base Case

Table 3.13: 30 Bus System Base Case Solution

Base Case	
Vse	0
δ_{se}	-114 degs
TCSC line	5-7
TCSC Impedance.	0.0460+0.1160 j

Table 3.14: 30 Bus System Capacitive Case Solution

Capacitive Case	
Vse	-0.0042
δ_{se}	-66 deg
Actual Impedance	0.0460 + 0.0928 j

Table 3.15: 30 Bus System Inductive Case Solution

Inductive Case	
Vse	-0.0022
δ_{se}	115 deg
Actual Impedance	0.0662 + 0.1369j

3.2.5 5 bus system with Multiple TCSCs

The series voltage model is applied on a 5 bus system with multiple TCSCs installed. In this case 2 one TCSC is installed between bus 3 and bus 4 and the second TCSC is installed between bus 4 and bus 5. This is shown in Fig.3.11.

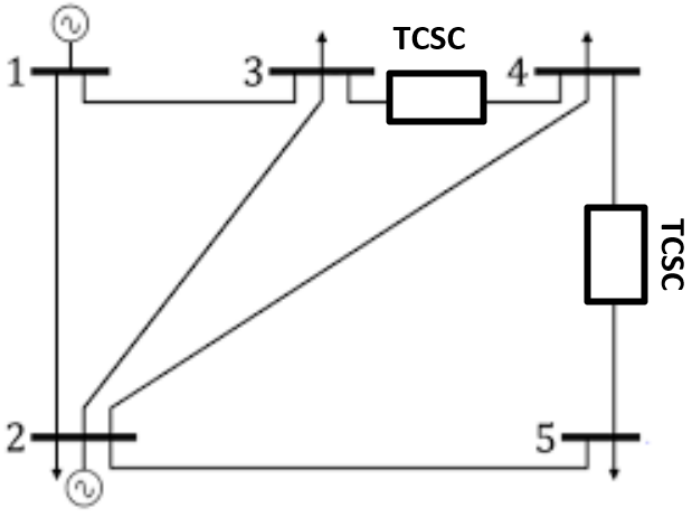

Figure 3.11: 5 Bus System Diagram with two TCSCs

Base Case

The results for the base case are shown in Table.?? and Table.3.17.

Table 3.16: 5 Bus System Base Case Power Flow Solution(Multiple TCSCs)

Bus No	Voltage(Volts)	Angle(Degrees)
1.	1	0
2.	1	-2.6615
3.	0.9865	-2.4826
4.	0.9834	-3.5106
5.	0.9793	-4.0554

Table 3.17: 5 Bus System Base Case TCSC Parameters(Multiple TCSCs)

	TCSC 1	TCSC 2
Vse	0	0
δ_{se}	-76	-91
Actual Impedance	0.03+0.06j	0.03+0.06j
Net Impedance	0.03+0.06j	0.03+0.06j

Mixed Operation Case 1-Capacitive and Inductive

In this case, TCSC 1 is in capacitive mode and Tcsc 2 is in inductive mode. This can be seen from the fact that the impedance for Tcsc 1 is less than the base impedance and the impedance for TCSC 2 is larger than the base impedance. The results are shown in Table.3.18 and Table.3.19.

Table 3.18: 5 Bus System Mixed Operation Case 1 Power Flow Solution

Bus No	Voltage(Volts)	Angle(Degrees)
1.	1	0
2.	1	-2.633
3.	0.987	-2.522
4.	0.983	-3.358
5.	0.979	-4.043

Table 3.19: 5 Bus System Mixed Operation Case 1 TCSC Parameters

	TCSC 1	TCSC 2
Vse	0.0051	-0.0042
δ_{se}	-81	-82
Actual Impedance	0.03+0.042j	0.03+0.078j
Net Impedance	0.0279+0.0424j	0.0242 + 0.089j

Mixed Operation Case 2-Capacitive and Inductive

In this case, TCSC 1 is in capacitive mode and Tcsc 2 is in inductive mode. This can be seen from the fact that the impedance for Tcsc 1 is less than the base impedance and the impedance for TCSC 2 is larger than the base impedance. The results are shown in table.3.20 and Table.3.21.

Table 3.20: 5 Bus System Mixed Operation Case 2 Power Flow Solution

Bus No	Voltage(Volts)	Angle(Degrees)
1.	1	0
2.	1	-2.682
3.	0.986	-2.454
4.	0.984	-3.637
5.	0.979	-4.046

Table 3.21: 5 Bus System Mixed Operation Case 2 TCSC Parameters

	TCSC 1	TCSC 2
Vse	0.0029	-0.0038
δ_{se}	-73	-97
Actual Impedance	0.03+0.042j	0.03+0.078j
Net Impedance	0.0329+0.0426j	0.0291+0.0755j

3.2.6 30 bus system with Multiple TCSCs

Multiple TCSCs are installed on a 30 Bus System in this section.The 30 Bus system diagram with multiple TCSCs are shown in Fig.3.12.

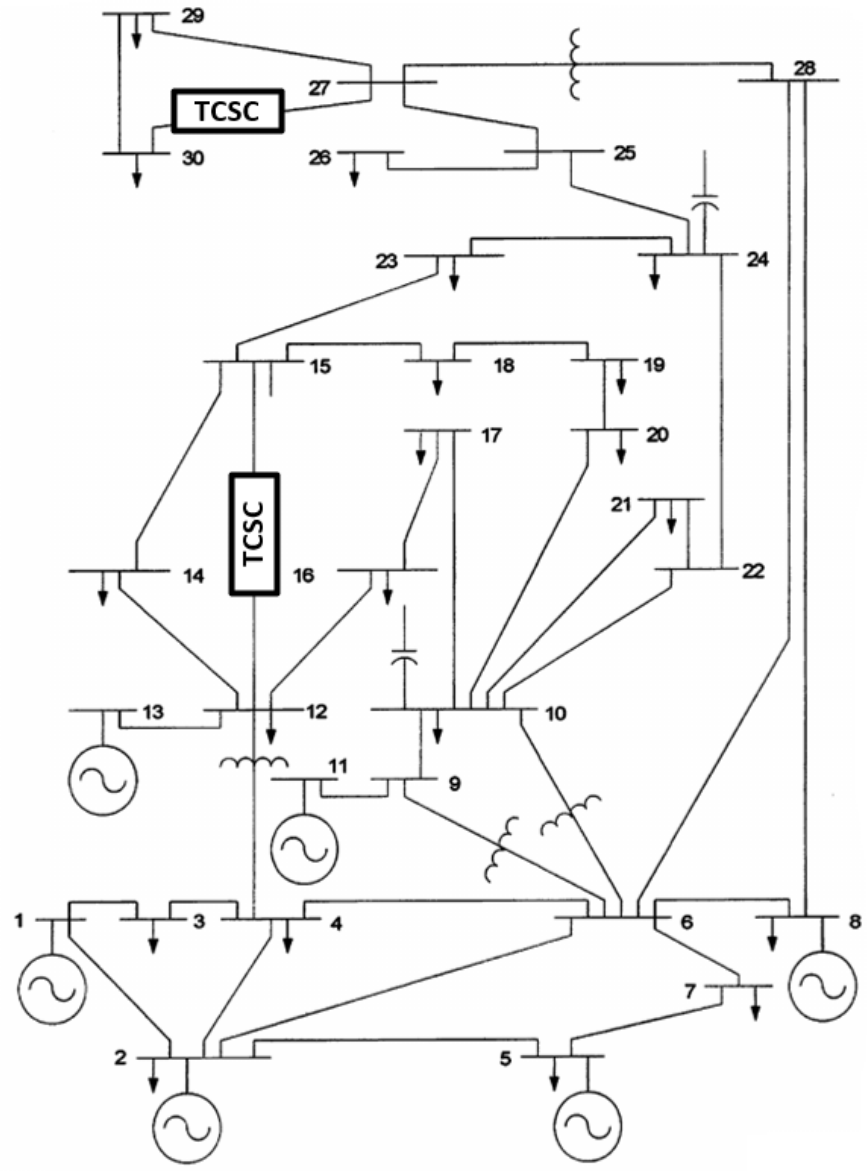

Figure 3.12: 30 Bus System Diagram with two TCSCs

Base Case

The results for the base case are shown in Table.3.22.

Table 3.22: 30 Bus System Base Case TCSC Parameters(Multiple TCSCs)

	TCSC 1	TCSC 2
Vse	0	0
δ_{se}	-115	-118
Actual Impedance	0.06620 + 0.130400i	0.32021 + 0.6027i
Net Impedance	0.0662 + 0.1304i	0.32021 + 0.6027i

Mixed Operation Case 1-Capacitive and Inductive

In this case, TCSC 1 is capacitive and TCSC 2 is inductive. The reactance in case of TCSC 1 is less than the base impedance. The reactance for TCSC 2 is larger than the base impedance. The results are shown in Table.3.23.

Table 3.23: 30 Bus System Mixed Operation Case 1 TCSC Parameters

	TCSC 1	TCSC 2
Vse	0.00350	-0.00812
δ_{se}	-118.5	-116.3
Actual Impedance	0.066 + 0.1043j	0.3202 + 0.7232i
Net Impedance	0.0634 + 0.1293i	0.31741 + 0.6017i

Mixed Operation Case 2-Capacitive and Inductive

In this case, TCSC 1 is inductive and TCSC 2 is capacitive. The reactance in case of TCSC 2 is less than the base impedance. The reactance for TCSC 1 is larger than the base impedance. The results are shown in Table.3.24.

Table 3.24: 30 Bus System Mixed Operation Case 2 TCSC Parameters

	TCSC 1	TCSC 2
Vse	0.00326	0.008973
δ_{se}	67.345	-121
Actual Impedance	0.06620 + 0.15648i	0.3202 + 0.48216i
Net Impedance	0.106338 + 0.1420i	0.3603 + 0.61438i

3.3 Variable Series Reactance Model for the TCSC

In this section, the TCSC is modelled as a variable reactance in series with the line impedance as shown in Fig.3.13.

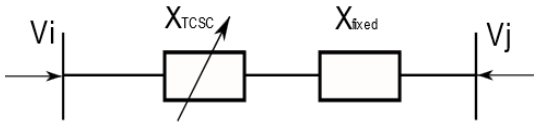

Figure 3.13: Variable Series Reactance Model

The impedance of the line between bus i and bus j is given by Eq. 5.1.

$$z_k = r_k + j(x_k + x_{tcsc}) = \frac{1}{g_k + b_k} \tag{3.13}$$

The conductance and susceptance are given by Eq.5.2 and Eq.5.3.

$$g_{nm} = \frac{r_{nm}}{r_{nm}^2 + (x_{nm} + x_{tcsc})^2} \tag{3.14}$$

$$b_{nm} = \frac{(x_{nm} + x_{tcsc})}{r_{nm}^2 + (x_{nm} + x_{tcsc})^2} \tag{3.15}$$

3.3.1 Modified NR power flow with Variable Reactance Model

A thyristor controlled series capacitor can be modelled in the Newton Raphson power flow using a variable reactance model. Additional variables need to be added

to the existing power flow method without modifying the existing Newton Raphson code by a great degree. Each variable introduces an additional mismatch equation. This is shown by the diagram below where jacobian terms are augmented to the existing jacobian of the AC Network. The additional mismatch equations are F1 to FnF and the additional variables are r1 to Rnf. This is shown in Fig.3.14.

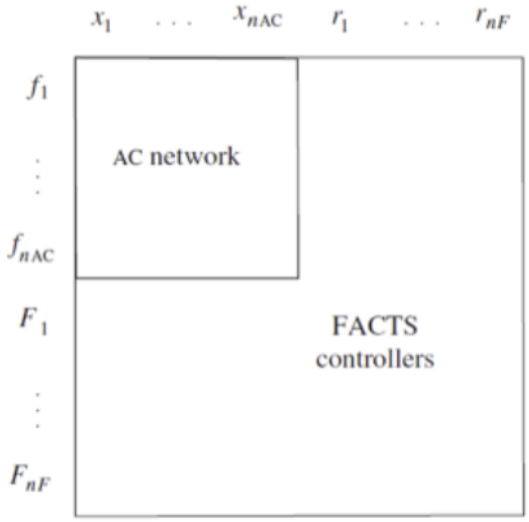

Figure 3.14: Augmented Jacobian with the Variable Reactance Model

Now different FACTS controllers have different terms which they introduce to the existing power flow depending on their control variable. TCSCs control real power by varying the line reactance. Thus the additional mismatch equation will be in the form of real power while the additional variable will be the variable reactance. A line in which the TCSC is installed can be modelled in the form of a variable reactance as previously shown in Fig.3.13. The reactance can either capacitive or inductive depending on the mode of operation.

The transfer admittance matrix of the series compensator is shown in Eq.3.16.

$$\begin{bmatrix} Ik \\ Im \end{bmatrix} = \begin{bmatrix} jB_{kk} & jB_{km} \\ jB_{mk} & jB_{mm} \end{bmatrix} \begin{bmatrix} Vk \\ Vm \end{bmatrix} \tag{3.16}$$

For inductive operation, the term B_{kk} and B_{km} are given by Eq.3.17 and Eq.3.18.

$$B_{kk} = B_{mm} = \frac{-1}{x_{tcsc}} \tag{3.17}$$

$$B_{km} = B_{mk} = \frac{1}{x_{tcsc}} \tag{3.18}$$

The reactance is variable which is equal to Xtcsc. The power flow equations for bus k are given by Eq.3.19 and EQ.3.20.

$$P_k = V_k V_m B_{km} sin(\delta_k - \delta_m) \tag{3.19}$$

$$Q_k = (V_k)^2 B_{kk} - V_k V_m B_{km} cos(\delta_k - \delta_m) \tag{3.20}$$

In the Newton Raphson power flow, the two terms given by Eq.3.19 and Eq.3.20 are added to the existing Jacobian in the form of an additional row and additional column for each TCSC added in the system. In order to do that, an additional mismatch equation needs to be added which is given by the power flow reference given by Eq.3.21.

$$\Delta P_{km} = P_{km,ref} - P_{km,calc} \tag{3.21}$$

As shown below, the modified jacobian contains the derivatives of this term with respect to the voltage and angle states given by Eq.3.22 and Eq.3.3.1. The additional variable we are solving for is the TCSC reactance which is able to satisfy the given power flow reference.

$$J = \begin{bmatrix} \frac{\partial Pk}{\partial \delta k} & \frac{\partial Pk}{\partial \delta m} & \frac{\partial Pk}{\partial Vk} & \frac{\partial Pk}{\partial Vm} & \frac{\partial Pk}{\partial Xtcsc} \\ \frac{\partial Pm}{\partial \delta k} & \frac{\partial Pm}{\partial \delta m} & \frac{\partial Pm}{\partial Vk} & \frac{\partial Pm}{\partial Vm} & \frac{\partial Pm}{\partial Xtcsc} \\ \frac{\partial Qk}{\partial \delta k} & \frac{\partial Qk}{\partial \delta m} & \frac{\partial Qk}{\partial Vk} & \frac{\partial Qk}{\partial Vm} & \frac{\partial Qk}{\partial Xtcsc} \\ \frac{\partial Qm}{\partial \delta k} & \frac{\partial Qm}{\partial \delta m} & \frac{\partial Qm}{\partial Vk} & \frac{\partial Qm}{\partial Vm} & \frac{\partial Qm}{\partial Xtcsc} \\ \frac{\partial P_{km}^{xtcsc}}{\partial \delta k} & \frac{^{xtcsc}}{km} & \frac{^{xtcsc}}{km} & \frac{\partial P_{km}^{xtcsc}}{\partial Vm} & \frac{\partial P_{km}^{xtcsc}}{\partial Xtcsc} \end{bmatrix} \tag{3.22}$$

$$\begin{bmatrix} \Delta P_k \\ \Delta P_m \\ \Delta Q_k \\ \Delta Q_m \\ \Delta P_{km}^{Xtcsc} \end{bmatrix} = J \begin{bmatrix} \Delta \delta_k \\ \Delta \delta_m \\ \Delta V_k \\ \Delta V_m \\ \Delta X_{tcsc} \end{bmatrix} \tag{3.23}$$

A flow chart of the entire modified TCSC newton Raphson code is shown in Algorithm 1.

Algorithm 1 NR Algorithm incorporating TCSC

1: Initialize the network.
2: Initialize the TCSC data including the sending end, receiving end, power flow reference. Make the Y bus network excluding the TCSC line.
3: Run a warm-start power flow excluding the TCSC line.
4: **while do**$(Tol) \leq (1e-5)$
5: Calculate PCAL, QCAL.(Calculated Power)
6: Calculate the TCSC bus power injection(bus k and m).
7: Calculate the Power Mismatches(DP and DQ).
8: Calculate the TCSC Power Mismatches. (Power flow reference mismatch).
9:
10: **if** $abs(DPQ) \leq Tol$ **then**
11: Power Flow has Converged.
12: **end if**
13: Calculate the Newton Raphson Jacobian.
14: Calculate the TCSS Jacobian.
15: $D = (JAC)^{-1} \times DPQ$
16: Update the State Variables and the TCSC Reactance.
17: Check Impedance Limits.
18: **end while**

It must be noted that the existing power flow data is modified by removing the line k-m which contains the TCSC in the Y bus since it is a variable reactance. The Y bus is used for modelling the fixed reactances. Since the Y bus does model the TCSC line, thus in order to account for the power flowing through line k-m, separate functions need to be added in the default NR power flow. Similarly, separate function

must be added to calculate the power mismatches for bus k and m as the TCSC is modelled by line k-m. It must be remembered that the TCSC reactance is changing after every iteration in the form of delta X thus the Y bus can not be used to model a variable reactance and hence the need for additional functions.

An example showing the addition of a new bus is shown below for a two bus system. Fig.3.15 shows a sample two bus power system without any TCSC installed.

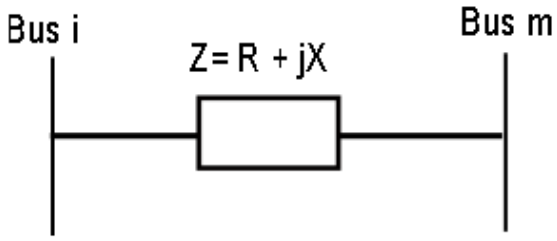

Figure 3.15: Fixed Impedance between Bus i and Bus m

Now if a TCSC needs to be installed between Bus i and Bus m, then the additional bus needs to be added between the two buses bus i and bus m. Line km models the TCSC reactance which is shown in Fig.3.16.

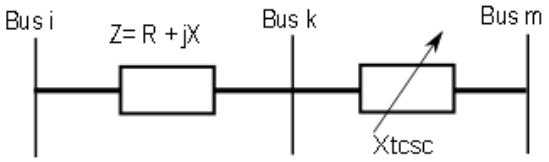

Figure 3.16: TCSC added to the Fixed Impedance between Bus i and Bus m

Thus the Simple Newton Raphson power functions and the Y bus models the fixed reactances only shown in Fig.3.17 while the additional functions are used to model the variable reactance shown in Fig.3.18. The two combined model the whole network shown in Fig.3.19.

Separate functions are added to a Newton Raphson power flow.These function modify the existing NR power flow to accommodate the addition of the TCSC line. A brief description of each additional function is given below.The function converges

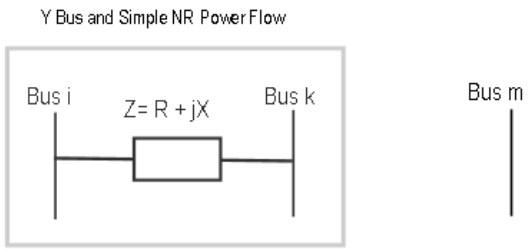

Figure 3.17: Fixed Impedance only between Bus i and Bus m

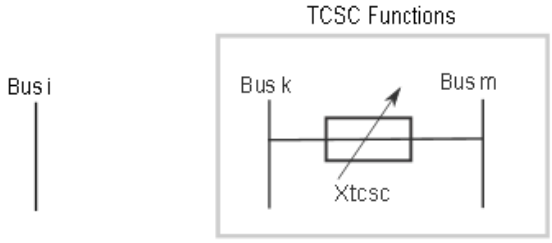

Figure 3.18: TCSC only between Bus i and Bus m

when the power mismatches including the power flow reference mismatch is less than a certain tolerance. The description of the additional TCSC functions are shown in Algorithm 2, Algorithm 3 and Algorithm 4.

1. TCSS Data: This adds an extra bus to the power system and modifies the existing power system.

2. TCSC calculated power: This function calculates the power flow in line k-m and adds that power flow to the default NR bus power injections.

3. TCSC power mismatches: This calculates the term delta Pkm and adds it to the last row of the power mismatches term.

4. TCSC jacobian : The TCSC jacobian calculates the derivatives of the state variables with respect to the power flow reference (real power through line km) . The additional state variable is the TCSC variable reactance.

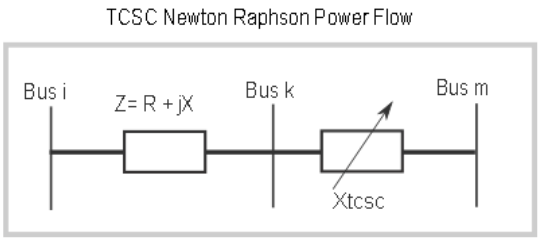

Figure 3.19: TCSC and Fixed Impedance Combined between Bus i and Bus m

3.3.2 IEEE 4 Bus System

The system used in this section is a modified version of the IEEE 4 bus radial system. The system configuration is shown in Fig.3.20. The system data is given in Table.3.25 and Table.3.26.

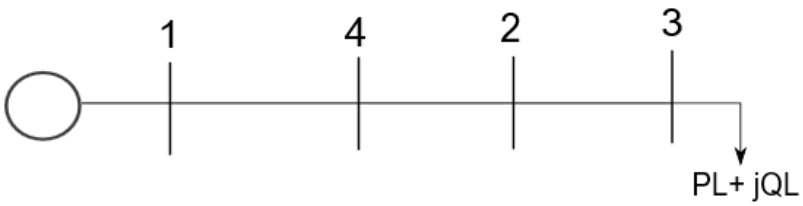

Figure 3.20: 4 Bus System Diagram

Table 3.25: 4 Bus System Data

Bus No.	Bus Type
1.	Slack bus
4.	PQ bus with zero load
2.	PQ bus with zero load
3.	PQ bus with load PL + j Q L

Algorithm 2 TCSC Calculated powers

1: **for** $ii = 1$ to $NTCSC(NumberofTCSCs)$ **do**
2: $B_{mm} = -1/X(ii)$ *and* $B_{mk} = 1/X(ii)$.(calculate the TCSC admittance)
3: **for** $kk = 1$ to $2(kk = 1(sendingbus)\, and\, kk = 2(recievingbus)$ **do**
4: Calculate the real and reactive power flow throughout the TCSC line.
5: A = VA (TCSC sending bus) − VA (TCSC receiving bus) .
6: $P_{cal} = VM(TCSCsendingbus) \times VM(TCSCreceivingbus) \times B_{mk} \times sin(A)$
7: $Q_{cal} = -VM(TCSCsendingbus)^2 \times B_{mm} \times VM(TCSCsendingbus) \times VM(TCSCreceivingbus) \times B_{mm} \times cos(A)$
8: Update the bus injection vector.
9: $P_{cal}(TCSCsendingbus) = P_{cal}(TCSCsendingbus) + P_{cal}$
10: $Q_{cal}(TCSCsendingbus) = Q_{cal}(TCSCsendingbus) + Q_{cal}$
11: Update the TCSC PQ power flow
12: **if** kk==1 (if the bus is the TCSS sending bus) **then**
13: TCSC PQ sending end = Pcal + i × Qcal
14: **else**
15: TCSC PQ recieving end= Pcal + j × Qcal
16: **end if**
17: Reverse the sending and receiving buses
18: **end for**
19: **end for**

Table 3.26: 4 Bus System Line Data

Branch No.	From Bus	To Bus	R	X	B
1.	1	4	.003	.006	0
2.	4	2	.003	.006	0
3.	2	3	.003	.006	0

3.3.3 Results for the IEEE 4 Bus System: Running Base case and TCSC code in tandem and comparison between the results

In order to verify the algorithm discussed in the previous section, several case scenarios were calculated by which different conclusions were obtained. The system studied in this section is a radial system which is a modified version of the IEEE 4 bus system. This is shown in Fig.3.21.

Algorithm 3 TCSC power mismatches

1: **if** ($It \geq 1$) **then**
2: **for** $ii = 1$ to $NTCSC(NumberofTCSCs)$ **do**
3: **if** Tcsc power flow control is ON **then**
4: **for** $kk = 1$ to $2(kk = 1(sendingbus)\, and\, kk = 2(recievingbus))$ **do**
5: A= VA (TCSC sending bus) − VA (TCSC receiving bus)
6: $P_{cal} = VM(TCSCsendingbus) \times VM(TCSCreceivingbus) \times B_{mk} \times sin(A)$
7: **if** (Flow is positive and the bus is TCSC sending bus) or (Flow is negative and the bus is the TCSS recieving bus) **then**
8: TCSC power mismatch = TCSC Power Flow reference − TCSC Calculated power
9: Break
10: **else**
11: Exit the if loop.
12: **end if**
13: Reverse the sending and receiving buses.
14: **end for**
15: **else**
16: TCSC power mismatch = 0(TCSC is bypassed)
17: **end if**
18: **end for**
19: **end if**

Algorithm 4 TCSC Jacobian

```
for ii = 1 to NTCSC(NumberofTCSCs) do
    for (Sending Bus and Receiving Bus ) do
        A= VA ( TCSC sending − TCSC receiving)
        (Hkm = - VM(Sending bus) × VM(Receiving bus) × Bmm × cos(A))
        (Nkm = VM(Sending bus)×VM(Receiving bus)×Bmm×sin(A))
        Modify Jacobian
        if ( It ≥ 1) then
            if ( Power flow control is on) then
                if (kk= Sending bus and Flow = Positive or kk= Receiving bus and
  Flow = Negative ) then
                    (Add JAC elements)
                end if
                (Add JAC elements)
            else
                (Jac x dPkm/dXtcsc=1)
            end if
            Switch Sending and receiving buses
        end if
    end for
end for
```

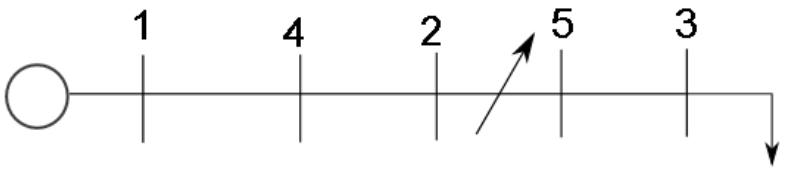

Figure 3.21: Modified version of IEEE 4 Bus System

The TCSC is installed on the line 2-5. The extra bus added is bus no 5 due to the addition of the TCSC. The 4 bus system without any tcsc installed is shown in Fig.3.22.

The Flow Chart of the procedure is shown in Fig.3.23.

Scenario 1

For the base case, the Power flow through the line 2-5 is 0.4006 units shown in Fig.3.24. The Power flow reference input into the TCSC code is 0.4006 units. However, the main difference is that instead of the Line 2-5 having a fixed reactance, the Line 2-5 has a variable reactance as shown in Fig.3.25.

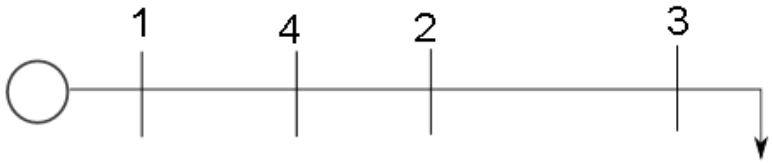

Figure 3.22: Original version of 4 Bus System

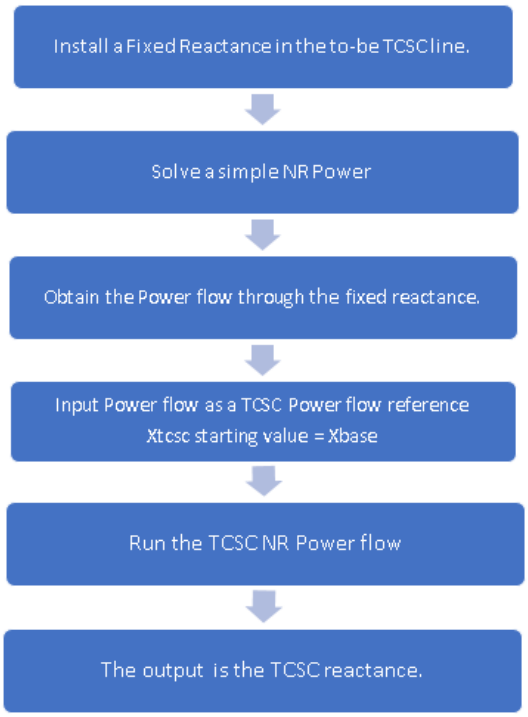

Figure 3.23: Flow of the Procedure used for comparing TCSC code with the base code

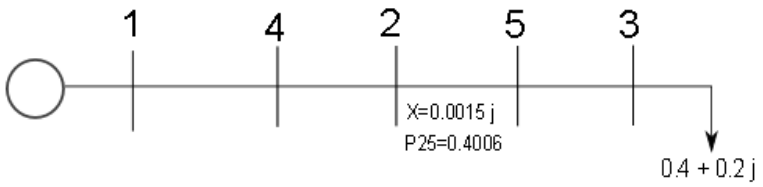

Figure 3.24: Base Case Scenario 1

The TCSC reactance of the converged NR power flow is 0.1971 j. Thus, there exist two different reactances which are able to satisfy a given power flow(i.e. a fixed load) in a radial system. One reactance is the solution of the TCSC code and the other

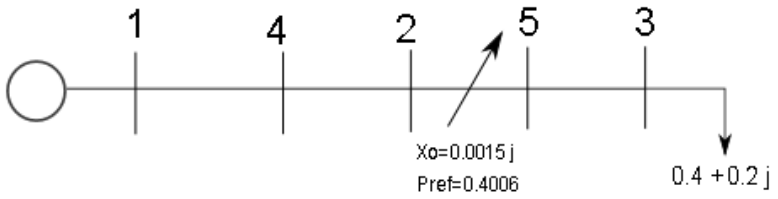

Figure 3.25: TCSC Case Scenario 1

reactance is a fixed reactance which was part of the base case shown in Table.3.28. However, the voltages and angles of the 5 buses are different in the base case solution and the TCSC solution shown in Table.3.27.

Table 3.27: Power Flow Solution Scenario 1

Bus No	Base Case VM	TCSC System VM	Base Case VA	TCSC System VA
1.	1.05	1.05	0	0
2.	1.0454	1.0449	-0.0033	-0.0031
3.	1.0428	1	-0.0055	-0.0803
4.	1.0477	1.0475	-0.0016	-0.0015
5.	1.0451	1.0024	-0.0038	-0.0785

Table 3.28: Reactance Parameters Scenario 1

Case	Power FLow in Line 2-5(pu)	Reactance of Line 2-5(pu)
Base Case	0.4006	0.0015
TCSC Code	0.4006	0.1971

Scenario 2

Another case scenario was studied to verify the above pattern with a different radial load as compared to Scenario 1. The second case scenario is discussed in this section. The Base Case system diagram is shown in Fig.3.26. The power flow reference is 0.6011 pu and the value of the fixed reactance is 0.0020 j. The starting value of the

reactance for the TCSC code is 0.0020 j. The TCSC system diagram is shown in Fig.3.27.

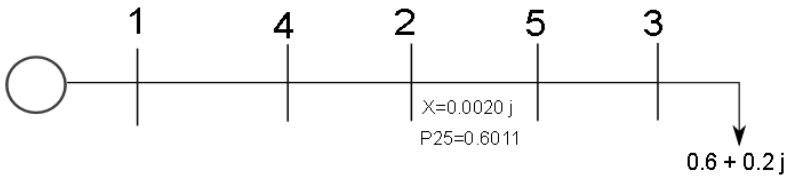

Figure 3.26: Base Case Scenario 2

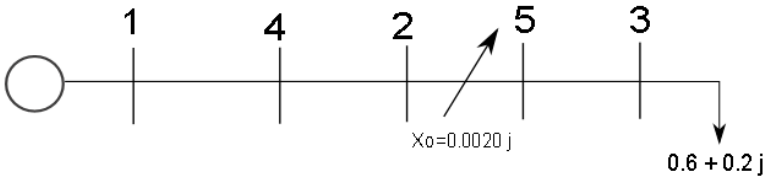

Figure 3.27: TCSC Case Scenario 2

Table 3.29: Power Flow Solution Scenario 2

Bus	Base Case VM	TCSC VM	Base Case VA	TCSC VA
1.	1.05	1.05	0	0
2.	1.0442	1.0443	-0.0055	-0.0055
3.	1.0409	1.0445	-0.0093	0
4.	1.0471	1.0471	-0.0027	-0.0027
5.	1.0438	1.0473	-0.0066	+0.0033

Table 3.30: Reactance Parameters Scenario 2

Case	Power FLow in Line 2-5	Reactance of Line 2-5
Base Case	0.6011	0.0020
TCSC Code	0.6011	-0.0161

As can be seen above, the voltage magnitude and angles of the base case and TCSC system are different as are the reactance of the line 2-5 however the power flow is still the same in both system through the TCSC line 2-5. The results are shown in Table.3.29 and Table.3.30.

3.3.3.1 Verification of the TCSC and Base Case Solutions through Matpower

Since the solution coming out of the TCSC code was different than the base case solution, a second check was performed to see if the TCSC solution actually existed if an equivalent fixed reactance was replaced in the system with its value being equal to the solution of the TCSC reactance. The system was then run in matpower to see if the voltages and angles from the matpower solution were the same as the TCSC solution. This is shown in Fig.3.28.

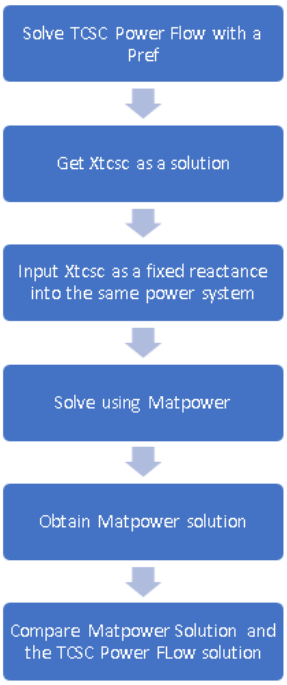

Figure 3.28: Verification of the TCSC and Base Case Solutions through Matpower procedure

This was done for the two systems studied in the earlier section. The results for the Matpower and the variable TCSC power flow were matching, thus the solution of the

variable TCSC code is correct. The verification results are shown here for Scenario 2.

Matpower verification of the Base Case

The base case system diagram for Scenario 2 is shown in Fig.3.29.

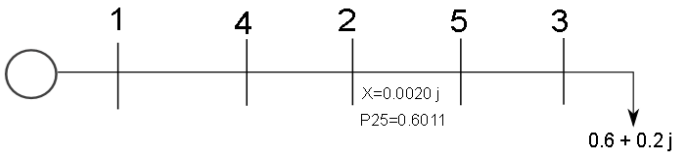

Figure 3.29: Base Case System Diagram Scenario 2

Matpower case format data is shown below which is same as the base case data input shown in Table.3.31. The comparison between Matpower solution and the base case solution are shown in Table.3.32 and Table.3.33.

Table 3.31: Base Case System Data Scenario 2

Branch No.	From Bus	To Bus	R	X	B
1.	1	4	.003	.006	0
2.	4	2	.003	.006	0
3.	2	5	0	.002	0
4.	5	3	.003	.006	0

Table 3.32: Base Case Scenario 2 Matpower Verification Results

Bus	Base Case VM	Matpower VM	Base Case VA	Matpower VA
1.	1.05	1.05	0	0
2.	1.0442	1.0442	-0.0055	-0.0055
3.	1.0409	1.0409	-0.0093	-0.0093
4.	1.0471	1.0471	-0.0027	-0.0027
5.	1.0438	1.0438	-0.0066	-0.0066

Table 3.33: Base Case Scenario 2 Reactance Verification Results

Case	Power flow in Line2-+5	React. of Line 2-5
Base Case	0.6011	0.0020
Matpower case	0.6011	0.002

Matpower verification of the Variable Reactance Solution

The system diagram for the TCSC system is shown in Fig.**??**. The comparison between Matpower solution and the base case solution are shown in Table.3.30 and Table.3.34. As can be seen, the matpower results are the same as the TCSC code which again shows that there exist two different reactances which can satisfy the same power flow reference.

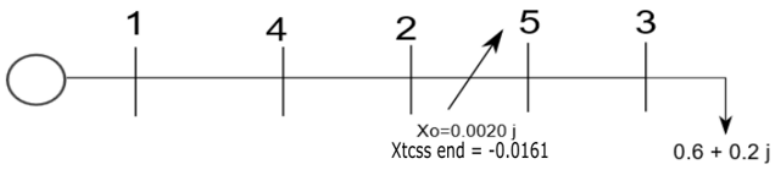

Figure 3.30: TCSC Case 1 System Diagram Scenario 2

Table 3.34: TCSC Case Scenario 2 Matpower Verification Results

Bus	Base Case VM	Matpower VM	Base Case VA	Matpower VA
1.	1.05	1.05	0	0
2.	1.0443	1.0443	-0.0055	-0.0055
3.	1.0445	1.044	5 0	0
4.	1.0471	1.0471	-0.0027	-0.0027
5.	1.0473	1.0473	+0.0033	+0.0033

Table 3.35: TCSC Case Scenario 2 Reactance Verification Results

Case	Power FLow in Line2-5	Reactance of Line 2-5
Base Case	0.6011	-0.0161
TCSC Code	0.6011	-0.0161

3.3.4 Comparison of TCSC reactance keeping the load fixed and multiple fixed reactances

Two base cases with two different fixed reactances are shown in Fig.3.31. The load was kept fixed. As can be seen, the power flow through the line 2-5 is still the same for both cases since the real load is the same for bus 3. Thus, it means that the real power flow is determined by the load and is same irrespective of the fixed reactance.

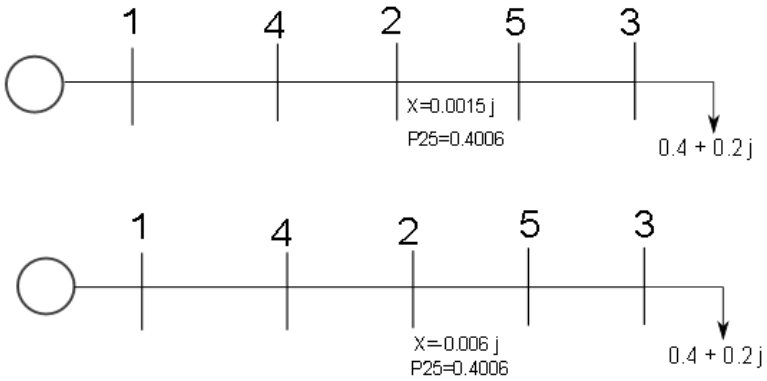

Figure 3.31: Two Base Cases with Fixed Reactances

Now the power flow reference which is 0.4006 pu for the above system is entered into the Variable TCSC code and the line 2-5 will be a variable reactance. Thus for both the base cases above, the solution of the variable TCSC code is given in Fig.3.32.

3.3.5 Region of Convergence

The TCSC code needs to be provided a maximum and a minimum limit for the variable reactance. This is important in terms of the convergence characteristics of the code. For the two systems studied in the first section, the region of convergence

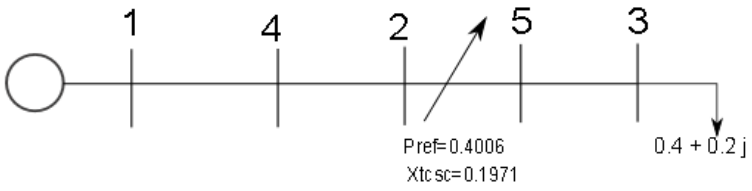

Figure 3.32: Variable Reactance Solution in case of Two Different Fixed Reactances

was checked. The maximum and minimum limit for the variable reactance were +1 and -1. For one system, the variable reactance solution is 0.1917 between x min=-0.9 and x max=+0.9. It is shown in Fig.3.33.

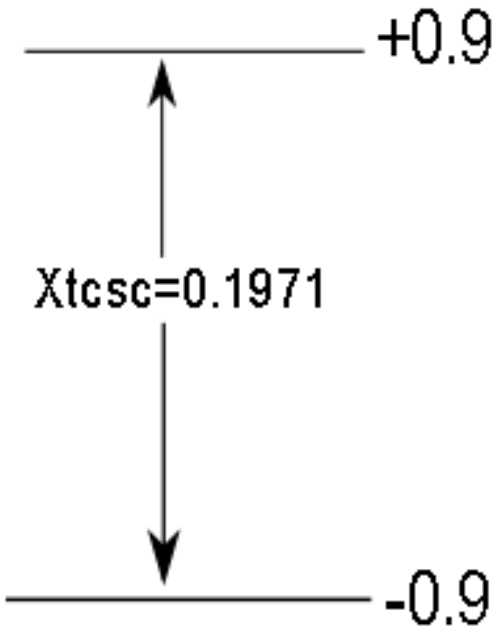

Figure 3.33: Region of Convergence Scenario 1

For the second system, the region of convergence is shown in Fig.3.34.

Thus overall, the solution of the variable TCSC code always converges to the same value sometimes within a certain percentage and sometimes between the maximum and minimum limit of the variable reactance.

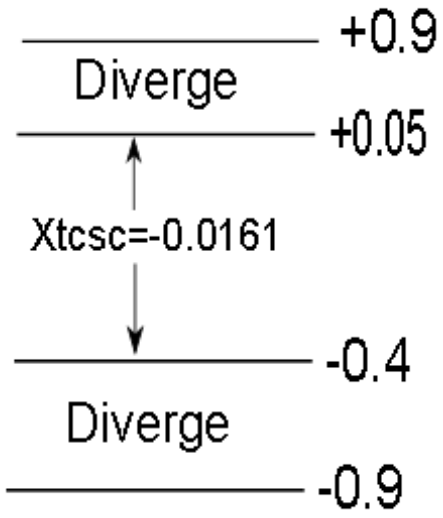

Figure 3.34: Region of Convergence Scenario 2

3.3.6 Increasing the number of loads in the radial system for the 4 Bus System

The analysis performed in the previous sections was done on a radial system with only one fixed load. The same results are now obtained for 2 loads in the radial system instead of one. The two loads are located such that one load is located at a bus towards the left of the tcsc line and one load is located at a bus towards the right of the tcsc line. The system diagram is shown in Fig.3.35.

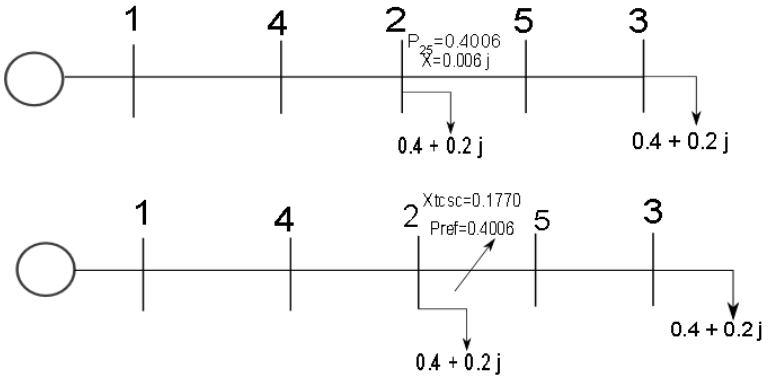

Figure 3.35: Base Case and TCSC Case with two loads Scenario 1

Similar pattern of results were obtained for the two loads as compared to the single load. The voltages and magnitudes of the base case and the variable TCSC code

are shown below as well as the summary of the results. The results are shown in Table.3.36 and Table.3.37.

Table 3.36: Power Flow Solution Scenario 1(Multiple Loads)

Bus	Base Case VM	Matpower VM	Base Case VA	Matpower VA
1.	1.05	1.05	0	0
2.	1.0407	1.0403	-0.0066	-0.0064
3.	1.0372	1.000	-0.0105	-0.0762
4.	1.0454	1.0452	-0.0033	-0.0032
5.	1.0396	1.0024	-0.0088	-0.0744

Table 3.37: Reactance Parameters Scenario 1(Multiple Loads)

Case	Power FLow in Line2-5	Reactance of Line 2-5
Base Case	0.4006	0.006
TCSC Code	0.4006	0.1770

Thus, there exist two reactance which are able to satisfy a given power flow, one of them is the fixed reactance and one of them is the solution of the variable tcsc code. Another system studied but with different loads is shown in Fig.3.36. Similar pattern in results as the previous case scenario is obtained.

Table 3.38: Power Flow Solution Scenario 2(Multiple Loads)

Bus No	Base Case VM	Matpower VM	Base Case VA	Matpower VA
1.	1.05	1.05	0	0
2.	1.0408	1.0403	-0.0039	-0.0037
3.	1.0414	1.00	0	-0.0735
4.	1.0454	1.0452	-0.0019	-0.0018
5.	1.0437	1.0024	+0.0017	-0.0717

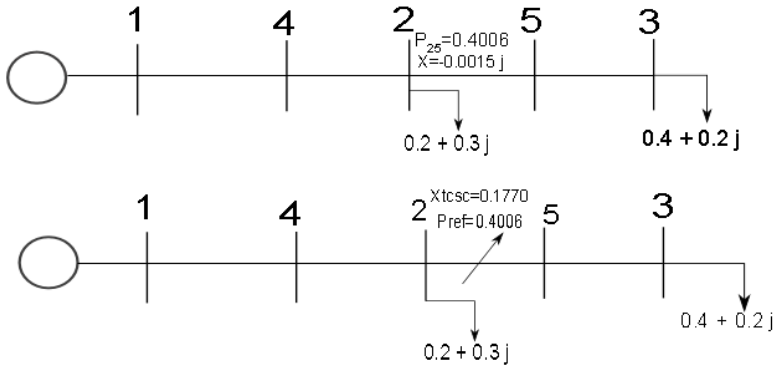

Figure 3.36: Base Case and TCSC Case with two loads Scenario 2

Table 3.39: Reactance Parameters Scenario 2(Multiple Loads)

Case	Power FLow in Line2-5	Reactance of Line 2-5
Base Case	0.4006	-0.0015
TCSC Code	0.4006	0.1770

Another case study was performed with two loads located at bus 5 and 3 after the tcsc bus shown in Fig.3.37.

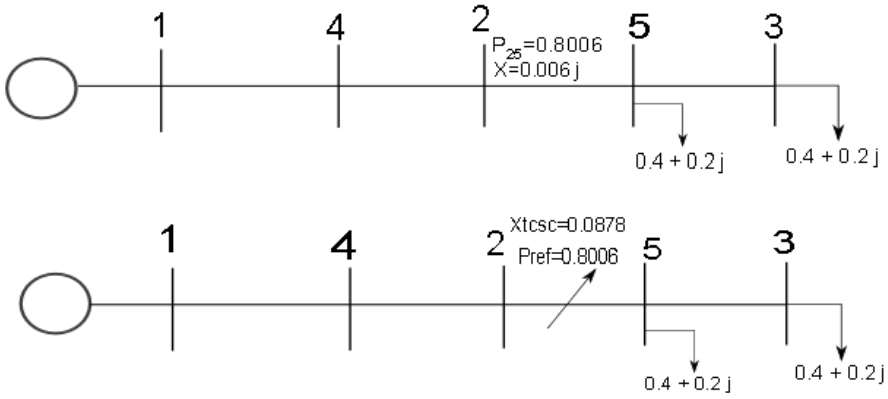

Figure 3.37: Base Case and TCSC Case with two loads Scenario 3

Table 3.40: Power Flow Solution Scenario 3(Multiple Loads)

Bus	Base Case VM	Matpower VM	Base Case VA	Matpower VA
1.	1.05	1.05	0	0
2.	1.0407	1.0399	-0.0066	-0.0062
3.	1.036	1.00	-0.0127	-0.0755
4.	1.0453	1.0450	-0.0033	-0.0031
5.	1.0384	1.0024	-0.0110	-.0737

Table 3.41: Reactance Parameters Scenario 3(Multiple Loads)

Case	Power FLow in Line2-5	Reactance of Line 2-5
Base Case	0.8006	0.006
TCSC Code	0.8006	0.0878

Another case study was performed with two loads located at bus 5 and 3 after the tcsc bus shown in Fig.3.38.

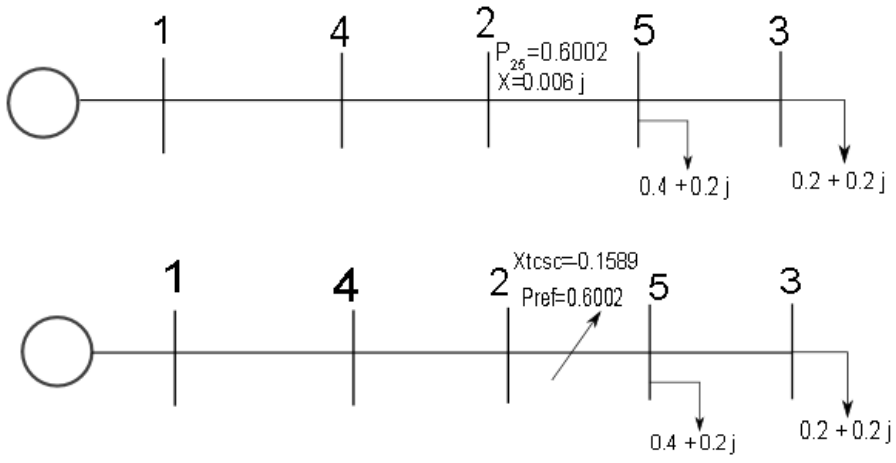

Figure 3.38: Base Case and TCSC Case with two loads Scenario 4

Table 3.42: Power Flow Solution Scenario 4(Multiple Loads)

Bus	Base Case VM	Matpower VM	Base Case VA	Matpower VA
1.	1.05	1.05	0	0
2.	1.0419	1.0427	-0.0044	-0.0048
3.	1.0378	1.0954	-0.0083	-0.0782
4.	1.0459	1.0464	-0.0022	-0.0024
5.	1.0396	1.0971	-0.0077	-0.0787

Table 3.43: Reactance Parameters Scenario 4(Multiple Loads)

Case	Power FLow in Line2-5	Reactance of Line 2-5
Base Case	0.6002	0.006
TCSC Code	0.6002	-0.1589

3.3.7 Parallel Radial System

Furthermore, a modified radial system was tested with multiple TCSCc installed in a single line. This was done in order to check if multiple TCSC installed in one line will converge to different reactance or to equal value. The first system shown in Fig.3.39 has one tcsc installed and the power flow reference is 0.2 MW for line 2-4. The converged value of the xtcsc is 0.1232.

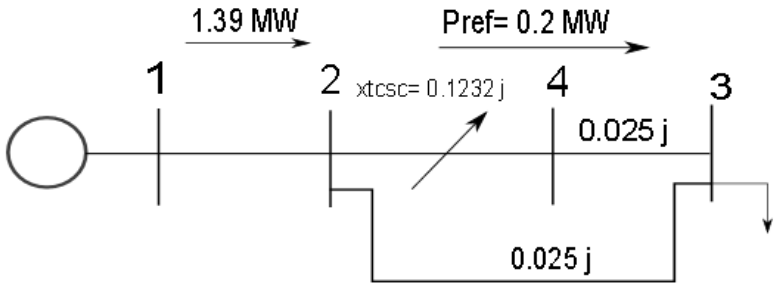

Figure 3.39: Parallel Radial System Diagram(One TCSC)

The second system shown in Fig.3.40 is the same as above but with 2 tcsc installed in series. The power flow reference is still the same. The reactance of one tcsc converges to a different value than the other. However it must be noted that the sum of the two reactances is equal to 0.1232 which was the solution with 1 tcsc only.

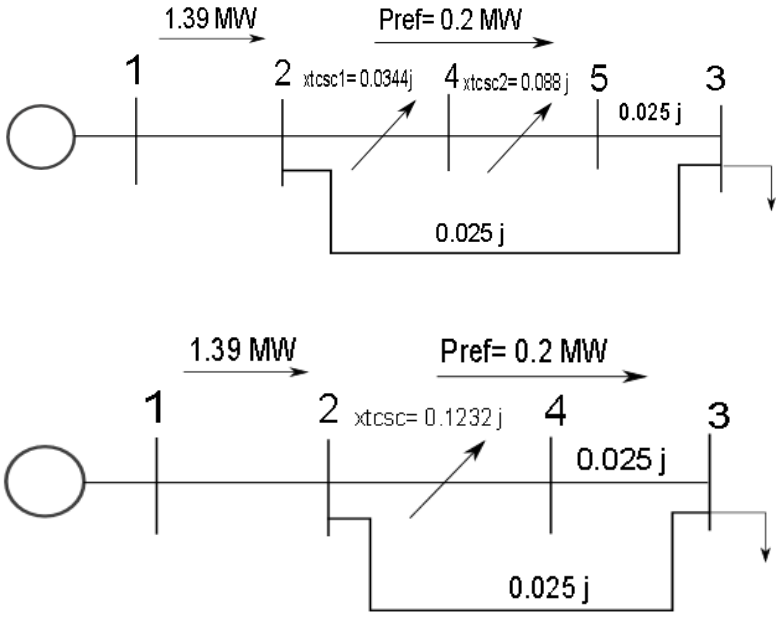

Figure 3.40: Parallel Radial System Diagram(Two TCSC)

With 3 tcscs installed in the line, each tcsc converges to a different value dependent upon the position shown in Fig.3.41. The sum of the three reactances is still equal to the value of the first system.

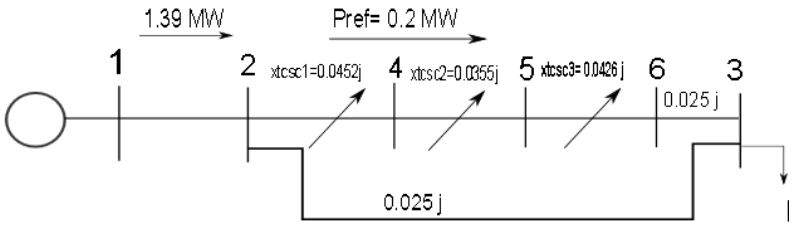

Figure 3.41: Parallel Radial System Diagram(Three TCSC)

The main takeaway is that the distribution of the reactance in unequal. The above

analysis was carried out with capacitive operation as well shown in Fig.3.42 and Fig.3.43.

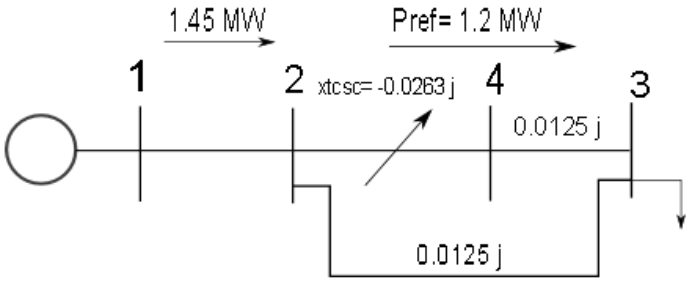

Figure 3.42: Parallel Radial System Diagram(Two TCSC) Capacitive Operation Base Case

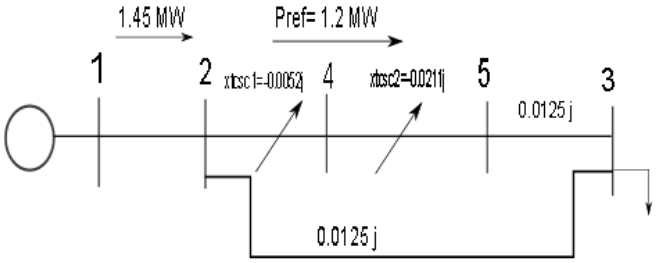

Figure 3.43: Parallel Radial System Diagram(Two TCSC) Capacitive Operation TCSC Case

Similar analysis was done for the capacitive operation as well. Again the capacitive reactance converges to unequal values but the sum is still equal to what the value of one capacitive reactance converges to in the first system.

3.3.7.1 Singularity issue with 2 TCSCs in series in one line

If two tcsc are installed in series in one line one after another, then the code discussed above has singularity error. This was done for a radial system. In order to see what is causing the singularity, sparsity was used as a possible solution to the singularity error however, that is not the case.

3.3.8 TWO TCSCs radial system

Two TCSCs were installed in the radial system for the IEEE 4 bus system. The two tcscs are independently controlled. The results will be shown for several scenarios. Overall, the results are summarized below:

- There exist two different solutions for the same power flow reference. One solution exists in case of fixed reactance(base case). The other solution exists in the case of variable reactance TCSC code. Since the reactance are different for a given power flow reference in the base case and TCSC case, the voltage and angles for the base case and TCSC power flow solution are different.

- Another important point which is different from the single tcsc case is that there exist several different solutions for the tcsc reactances depending on the starting point of the TCSC reactance. This is the case for a given power flow reference. In all such solutions, the voltage and angles of all buses except the two buses linking one tcsc to the second tcsc are same. This creates the two different solutions. The sum of the two reactance still remains the same across different solutions. .

3.3.8.1 Results

Scenario 1

The base case for scenario 1 is shown in Fig.3.44. The system diagram with TCSCs for scenario 1 is shown in Fig.3.45.The results are shown in Table.3.44 and Table.3.45.

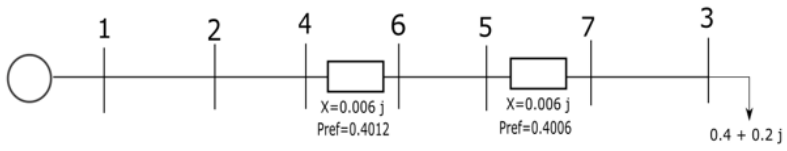

Figure 3.44: Base Case Scenario 1(Multiple TCSCs Radial System)

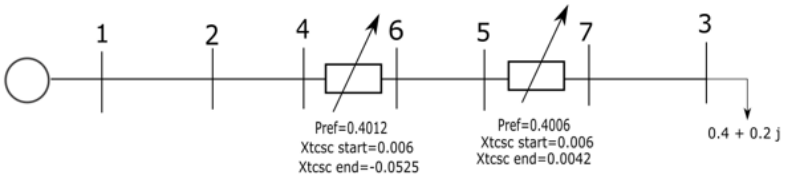

Figure 3.45: TCSC Case Scenario 1(Multiple TCSCs Radial System)

Table 3.44: Power Flow Solution Scenario 1(Multiple TCSCs Radial System)

Bus	Base Case VM	Matpower VM	Base Case VA	Matpower VA
1.	1.05	1.05	0	0
2.	0.9975	0.9976	-0.0036	-0.0018
3.	0.9878	1	-0.0121	0.0121
4.	0.9975	0.9953	-0.0018	-0.0037
5.	0.9914	1.0032	-0.0079	0.0156
6.	0.9939	1.0056	-0.0060	0.0174
7.	0.9902	1.0024	-0.0121	0.0139

Table 3.45: Reactance Parameters Scenario 1(Multiple TCSCs Radial System)

Case	Power FLow in Line4-6	Reactance of Line 4-6
Base Case	0.4012	0.006
TCSC Code	0.4012	-0.0525
Case	Power FLow in Line 5-7	Reactance of Line 5-7
Base Case	0.4006	0.006
TCSC Code	0.4006	0.0042

Scenario 2

The base case system diagram is shown in Fig.3.46. The system diagram with TCSC is shown in Fig.3.47. The results are shown in Table.3.46 and Table.3.47.

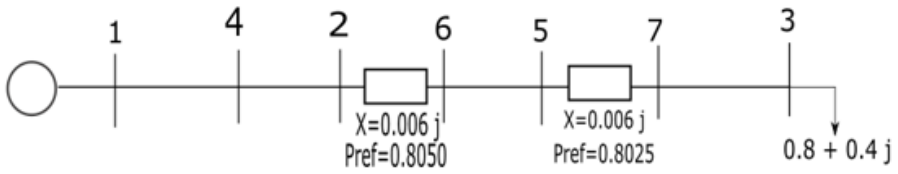

Figure 3.46: Base Case Scenario 2(Multiple TCSCs Radial System)

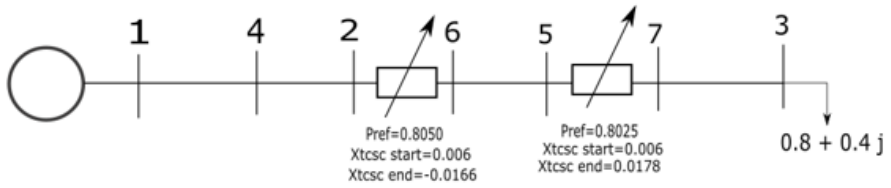

Figure 3.47: TCSC Case Scenario 2(Multiple TCSCs Radial System)

Table 3.46: Power Flow Solution Scenario 2(Multiple TCSCs Radial System)

Bus No	Base Case VM	Matpower VM	Base Case VA	Matpower VA
1.	1	1	0	0
2.	0.99	0.9901	-0.0072	-0.0073
3.	0.9751	0.9798	-0.0246	-0.0157
4.	0.9950	0.9951	-0.0036	-0.0036
5.	0.9825	0.9921	-0.0158	0.0027
6.	0.9875	0.9971	-0.0122	0.0063
7.	0.9800	0.9847	-0.0208	-0.0119

Scenario 3(same as scenario 2 except different x start- same x base and same power flow ref)

The base case system diagram is shown in Fig.3.48. The system diagram with TCSCs is shown in Fig.3.49. The results are shown in Table.3.48 and Table.3.49.

Table 3.47: Reactance Parameters Scenario 2(Multiple TCSCs Radial System)

Case	Power FLow in Line2-6	Reactance of Line 2-6
Base Case	0.8050	0.006
TCSC Code	0.8050	-0.0166
Case	Power FLow in Line 5-7	Reactance of Line 5-7
Base Case	0.8025	0.006
TCSC Code	0.8025	0.0178

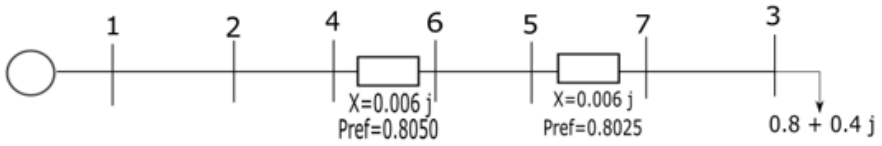

Figure 3.48: Base Case Scenario 3(Multiple TCSCs Radial System)

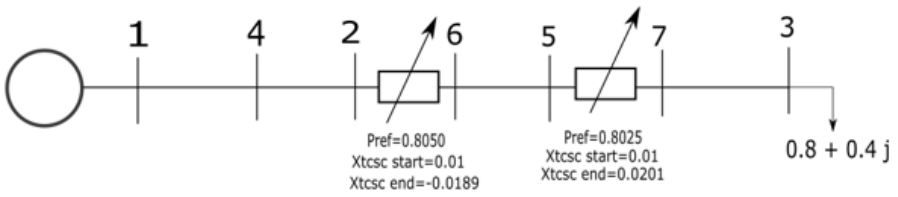

Figure 3.49: TCSC Case Scenario 3(Multiple TCSCs Radial System)

Table 3.48: Power Flow Solution Scenario 3(Multiple TCSCs Radial System)

Bus No	Base Case VM	Matpower VM	Base Case VA	Matpower VA
1.	1	1	0	0
2.	0.99	0.9901	-0.0072	-0.0073
3.	0.9751	0.9798	-0.0246	-0.0157
4.	0.9950	0.9951	-0.0036	-0.0036
5.	0.9825	0.9921	-0.0158	0.0027
6.	0.9875	0.9971	-0.0122	0.0063
7.	0.9800	0.9847	-0.0208	-0.0119

Table 3.49: Reactance Parameters Scenario 3(Multiple TCSCs Radial System)

Case	Power FLow in Line2-6	Reactance of Line 2-6
Base Case	0.8050	0.006
TCSC Code	0.8050	-0.0189
Case	Power FLow in Line 5-7	Reactance of Line 5-7
Base Case	0.8025	0.006
TCSC Code	0.8025	0.0201

3.3.9 Verifying the solution of the base case solutions through a Delta Pkm solution

Another method used by to verify the solution of the TCSC code was using a modified version of the Newton Raphson power flow solution. The modified Newton Raphson Power flow solution is shown in Alglorithm.5 where the Steps 4,5,6 and 7 are the steps involved in a normal Newton Raphson power flow while Steps 8,9,10,11,12,13 and 14 are the additional steps added in the modified version of the NR power flow. The idea here is to calculate the mismatch between the Power flow reference and the actual real power flowing in the TCSC line and then based on the mismatch calculate the change in reactance needed for the power flow solution to converge to the power flow reference in the TCSC line. The mismatch and the update in the TCSC reactance is performed within a Newton Raphson iteration after the state variables are updated. Since the TCSC reactance is updated in each iteration, the Y bus needs to be updated in each iteration also. This step is unlike the normal power flow where the Y bus remains the same for a Newton Raphson power flow.

The application of this code to a radial system is shown in the next section.

The power flow in the line k-m is given by Eq.3.24.

$$P_k = V_k V_m B_{km} sin(\delta k - \delta m) \tag{3.24}$$

Algorithm 5 Modified NR Power Flow

1: Initializing the Power FLow Data + Y bus
2: Initialize the Power FLow Reference (Pref) in the TCSC Line
3: **while** $Tol \geq 0$ **do**
4: Calculated Powers
5: Power Mismatches
6: Newton Raphson Jacobian
7: D=JAC/DPQ
8: State Variable Update
9: Calculate the Actual Real Power in the TCSC line
10: Calculate the Power Mismatch in the TCSC Line dPkm=Pref- Pact
11: Calculate dPk/dXtcsc
12: Calculate dXtcsc = dPkm / (dPk/dXtcsc)
13: Xtcsc new=Xtcsc old + delta Xtcsc
14: Update the Ybus with Xtcsc new.
15: **end while**

The derivative dPkm/dXtcsc in the line k-m is given by Eq.3.25.

$$\frac{dP_{km}}{dX_{tcsc}} = V_k V_m sin(\delta k - \delta m) \frac{1}{(Xtcsc)^2} \tag{3.25}$$

The change in reactance $\Delta Xtcsc$ is given by Eq.3.26.

$$\Delta Xtcsc = \frac{P_{km} - P_{ref}}{\frac{dPkm}{dXtcsc}} \tag{3.26}$$

3.3.9.1 Applying the Internal Reactance change to a radial system

Scenario 1

The system diagram for the base case is shown in Fig.3.50.

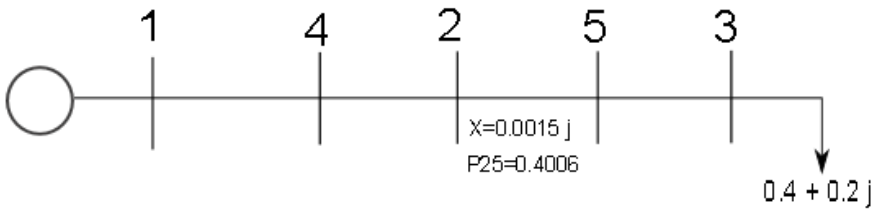

Figure 3.50: Scenario 1 Base case internal reactance change

The Power flow through the line 2-5 is 0.4006 units. The reactance in the line 2-5 is fixed at 0.0015j.The Power flow reference input into the TCSC code is 0.4006 units. However, the main difference is that instead of the Line 2-5 having a fixed reactance, the Line 2-5 has a variable reactance in the modified NR power flow. Xo is the starting reactance of the line which is 0.0015 j.

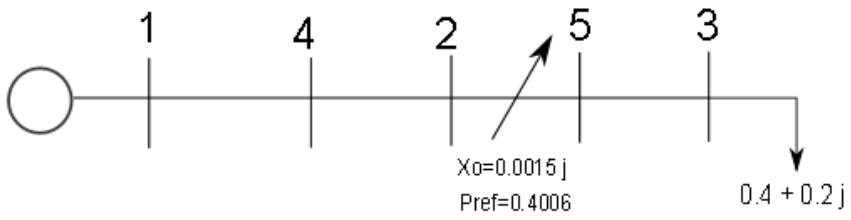

Figure 3.51: Scenario 1 TCSC case internal reactance change

The TCSC reactance of the converged NR power flow is 0.0015j.

Scenario 2

A second case was tested as shown in Fig.3.52 with a different fixed reactance. All other system parameters remain the same as scenario 1.

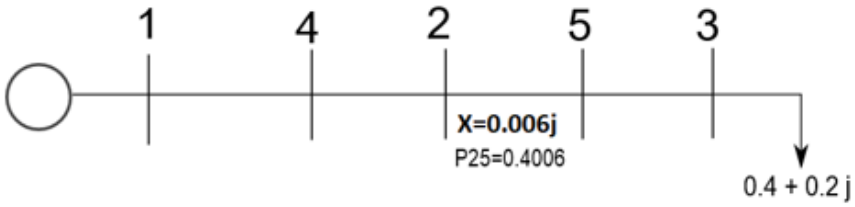

Figure 3.52: Scenario 2 Base case internal reactance change

The Power flow through the line 2-5 is 0.4006 units. The reactance in the line 2-5 is fixed at 0.006j.The Power flow reference input into the TCSC code is 0.4006 units. Xo is the starting reactance of the line which is 0.006 j. This is shown in Fig.3.53.

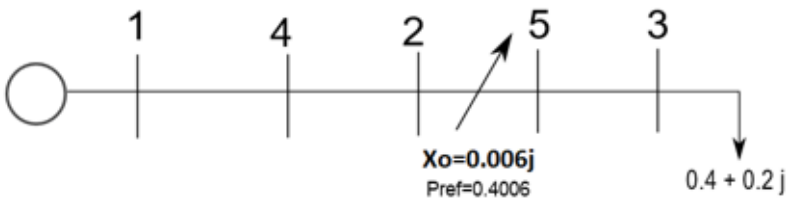

Figure 3.53: Scenario 2 TCSC case internal reactance change

The TCSC reactance of the converged NR power flow is 0.006j. Summarizing scenario 1 and 2, both cases have the same Power flow reference which 0.4006 units. The base reactance for case 1 and 2 is 0.0015i and 0.006i respectively. The Power flow reference is determined by the load at bus 3 and thus is same for case 1 and 2 irrespective of the base reactance. This results in the TCSC code giving the solution of the variable reactance the same as the base reactance in case 1 and case 2 which 0.0015i and 0.006i as both reactances will satisfy the power flow reference of 0.4006 units.

3.3.9.2 Applying the Internal Reactance change to a Parallel Radial System

Algorithm.5 is applied to a parallel radial system. The system diagram is shown in Fig.3.54. The system data is shown in Fig.3.55.

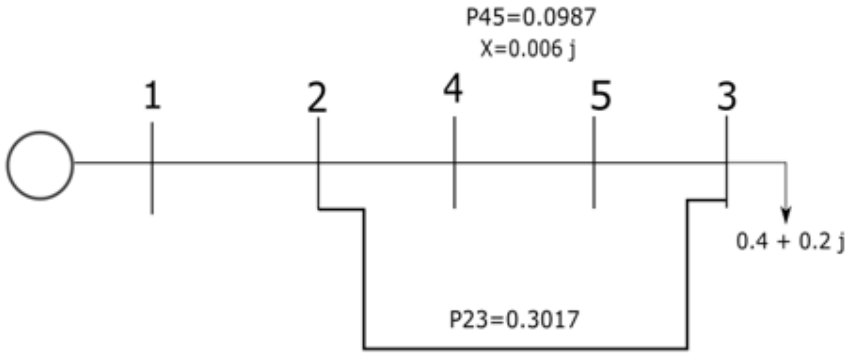

Figure 3.54: Base case Parallel Radial System Internal Reactance Change

MATPOWER CASE DATA					
Branch data					
Branch #	From bus	To bus	R	X	B
1	1	2	0.003	0.006	0
2	2	4	0.003	0.006	0
3	4	5	0	0.006	0
4	5	3	0.003	0.006	0
5	2	3	0.003	0.006	

Figure 3.55: Base case Parallel Radial System System Data

The base case results in a power flow of 0.0987 pu in the line 4-5 and 0.3017 pu in line 2-3. Algorithm.5 was run on the system and the results are shown in Fig.3.56.

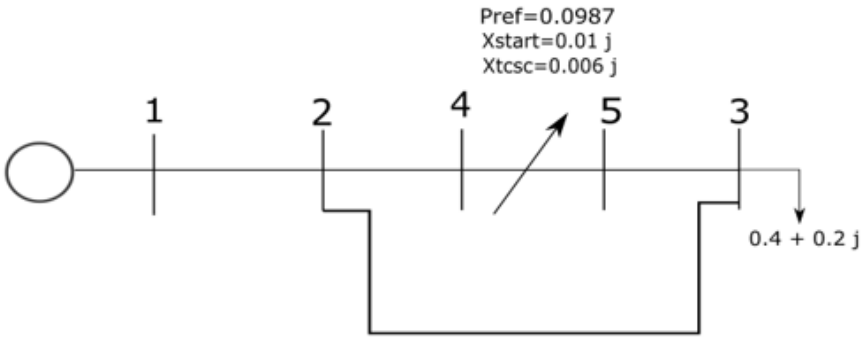

Figure 3.56: TCSC case Parallel Radial System Internal Reactance Change

The power reference in line 4-5 is set as 0.0987. The starting reactance of the TCSC is set as 0.01j. The TCSC reactance converges to 0.006j which is the base reactance. The results for the first 14 iterations are shown in Fig.3.57.

Iteration	TSCC Reactance	Power Flow in line 4-5
1	0.01	0.09163
2	0.0092	0.09163
3	0.0079	0.08595
4	0.0072	0.090931
5	0.0068	0.093598
6	0.0065	0.095219
7	0.0064	0.096272
8	0.0063	0.096984
9	0.0062	0.097476
10	0.0061	0.097821
11	0.0061	0.098067
12	0.0061	0.098242
13	0.0060	0.098368
14	0.0060	0.098459

Figure 3.57: Iteration Convergence

Another case scenario was tested with the system diagram shown in Fig.3.58.

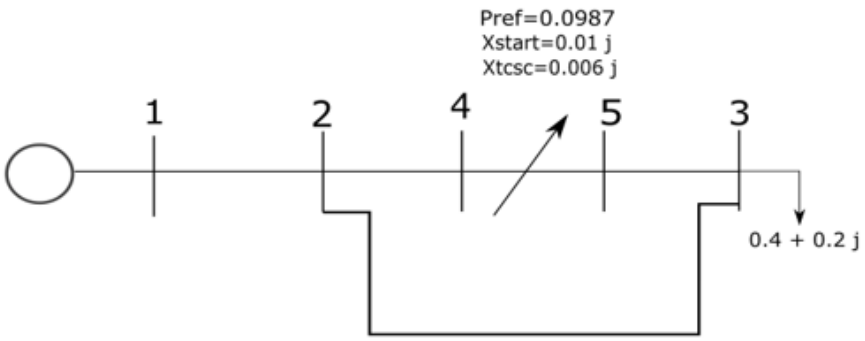

Figure 3.58: TCSC System Diagram Case 2 Parallel Radial System Internal Reactance Change

The starting reactance of the TCSC was 0.01 j and the TCSC reactance converges to 0.006j. The TCSC power flow converges to 0.0987 units which is the base power flow in line 4-5. Given the above two cases, it can seen that the TCSC code is able to converge to the base reactance within a wide range of TCSC starting reactance.

3.4 UPFC Models

A Newton Raphson Power Flow Model incorporating UPFC Model is formulated in this section. A UPFC has additional power flow control capabilities as compared to a TCSC. A UPFC is able to provide the following controls:

- It can control the voltage at bus i at which the shunt voltage source is attached.
- It can control the real and reactive power through the transmission line connecting bus i and bus j.

3.4.1 UPFC Circuit Model

The UPFC circuit model is shown in Fig.3.59 and Fig.3.60. The model shown in Fig.3.59 shows the shunt and series voltage sources along with the series and shunt transformer impedances. Bus i is the bus at which the voltage is controlled by exchnaging reactive power with the shunt voltage source. The series voltage source controls the flow of real and reactive power by injecting either a capacitive or inductive impedance in the transmission line. An equivalent model which can also be used in the Newton Raphson Power flow is shown in Fig.3.60. It models the UPFC in terms of a PV and a PQ bus where the PV Bus models bus i and PQ bus models bus j in Fig.3.59.

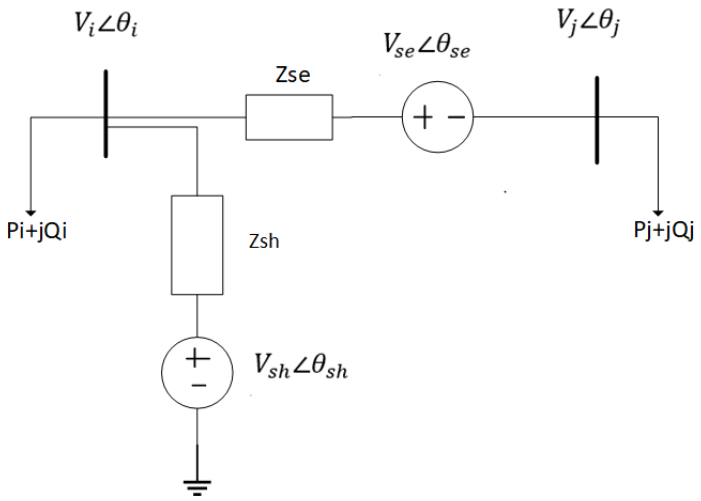

Figure 3.59: Circuit Diagram of UPFC-Series and Shunt Voltage Source

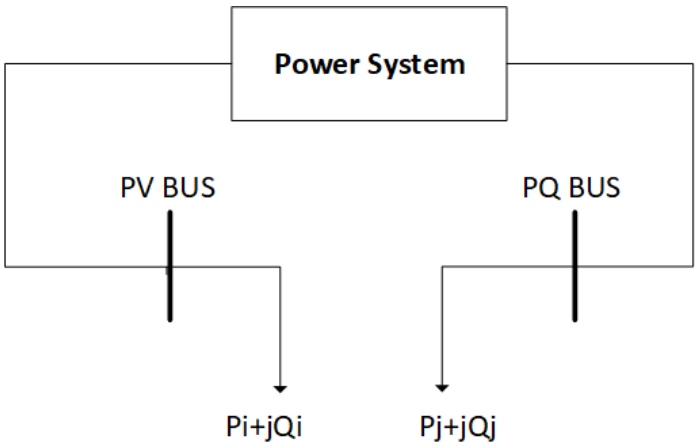

Figure 3.60: UPFC Bus Injection Model

Eq.3.27,Eq.3.28 and Eq.3.29 show the real,reactive and apparent power capacity of the series voltage source respectively.

$$P_{se} = V_{se}[V_j sin(\delta se - \delta j) - V_i sin(\delta se - \delta i)]/X_{se} \tag{3.27}$$

$$Q_{se} = V_{se}[V_i cos(\delta se - \delta i) - V_j cos(\delta se - \delta i) - V_{se}]/X_{se} \tag{3.28}$$

$$MVA_{se} = \sqrt{Pse^2 + Qse^2} \tag{3.29}$$

Eq.3.30,Eq.3.31 and Eq.3.32 show the real,reactive and apparent power flow through the shunt voltage source respectively.

$$P_{sh} = V_{sh}[V_i sin(\delta sh - \delta i)]/X_{sh} \tag{3.30}$$

$$Q_{sh} = V_{sh}[V_i cos(\delta sh - \delta i) - V_{sh}]/X_{sh} \tag{3.31}$$

$$MVA_{sh} = \sqrt{Psh^2 + Qsh^2} \tag{3.32}$$

Eq.3.33 is the total real power consumed or generated by the UPFC. It is zero since the UPFC neither consumes nor generates any real power but can only control the

flow of real power.

$$P_{sh} + P_{se} = 0 \tag{3.33}$$

Eq.3.34 and Eq.3.35 are the real and reactive power reference for the UPFC which will be the real and reactive power flowing through Bus j. Eq.3.36 indicates that the real power flowing through bus i and bus j is equal which stems from the fact that the UPFC neither consumes nor generates any real power.

$$P_j = V_j[V_{se}sin(\delta j - \delta se) - V_i sin(\delta j - \delta i)]/X_{se} \tag{3.34}$$

$$Q_j = V_j[V_i cos(\delta j - \delta i) - V_{se}cos(\delta j - \delta se) - V_j]/X_{se} \tag{3.35}$$

$$P_i - P_j = 0 \tag{3.36}$$

Eq.3.37,Eq.3.38 and Eq.3.39 show the reactive power flowing through bus i,reactive power flowing through the transmission line ij and the reactive power flowing through the shunt voltage source respectively.

$$Q_i = Q_{ij} + Q_{ish} \tag{3.37}$$

$$Q_{ij} = V_i[V_i + V_j cos(\delta i - \delta j) - V_{se}cos(\delta i - \delta se)]/X_{se} \tag{3.38}$$

$$Q_{ish} = V_i[V_i - V_{sh}cos(\delta i - \delta sh)]/X_{sh} \tag{3.39}$$

In order to incorporate the Above UPFC equations into the Newton Raphson power flow model, four new state variables need to be added which are the series and shunt voltage source magnitude and angles. For each UPFC model added, there will be four new state variables. Since there are four new state variables, there needs to be four extra mismatch equations. The four mismatch equations can be obtained from the following references:

- The Real Power Flow Reference at bus j.

- The Reactive Power Flow Reference at bus j.
- The Voltage Reference at bus i.
- The Real Power Exchanged between the shunt and series voltage source.

The Jacobian matrix for the modified NR power flow model is shown in Eq.3.40.

Eq.3.41,Eq.3.42,Eq.3.43 and Eq.3.44 show the expanded version of J1,J2,J3 and J4 of Eq.3.40.

$$\begin{bmatrix} \Delta F \\ \Delta G \\ \Delta P_{\Sigma} \\ (V_i - V_i^{spec}) \\ .... \\ \Delta Pi \\ \Delta Qi \\ \Delta Pj \\ \Delta Qj \end{bmatrix} = \begin{bmatrix} J1 & J2 \\ J3 & J4 \end{bmatrix} \begin{bmatrix} \Delta\delta se \\ \Delta V se \\ \Delta\delta sh \\ \Delta V sh \\ .... \\ \Delta\delta i \\ \Delta V i \\ \Delta\delta j \\ \Delta V j \end{bmatrix} \tag{3.40}$$

$$J1 = \begin{bmatrix} \frac{\partial F}{\partial \delta se} & \frac{\partial F}{\partial V se} & \frac{\partial F}{\partial \delta sh} & \frac{\partial F}{\partial V sh} \\ \frac{\partial G}{\partial \delta se} & \frac{\partial G}{\partial V se} & \frac{\partial G}{\partial \delta sh} & \frac{\partial G}{\partial V sh} \\ \frac{\partial P_{\Sigma}}{\partial \delta se} & \frac{\partial P_{\Sigma}}{\partial V se} & \frac{\partial P_{\Sigma}}{\partial \delta sh} & \frac{\partial P_{\Sigma}}{\partial V sh} \\ \frac{\partial (V_i - V_i^{spec})}{\partial \delta se} & \frac{\partial (V_i - V_i^{spec})}{\partial V se} & \frac{\partial (V_i - V_i^{spec})}{\partial \delta sh} & \frac{\partial (V_i - V_i^{spec})}{\partial V sh} \end{bmatrix} \tag{3.41}$$

$$J2 = \begin{bmatrix} \frac{\partial F}{\partial \delta i} & \frac{\partial F}{\partial V i} & \frac{\partial F}{\partial \delta j} & \frac{\partial F}{\partial V j} \\ \frac{\partial G}{\partial \delta i} & \frac{\partial G}{\partial V i} & \frac{\partial G}{\partial \delta j} & \frac{\partial G}{\partial V j} \\ \frac{\partial P_{\Sigma}}{\partial \delta i} & \frac{\partial P_{\Sigma}}{\partial V i} & \frac{\partial P_{\Sigma}}{\partial \delta j} & \frac{\partial P_{\Sigma}}{\partial V j} \\ \frac{\partial (V_i - V_i^{spec})}{\partial \delta i} & \frac{\partial (V_i - V_i^{spec})}{\partial V i} & \frac{\partial (V_i - V_i^{spec})}{\partial \delta j} & \frac{\partial (V_i - V_i^{spec})}{\partial V j} \end{bmatrix} \tag{3.42}$$

$$J3 = \begin{bmatrix} \frac{\partial Pi}{\partial \delta se} & \frac{\partial Pi}{\partial Vse} & \frac{\partial Pi}{\partial \delta sh} & \frac{\partial Pi}{\partial Vsh} \\ \frac{\partial Qi}{\partial \delta se} & \frac{\partial Qi}{\partial Vse} & \frac{\partial Qi}{\partial \delta sh} & \frac{\partial Qi}{\partial Vsh} \\ \frac{\partial Pj}{\partial \delta se} & \frac{\partial Pj}{\partial Vse} & \frac{\partial Pj}{\partial \delta sh} & \frac{\partial Pj}{\partial Vsh} \\ \frac{\partial Qj}{\partial \delta se} & \frac{\partial Qj}{\partial Vse} & \frac{\partial Qj}{\partial \delta sh} & \frac{\partial Qj}{\partial Vsh} \end{bmatrix} \tag{3.43}$$

$$J4 = \begin{bmatrix} \frac{\partial Pi}{\partial \delta i} & \frac{\partial Pi}{\partial Vi} & \frac{\partial Pi}{\partial \delta j} & \frac{\partial Pi}{\partial Vj} \\ \frac{\partial Qi}{\partial \delta i} & \frac{\partial Qi}{\partial Vi} & \frac{\partial Qi}{\partial \delta j} & \frac{\partial Qi}{\partial Vj} \\ \frac{\partial Pj}{\partial \delta i} & \frac{\partial Pj}{\partial Vi} & \frac{\partial Pj}{\partial \delta j} & \frac{\partial Pj}{\partial Vj} \\ \frac{\partial Qj}{\partial \delta i} & \frac{\partial Qj}{\partial Vi} & \frac{\partial Qj}{\partial \delta j} & \frac{\partial Qj}{\partial Vj} \end{bmatrix} \tag{3.44}$$

The four extra mismatch equations which are added in Eq.3.40 are expanded below. Eq.3.45 and Eq.3.46 are the real power mismatch equation.Eq.3.47 and Eq.3.48 are the reactive power mismatch equation. Eq.3.49,Eq.3.50 and Eq.3.51 are the mismatch equation which shows the real and reactive power exchanged between the series and shunt voltage sources. The reference value for this is zero.

$$P_{ji} = (V_j)^2 g_{ij} - V_i V_j (g_{ij} cos\delta_{ji} + b_{ij} sin\delta_{ji}) + V_j V_{se} (g_{ij} cos(\delta_j - \delta_{se}) + b_{ij} sin(\delta_j - \delta_{se})) \tag{3.45}$$

$$\Delta F = P_{ji} - P_{ref} \tag{3.46}$$

$$Q_{ji} = -(V_j)^2 b_{ij} - V_i V_j (g_{ij} sin\delta_{ji} - b_{ij} cos\delta_{ji}) + V_j V_{se} (g_{ij} sin(\delta_j - \delta_{se}) -$$

$$b_{ij} cos(\delta_j - \delta_{se})) \tag{3.47}$$

$$\Delta G = Q_{ji} - Q_{ref} \tag{3.48}$$

$$PE_{se} = -V_i V_{se}(g_{ij}cos(\delta i - \delta se) - b_{ij}sin(\delta i - \delta se)$$

$$+ V_j V_{se}(g_{ij}cos(\delta j - \delta se) - b_{ij}sin(\delta j - \delta se)) \quad (3.49)$$

$$PE_{sh} = (V_{sh})^2 g_s - V_i V_{sh}(g_s cos(\delta i - \delta sh) - b_s sin(\delta i - \delta sh)) \quad (3.50)$$

$$\Delta P_{\Sigma} = PE_{sh} - PE_{se} \quad (3.51)$$

3.4.2 5 Bus System

The Modified NR power flow model was simulated on a 5 bus system as shown in Fig.**??**. THe UPFC is installed between bus 4 and bus 5.

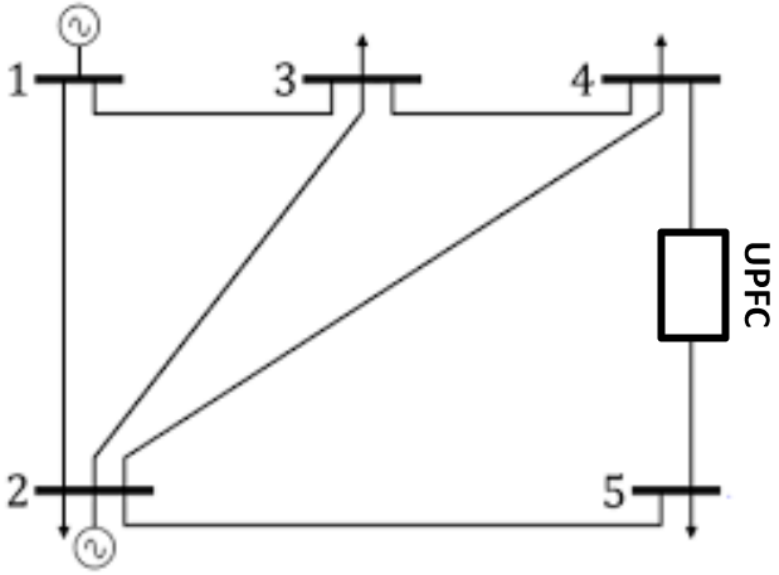

Figure 3.61: 5 Bus system with 1 UPFc

The reference values are shown in Table.3.50. The UPFC State Variables are shown in Table.3.51. The power flow solution is shown in Table.3.52.

Table 3.50: Specified Parameters for the UPFC 5 Bus System

Specified Parameters for the UPFC	
P_{ref}	-18 MW
Q_{ref}	-1.5 MVAR
V_{spec}	0.9954 V

Table 3.51: UPFC State Variables for the UPFC 5 Bus System

UPFC Parameters	
V_{se}	0.0545 V
δ_{se}	71.6238 deg
V_{sh}	1.0139 V
δ_{sh}	-2.5314 deg

Table 3.52: 5 Bus System Volts and Angles

Bus No	Voltage	Angle(Degrees)
1.	1	0
2.	0.99	-2.2185
3.	0.9919	-2.1059
4.	0.9954	-2.5422
5.	0.9823	-4.9702

3.4.3 30 Bus System

The modifed NR power flow is also simulated on a 30 Bus system. 2 UPFCs are installed on the 30 Bus system. Thus 8 new state variables are added in the modified jacobian. The specified parameters for the two UPFCs are shown in Table.3.53. The UPFC state variables are shown in Table.3.54.

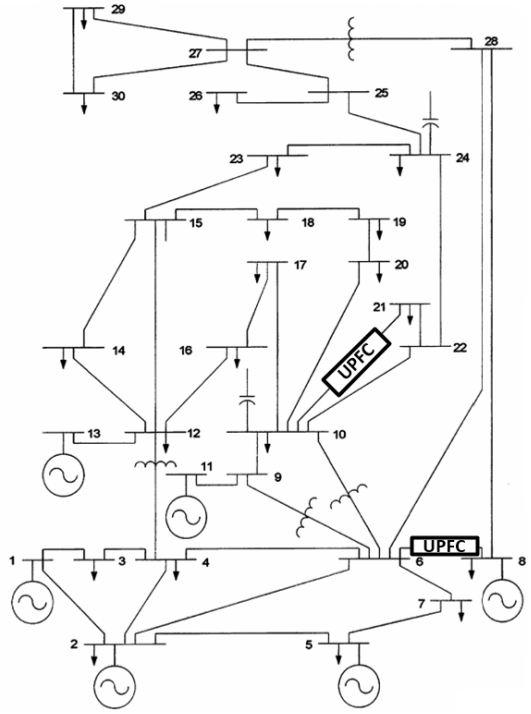

Figure 3.62: 30 Bus system with 2 UPFc

Table 3.53: Specified Parameters for the UPFC 30 Bus System

Specified Parameters for UPFC 6-8	
P_{ref}	30.08 MW
Q_{ref}	12 MVAR
V_{spec}	1.0121 V
Specified Parameters for UPFC 10-21	
P_{ref}	18.66 MW
Q_{ref}	3.27 MVAR
V_{spec}	1.0438 V

Table 3.54: UPFC State Variables for the 30 Bus System

UPFC Parameters for UPFC 6-8	
V_{se}	0.0019 V
δ_{se}	-102.52 deg
V_{sh}	1.0126 V
δ_{sh}	-11.09 deg
UPFC Parameters for UPFC 10-21	
V_{se}	0.0016 V
δ_{se}	-159.4 deg
V_{sh}	1.0440 V
δ_{sh}	-15.73 deg

3.5 Summary

In this chapter, the different models of FACTs devices were simulated in a Newton Raphson power flow. The Newton Raphson power flow has to be modified to take into account the control references of the FACTs devices. Additional state variables are introduced for the magnitude and angle of the voltage sources used to model either a series or a shunt voltage source. This Newton Raphson power flow is easy to use as it utilizes the NRPF formulation which already exists. Furthermore, it can be used in OPF formulations where FACTs devices are modelled as bus injections. The solution of the OPF can be divided into two steps where the first step involves calculating the external variables of the power system. The second step involves calculating the internal variables of the FACTs devices using the models as explained in this chapter. An application of this is shown in the next chapter.

CHAPTER 4: OPTIMAL POWER FLOW METHODOLOGY WITH UPFC INTEGRATED POWER GRID FOR LINE LOADING OPTIMIZATION

4.1 Introduction

The OPF Problem is frequently used by power sytem operators to find an optimal solution to a certain objective function. The LPOPF is more effective and robust to use among different OPFs as it uses a linearised version of the ACPF equations in its formulation. With respect to the application of FACTs devices, the LPOPF is an effective choice. The LPOPF can be used to determine the operating settings of FACTs devices with respect to a given objective function. In most cases, the FACTs devices are either used to reduce congestion or solve bottlenecks. These can be included in terms of line inequality constraints.

4.1.1 Main Contributions

In this chapter, a LPOPF based formulation incorporating FACTS devices specifically UPFC has been described. The objective of the OPF model is to reduce the stress on the power system by reducing the line loading ratio on heavily loaded lines. This can be done by rerrouting power flow from heavily loaded lines to lightly loaded lines as much as possible. Since the main objective of the LPOPF is to reduce line loading ratio of high loaded lines, the target of the OPF is to obtain as high a reduction as possible with more accuracy and more speed. The following modifications and features of the LPOPF help to achieve the above:

- The LPOPF model is able to obtain maximum reduction in line loading ratio by improving accuracy in each LPOPF iteration. This is made sure by making the solution of each iteration accurate so that the iterations can be continued on for

as much as possible.The LPOPF model incorporating UPFC devices with the objective function of reducing line loading improves accuracy by adjusting the control variables in small steps according to the accuracy of the linearisation of the equations included in the LPOPF. The accuarcy of the linearisation is judged using a gradient method. Some iterations may more more accurate as compared to others. If the accuracy of the linearisation is higher in one iteration, a higher change in control variables can be allowed while if linearisation is less accurate, a smaller change in control variables should be allowed.

- The LPOPF model uses the Bus injection model of UPFC in the ACPF equations. The bus injection model of UPFC models the UPFC as a PV and PQ Bus. The PV and PQ buses are already part of a normal power system so the existing LPOPF models do not need to be modified much. The PV and PQ bus then can model the real and reactive injections of the UPFC. This makes it easy to model the UPFC in the LPOPF model. The incorporation of the Bus injection model of the UPFC makes the LPOPF robust. As compared to the Bus injection model, if the equivalent circuit model of UPFC is included in terms of the Series and Shunt Voltage Sources, there will be two more line equations and four more state variables.

- After each LPOPF iteration, if the solution of the LPOPF is not feasible, the sensitivities are still updated at the infeasible operating point. The infeasible operating point is passed on to the next LPOPF iteration. The solution of the next iteration may or moay not be feasible. In both cases, this gives a larger solution space for the LPOPF. This will allow the LPOPF to run more iterations and hence possibly obtain a larger reduction in line loading in some cases. Do remember that it is important to arrive at a solution that is feasible when it converges however the intermediate LPOPF iteration solutions can be

infeasible.

4.2 Problem Formulation

4.2.1 UPFC Bus Injection Model

The UPFC Circuit diagram is shown in Fig.4.1.

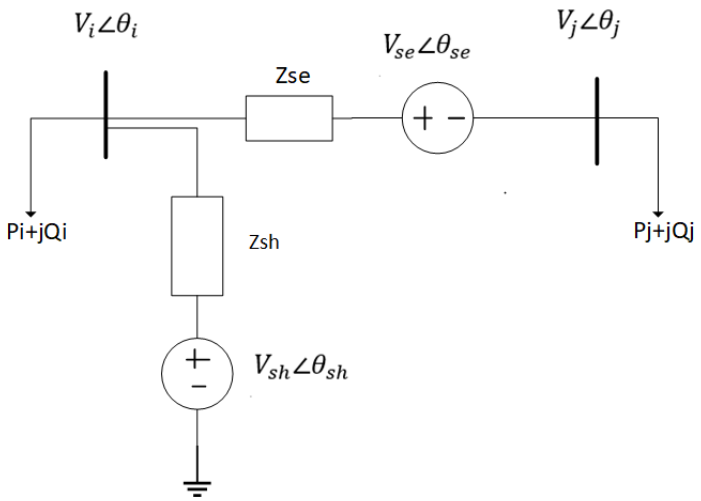

Figure 4.1: Circuit Diagram of UPFC

Equations 3.1-3.14 model the UPFC circuit digram effectively.

$$P_{se} = V_{se}[V_j sin(\delta se - \delta j) - V_i sin(\delta se - \delta i)]/X_{se} \tag{4.1}$$

$$Q_{se} = V_{se}[V_i cos(\delta se - \delta i) - V_j cos(\delta se - \delta i) - V_{se}]/X_{se} \tag{4.2}$$

$$Q_{se} = V_{se}[V_i cos(\delta se - \delta i) - V_j cos(\delta se - \delta i) - V_{se}]/X_{se} \tag{4.3}$$

$$MVA_{se} = \sqrt{P_{se}^2 + Q_{se}^2} \tag{4.4}$$

$$P_{sh} = V_{sh}[V_i sin(\delta_{sh} - \delta_i)]/X_{sh} \tag{4.5}$$

$$Q_{sh} = V_{sh}[V_i cos(\delta_{sh} - \delta_i) - V_{sh}]/X_{sh} \tag{4.6}$$

$$MVA_{sh} = \sqrt{P_{sh}^2 + Q_{sh}^2} \tag{4.7}$$

$$P_{sh} + P_{se} = 0 \tag{4.8}$$

$$P_j = V_j[V_{se}sin(\delta_j - \delta_{se}) - V_i sin(\delta_j - \delta_i)]/X_{se} \tag{4.9}$$

$$Q_j = V_j[V_i cos(\delta_j - \delta_i) - V_{se}cos(\delta_j - \delta_{se}) - V_j]/X_{se} \tag{4.10}$$

$$P_i - P_j = 0 \tag{4.11}$$

$$Q_i = Q_{ij} + Q_{ish} \tag{4.12}$$

$$Q_{ij} = V_i[V_i + V_j cos(\delta_i - \delta_j) - V_{se}cos(\delta_i - \delta_{se})]/X_{se} \tag{4.13}$$

$$Q_{ish} = V_i[V_i - V_{sh}cos(\delta_i - \delta_{sh})]/X_{sh} \tag{4.14}$$

The UPFC Bus injection Model is shown in Fig.4.2 and Fig.4.3. It consists of a PV bus and a PQ bus. The PV Bus is located at the bus where the shunt voltage source is located.

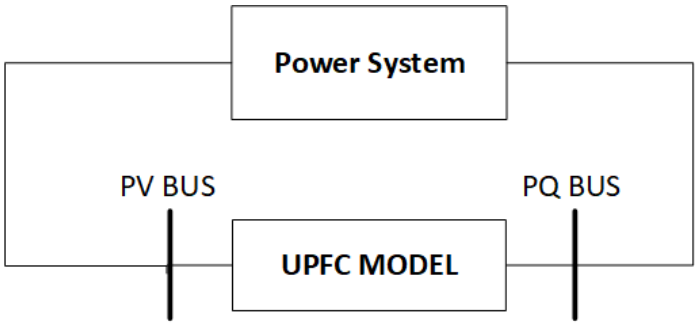

Figure 4.2: Connection of UPFC with the Power SYstem

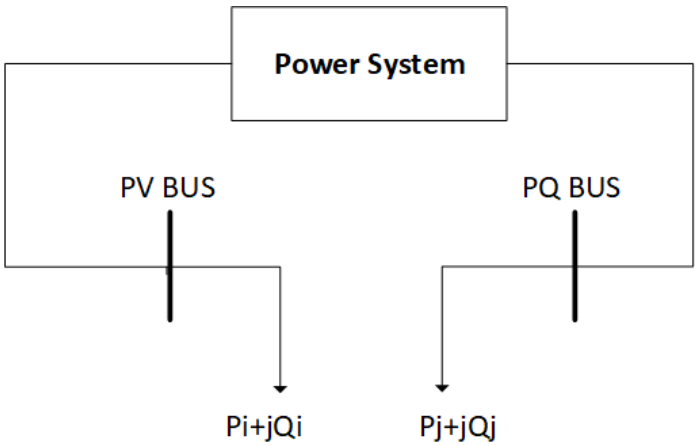

Figure 4.3: UPFC model in Power FLow Calculation

The UPFC parameter equations linking the external UPFC and internal UPFC parameters can be represented by a vector as shown in Eq. 4.15, Eq.4.16 and Eq.4.17.

$$F(x_{upfc}, xp) = 0 \tag{4.15}$$

$$x_{upfc} = [V_{sh}, V_{se}, \delta_{sh}, \delta_{se}] \tag{4.16}$$

$$x_p = [V_j, \delta_i, \delta_j, Q_i, V_{desired}, P_{desired}, Q_{desired}] \tag{4.17}$$

The vector F in Eq. 4.15 is a set of equations. These equations are expressed in Eq .4.18-Eq.**??**.

$$Vj[V_{se}sin(\delta_j - \delta_{se}) - V_{desired}sin(\delta_j - \delta_i)]]/Xse - P_{desired} = 0 \tag{4.18}$$

$$Vj[V_{desired}cos(\delta_j - \delta_i) - V_{se}cos(\delta_j - \delta_{se}] - Vj]/X_{se} - Q_{desired} = 0 \tag{4.19}$$

$$Vse[V_j sin(\delta_{se} - \delta_j) - V_{desired}sin(\delta_{se} - \delta_i]/X_{se} - V_{sh}V_{desired}sin(\delta_{sh} - \delta_i]/X_{sh} = 0 \tag{4.20}$$

$$V_{desired}[V_{desired} + V_j cos(\delta_i - \delta_j) - V_{se} cos(\delta_i - \delta_{se})]/X_{se} V_{desired}$$
$$+ V_{desired}[V_{desired} - V_{sh} cos(\delta_i - \delta_{sh})]/X_{sh} - Q_i = 0$$

4.2.2 LPOPF Formulation of LPOPF incorporating UPFC

The state variables in the LPOPF are voltages and angles. The control variables are the real generation, reactive generation and UPFC power injections. The objective function of the LPOPF model is given by Eq.4.21.

$$\text{Min Average Loading ratio} = \frac{1}{nl} \quad \frac{\Sigma MVA}{\Sigma MVA_{max}} \tag{4.21}$$

Let MVA_i denote the apparent power on a given line i,$MVA_{i.max}$ denote the maximum apparent power on a given line i,nl denote the number of lines. The objective function is linearised as given by Eq.4.22.

$$\text{Min} \quad \Delta z = \sum_{i=1}^{n} \frac{(MVA \times \Delta x)}{MVA_{max}} \tag{4.22}$$

x denote the system state variable vector and $deltax$ is the change in the system state variable vector. This vector will contain the change in each system state variable,such as the change in each angle and each voltage of the power system state. Since the apparent power on a line can be calculated both from the receiving end or the sending end of the line, Eq.4.22 is modified to define the apparent power on a line as the average of both the sending and recieving end of the line. The new equation is given by EQ.4.23.

$$\text{Min} \quad \Delta z = \sum_{k=1}^{n} \frac{((MVA_{ij} + MVA_{ji}) \times \Delta x)}{(2nl) \times MVA_{max}} \tag{4.23}$$

In the study, only the lines whose loadings are greater than 0.5 are included in the

objective function. The reason for this is that under stressful power system state, it is important to reduce the loading on high loaded lines as those lines are directly affecting system security. It is not important to reduce the averge loading on all lines as sometimes by reducing the average loading on all the lines, it could mean sometimes that the loading on some highly loaded lines may increase. The equality constraints included in the LPOPF are the real power and reactive power balance constraints.

The real power balance constraint is given by EQ.4.24.

$$\frac{dP}{d\delta}\ \Delta\delta + \frac{dP}{dV}\,\Delta V + \frac{dP}{dPg} \times -\Delta Pg + \frac{dP}{dQg} \times -\Delta Qg = 0 \tag{4.24}$$

The reactive power balance constraint is given by EQ.4.25.

$$\frac{dQ}{d\delta}\ \Delta\delta + \frac{dQ}{dV}\,\Delta V + \frac{dQ}{dPg} \times -\Delta Pg + \frac{dQ}{dQg} \times -\Delta Qg = 0 \tag{4.25}$$

The real power balance constraint on the UPFC PV and UPFC PQ Bus are discussed next. The Real Power Balance on the UPFC PQ Bus is given by Eq.4.26.

$$\frac{dP}{d\delta}\ \Delta\delta + \frac{dP}{dV}\,\Delta V + \frac{dP}{dPg} \times -\Delta Pg = 0 \tag{4.26}$$

The Real Power Balance on the UPFC PV Bus is given by Eq.4.27.

$$\frac{dP}{d\delta}\ \Delta\delta + \frac{dP}{dV}\,\Delta V + \frac{dP}{dVdes}\,\Delta Vdes + \frac{dP}{dPg} \times -\Delta Pg = 0 \tag{4.27}$$

The Reactive Power Balance on the UPFC PQ Bus is given by Eq.4.28.

$$\frac{dQ}{d\delta}\ \Delta\delta + \frac{dQ}{dV}\,\Delta V + \frac{dQ}{dQg} \times -\Delta Qg = 0 \tag{4.28}$$

The Reactive Power Balance on the UPFC PV Bus is given by Eq.4.29.

$$\frac{dQ}{d\delta}\ \Delta\delta + \frac{dQ}{dV}\,\Delta V + \frac{dQ}{dVdes}\,\Delta Vdes + \frac{dQ}{dPg} \times -\Delta Qg = 0 \tag{4.29}$$

The difference between the UPFC PQ and PV bus is that the injection on the PQ bus is treated like negative generation and the bus injection on the PV bus is treated like positive generation. The negative generation on the PQ bus is in fact mimicing a load but in the LPOPF it is more easier to model the load as negative generation because the OPF modelling already includes generation variables. The Vdes variable in the equations above is the voltage at the PV bus of the UPFC model. Since the UPFC does not consume nor produce any real power,Eq.4.30 and Eq.4.31 is included in the OPF.

$$\text{Power injection at PQ bus} = \text{Power injection at PV bus} \tag{4.30}$$

$$Pi = Pj \tag{4.31}$$

Eq.4.31 needs to be linearised to be included in the LPOPF. The linearised equation is given by Eq.4.32.

$$\Delta Pi = \Delta Pj \tag{4.32}$$

If the change in the real injections at both PQ and PV bus are equal and the real injection at the start of OPF is the same then the real injection after the LPOPF converges will also be same.

The inequality constraints included are the line flow constraints and the UPFC rating constraints. The inequality constraints of the UPFC include the series and shunt MVA ratings of the converters, maximum voltage of the series and shunt converters. Since the UPFC is modelled as a PQ and a PV bus and its internal parameters which are the voltage and angles of the series and shunt converters are not included directly

in the OPF model and furthermore,the inequalities of the UPFC's internal parameters need to be included in the LPOPF model, a linearised mathematical relation needs to be made between the UPFC's ratings and the UPFC's external parameters. Keep in mind that the a nonlinear mathematical relation already exists between the UPFC's ratins and the UPFC's external parameters but a linearised mathematical relation needs to be derived since the model is Linearised OPF. This linear relation is necessary for the UPFC inequality constraints to be formulated. The inequality constraints of the UPFC which represent the UPFC ratings are given by Eq.4.33-Eq.4.37.

$$Psh_{min} \leq Psh(x) + \frac{\partial Psh}{\partial x} \ \Delta x \leq Psh_{max} \tag{4.33}$$

$$MVash_{min} \leq MVAsh(x) + \frac{\partial MVAsh}{\partial x} \ \Delta x \leq MVAsh_{max} \tag{4.34}$$

$$MVAse_{min} \leq MVAse(x) + \frac{\partial MVAse}{\partial x} \ \Delta x \leq MVAse_{max} \tag{4.35}$$

$$Vsh_{min} \leq Vsh(x) + \frac{\partial Vsh}{\partial x} \ \Delta x \leq Vsh_{max} \tag{4.36}$$

$$Vse_{min} \leq Vse(x) + \frac{\partial Vse}{\partial x} \ \Delta x \leq Vse_{max} \tag{4.37}$$

In order to calculate the derivatives of the UPFC Internal Parameters with respect to the state variables of the power system, the partial derivatives of the vector set of equations F in Eq.4.15 needs to be taken using the chain rule. This is shown in Eq.4.38 and Eq.4.39.

$$\Big[\frac{\partial F}{\partial x_{upfc}} \ \ \frac{\partial x_{upfc}}{\partial x_p}\Big] + \frac{\partial F}{\partial x_p} \ = 0 \tag{4.38}$$

$$-\Big[\frac{\partial F}{\partial x_{upfc}}\Big]^{-1} \frac{\partial F}{\partial x_p} \ = \frac{\partial x_{upfc}}{\partial x_p} \tag{4.39}$$

From Eq.4.39, Eq.4.40 and Eq.4.41 can be obtained. These represent the partial derivatives of Vse and Vsh with respect to the state variables of the power system.

$$\frac{\partial x_{upfc}}{\partial x_p} = \frac{\partial V_{se}}{\partial x_p} \tag{4.40}$$

$$\frac{\partial x_{upfc}}{\partial x_p} = \frac{\partial V_{sh}}{\partial x_p} \tag{4.41}$$

The partial derivatives of UPFC Shunt real Power(Psh), Shunt MVA Rating (MVAsh) and Series MVA Rating(MVAse) with respect to the state variables need to be calculated. The vector H is given in Eq.4.42 and Eq.4.43.

$$H = \begin{bmatrix} P_{sh} \\ MVA_{sh} \\ MVA_{se} \end{bmatrix} \tag{4.42}$$

$$H = \begin{bmatrix} V_{sh}[V_i sin(\delta_{sh} - \delta_i)]/X_{sh} \\ \sqrt{P_{sh}^2 + Q_{sh}^2} \\ \sqrt{P_{se}^2 + Q_{se}^2} \end{bmatrix} \tag{4.43}$$

Using the chain rule applied on vector H, the partial derivatives of UPFC Shunt real Power Psh, Shunt MVA Rating MVAsh and Series MVA Rating MVAse with respect to the state variables are calculated given by Eq.4.44 and Eq.4.45.

$$\frac{\partial H}{\partial x_p} = \left[\frac{\partial H}{\partial x_{upfc}} \quad \frac{\partial x_{upfc}}{\partial x_p} \right] + \frac{\partial H}{\partial x_p} \tag{4.44}$$

$$\frac{\partial upfc_{var}}{\partial x_p} = \left[\frac{\partial P_{sh}}{\partial x_p} , \frac{\partial MVA_{sh}}{\partial x_p} , \frac{\partial MVA_{se}}{\partial x_p}, \frac{\partial V_{se}}{\partial x_p} , \frac{\partial V_{sh}}{\partial x_p} \right] \tag{4.45}$$

4.2.3 Flow Chart of LPOPF algorithm

The flow chart of LPOPF algorithm is shown in the Fig.4.4. The algorithm is started with an initial UPFC operating Point. The algorithm contains a while loop

which stops itearting when the convergence criterion is reached. The convergence is reached when the reduciton in line loading ratio is less than the Tolerance and the operating point is feasible. The objective function is described in Eq.**??**. After the while loop, the sensitivities and the partial derivatives are calculated. These include the sensitivities given in Eq.4.45.The LPOPF is solved in Matlab using LINPROG. The state variables are updated. The control variables in his algorithm are the UPFC bus injections at the PV and PQ bus, Real and Reactive Generation and the Generation Bus Voltages. These are entered as an input to the ACPF data. The ACPF is run with the updated control variables. The ACPF solution is obtained. The LPOPF solution and ACPF solution will not be exactly the same as the LPOPF is a linearised version of the ACPF equations so there will be some error between the two solutions. The solution passed on to the next iteration is the ACPF solution. At this point, the new objective function cost is calculated given by Eq.4.46.

Then, Sigma is calculated which represents the accuracy of the LPOPF solution given by Eq.**??**.

$$\text{Sigma } = \frac{(\text{objective startpoint} - \text{ objective newpoint}}{\text{objective startpoint} - \text{objective linear proj}} \tag{4.46}$$

The value of delta which is the maximum change allowed in variables is updated based on Sigma. At this point, the following three checks are made:

- if the new operating point is feasible e.g. most common violation is that the line flow is exceeding line flow maximum MVA
- if sigma is greater than zero which means that the LPOPF is accurate
- if (objective startpoint - objective linear proj) is reducing which means that the LPOPF estimates the gradient of objective function in the right direction

If all of these are true, then the new operating point cost reduction is stored. However, if any of these are not true, the new cost reduction is not acceptable. Still, in

both cases, the solution is passed on to the next LPOPF iteration as discussed previously. This give the LPOPF a larger solution space. In cases where the solution the current iteration is infeasible, updating the sensitivities allows the LPOPF to proceed towards a feasible solution in the proceeding iterations. The LPOPF converges when there is no more further reduction in the objective function cost,sigma is greater than zero and the current operating point is feasible. All these three conditions need to be true at the end of the LPOPF iteration if the LPOPF has to reach convergence. The algorithm flow is shown in Algorithm.9.

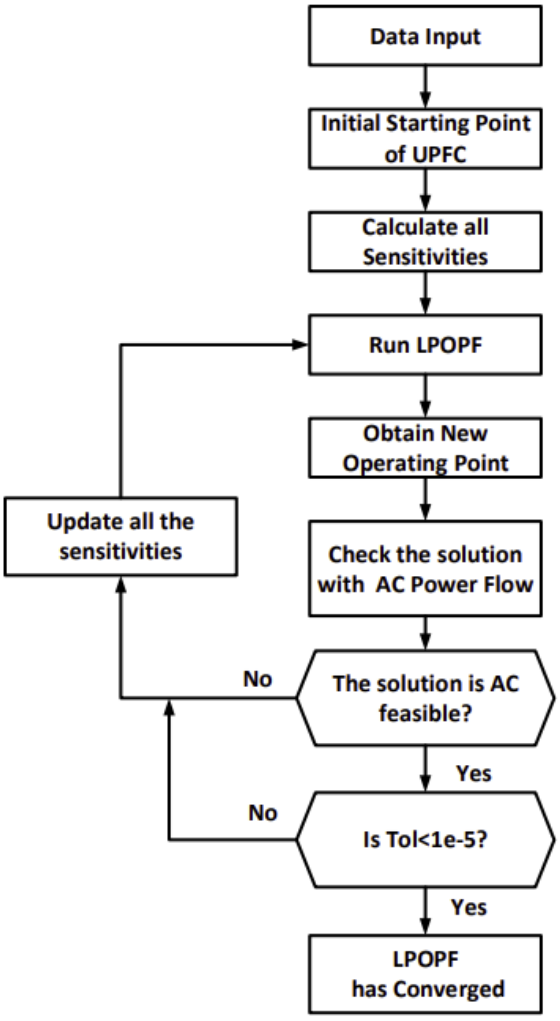

Figure 4.4: Flow Chart of the LPOPF algorithm

Algorithm 6 Proposed LPOPF Algorithm

Initialize network parameters.
Initialize the UPFC Operating Point.
Run ACPF.
Find which lines have Loading Ratio more than 0.5. Calculate the Objective Function Loading Ratio.
while do$(iter) \leq (Maxiterations)$
Calculate the Objective Function Start Point.
Calculate the Sensitivity/partial derivatives.
Set up the LPOPF equations in matrix form.
Solve the LPOPF.
Obtain the New Operating Point. $(P_{des}, Q_{des}, V_{des}, P_{gen}, Q_{gen}, V_{pv})$.
Input the New Operating Point in ACPF. $(P_{des}, Q_{des}, V_{des}, P_{gen}, Q_{gen}, V_{pv})$.
Run ACPF.
The solution of the ACPF is obtained.
Calculate the new $V_{se}, \delta_{se}, V_{sh}, \delta_{sh}$.
Calculate Sigma.

if $Sigma \geq 0.1$ **then**
Increase the maximum change in control Variables.
else if $Sigma \leq 0$ **then**
Reduce the maximum change in Control Variables.
else if $(objectivestartpoint - objectivelinearproj) \leq 0$ **then**
Reduce the maximum change in Control Variables.
end if

if $Sigma \geq 0.1$ and $(objectivestartpoint - objectivelinearproj) \geq 0$ and $(LineLimitsnotexceedinginACPFsolution) \equiv 0$ **then**
The new operating point is feasible and the objective function cost reduction is stored.
else
The new operating point is not feasible. The objective function cost change is not stored.
end if

if $(Tol = (objectivestartpoint - objectivenewpoint)) \leq (1e-5)$ and (Operating Point is feasible) **then**
The LPOPF has Converged.
else
Continue with the next iteration.
end if
end while

4.2.3.1 Parameters of the Model

The inputs and outputs of the algorithm are listed below: The inputs are:

- Initial Operating Point of UPFC(Pref,Qref,Vref)
- Real and Reactive Generation Setpoints(Pgen,Qgen)
- Voltage and Angle of Buses
- Power System Line Parameters(R,X)
- Line Flow Limits(MVAmax)
- UPFC Max Ratings(MVAsh,Psh,MVAse)
- Loading Ratio before OPF
- List of High Loaded Lines

The outputs are:

- Optimal Operating Point of UPFC(Pref,Qref,Vref)
- Real and Reactive Generation Setpoints
- Optimal Line Flows
- Loading Ratio after OPF

4.2.4 Comparison with the Previous Models

A comparison is provided in the flow charts between previous model published by Dr.Vijay and the proposed formulation in Fig.4.5. The differences are summarised in Table.4.1.

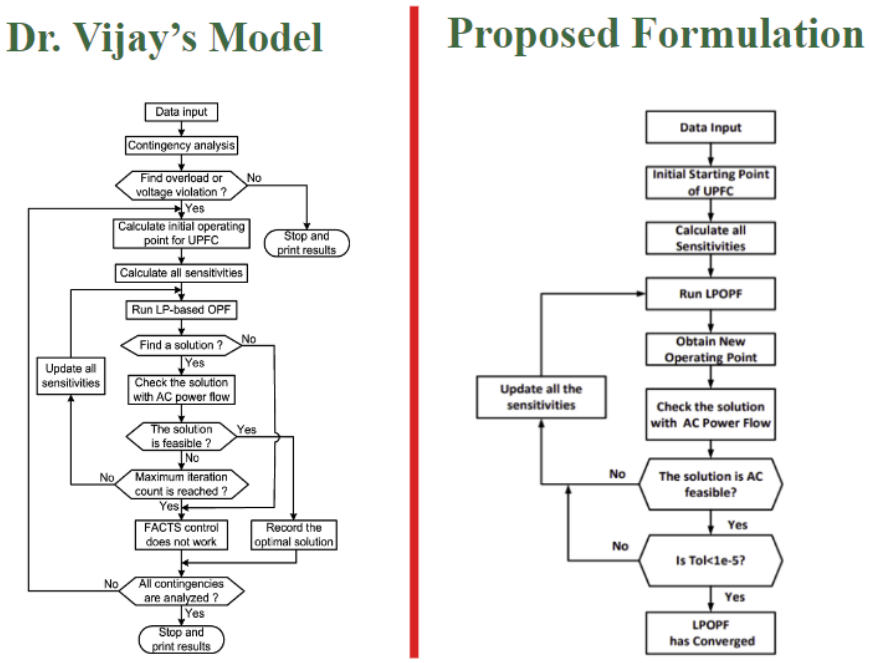

Figure 4.5: A side by side comparison of the Proposed Model with Dr.Vijay's Model

Table 4.1: Summary of Comparison between Proposed Model and New Model

Proposed Model	**Dr.Vijay's Model**
The main objective of the proposed algorithm is to maximize reduction in line loading of heavily loaded lines. Convergence is achieved when the change in loading ratio is less than 1e-5.	Previous model converged when the overload/voltage violation was corrected.

Continuation of Table 6.1	
The proposed formulation has to maintain accuracy in its solutions as it runs for more iterations compared with Dr. Vijayâs model.Solutions of the proposed OPF need to be accurate in order for the LPOPF to transfer solutions across iterations.	Dr. Vijayâs model runs for maximum 2 iterations since the LPOPF converges when the overload/voltage violation is corrected.
The proposed algorithm allows real and reactive generation to vary in one thesis chapter. The proposed algorithm needs to maintain its accuracy if the generation has to be allowed to change.	Dr. Vijayâs model does not allow any change in real and reactive generation.

4.2.5 Results

The algorithm was tested on a 39 bus system and a 118 bus system.

4.2.5.1 39 Bus System

The 39 Bus system has 10 generators and 46 lines. Since the objective of the case study was to show that the UPFC is able to reduce the line loading under stressed loading conditionss, thus the line 4-5 is switched out. This increases the loading on highly loaded lines(lines with loading ratio more than 0.5) from 0.6181 to around

0.66.

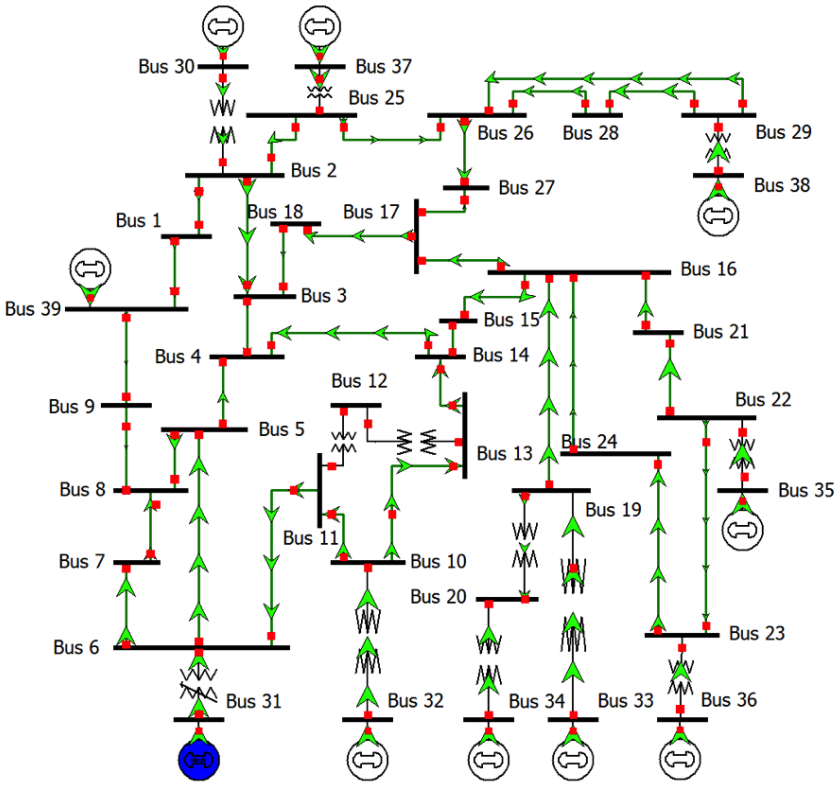

Figure 4.6: 39 Bus System

The UPFC ratings are shown in the table 4.2 below. The ratings are particularly important since they will determine the reduction in loading that is possible. The series voltage source rating (MVASE) determines how effectively the UPFC is able to change the amount of power flowing through the line or under some circumstances, if it is able to change the direction of power flowing through the line. The shunt power rating(MVASH) is relevant to the reactive power support that the UPFC is able to offer in terms of how much reactive power it is able to absorb or supply. By doing so, it is able to change the voltage at the PV bus and hence it can also aid in rerouting power by controlling the voltage. Another important factor to keep in mind for later is that the more higher the rating of the UPFC, the higher the cost. This is not considered for now. The list of branches which have loading more than 50 percent are shown in Table 4.3.

Table 4.2: UPFC Ratings

Parameter	Min	Max
V_{se}	-0.5 V	0.5 V
V_{sh}	0.8 V	1.5 V
MVA_{se}	0 MVA	200 MVA
MVA_{sh}	0 MVA	200 MVA
P_{sh}	-80 MW	80 MW

Table 4.3: List of Highly Loaded Branches 39 Bus System

From Node	To Node
13	14
4	14
15	16
2	3
29	38
28	29
25	37
23	36
23	24
22	35
21	22
2	25
6	7
10	13
10	32
16	19
16	21
19	33
20	34

Case A 1 UPFC

In Case A, a UPFC was installed on line 16-17. The reduction in loading is shown in Table 4.4.

Table 4.4: Change in Loading Ratio Case A

UPFC Location	Line 16-17
Loading Ratio before OPF	0.6645
Loading Ratio after OPF	0.6393
Reduction in Loading Ratio	0.0252

The loading of all lines for Case A before and after OPF is shown Fig. 4.7. As shown in Fig. 4.7, the UPFC is able to reduce the loading ratio in 2 to 3 lines. Some lines have the same loading ratio before and after opf. That is because the UPFC can not effect a change in loading in those lines which are located far away from the UPFC.

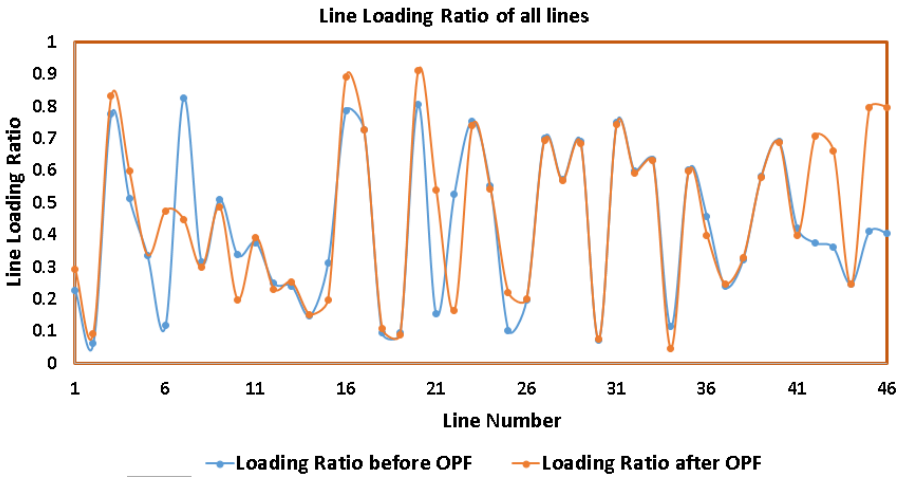

Figure 4.7: Loading Ratio for Lines Case A

The line locations with the highest reduction are shown in Fig.4.8. As seen, the lines are located close to the location of the UPFC.

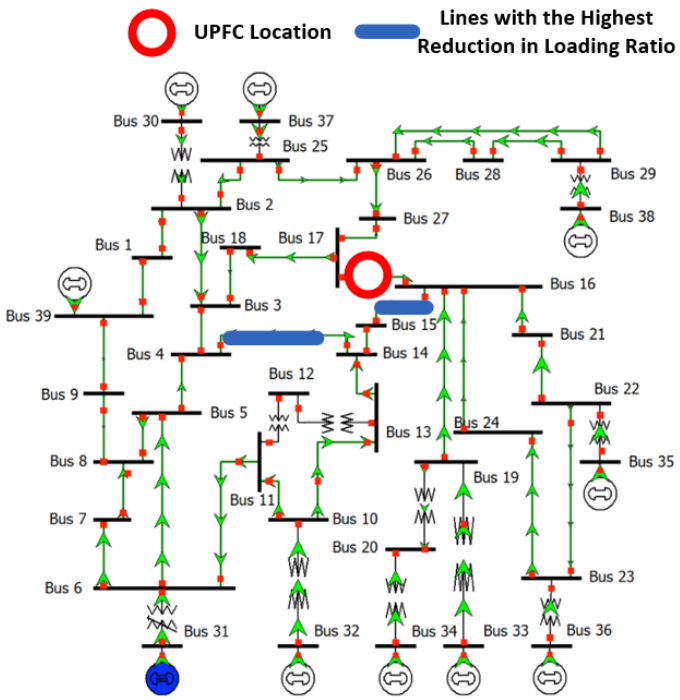

Figure 4.8: Lines with Highest Reduction Case A

The UPFC operating point before and after the OPF is shown in the table 4.5. The main thing to note here is that the UPFC rating for the series voltage ource changes from 10 MVA to 65 MVA respectively. Since the initial start point for the OPF is the normal power flowing through the line 16-17 in the 39 bus system, thus the UPFC series rating is comparatively lower(10 MVA) and the voltage Vse is 0.0439 V. Since the OPF changes the power flowing through the line 16-17 in order to reduce the loading ratio, the UPFC reroutes power flow by injecting a series voltage which is 0.2570 at an inductive angle. Thus the UPFC series power rating increases from 10 MVA to 65 MVA. The shunt rating of the UPFc increases from 21 MVA to 38 MVA as the desired voltage at the PV bus is raised from 0.991 V to 1.0428 V. The shunt source has to provide some reactive support. This indicates that the UPFC is effective at reducing the line loading ratio.

Table 4.5: UPFC operating point in Case A

UPFC Parameter(16-17 Upfc)	Before OPF	After OPF
V_{se}	0.0439	0.2570
δ_{se}	87 deg	61 deg
MVA_{se}	10 MVA	65 MVA
MVA_{sh}	21 MVA	38 MVA
P_{sh}	0.9 MW	27 MW
P_{des}	238 MW	458 MW
Q_{des}	-66 Mvar	-47 Mvar
V_{des}	0.991 V	1.0428 V

Since the case only only studies the effect of UPFC only on the change in loading ratio, thus the real and reactive generation is not allowed to change during each LPOPF iteration. However, it must be noted that the LPOPF is a linear approximation of the actual ACPF equations. Thus, after each iteration when the LPOPF output is entered as an input to the ACPF, there are bound to be differences between the LPOPF output(LPOPF Real and Reactive Generations Setpoints) and ACPF output(ACPF Real and Reactive Generation Setpoints). In other terms, this can also be called the error of the LPOPF which is the difference between the ACPF Real Generation setpoint and LPOPF Real Generation setpoints and the same is the case for Reactive Generation setpoints. This difference between the LPOPF and ACPF output can accumulate over several iterations of the LPOPF till the LPOPF converges. The ideal situation will be that the before OPF Real and Reactive Generation Setpoints should be same as after OPF Real and Reactive Generation Setpoints. However, as discussed before, there will be error. This error is shown in Fig. 4.9 and Fig. 4.10 respectively. The highest error is at bus 31 which is the slack bus. These errors may seem at high first but if seen from a percentage point of view are relatively small.

The percentage error is shown in 4.6. Both errors are less than 3.5 percent which is acceptable from LPOPF point of view.

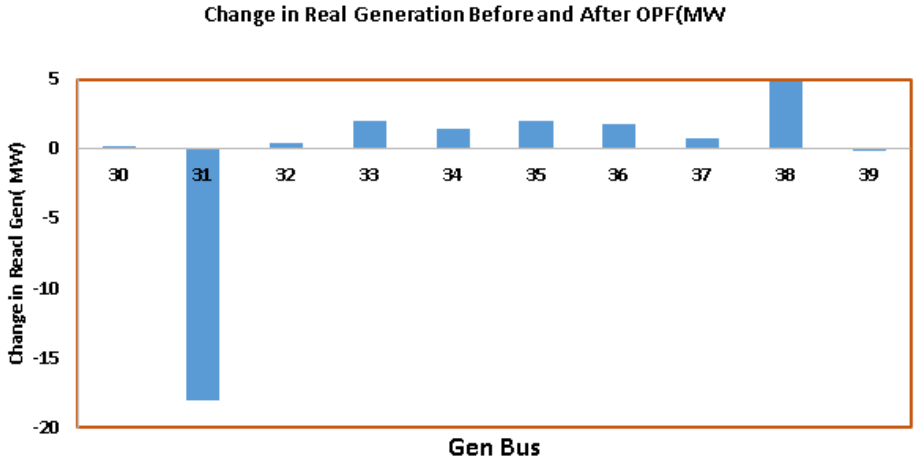

Figure 4.9: Change in Real Generation before and after OPF in MW

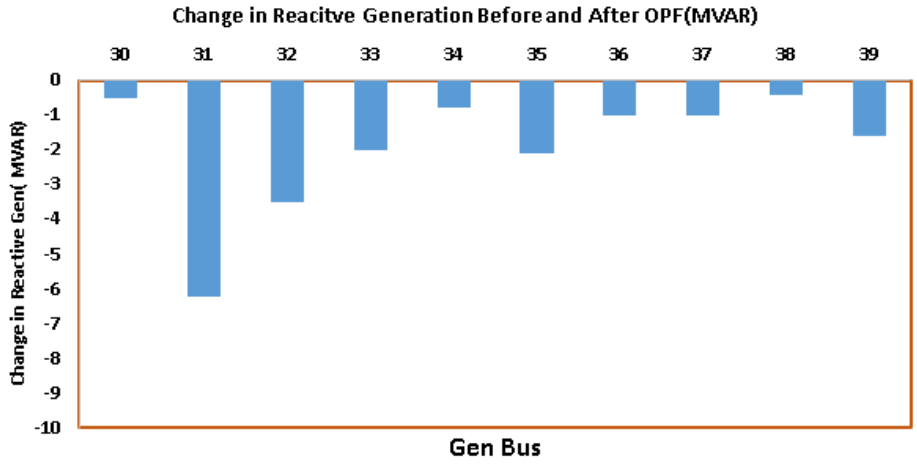

Figure 4.10: Change in Reactive Generation before and after OPF in MVar

Table 4.6: Percentage Change in Pgen and Qgen

Bus 31 Pgen before OPF	683.06 MW
Bus 31 Pgen after OPF	665 MW
Percentage Error in Pgen at Bus 31	2.6 percent
Bus 31 Qgen before OPF	174 MW
Bus 31 Qgen after OPF	168 MW
Percent error in Qgen Bus 31	3.4 percent

Case B 1 UPFC

The UPFC is installed on line 3-4 in Case B. The reduction in loading ratio is shown in Table 4.7. The reduction is significant given the real and reactive generation is not allowed to change.

Table 4.7: Change in Loading Ratio Case B

UPFC Location	Line 3-4
Loading Ratio before OPF	0.6682
Loading Ratio after OPF	0.6341
Reduction in Loading Ratio	0.0341

The reduction in loading ratio is brought about by reducing the loading on certain lines. Do note that the loading ratio can increase in some lines after opf. In this case, as you can see in Fig. 4.11, few lines which have loading ratio less than 50 before the OPF have loading ratio more than 50 after the opf. This is understandable given that power flow will be rerouted from heavily loaded lines to lightly loaded lines.

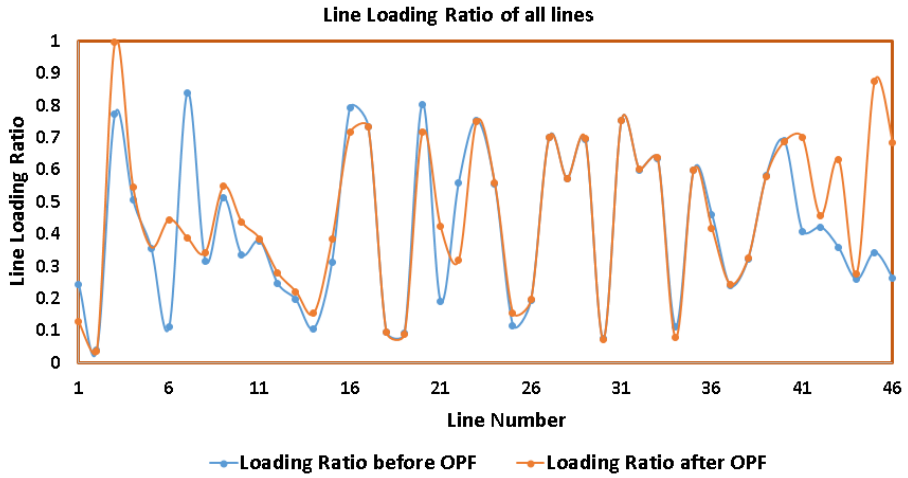

Figure 4.11: Loading Ratio for Lines Case B

The line locations with the highest reduction are shown in Fig.4.12. As seen, the lines are located close to the location of the UPFC.

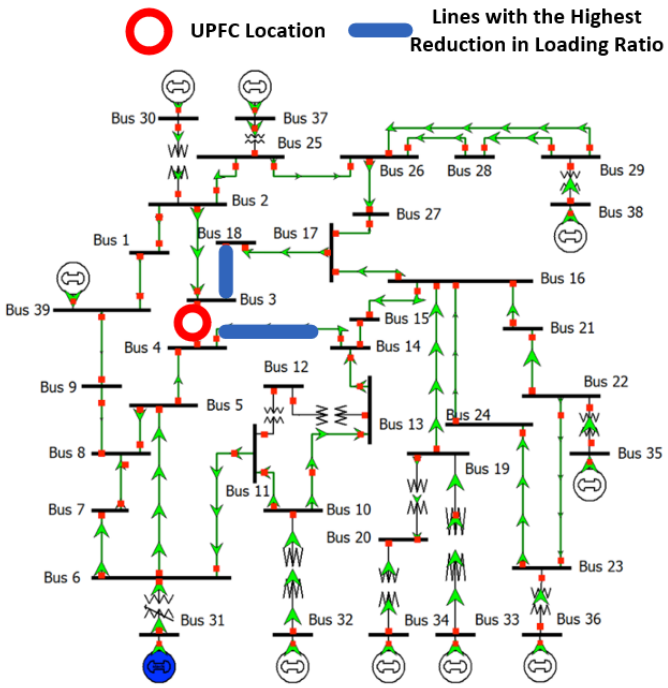

Figure 4.12: Lines with Highest Reduction Case B

The UPFC operating point before and after the OPF is shown in table .4.8. As can be seen, as discussed for Case A, the series voltage source magnitude increases

from 0.0311 V to 0.2926 V. The relatively low series voltage magnitude before OPF is again due to the reason that the power flow in line 3-4 is the same as in the 39 bus system. However, after the OPF, both the series voltage source magnitude and the series power flow rating increases significantly. This shows that the UPFC is essential to reducing the line loading ratio. The shunt voltage source power rating increases from 66 MVA to 113 MVa to support the higher voltage at the PV Bus.

Table 4.8: UPFC operating point in Case B

UPFC Parameter(3-4 Upfc)	Before OPF	After OPF
V_{se}	0.0311	0.2926
δ_{se}	42 deg	57 deg
MVA_{se}	6 MVA	59 MVA
MVA_{sh}	66 MVA	113 MVA
P_{sh}	-2 MW	36 MW
P_{des}	88.00 MW	316 MW
Q_{des}	160 Mvar	295 Mvar
V_{des}	0.952 V	1.036 V

The error in Real and Reactive Generation setpoints for Case B are shown in Fig.4.13 and Fig.4.14. The maximum error is 3.5 percent which is acceptable for the LPOPF. The errors are given in Table.**??**.

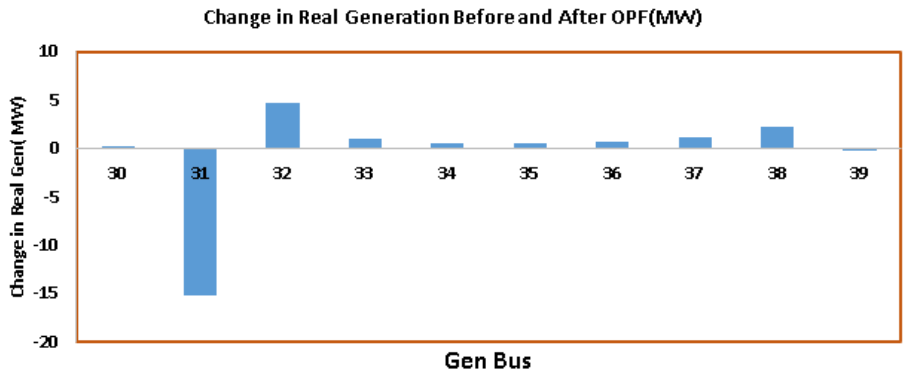

Figure 4.13: Change in Real Generation Case B

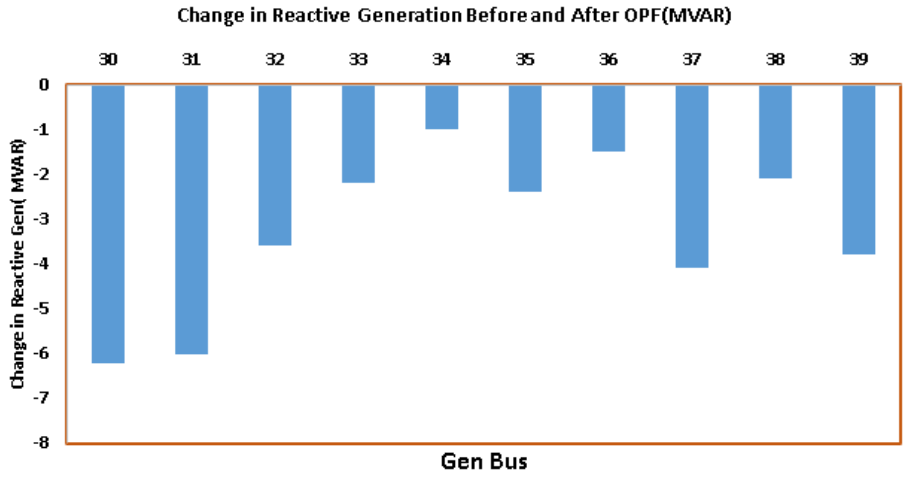

Figure 4.14: Change in Reactive Generation Case B

Table 4.9: Percentage Change in Pgen and Qgen Case B

Bus 31 Pgen before OPF	683.06 MW
Bus 31 Pgen after OPF	668 MW
Percentage Error in Pgen at Bus 31	2.53 percent
Bus 31 Qgen before OPF	174 MVar
Bus 31 Qgen after OPF	167 MVar
Percent error in Qgen Bus 31	3.43 percent

The Fig.4.15, Fig.4.16, Fig.4.18, Fig.4.19,Fig.4.20,Fig.4.21 and Fig.4.22 show the

convergence pattern of the control parameters and the objective function cost.As can be seen the LPOPF takes 26 iterations to converge. As can been from Fig.4.20 and Fig.4.21, the value of Pdesired oscillates around 300 MW and the value of Qdes oscillates around 300 MVAR before they both settle at their final values. This shows that the limiting characterisitics must be related to the maximum real and reactive injection allowed at the UPFC Buses. Since none of the UPFC ratings are near their limits, thus the other factor limiting the UPFC injections are the line flow limits of the lines connecting the UPFC buses to its neighbouring buses. If the loading ratio of the lines are seen after the OPF converges, then it can be seen that from Fig.4.23, that the loading ratio for this line is at 1. Thus this is the limit factor in this case limiting further reduction in Objective function cost. However, the limit factor is case-dependent.

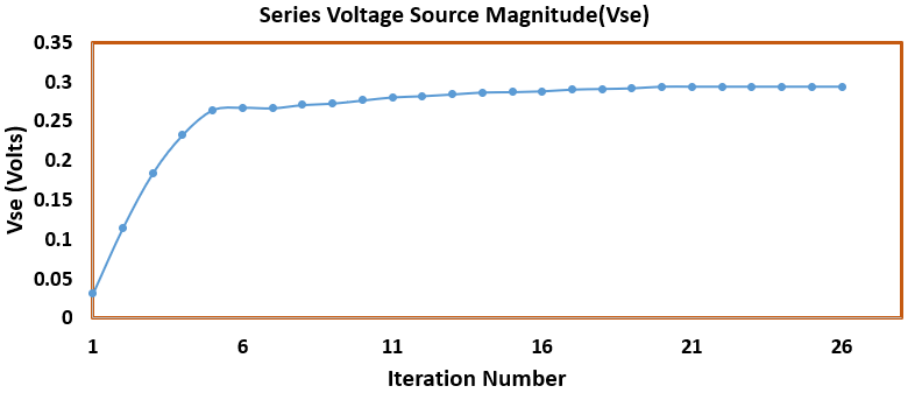

Figure 4.15: Series Voltage Source Magnitude Vse

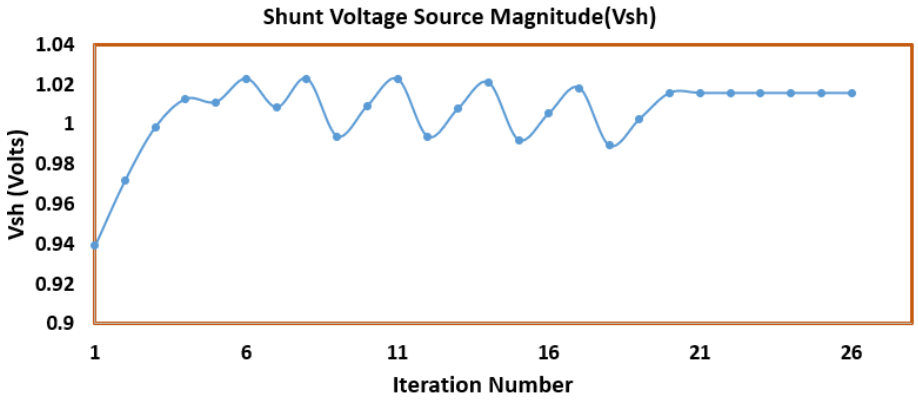

Figure 4.16: Shunt Voltage Source Magnitude Vsh

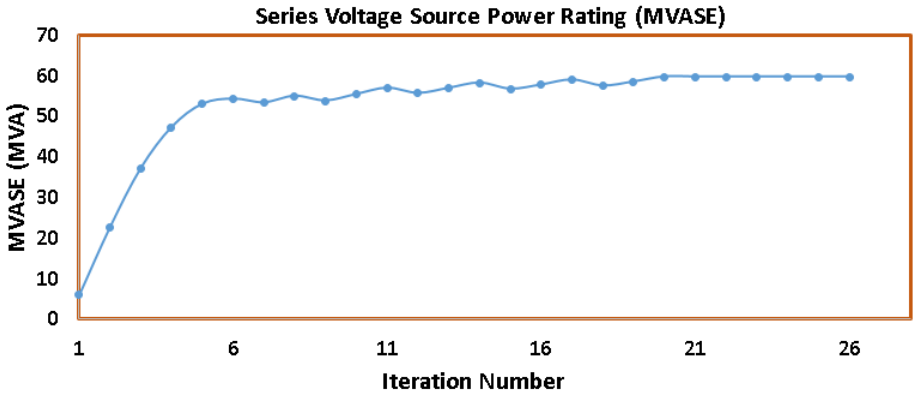

Figure 4.17: UPFC Series Power Ratings

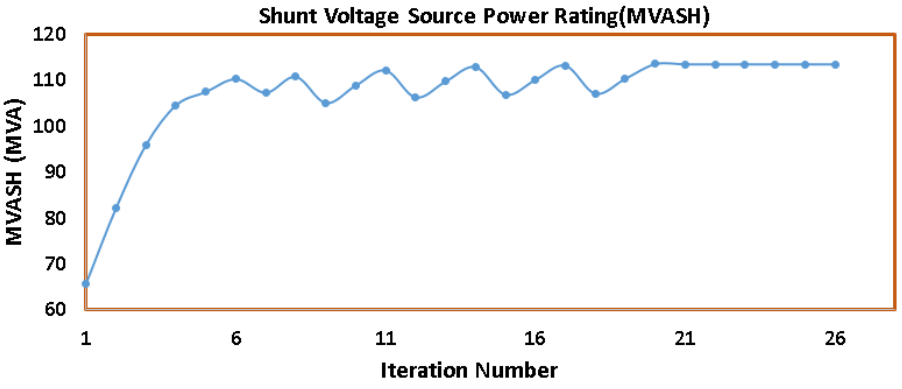

Figure 4.18: UPFC Shunt Power Ratings

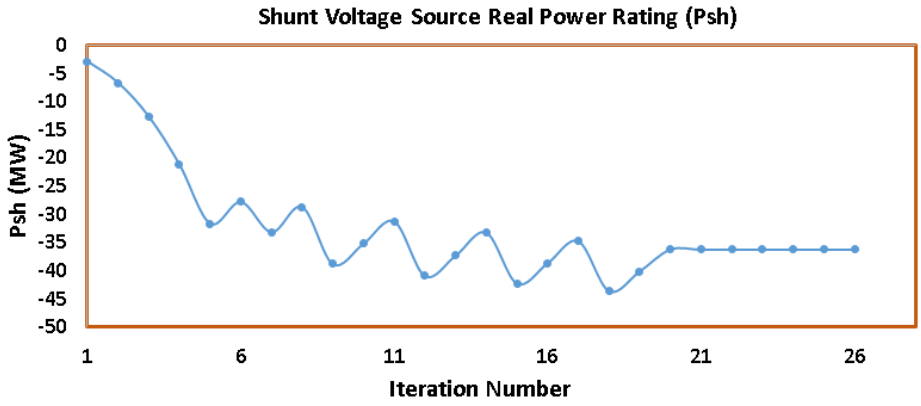

Figure 4.19: UPFC Shunt Real Power Ratings

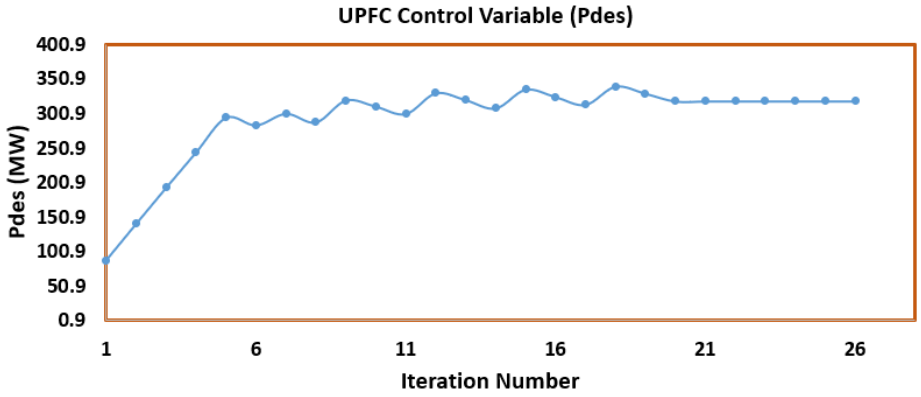

Figure 4.20: UPFC Pdesired

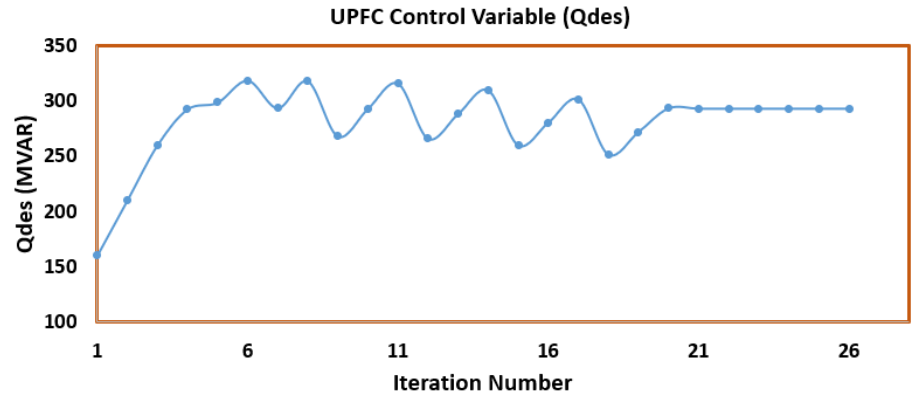

Figure 4.21: UPFC Qdesired

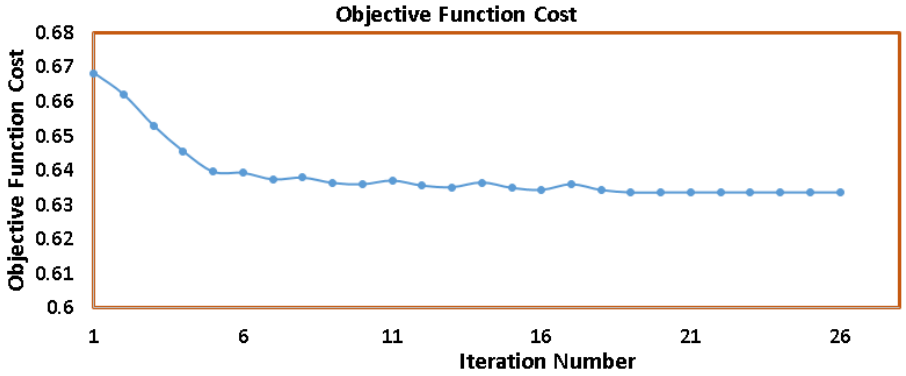

Figure 4.22: Loading Ratio-Objective Function Cost

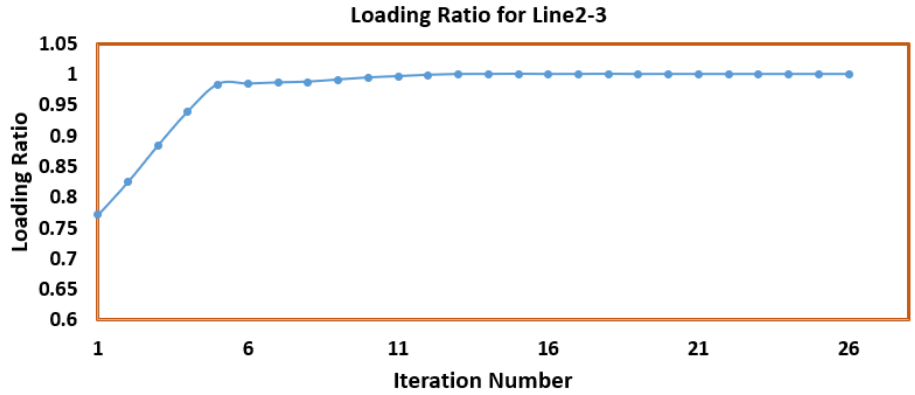

Figure 4.23: Loading Ratio for Line2-3

Case C 1 UPFC(Less Ideal UPFC Location)

In Case C, the UPFC is installed on line 13-14. The reduction in loading in this case is 0.0066 which is shown in Table.4.10. It is comparatively less than Case A and Case B where it was 0.0252 and 0.0341 respectively. This shows that the UPFC location is important. Lines selected in Case A and Case B were 16-17 and 3-4 which were transmission corridors and thus more helpful in rerouting power flow and hence reducing the loading ratio. Other factors which affect the effective UPFC location include topology and other parameters as well.

Table 4.10: Change in Loading Ratio Case C

UPFC Location	13-14
Loading Ratio before OPF	0.6581
Loading Ratio after OPF	0.6515
Reduction in Loading Ratio	0.0066

The UPFC parameters are shown in Table .**??**. The series voltage source power rating increases from 50 MVA to 125 MVA and the series voltage source magnitude changes from 0.0999 to 0.2402. Furthermore, the shunt voltage source power rating increases from 24 MVA to 151 MVA. Thus, the UPFC is utilizing the series and shunt power rating capacity by more than 60 percent. Do keep in mind that the reduction in loading is comparitiviely lower in Case C as compared ot Case A and B. This indicates that the algorithm allowed the UPFC to utilize it's capacity at its maximum to reduce the loading ratio. This again emphasizes the conclusion made previously that the location of the UPFC is not optimal in this case.

Table 4.11: UPFC operating point in Case C

UPFC Parameter(13-14 Upfc)	Before OPF	After OPF
V_{se}	0.0999	0.2402
δ_{se}	42 deg	57 deg
MVA_{se}	50 MVA	125 MVA
MVA_{sh}	24 MVA	151 MVA
P_{sh}	3 MW	-10 MW
P_{des}	481.00 MW	318.48 MW
Q_{des}	-34.0 Mvar	-68.45 Mvar
V_{des}	0.957 V	0.972 V

The change in real and reactive generation for Case C are shown in Fig. 4.24 and

Fig. 4.25. The maximum error in Fig. 4.24 and Fig. 4.25 is 4 MW and 4 MVAR respectively. This shows that the LPOPF is indeed accurate to an acceptable extent for Case C.

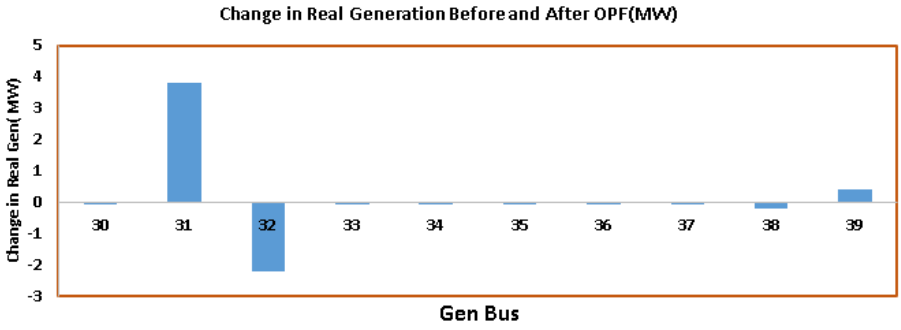

Figure 4.24: Change in Pgen for Case C

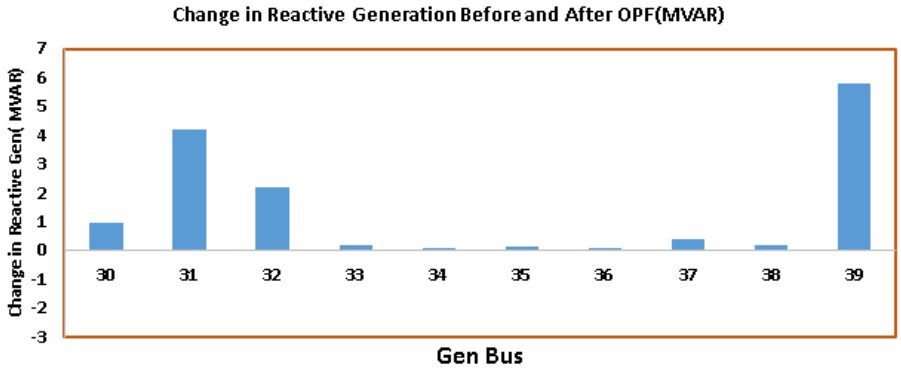

Figure 4.25: Change in Qgen for Case C

4.2.5.2 Comparison with Previous Model

A comparison is made between the previous model and the proposed model shown in Table.4.12. It can seen that the proposed model obtains a reduction in loading ratio which is 2.5 times that of the previous model. Thus, there is an improvement in the results.

Table 4.12: Loading Ratio Comparison of Dr.Vijay's Model and Proposed Model

UPFC Location	16-17
Reduction in Loading Ratio(Dr.Vijay's Model)	0.014
Reduction in Loading Ratio(Proposed Model)	2.5 times 0.014

4.2.5.3 118 Bus System

The LPOPF code was simulated on a 118 Bus system. The 118 Bus system diagram is shown in Fig. 4.26. It is a relativly larger system as compared to the 39 Bus system. It has 186 branches and 54 generators. The generation is evenly spread out across the whole system thus there are no specific generation centers. As a result, there are no specific transmission corridors connecting the generation centers to load centers. The 118 bus system was simulated for four cases. In the first two cases, one UPFC is installed while in the other two cases,two UPFCs were installed. Since the 118 bus system is a large system compared to the 39 Bus System, thus one UPFC only will be less beneficial as compared to two UPFCs to create an effect in line loading for a bunch of lines. One UPFC may be sufficient to overcome the bottleneck on one line but may not help in reducing the line loading ratio on a number of lines. It may also be added that the high loaded lines may not necessarily lie in close vicinity thus one UPFC alone located far away may not be able to effect the line loading on lines located far away from the UPFC.

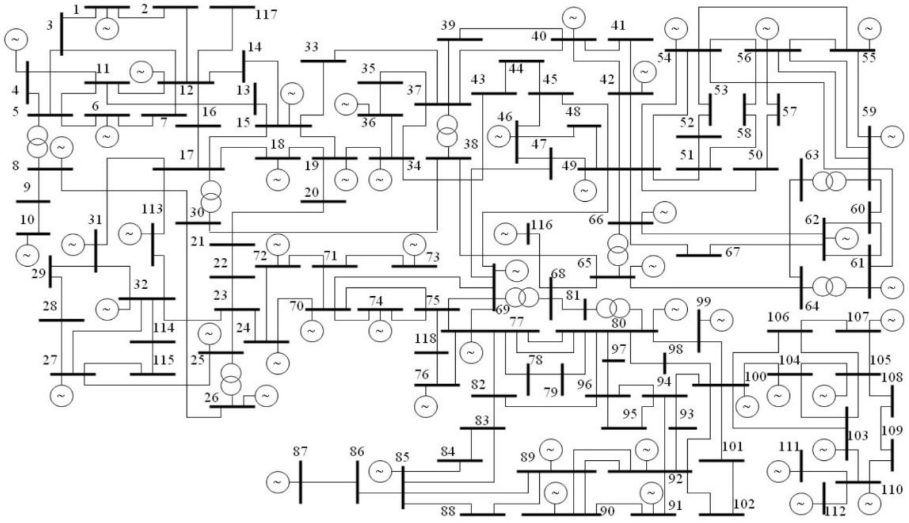

Figure 4.26: 118 Bus System

The UPFC ratings selected were 200 MVA series and shunt ratings. The maximum and minimum series voltage ratings were 0.5V and -0.5V respectively. The maximum and minimum shunt voltage ratings were 1.5V and 0,8V respectively. They are shown in Table.4.13.

Table 4.13: UPFC Ratings in the 118 Bus SYstem

Parameter	Min	Max
V_{se}	-0.5 V	0.5 V
V_{sh}	0.8 V	1.5 V
MVA_{se}	0 MVA	200 MVA
MVA_{sh}	0 MVA	200 MVA
P_{sh}	-80 MW	80 MW

Table 4.14: List of Highly Loaded Branches 118 Bus System

From Node	To Node
3	5
5	6
8	9
8	5
9	10
5	11
17	18
23	25
25	27
30	17
26	26
26	30
23	32
37	39
38	65
64	65
47	69
68	69
69	77
78	77
85	89
89	92
110	112

Case A

In Case A, the UPFC was installed on line 81-80. The reduction in line loading is shown in Table. 4.15. The location of the UPFC installed is shown in Fig.4.27.

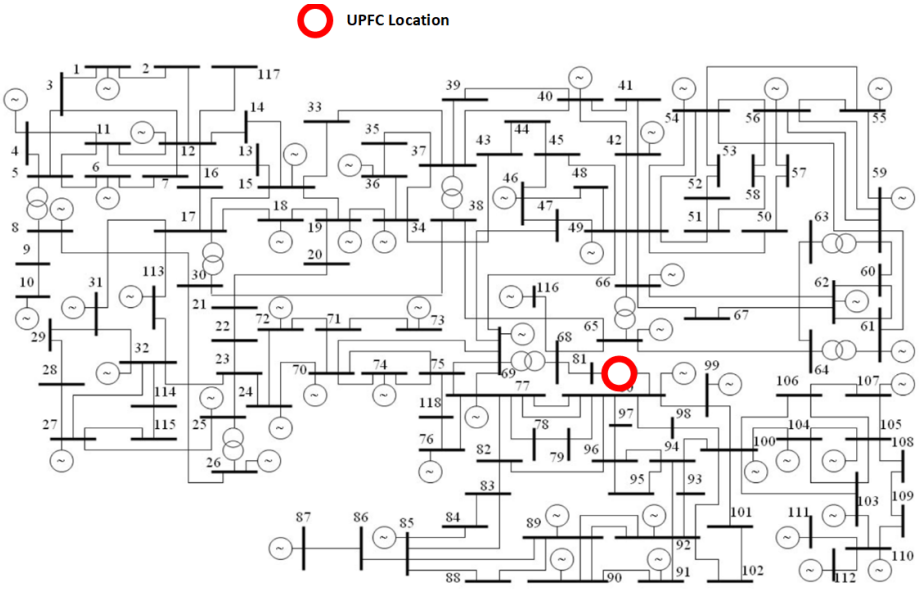

Figure 4.27: Location of UPFC Case A 118 Bus System

Table 4.15: Change in Loading Ratio for Case A-118 Bus System

UPFC Location	81-80
Loading Ratio before OPF	0.6489
Loading Ratio after OPF	0.6305
Reduction in Loading Ratio after OPF	0.0184
Number of LPOPF iterations	4

The loading ratio of all lines in Case A before and after opf is shown in Fig.4.28. As can be seen, a couple of lines have lower loading after opf as compared to before opf power flow solution but majority of lines have around the same loading ratio after LPOPF converges as it was at the start of the OPF.

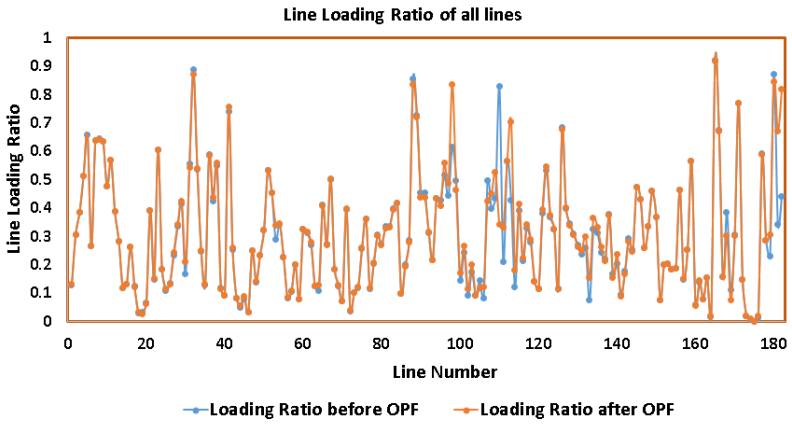

Figure 4.28: Loading Ratio Case A

The lines where the highest reduction in line loading ratio takes place are shown in Fig.4.29. AS can be seen, they are located at close to the UPFC location.

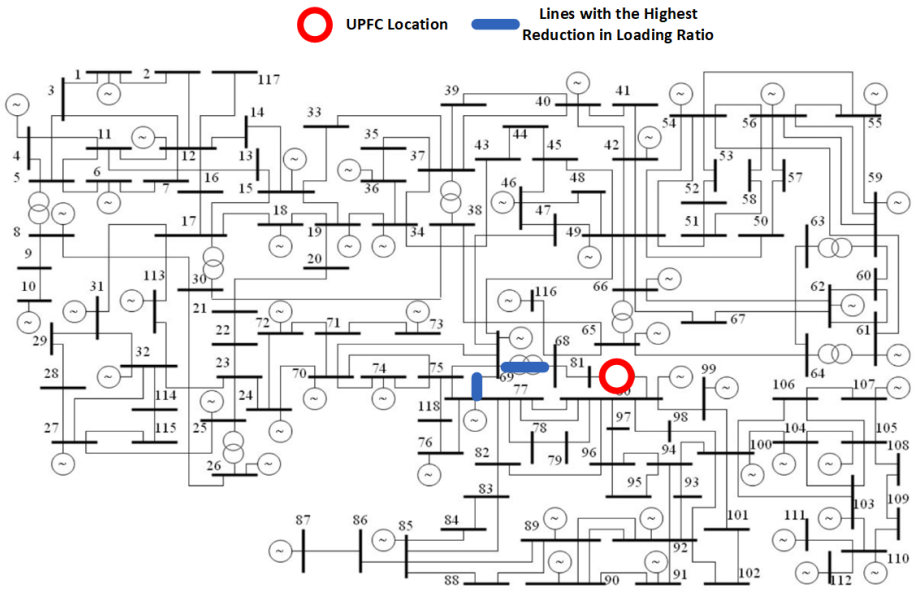

Figure 4.29: Lines with the Highest reduction in line loading Case A

The change in UPFC Parameters is shown in Table.4.16.

Table 4.16: UPFC 81-80 Parameters Case A

UPFC Parameter(81-80 UPFC)	Before OPF	After OPF
V_{se}	0.0288	0.3088
δ_{se}	55.8 deg	-52.42 deg
MVA_{se}	1 MVA	14 MVA
MVA_{sh}	17 MVA	30 MVA
P_{sh}	-0.1 MW	10 MW
P_{des}	34.000 MW	-104.56 MW
Q_{des}	33 Mvar	65.38 Mvar
V_{des}	1.050 V	1.077 V

The Fig. 4.30 and Fig. 4.31 show the change in Real Generation and Reactive Generation setpoints before and after the LPOPF converges.As discussed for the 39 Bus case, this should ideally be zero. However, since LPOPF inherently has an error due to linear modelling of the ACPF equations, there is some change in the Real and Reactive Generation setpoints. The error in Case A is negligible.

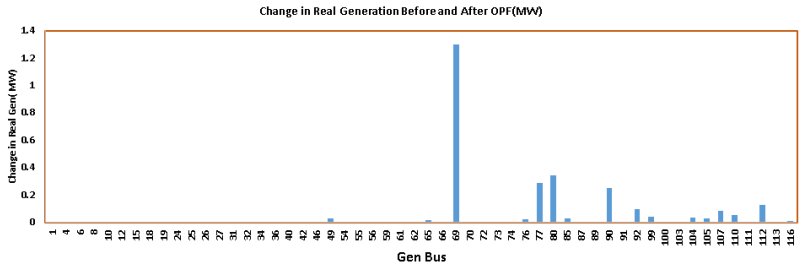

Figure 4.30: Change In Real Generation(MW) Case A

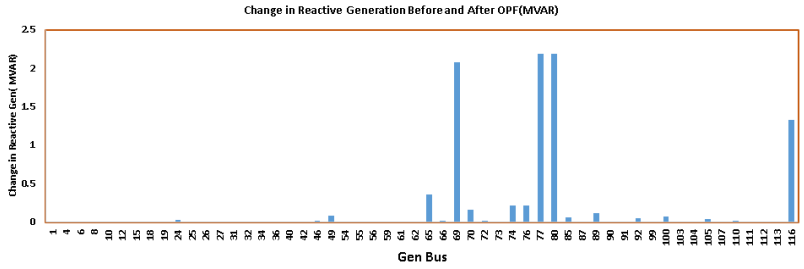

Figure 4.31: Change In Reactive Generation(MVAR) Case A

Case B

In Case B, a UPFC was installed on line 30-17. The location of the UPFC installed is shown in Fig.4.32.

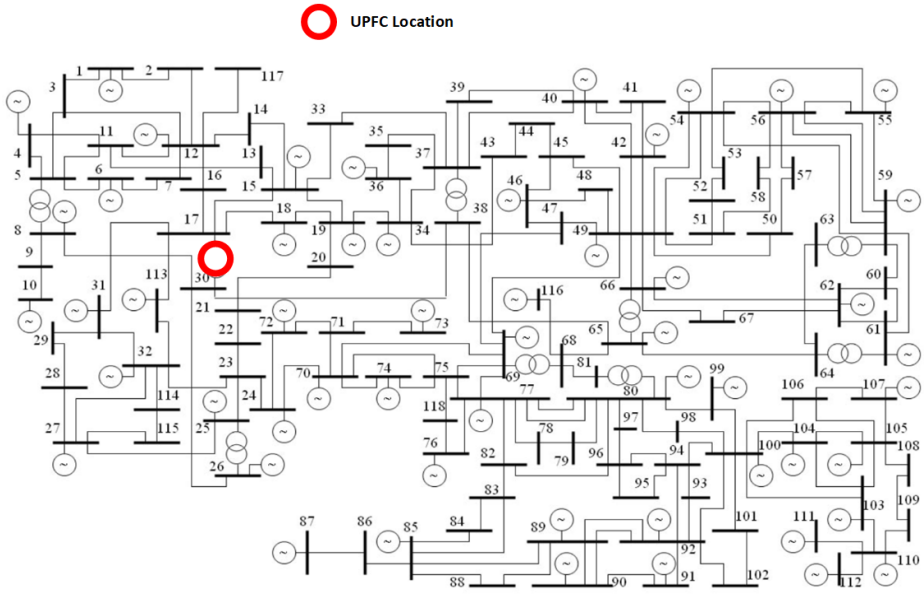

Figure 4.32: Location of UPFC Case B 118 Bus System

The reduction in loading ratio is shown in Table.4.17. It is higher as compared to Case A.

Table 4.17: Change in Loading Ratio for Case B-118 Bus System

UPFC Location	30-17
Loading Ratio before OPF	0.6491
Loading Ratio after OPF	0.6279
Reduction in Loading Ratio after OPF	0.0212
Number of LPOPF iterations	5

The change in UPFC Parameters is shown in Table.4.18.

Table 4.18: UPFC 30-17 Parameters Case B

UPFC Parameter(30-17 UPFC)	Before OPF	After OPF
V_{se}	0.1223	0.43
δ_{se}	55.8 deg	109 deg
MVA_{se}	31 MVA	105 MVA
MVA_{sh}	56 MVA	128 MVA
P_{sh}	-2 MW	-55 MW
P_{des}	242.00 MW	418.72 MW
Q_{des}	54.00 Mvar	-44.22 Mvar
V_{des}	0.991 V	0.949 V

The loading ratio of all lines in Case B before and after opf is shown in Fig.4.33. In Case B, only a few lines have smaller loading after opf as compared to before opf.

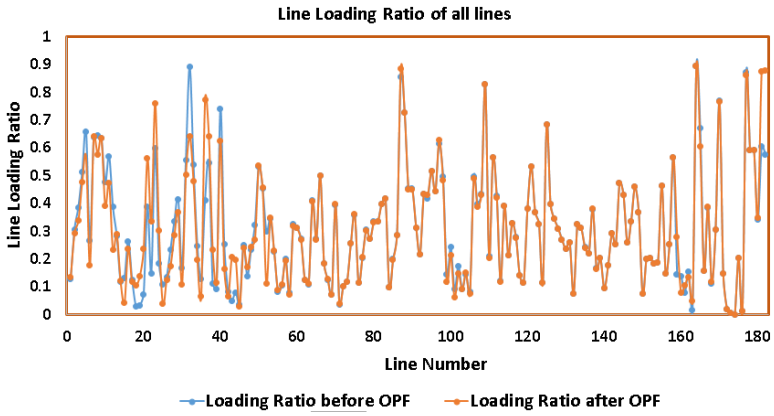

Figure 4.33: Loading Ratio Case B

The location of lines with the highest reduction in line loading ratio is shown in Fig.4.34. Compared to Case A, the lines with the highest reduction in line loading have different location as the UPFC location has changed. They are now located close to where the UPFC is located.

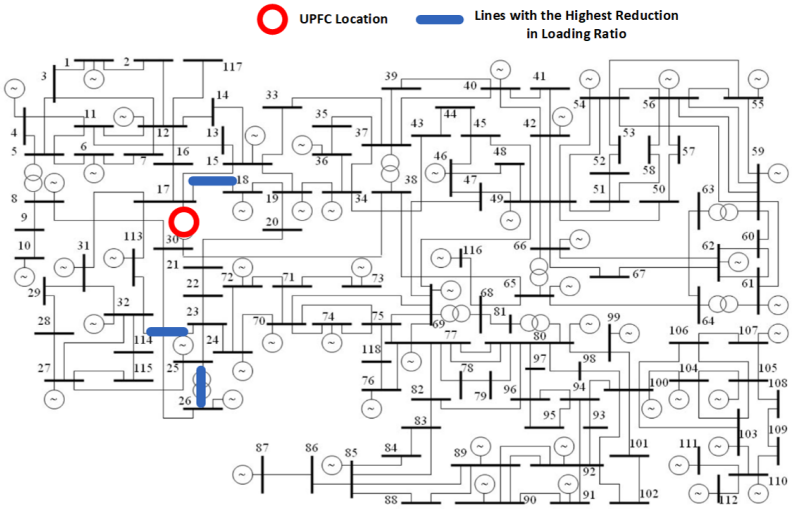

Figure 4.34: Lines with the Highest reduction in line loading Case B

The error in real and reactive generation setpoints is shown in Fig.4.35 and Fig.4.36. In Case B, this error is negligible.

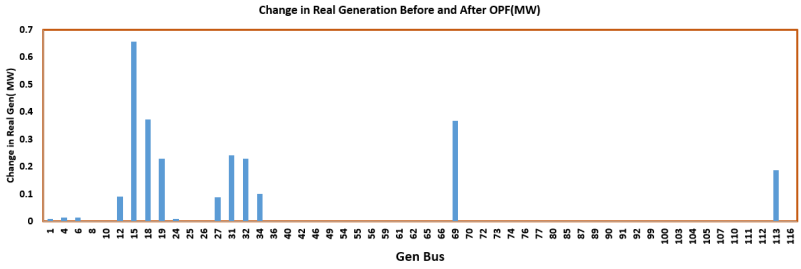

Figure 4.35: Change In Real Generation(MW) Case B

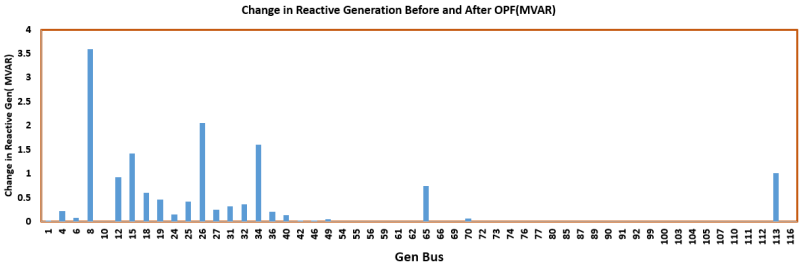

Figure 4.36: Change In Reactive Generation(MVAR) Case B

Case C

Two UPFCs were installed on the system on line 63-64 and 80-81. The locations are shown in Fig. 4.37.

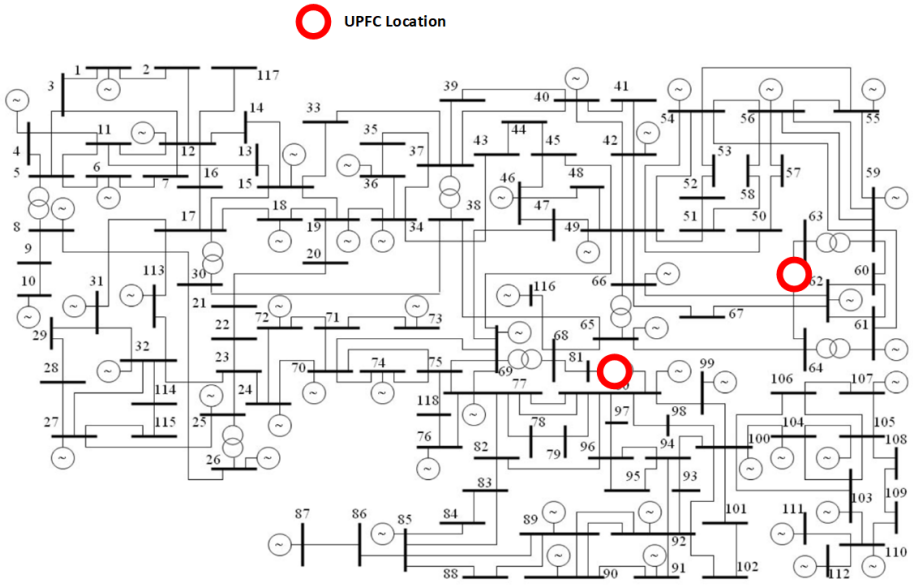

Figure 4.37: Location of UPFC Case C 118 Bus System

The reduction in loading ratio is shown in Table .4.19. The reduction in loading ratio is significant given the 118 Bus system is a large power system. The 39 Bus system Case A had a reduction in loading ratio of 0.0252 and Case B had a reduction of 0.0341. The reduction is comparable to that for the smaller 39 Bus System.

Table 4.19: Change in Loading Ratio for Case C-118 Bus System

UPFC Locations	63-64 and 80-81
Loading Ratio before OPF	0.6499
Loading Ratio after OPF	0.6146
Reduction in Loading Ratio after OPF	0.0353
Number of LPOPF Iterations	30

The Loading ratio of all lines before and after opf are shown in Fig. 4.38. As seen for the 39 Bus system, some lines have higher loading before opf versus after opf while some lines have the opposite pattern. However, overall there is a reduction in the loading ratio for high loaded lines.

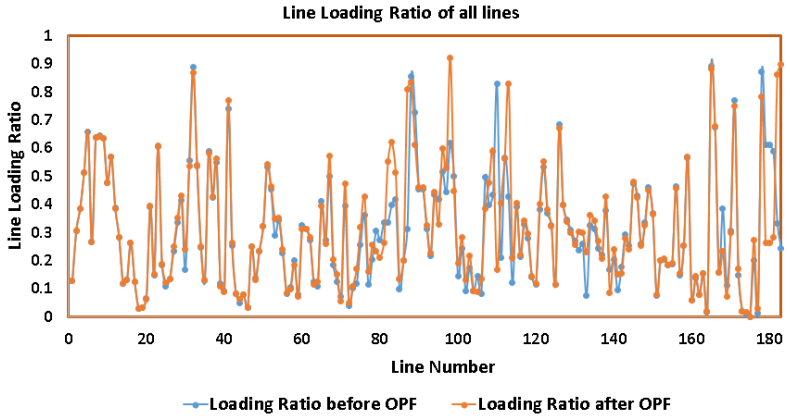

Figure 4.38: Loading Ratio Case C

The location of lines with the highest reduction in line loading ratio is shown in Fig.4.39.

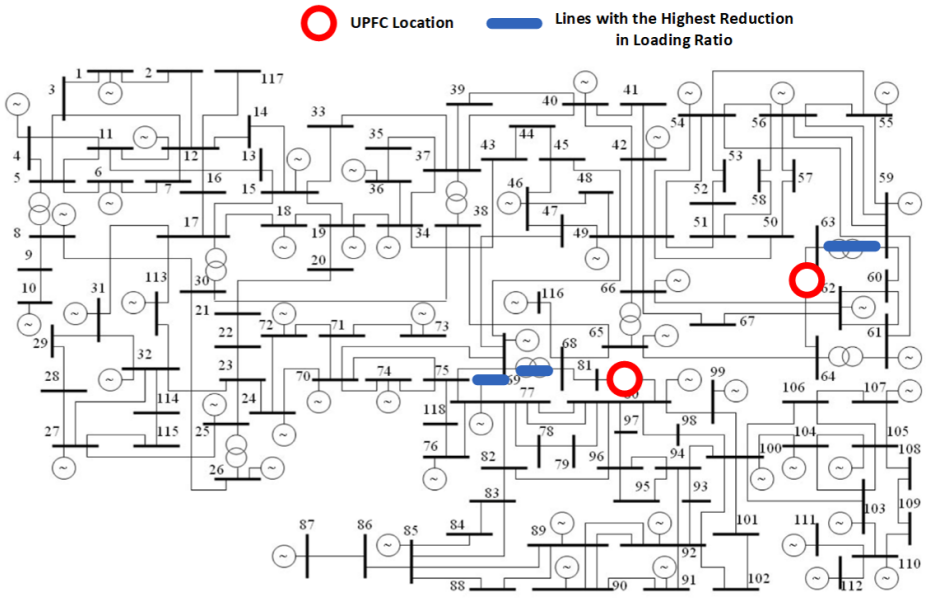

Figure 4.39: Lines with the Highest reduction in line loading Case C

The UPFC operating point before and after the OPF are shown in the table .4.20 and table .4.21. As can be seen in table .4.20 and table .4.21, the voltage source magnitude and series voltage source power rating increase after the OPF for both UPFC locations emphasizing the facr that UPFC is essential to reducing the line loading when the real and reactive gen setpoints are not allowed to change in Case A. The shunt voltage source power rating also increases because the desired voltage increases at the two UPFC's PV bus locations.

Table 4.20: UPFC Parameters for UPFC 63-64

UPFC Parameter(63-64 UPFC)	Before OPF	After OPF
V_{se}	0.0499	0.1483
δ_{se}	-90 deg	81 deg
MVA_{se}	8 MVA	26 MVA
MVA_{sh}	21 MVA	56 MVA
P_{sh}	1.5 MW	-3 MW
P_{des}	-165.00 MW	-40.66 MW
Q_{des}	-33.00 Mvar	11.02 Mvar
V_{des}	1.013 V	1.010 V

Table 4.21: UPFC Parameters for UPFC 81-80

UPFC Parameter(81-80 UPFC)	Before OPF	After OPF
V_{se}	0.0148	0.2816
δ_{se}	-68 deg	114 deg
MVA_{se}	0.7 MVA	15 MVA
MVA_{sh}	32 MVA	45 MVA
P_{sh}	-0.4 MW	10 MW
P_{des}	-34 MW	101.10 MW
Q_{des}	-33 Mvar	-53.07 Mar
V_{des}	1.04 V	1.071 V

The Fig. 4.40 and Fig. 4.41 show the change in Real Generation and Reactive Generation setpoints before and after the LPOPF converges. As discussed for the 39 Bus case, this should ideally be zero. However, since LPOPF inherently has an error due to linear modelling of the ACPF equations, there is some change in the Real and Reactive Generation setpoints. In Case A, the maximum error in Real

Generation setpoint occurs at bus 69 and that for the Reactive Generation setpoint occurs at bus 59 as shown in Table .4.22. The percent error is 0.13 percent in case of Real Generation while that for the reactive generation is 8.3 percent. This is also acceptable given that there are 54 generators and the average error is significantly less than 8.3 percent as can be judged from Fig .4.41.

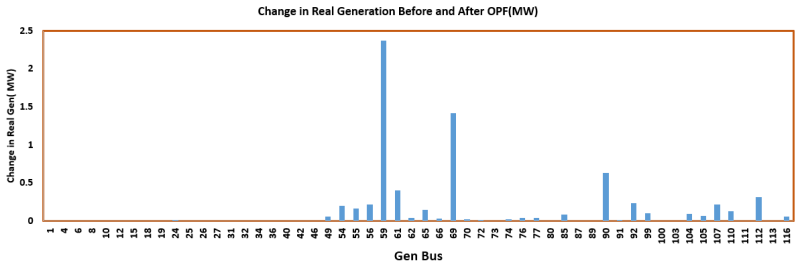

Figure 4.40: Change In Real Generation(MW) Case C

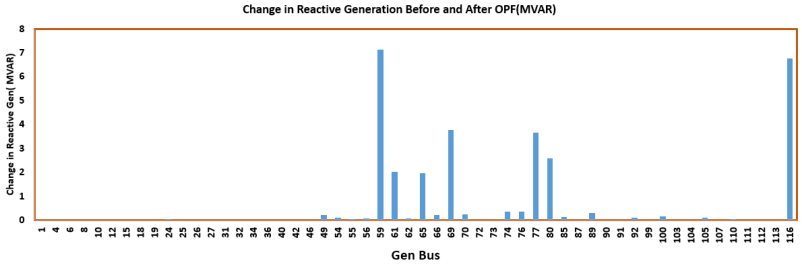

Figure 4.41: Change In Reactive Generation(MVAR) Case C

Table 4.22: Maximum Percentage Change in Pgen and QGen Case C

Bus 69 PGen before OPF	761.66 MW
Bus 69 PGen after OPF	762.69 MW
Percentage Error in PGen at Bus 69	0.13 percent
Bus 59 QGen before OPF	97.00 MVAR
Bus 59 QGen after OPF	105.39 MVAR
Percent error in QGen Bus 59	8.3 percent

Case D

The location of the UPFCs installed are 65-68 and 30-17. The locations are shown in Fig. 4.42.

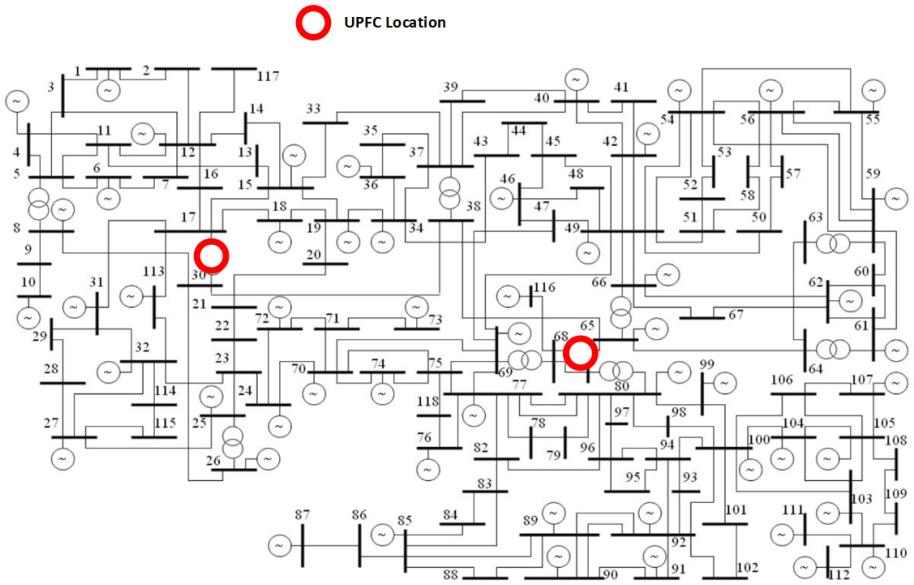

Figure 4.42: Location of UPFC Case D 118 Bus System

The reduction in loading ratio is shown in Table. 4.23.

Table 4.23: Change in Loading Ratio for Case D-118 Bus System

UPFC Location	65-68 and 30-17
Loading Ratio before OPF	0.6516
Loading Ratio after OPF	0.6208
Reduction in Loading Ratio after OPF	0.0308

The UPFC operating point before and after the OPF is shown in the Table .4.24 and Table .4.25.

Table 4.24: UPFC 65-68 Parameters

UPFC Parameter(65-68 UPFC)	Before OPF	After OPF
V_{se}	0.0226	0.0759
δ_{se}	-113 deg	125 deg
MVA_{se}	2 MVA	7.5 MVA
MVA_{sh}	34 MVA	40 MVA
P_{sh}	-0.1 MW	6.5 MW
P_{des}	-69.00 MW	-37.04 MW
Q_{des}	-72.00	-51.44 Mvar
V_{des}	1.012 V	1.010 V

Table 4.25: UPFC 30-17 Parameters

UPFC Parameter(30-17 UPFC)	Before OPF	After OPF
V_{se}	0.1237	0.4348
δ_{se}	82.0807 deg	109 deg
MVA_{se}	31 MVA	103 MVA
MVA_{sh}	29 MVA	102 MVA
P_{sh}	0.9 MW	-58 MW
P_{des}	242.00	418.68 MW
Q_{des}	54.00	-50.39Mar
V_{des}	1.005 V	0.958 V

The loading ratio for Case D is shown in Fig.4.43.

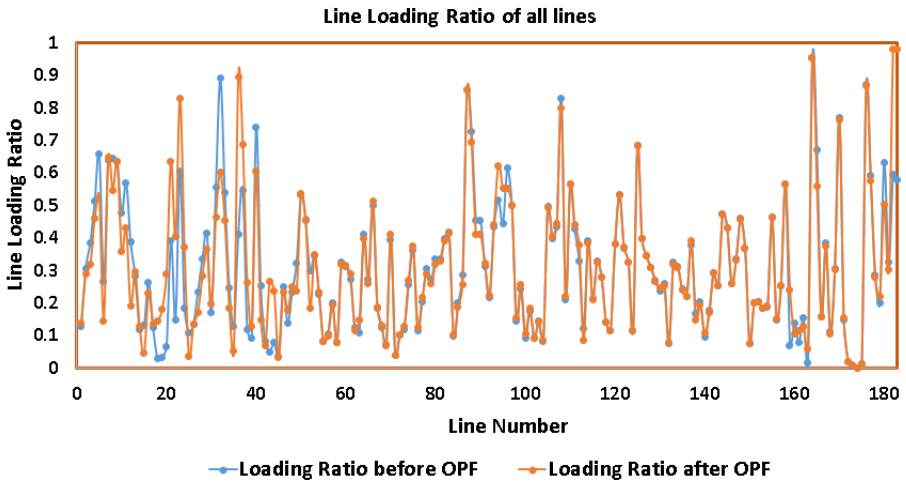

Figure 4.43: Loading Ratio Case D(118 BUS)

The location of lines with the highest reduction in line loading ratio is shown in Fig.4.44. In this case, no line is located near UPFC 65-68 signifying that it is not an optimal location for the UPFC. All the lines are located near UPFC 30-17 signifying that it is an effective UPFC location.

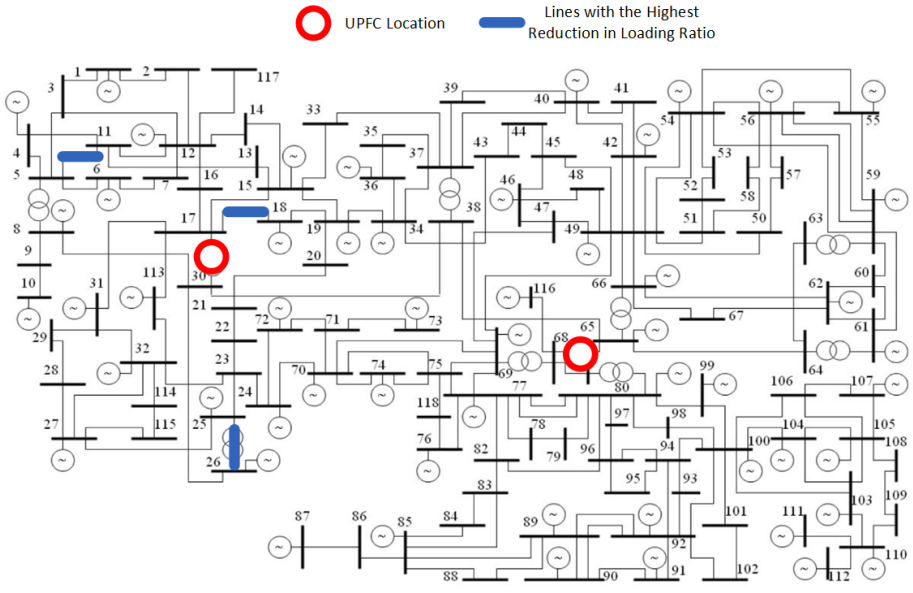

Figure 4.44: Lines with the Highest reduction in line loading Case D

The error in real and reactive generation setpoints is shown in Fig.4.45 and Fig.4.46.

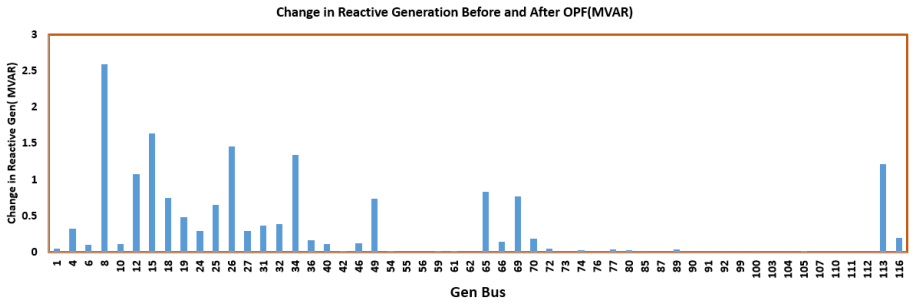

Figure 4.45: Change In Reactive Generation(MVAR) Case D

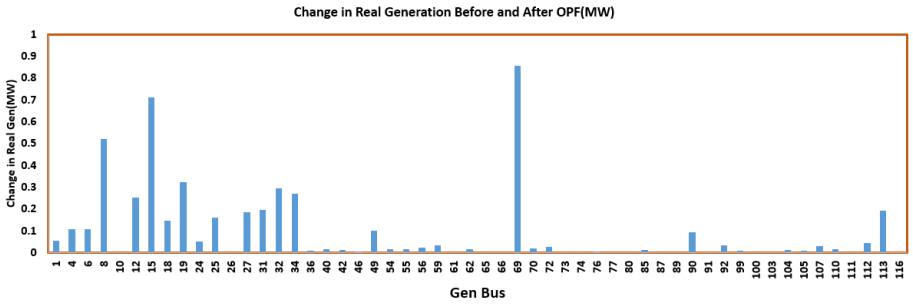

Figure 4.46: Change In Real Generation(MW) Case D

4.2.5.4 Summary and Main Contribution

The Main contribution of this chapter is listed below:

- The proposed LPOPF algorithm is able to optimally manage the power flow in a system by providing a feasible solution which is accurate and computationally efficient. The solution is feasible with regards to the UPFC power and voltage ratings defined in the LPOPF. Compared with the model already published, it is giving a larger reduction in the line loading ratio thus it is able to show that it maximises the benefit of UPFC towards achieving the optimal power flows in a power system. The results have been verified for the 39 Bus and 118 Bus System thus the algorithm is effective for larger systems as well.

The summary of the cases studied thus far is shown in Tabel.6.21.

Table 4.26: Summary of the Cases studied

39 Bus System			
Location of UPFC	Loading Ratio Before OPF	Loading Ratio After OPF	Reduction in Loading Ratio
16-17	0.6645	0.6393	0.0252
3-4	0.6682	0.6341	0.0341
13-14	0.6581	0.6515	0.0066
118 Bus System			
Location of UPFC	Loading Ratio Before OPF	Loading Ratio After OPF	Reduction in Loading Ratio
81-80	0.6489	0.6305	0.0185
30-17	0.6491	0.6279	0.0212
63-64 and 80-81	0.6499	0.6146	0.0353
65-68 and 30-17	0.6516	0.6208	0.0308

Some Points can be concluded from this chapter which are discussed below:

- The choice of the location of the UPFC is vital for bringing an effective reduction in the loading ratio. UPFC located on lines which are transmission corridors connecting generation centers to load centers produce the most optimal results. 39 Bus System 1 UPFC Case B has the largest reduction in loading ratio as the location of UPFC in this case is more optimal as compared to 39 Bus SYstem 1 UPFC CAse A and Case C. Similar conclusion can be made for the 118 Bus System where Case B has a larger reduction compared to Case A. This algorithm can provide quantitative insight into what are the optimal locations for the UPFC if the objective is to reduce the line loading ratio in high loaded lines. There are other factors which are important as well. Topology of the power system is another important factor. In 118 Bus system, since the generation

and load is evenly distributed across the entire system, thus there is no specific transmission corridor which is vital to reducing the line loading ratio. In such a topology, furthermore, high loaded lines may be spread out across different zones. Thus, it is important to locate UPFCs in those zones so that bottlenecks can be solved and line loading could be reduced further. This was seen when the UPFC is located in line 81-80 as opposed to the case where the UPFC is located in line 30-17. The UPFCs are located in different zones in both cases as the high loaded lines are located around different locations.

- It can be seen that even for larger 118 bus system, the reduction in loading ratio is comparable to that for the 39 Bus system. If you compare 39 Bus System 1 UPFC Case A and B with the 118 Bus system 2 UPFC Case C and D, the reduction in loading ratio is almost in the same range. Thus, if the objective of the power system operator is to reduce the line loading ratio in high loaded lines, it can be useful even for larger systems keeping in mind the cost. The 118 Bus system has 186 branches while the 39 Bus system has 47 branches, however only one more UPFC is required for the 118 bus system to produce the same reduction in line loading ratio as that for the 39 Bus system. As was seen from the discussion in previous subsections, the UPFC capacity was not fully utilized in all the cases. Given the recent introduction of Distributed FACTs devices, modular SSSCs can be installed which have comparitively lower ratings as compared to traditional UPFCs and hence lower costs. This can be useful for larger power systems such as the 118 Bus system where multiple modular SSSCs will be more beneficial to reduce the line loading and reduce congestion. The results of this chapter can be used further study the effect of modular SSSCs on line loading ratio.

CHAPTER 5: OPTIMAL POWER FLOW METHODOLOGY WITH UPFC AND SYNCHRONOUS GENERATOR FOR LINE LOADING OPTIMIZATION

5.1 Introduction

The line loading is an important parameter for mainting system security. In case of contingencies, it is important to maintian as large a security margin as is possible. In order to increase the security margin, the line loading of the heavily loaded lines must be reduced. FACTs devices offer control of power flow and hence are useful to control loading levels of lines in proximity to where the FACTs is installed. Varying the generation can change power flows and hence reach a power flow solution which is more secure speaking from the line loading level. Combining the use of generation and UPFCs can bring advantages to reducing the line loading than using each of them individually. Generation offers a large degree of control of line flows over a large region in the power system. UPFC can provide more direct control over a more smaller region which covers the neighbouring lines adjacent to the line the UPFC is installed on. Thus, it is important to optimize the use of generation and UPFCs in a single OPF formulation to gain a more optimal solution.

The major contributions of this chapter are:

1. A formulation has been presented which finds out the optimal parameter settings of UPFC when generation control is allowed. The objective of the LPOPF formulation is to manage the line loading of the power system. Generation control is divided into three categories which are real generation control, reactive generation control and the combined used of real and reactive generation control.

5.2 Formulation

In this chapter, an LPOPF formulation has been presented which outputs the optimal parameter settings of the UPFC when generation control is allowed. The generation control is allowed into three categories which are real generation control, reactive generation control and the combined use of real and reactive generation control. The formulation used in this chapter is similar to the formulation used in the last chapter except that within each LPOPF iteration, generation is allowed to vary depending on which generation control category is being used. The categories are defined below:

- Scenario 1: All Real generation and Only Slack Bus Reactive Generation can Vary during the LPOPF. The input to the LPOPF includes reactive generation setpoints from all generators(other than the slack bus).
- Scenario 2: All Reactive generation and Only Slack Bus Real Generation can Vary during the LPOPF.The input to the LPOPF includes real generation setpoints from all generators(other than the slack bus).
- Scenario 3: All Reactive and Real Generation can Vary during the LPOPF.

Table 5.1: Generation Control Description

Scenario	Pgen Control	Qgen Control
1	All Pgen	Slack Qgen
2	Slack Pgen	All Qgen
3	All Pgen	All Qgen

A flow chart of the algorithm has been presented below:

The line loading gained as an output from the LPOPF incorporating UPFC and Generation control needs to be compared with a benchmark. The benchmark is the

line loading gained as an output from the LPOPF incorporating only Generation Control. Thus, in this manner if we compare the two line loadings, the contribution of UPFC to the reduction in line loading is obtained. This way, the effectiveness of the UPFC is obtained under the circumstances when the generation control is allowed. This is shown in Table.5.2. The effectiveness of the UPFC can be compared as shown below:

- If (A-B) $>$ (A-C) then the UPFC is not effective in reducing line loading ratio when generation control is allowed. This suggests that UPFC should not be installed in the system.
- If (A-B) $<$ (A-C) then the UPFC is effective in reducing line loading when generation control is allowed. This suggests that UPFC should be installed in the system.

Table 5.2: Comparison of Change in Loading Ratio

LPOPF With Generation Control Only(Base Case)	
Loading Ratio before OPF	A
Loading Ratio after OPF	B
Reduction in Loading Ratio	(A-B)
LPOPF With Generation Control and UPFC Control Only	
Loading Ratio before OPF	A
Loading Ratio after OPF	C
Reduction in Loading Ratio	(A-C)

5.3 Results for 39 Bus System

In this section, the 39 Bus System is studied. It is assumed that the line 4-5 is not in operation. Thus, the system is more constrained. The location of the heavily loaded lines in the system are shown in Fig.5.1.

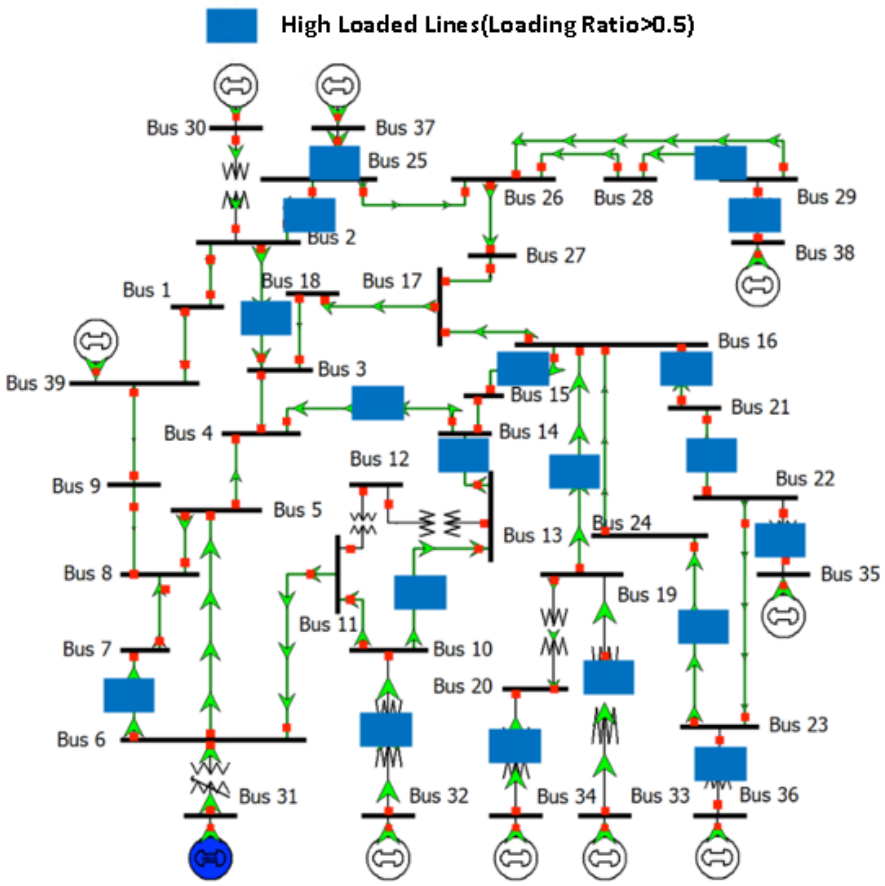

Figure 5.1: Location of High Loaded Lines 39 Bus System

5.3.1 Base Case(No UPFC)

In this case, no upfc is installed in the system. The results of this case will be used as a benchmark for comparison with cases where a UPFC is installed in the system.

5.3.1.1 Base Case Scenario 1: All Pgen+Slack Bus Qgen

The line loading ratio for this scenario is shown in Table.5.3. Since the real generation at all generation buses is allowed to vary, thus there is considerable change in real power flow before vs after opf as shown in Fig.5.3. The reactive power flow changes slightly due to the change in Slack bus reactive generation. This can be seen in Fig.5.4.

Table 5.3: No UPFC Case : Scenario 1 Loading Ratio Results

Generation Control	Before OPF	After OPF
All Pgen + Slack Bus Qgen	0.7289	0.6163

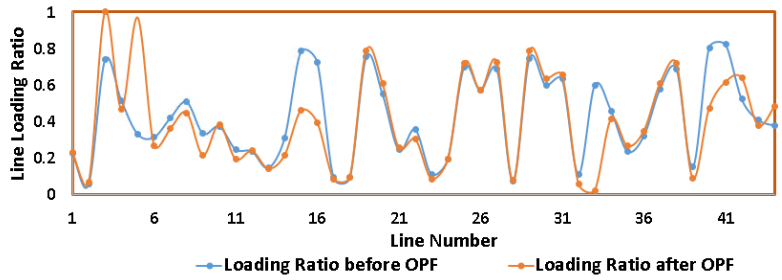

Figure 5.2: Base Case Scenario 1 Line Loading Ratio

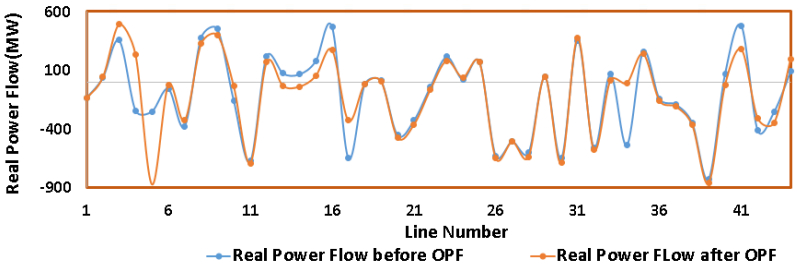

Figure 5.3: Base Case Scenario 1 Real Power Flow

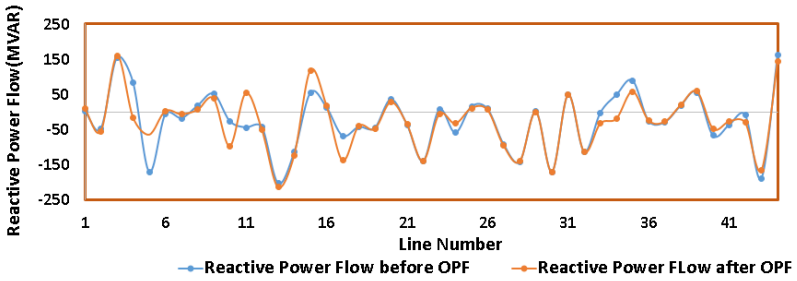

Figure 5.4: Base Case Scenario 1 Reactive Power Flow

5.3.1.2 Base Case Scenario 2: All Qgen+Slack Bus Pgen

In this scenario, the reactive generation at all generation buses is allowed to vary. The real power almost remains the same before vs after opf as only the slack bus real

generation is allowed to change as shown in Fig.5.6. The reduction in line loading is significantly less in scenario 2 compared with scenario 1 as the line flows comprise a larger percentage of the real power flow compared with the reactive power flow.

Table 5.4: No UPFC Case : Scenario 2 Loading Ratio Results

Generation Control	Before OPF	After OPF
All Qgen + Slack Bus Pgen	0.7289	0.7267

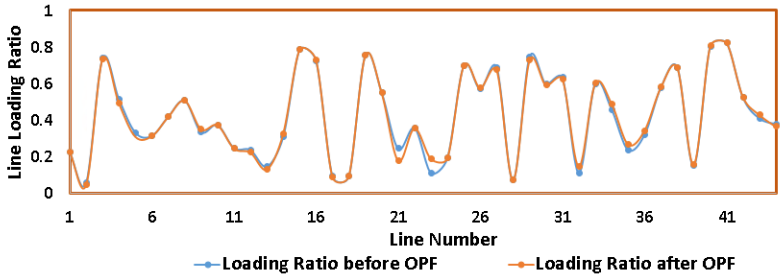

Figure 5.5: Base Case Scenario 2 Line Loading Ratio

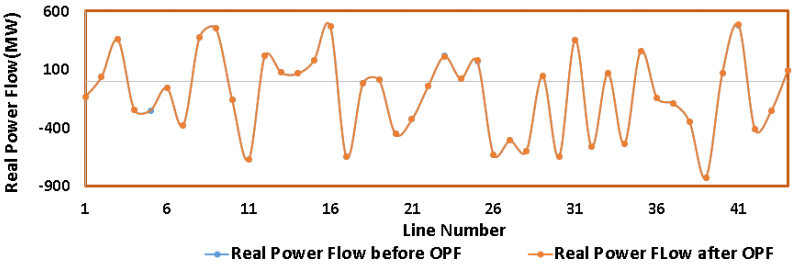

Figure 5.6: Base Case Scenario 2 Real Power Flow

5.3.1.3 Base Case Scenario 3: All Pgen+All Qgen

Table 5.5: No UPFC Case : Scenario 3 Loading Ratio Results

Generation Control	Before OPF	After OPF
All Pgen + All Qgen	0.7289	0.6070

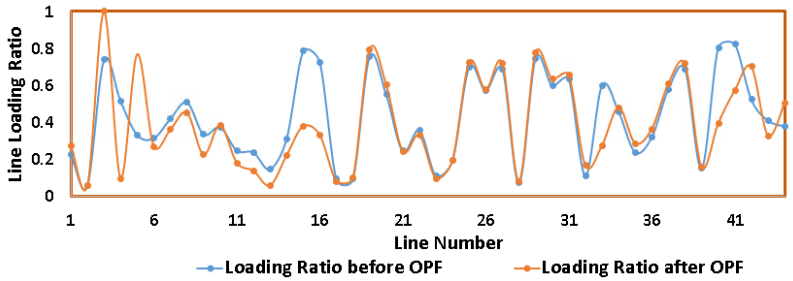

Figure 5.7: Base Case Scenario 3 Line Loading Ratio

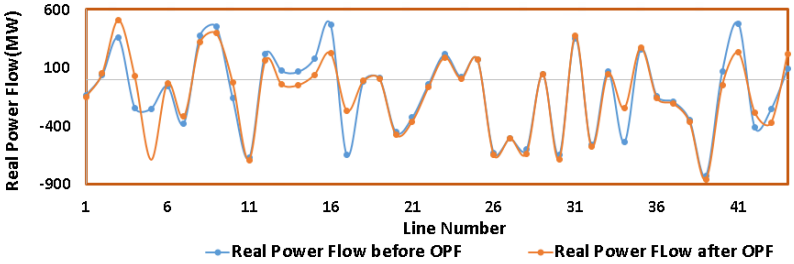

Figure 5.8: Base Case Scenario 3 Real Power Flow

5.3.2 Case A: UPFC Installed on Line 3-18

5.3.2.1 Case A Scenario 1: All Pgen+Slack Bus Qgen

In this case, a UPFC is installed on Line connecting buses 3 and 18.As can be seen in Table. 5.6, the UPFC provides additional reduction in line loading in Scenario 1. Thus the UPFC is beneficial in this scenario. Since the real generation setpoints are allowed to change during the LPOPF, the real power flow has more leverage to vary during the OPF as shown in Fig.5.10. The change in loading ratio and the change in reactive power flow are shown in Fig.5.9 and Fig.5.11. It is important to note that the reducing the loading ratio of heavily loaded lines can not occur without increasing the loading ratio of lighty loaded lines. This can be seen in Fig.5.9, where some lines which loading ratio more than 0.5 before opf have loading ratio after opf less than 0.5 and vice versa. Thus, power is rerouted from heavily loaded lines to lightly loaded lines. However, this is not the case necessarily as lines connecting generation buses to rest of power system can not have power rerouted as there is no alternate route.

For these lines, loading ratio will likely remain above 0.5.

Table 5.6: Case A : Scenario 1 Loading Ratio Results

LPOPF With Generation Control Only	
Loading Ratio before OPF	0.7289
Loading Ratio after OPF	0.6163
LPOPF With Generation Control and UPFC Control Only	
Loading Ratio before OPF	0.7289
Loading Ratio after OPF	0.5433

Table 5.7: UPFC 3-18 Parameters Case A: Scenario 1

UPFC Parameter(3-18 UPFC)	Before OPF	After OPF
MVA_{se}	0.1 MVA	100 MVA
MVA_{sh}	1 MVA	20 MVA
P_{sh}	0.4 MW	-2 MW
Q_{sh}	0.5 MVAR	5 MVAR

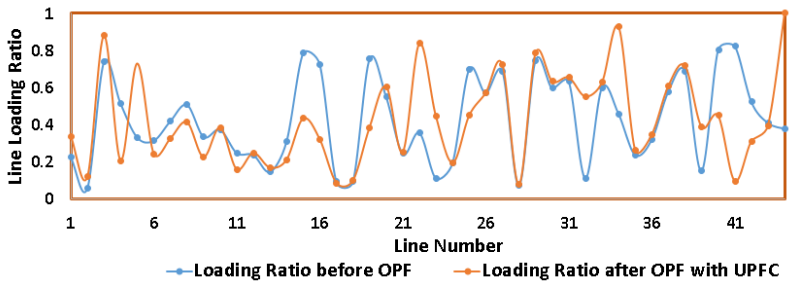

Figure 5.9: Case A Scenario 1 Line Loading Ratio

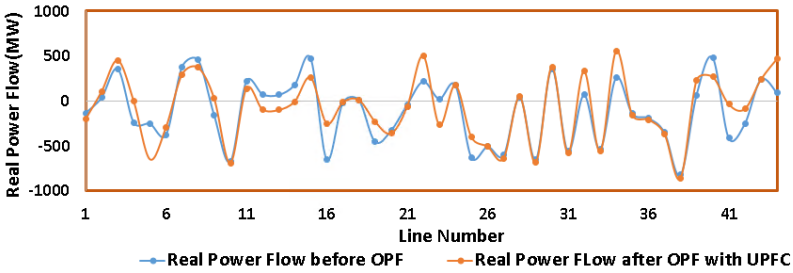

Figure 5.10: Case A Scenario 1 Real Power Flow

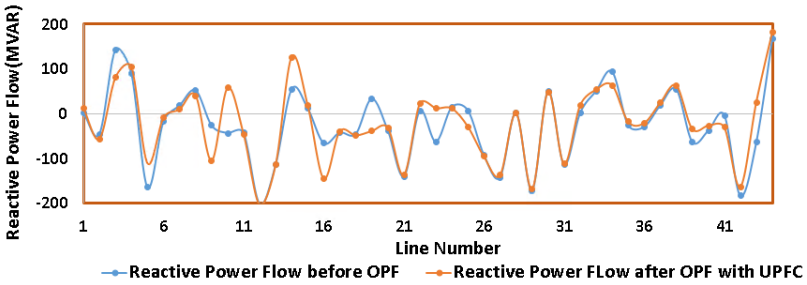

Figure 5.11: Case A Scenario 1 Reactive Power Flow

As can be seen in Fig.5.12, the voltage limits are being met after the OPF.

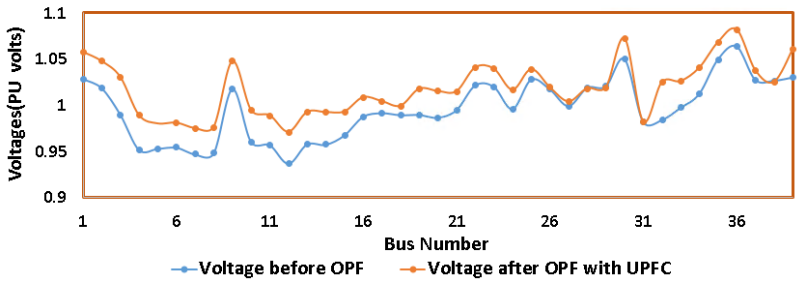

Figure 5.12: Case A Scenario 1 Voltages

5.3.2.2 Case A Scenario 2: All Qgen+Slack Bus Pgen

In this scenario, the UPFC is able to provide a larger reduction in line loading compared with without UPFC case. The line loading ratio, the real power flow and reactive power flow are shown in Fig.5.13, Fig.5.14 and Fig.5.15. As can be seen in Fig.5.14, the real power flow is not changing signficantly compared with Scenario 1 because in Scenario 2, only the real generation at the slack bus is allowed to vary

during the OPF. Thus, there is less leverage for the real power flow to change. However, the reactive power flow is changing more in scenario 2 compared with scenario 1 since in scenario 2, the reactive generation can vary in all generation buses thus there is more leverage for the reactive power flow to change. Since the real power flow comprises a larger portion of the line flows, thus there is less reduction in line loading in scenario 2 compared with scenario 1 because in scenario 1, the real generation at all generation buses is allowed to vary during the OPF. The important point to note is that even with the limited control provided by reactive generation in scenario 2, the UPFC provides additional control to help reduce the line loading ratio of heavily loaded lines.

Table 5.8: Case A : Scenario 2 Loading Ratio Results

LPOPF With Generation Control Only	
Loading Ratio before OPF	0.7289
Loading Ratio after OPF	0.7267
LPOPF With Generation Control and UPFC Control Only	
Loading Ratio before OPF	0.7289
Loading Ratio after OPF	0.695

Table 5.9: UPFC 3-18 Parameters Case A: Scenario 2

UPFC Parameter(3-18 UPFC)	Before OPF	After OPF
MVA_{se}	0.1 MVA	50 MVA
MVA_{sh}	1 MVA	250 MVA
P_{sh}	0.4 MW	15 MW
Q_{sh}	0.5 MVAR	-250 MVAR

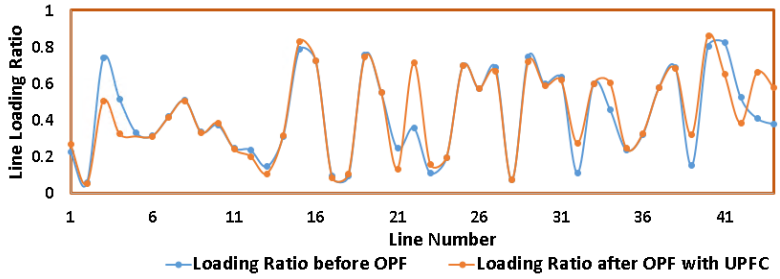

Figure 5.13: Case A Scenario 2 Line Loading Ratio

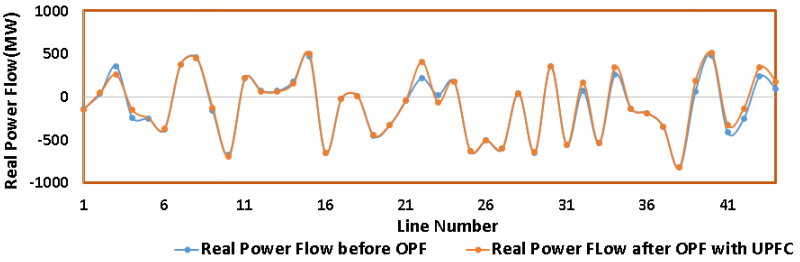

Figure 5.14: Case A Scenario 2 Real Power Flow

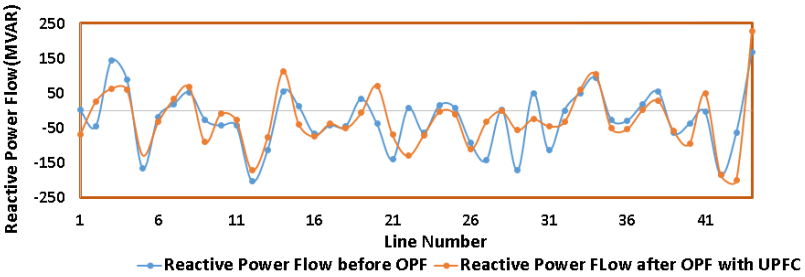

Figure 5.15: Case A Scenario 2 Reactive Power Flow

5.3.2.3 Case A Scenario 3: All Qgen+All Pgen

In this scenario, both real and reactive generation is allowed to vary during the OPF. The line loading ratio for the with and without UPFC cases is shown in Table.5.10. Comparing the results with Scenario 1, the line loading is approximately similar after OPF in both with and without UPFC cases for Scenario 1 and Scenario 3. This can be attributed to the fact that Scenario 1 is "All Pgen+ SLack Bus Qgen" and Scenario 3 is "ALL Qgen+ All Pgen". Since most of the line flows are determined

by the real power flow thus the additional control offered by the reactive generation is very less towards reducing the line loading ratio. Thus, as can be seen the results are similar to Scenario 1.

Table 5.10: Case A : Scenario 3 Loading Ratio Results

LPOPF With Generation Control Only	
Loading Ratio before OPF	0.7289
Loading Ratio after OPF	0.6070
LPOPF With Generation Control and UPFC Control Only	
Loading Ratio before OPF	0.7289
Loading Ratio after OPF	0.5416

Table 5.11: UPFC 3-18 Parameters Case A: Scenario 3

UPFC Parameter(3-18 UPFC)	Before OPF	After OPF
MVA_{se}	0.1 MVA	150 MVA
MVA_{sh}	1 MVA	250 MVA
P_{sh}	0.4 MW	40 MW
Q_{sh}	0.5 MVAR	-250 MVAR

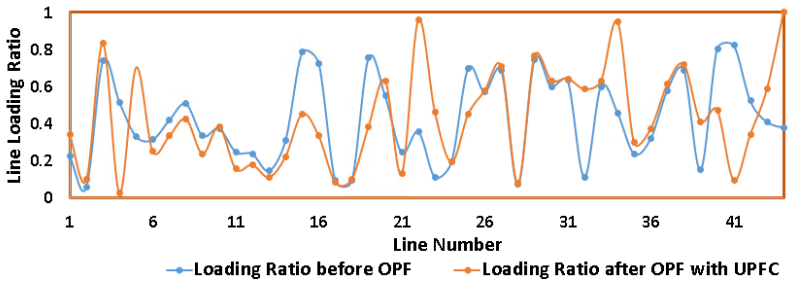

Figure 5.16: Case A Scenario 3 Line Loading Ratio

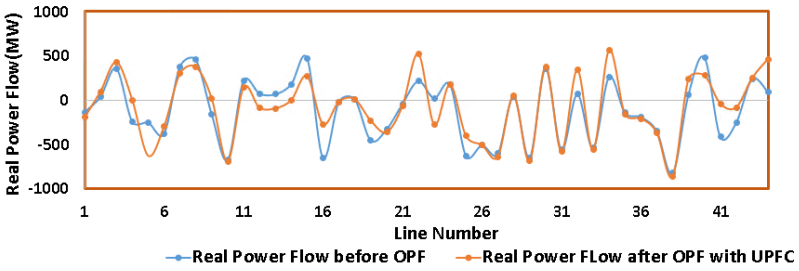

Figure 5.17: Case A Scenario 3 Real Power Flow

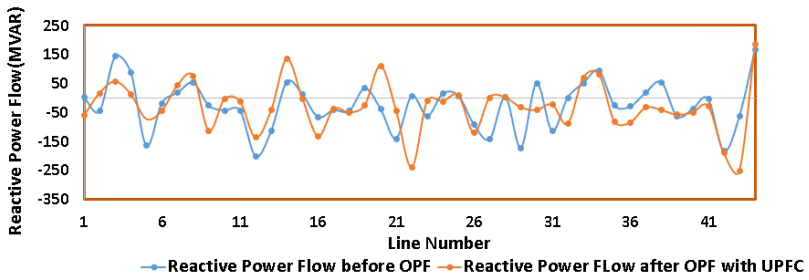

Figure 5.18: Case A Scenario 3 Reactive Power Flow

A summary of Case A results is shown in Table.5.12.

Table 5.12: Summary of Case A Results

Generation Control	UPFC Installed	Before OPF	After OPF
All Pgen + Slack Qgen	No	0.7289	0.6163
All Pgen + Slack Qgen	Yes	0.7289	0.5433
All Qgen + Slack Pgen	No	0.7289	0.7267
All Qgen + Slack Pgen	Yes	0.7289	0.695
All Qgen + All Pgen	No	0.7289	0.6070
All Qgen + All Pgen	Yes	0.7289	0.5416

5.3.2.4 Case D

In this section, load is varied with the UPFC installed on the same line. A few select loads on some buses are increaseed in load. Loads on Bus 12,15,16,23, 25 and 26 are increased by 2 percent for both real and reactive power.

Table 5.13: Case D Load Variation

Bus No.	Real Load	Reactive Load	Percent Increase
12	15	88	2
15	350	153	2
16	350	33	2
23	249	85	2
25	224	48	2
26	139	17	2

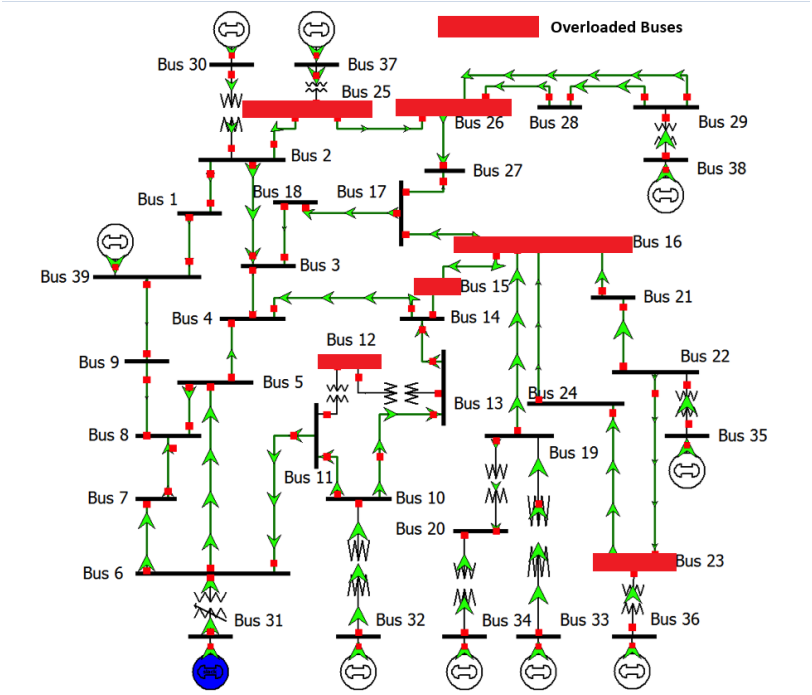

Figure 5.19: Case D 39 Bus system

The line loading ratios of the system for various control scenarios are shown in Fig.5.21, Fig.5.20 and Fig.5.22. As can be seen that in Fig.5.20, the line loading of all lines before and after opf is the same. Thus for Scenario 2, there is no change in the power system state. This is because one of the lines has a loading ratio almost 1. Thus, the presence of UPFC is not able to help in this case.

Table 5.14: Case D : Scenario 1 Loading Ratio Results

LPOPF With Generation Control Only	
Loading Ratio before OPF	0.7915
Loading Ratio after OPF	0.7004
LPOPF With Generation Control and UPFC Control Only	
Loading Ratio before OPF	0.7915
Loading Ratio after OPF	0.5852

Table 5.15: Case D : Scenario 2 Loading Ratio Results

LPOPF With Generation Control Only	
Loading Ratio before OPF	0.7915
Loading Ratio after OPF	0.7915
LPOPF With Generation Control and UPFC Control Only	
Loading Ratio before OPF	0.7915
Loading Ratio after OPF	0.7915

Table 5.16: Case D : Scenario 3 Loading Ratio Results

LPOPF With Generation Control Only	
Loading Ratio before OPF	0.7915
Loading Ratio after OPF	0.6873
LPOPF With Generation Control and UPFC Control Only	
Loading Ratio before OPF	0.7915
Loading Ratio after OPF	0.5553

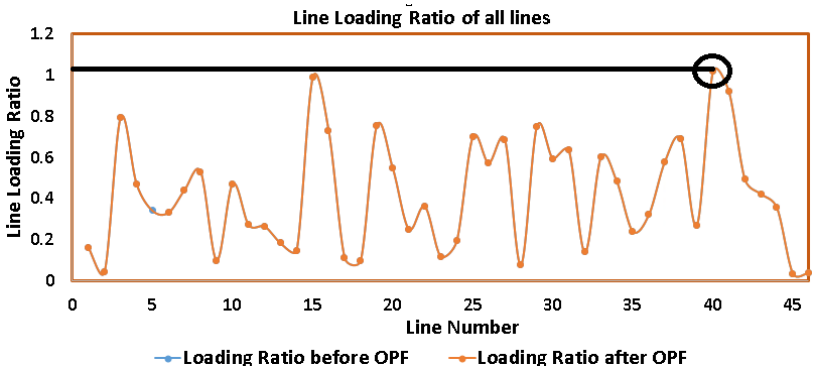

Figure 5.20: Case D Scenario 2 Line Loading Ratio

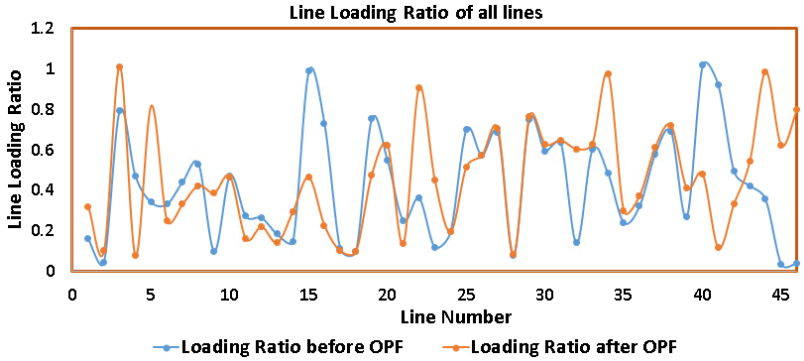

Figure 5.21: Case D Scenario 3 Line Loading Ratio

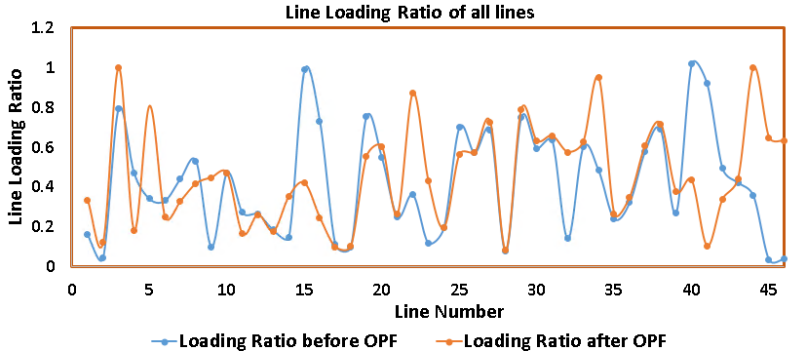

Figure 5.22: Case D Scenario 1 Line Loading Ratio

Table 5.17: UPFC 3-18 Parameters Case D: Scenario 1

UPFC Parameter(3-18 UPFC)	After OPF
MVA_{se}	106 MVA
MVA_{sh}	110 MVA
Vse	0.3250 V

Table 5.18: UPFC 3-18 Parameters Case D: Scenario 3

UPFC Parameter(3-18 UPFC)	After OPF
MVA_{se}	113 MVA
MVA_{sh}	250 MVA
Vse	0.3374 V

5.3.3 Case B: UPFC Installed on Line 11-12

5.3.3.1 Case B Scenario 1: All Pgen+Slack Bus Qgen

In this case, a UPFC is installed on Line connecting buses 11 and 12.As can be seen in Table. 5.19, the UPFC provides reduction in line loading ratio additional to the generation controls. Thus the UPFC installed on this location is effective in this scenario. Note that the additional reduction provided by the UPFC is small. However this must be taken in perspective as the control provided by UPFC is within its neighbouring region of installation while the control offered by real generation at the 9 generation buses collectively is across the entire power system. The paramters of the UPFC are shown in Table.5.20. As was discussed for Case A Scenario 1, the real generation control at all generation buses allows more leverage for the real power flow to change as compared with the reactive power flow. This can be seen in Fig.5.24 and Fig.5.25. The line loading ratio is shown in Fig.5.23.

Table 5.19: Case B : Scenario 1 Loading Ratio Results

Generation Control	UPFC Installed	Before OPF	After OPF
All Pgen + Slack Bus Qgen	No	0.7289	0.6163
All Pgen + Slack Bus Qgen	Yes	0.7289	0.6044

Table 5.20: UPFC 11-12 Parameters Case B: Scenario 1

UPFC Parameters	Before OPF	After OPF
MVA_{se}	0.05 MVA	200 MVA
MVA_{sh}	30 MVA	4 MVA
P_{sh}	0.4 MW	-4 MW
Q_{sh}	-30 MVAR	1 MVAR

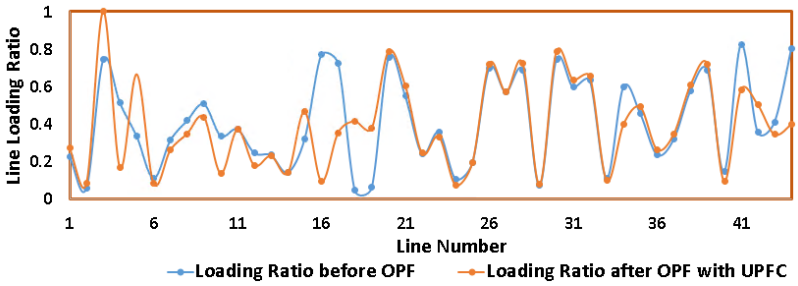

Figure 5.23: Case B Scenario 1 Line Loading Ratio

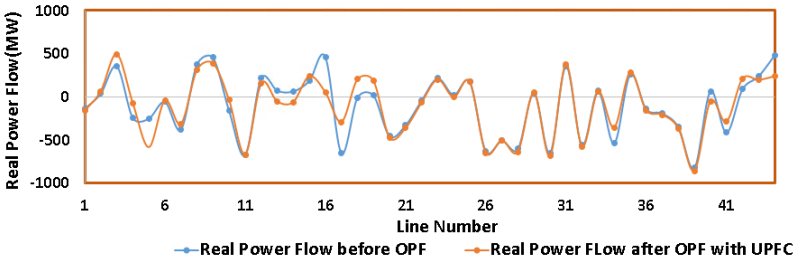

Figure 5.24: Case B Scenario 1 Real Power Flow

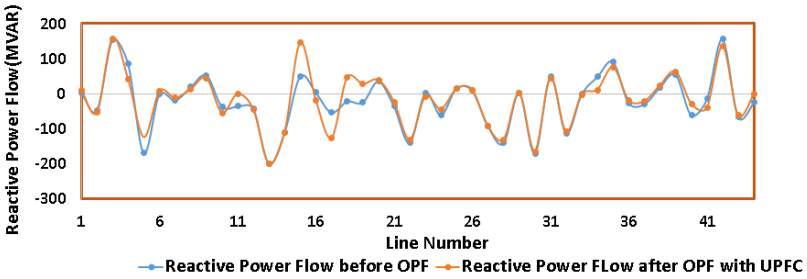

Figure 5.25: Case B Scenario 1 Reactive Power Flow

5.3.3.2 Case B Scenario 2: All Qgen+Slack Bus Pgen

In this scenario, the UPFC is able to provide additional reduction in line loading ratio compared with the without UPFC case. The UPFC parameters are shown in Table.5.22. As can be seen, UPFC utilizes its reactive capacity support by providing 250 MVAR to the power system. As was discussed previously for Case A, since only the slack bus real generation is allowed to vary, the real power flow does not change signficantly during the OPF. Since the reactive generation can change at all generation buses, thus the reactive power flow changes significantly during the OPF. This can be seen in Fig.5.28 and Fig.5.27.

Table 5.21: Case B : Scenario 2 Loading Ratio Results

Generation Control	UPFC Installed	Before OPF	After OPF
All Qgen + Slack Bus Pgen	No	0.7289	0.7267
All Qgen + Slack Bus Pgen	Yes	0.7289	0.6997

Table 5.22: UPFC 11-12 Parameters Case B: Scenario 2

UPFC Parameters	Before OPF	After OPF
MVA_{se}	0.05 MVA	200 MVA
MVA_{sh}	30 MVA	250 MVA
P_{sh}	0.4 MW	40 MW
Q_{sh}	-30 MVAR	-250 MVAR

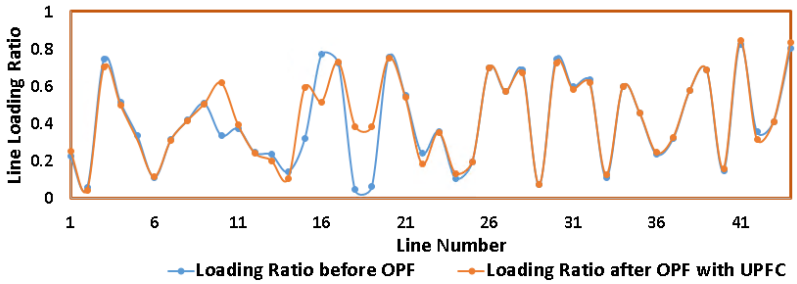

Figure 5.26: Case B Scenario 2 Line Loading Ratio

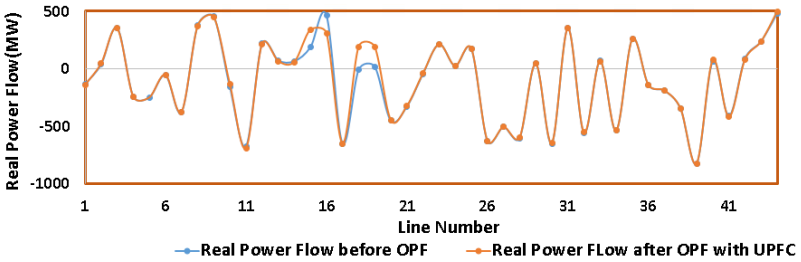

Figure 5.27: Case B Scenario 2 Real Power Flow

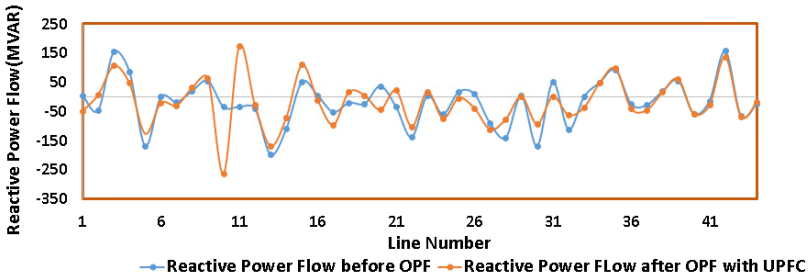

Figure 5.28: Case B Scenario 2 Reactive Power Flow

5.3.3.3 Case B Scenario 3: All Qgen+All Pgen

In this scenario, all real and reactive generation can vary. The UPFC is providing additional reduction in line loading as shown in Table.5.23. Compared with Scenario 1 where only slack bus qgen is allowed to vary, in this scenario UPFC is able to provide additonal reactive support since the all reactive generation can vary in Scenario 3. This allows more leverage for the reactive flows to change and hence more leverage for the UPFC PV and PQ buses to change its reactive injections. This can be seen

in Table.5.24 where the UPFC reactive power rating is 220 MVA compared with Scenario 1 where it is 4 MVA.

Table 5.23: Case B : Scenario 3 Loading Ratio Results

Generation Control	UPFC Installed	Before OPF	After OPF
All Qgen + ALL Pgen	No	0.7289	0.616
All Qgen + ALL Pgen	Yes	0.7289	0.5886

Table 5.24: UPFC 11-12 Parameters Case B: Scenario 3

UPFC Parameters	Before OPF	After OPF
MVA_{se}	0.05 MVA	210 MVA
MVA_{sh}	30 MVA	220 MVA
P_{sh}	0.4 MW	30 MW
Q_{sh}	-30 MVAR	-220 MVAR

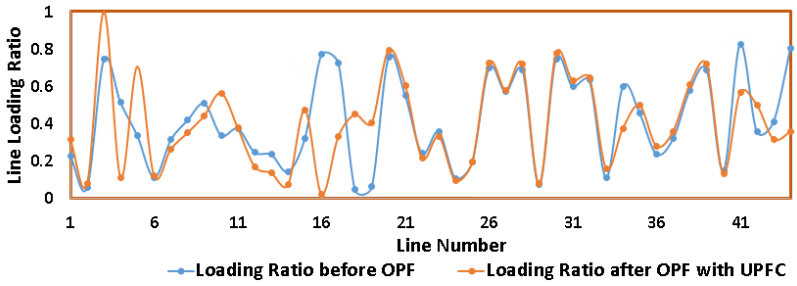

Figure 5.29: Case B Scenario 3 Line Loading Ratio

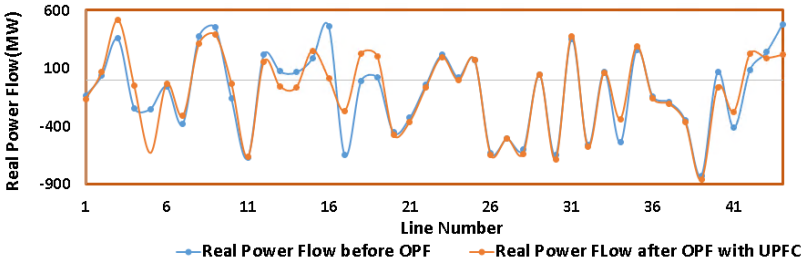

Figure 5.30: Case B Scenario 3 Real Power Flow

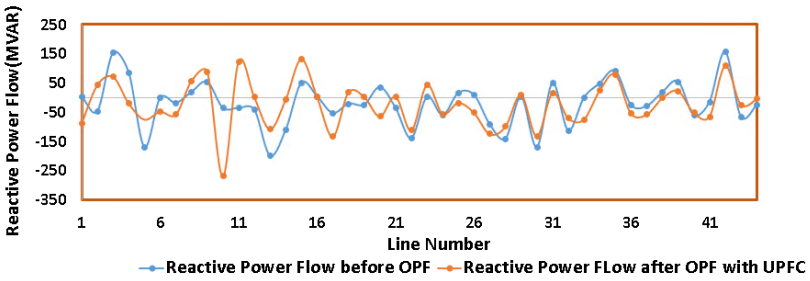

Figure 5.31: Case B Scenario 3 Reactive Power Flow

A summary of Case B results is shown in Table.5.25.

Table 5.25: Summary of Case B Results

Generation Control	UPFC Installed	Before OPF	After OPF
All Pgen + Slack Qgen	No	0.7289	0.6163
All Pgen + Slack Qgen	Yes	0.7289	0.6044
All Qgen + Slack Pgen	No	0.7289	0.7267
All Qgen + Slack Pgen	Yes	0.7289	0.6997
All Qgen + All Pgen	No	0.7289	0.6070
All Qgen + All Pgen	Yes	0.7289	0.5886

5.3.3.4 Case E

In this section, load is varied with the UPFC installed on the same line. A few select loads on some buses are increaseed in load. Loads on Bus 12,15,16,23, 25 and 26 are increased by 2 percent for both real and reactive power. The load variation is shown in Table.5.26 and in Fig.5.32.

Table 5.26: Case E Load Variation

Bus No.	Real Load	Reactive Load	Percent Increase
12	15	88	2
15	350	153	2
16	350	33	2
23	249	85	2
25	224	48	2
26	139	17	2

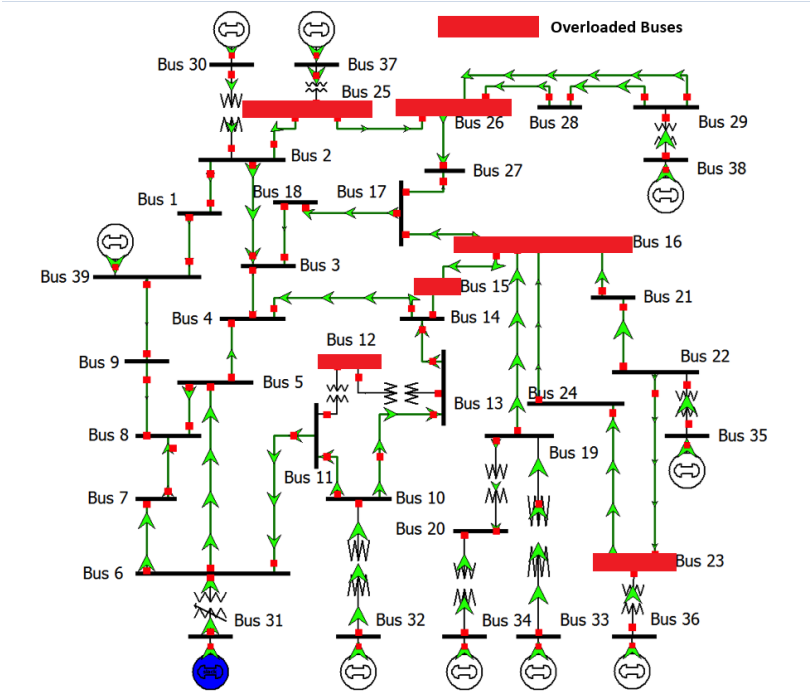

Figure 5.32: Case E 39 Bus system

The loading ratio before and after opf for all three control scenarios are shown in Table.5.27, Table.5.28 and Table.5.29. It is seen that the UPFC is beneficial in all three control scenarios. The UPFC parameters for control scenarios 1 and 3 are shown in Table.5.33 and Table.5.34. The line loading ratio for the control scenarios 1 and 3 are shown in Fig.5.33 and Fig.5.34.

Table 5.27: Case E : Scenario 1 Loading Ratio Results

LPOPF With Generation Control Only	
Loading Ratio before OPF	0.7915
Loading Ratio after OPF	0.7004
LPOPF With Generation Control and UPFC Control Only	
Loading Ratio before OPF	0.7915
Loading Ratio after OPF	0.6636

Table 5.28: Case E : Scenario 2 Loading Ratio Results

LPOPF With Generation Control Only	
Loading Ratio before OPF	0.7915
Loading Ratio after OPF	0.7915
LPOPF With Generation Control and UPFC Control Only	
Loading Ratio before OPF	0.7915
Loading Ratio after OPF	0.7915

Table 5.29: Case E : Scenario 3 Loading Ratio Results

LPOPF With Generation Control Only	
Loading Ratio before OPF	0.7915
Loading Ratio after OPF	0.6873
LPOPF With Generation Control and UPFC Control Only	
Loading Ratio before OPF	0.7915
Loading Ratio after OPF	0.6433

Table 5.30: UPFC 11-12 Parameters Case E: Scenario 1

UPFC Parameter(11-12 UPFC)	After OPF
MVA_{se}	183 MVA
MVA_{sh}	15 MVA
Vse	0.56 V

Table 5.31: UPFC 11-12 Parameters Case E: Scenario 3

UPFC Parameter(11-12 UPFC)	After OPF
MVA_{se}	182 MVA
MVA_{sh}	94 MVA
Vse	0.56 V

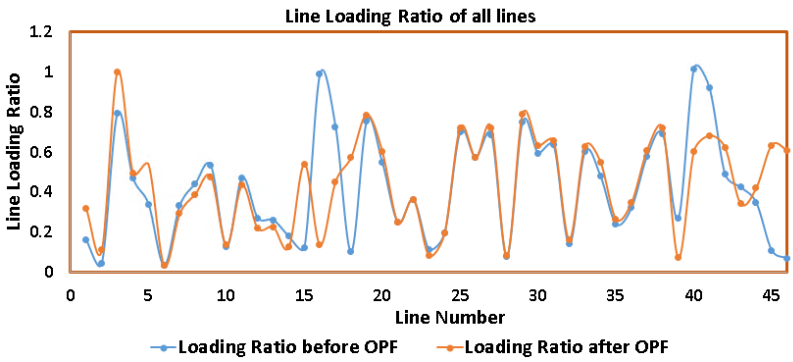

Figure 5.33: Case E Scenario 1 Line Loading Ratio

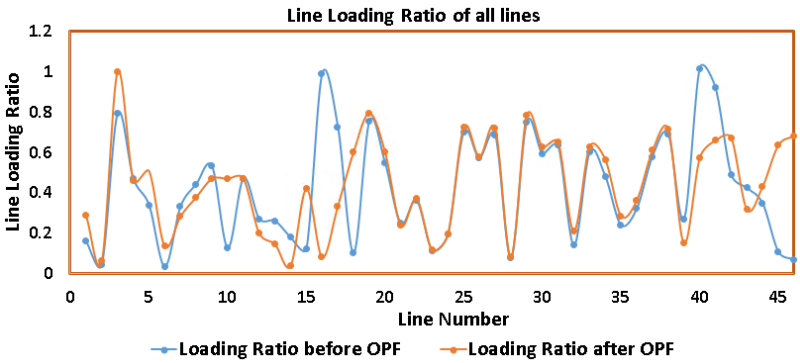

Figure 5.34: Case E Scenario 3 Line Loading Ratio

5.3.4 Case C: UPFC Installed on Line 16-17

5.3.4.1 Case C Scenario 1: All Pgen+Slack Bus Qgen

The UPFC is installed on the line connecting buse 16 and 17. This location is effective as it can be seen that the UPFC brings additional reduction in line loading ratio. The parameters of the UPFC are shown in Table.5.33. The loading ratio, the real flow and reactive flow are shown in Fig.5.35, Fig.5.36 and Fig.5.37.

Table 5.32: Case C : Scenario 1 Loading Ratio Results

Generation Control	UPFC Installed	Before OPF	After OPF
All Pgen + Slack Bus Qgen	No	0.7289	0.6163
All Pgen + Slack Bus Qgen	Yes	0.7289	0.6062

Table 5.33: UPFC Parameters Case C: Scenario 1

UPFC Parameters	Before OPF	After OPF
MVA_{se}	2.5 MVA	200 MVA
MVA_{sh}	2 MVA	80 MVA
P_{sh}	0.4 MW	-25 MW
Q_{sh}	1 MVAR	70 MVAR

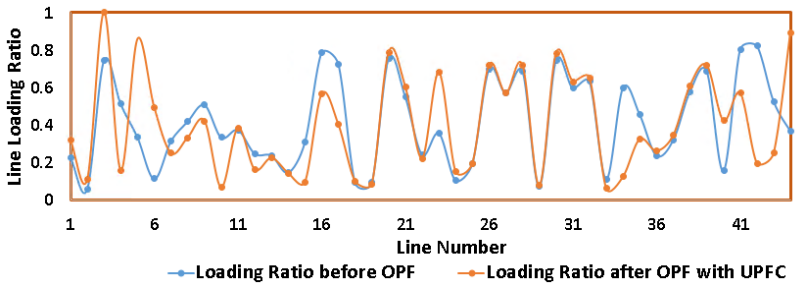

Figure 5.35: Case C Scenario 1 Line Loading Ratio

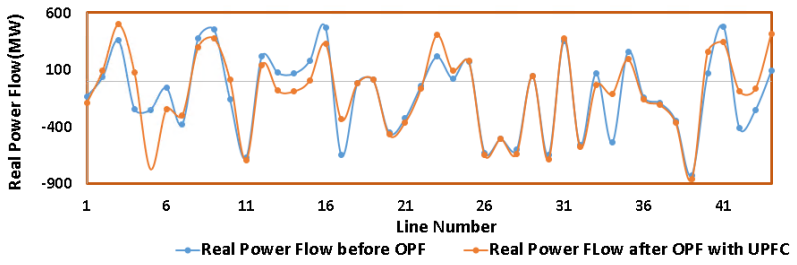

Figure 5.36: Case C Scenario 1 Real Power Flow

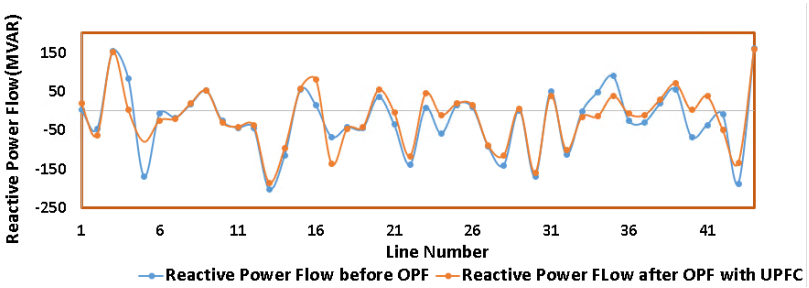

Figure 5.37: Case C Scenario 1 Reactive Power Flow

5.3.4.2 Case C Scenario 2: All Qgen+Slack Bus Pgen

The UPFC is effective in this scenario as well where it is able to provide additional control of the loading ratios in additon to the generation control. Since the reactive generation at every generation bus is allowed to change, thus the UPFC has more leverage for providing reactive support through its shunt source compared with Scenario 1. However, since real power flows are limited by change in Slack bus Pgen only, thus the series power rating MVAse of the UPFC is less in Scenario 2(70 MVA) versus Scenario 1(200 MVA). The UPFC has less leverage to reroute power in Scenario 2 as the line flows comprise a larger portion of the real power compared with the reactive power flow.

Table 5.34: Case C : Scenario 2 Loading Ratio Results

Generation Control	UPFC Installed	Before OPF	After OPF
All Pgen + Slack Bus Qgen	No	0.7289	0.7267
All Pgen + Slack Bus Qgen	Yes	0.7289	0.7166

Table 5.35: UPFC Parameters Case C: Scenario 2

UPFC Parameters	Before OPF	After OPF
MVA_{se}	2.5 MVA	70 MVA
MVA_{sh}	2 MVA	180 MVA
P_{sh}	0.4 MW	-35 MW
Q_{sh}	1 MVAR	-160 MVAR

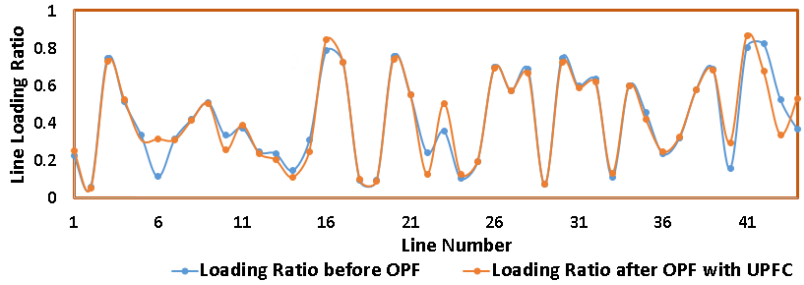

Figure 5.38: Case C Scenario 2 Line Loading Ratio

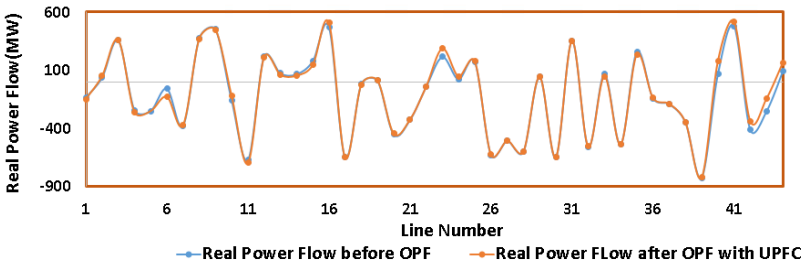

Figure 5.39: Case C Scenario 2 Real Power Flow

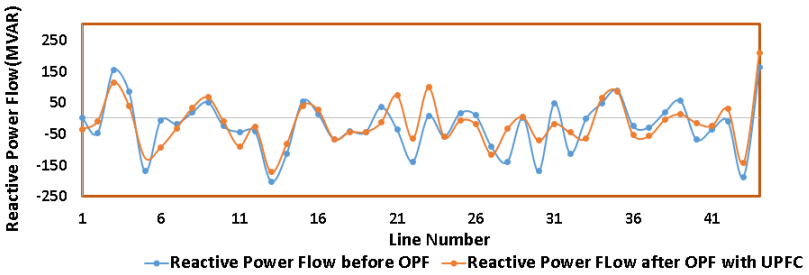

Figure 5.40: Case C Scenario 2 Reactive Power Flow

5.3.4.3 Case C Scenario 3: All Qgen+ALL Pgen

In this scenario, the UPFC is not effective in providing additional control over the line loading as shown in Table.5.36. This is mainly because this scenario allows real and reactive generation to vary at all generation buses thus the control offered by generation is significantly more than the UPFC. Thus the effectiveness of UPFC is negligible. The parameters of the UPFC are shown in Table.5.37.

Table 5.36: Case C : Scenario 3 Loading Ratio Results

Generation Control	UPFC Installed	Before OPF	After OPF
All Pgen + Slack Bus Qgen	No	0.7289	0.6070
All Pgen + Slack Bus Qgen	Yes	0.7289	0.6085

Table 5.37: UPFC Parameters Case C: Scenario 3

UPFC Parameters	Before OPF	After OPF
MVA_{se}	2.5 MVA	200 MVA
MVA_{sh}	2 MVA	200 MVA
P_{sh}	0.4 MW	-70 MW
Q_{sh}	1 MVAR	-180 MVAR

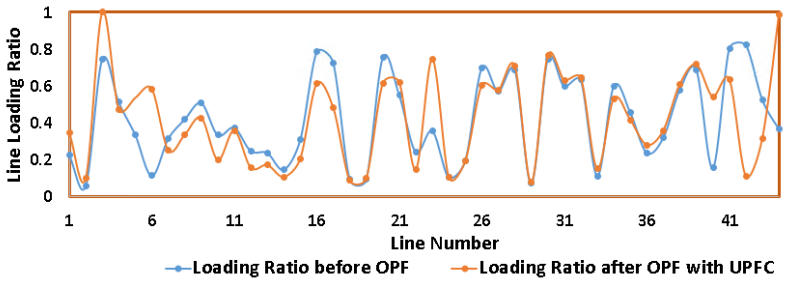

Figure 5.41: Case C Scenario 3 Line Loading Ratio

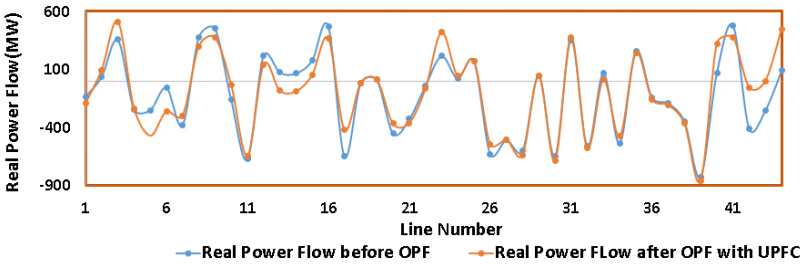

Figure 5.42: Case C Scenario 3 Real Power Flow

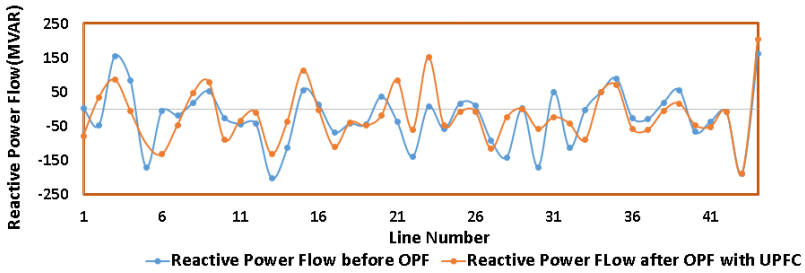

Figure 5.43: Case C Scenario 3 Reactive Power Flow

A summary of the results for Case C are shown in Table.5.38.

Table 5.38: Summary of Case C Results

Generation Control	UPFC Installed	Before OPF	After OPF
All Pgen + Slack Qgen	No	0.7289	0.6163
All Pgen + Slack Qgen	Yes	0.7289	0.6062
All Qgen + Slack Pgen	No	0.7289	0.7267
All Qgen + Slack Pgen	Yes	0.7289	0.7166
All Qgen + All Pgen	No	0.7289	0.6070
All Qgen + All Pgen	Yes	0.7289	0.6085

5.3.5 A Discussion on Voltage Improvement with UPFC 39 Bus system

5.3.6 A Discussion on UPFC Control REgion

Overall, the UPFC in combination with generation control is able to create a larger reduction in line loading ratio compared with generation control only(no UPFC case).

However, the location of the UPFC must be effective in order for the UPFC to be effective. The optimal location of the UPFC depends on several factors. The most important factor is loading levels and the system topology. In the system studied in this section, most of the heavily loaded lines are located in the center region of the system(6 lines of the 19 lines) denoted by the red rectangle shown in Fig.**??**. The other heavily loaded lines are branches connecting the generators to the rest of the system. These are shown by the lines marked inside the green circles. To reduce the line loading of the lines inside the green circle, generation can be adjusted at respective buses. The line loadings of the lines located in the center region can be controlled by adjusting generation. However,the degree of generation control reduces as we move inwards from the generation buses towards the area inside the red rectangle. Thus, if a UPFC is located within the red rectangle, additional control can be provided for lines located in proximity to UPFC location. This will help reduce the line loading further for these lines in particular.The results confirm what has been discussed so far. The UPFC installed on Line 3-18,16- 17 and 11-12 give higher reductions compared to without UPFC cases.

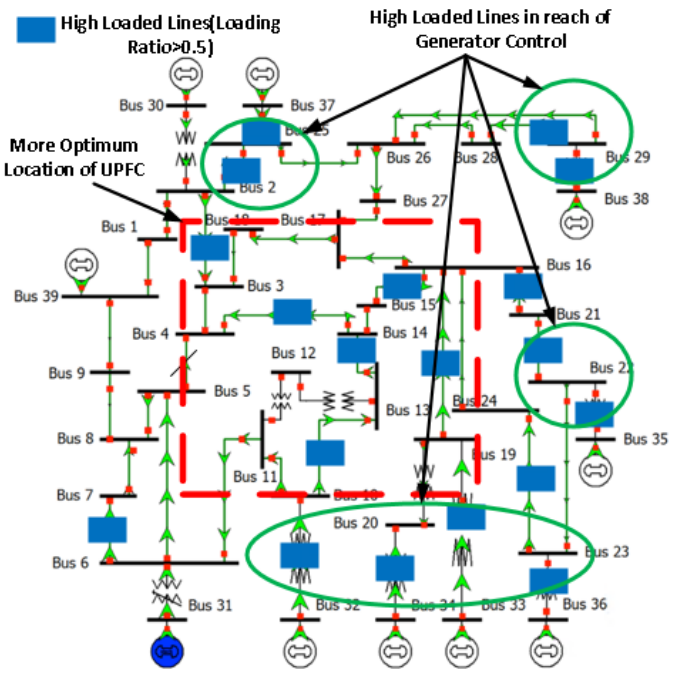

Figure 5.44: Control Region of UPFC

5.4 Results for 118 Bus System

The 118 bus system is a larger system as compared to the 39 bus system. It has 54 generators and 183 branches. The generators are located across the 118 bus system unlike the 39 bus system where generators were located on the outer buses of the system.

5.4.1 Base Case(No UPFC)

5.4.1.1 Base Case Scenario 1: All Pgen+Slack Bus Qgen

In scenario 1, all the real generation can vary. The change in line loading ratio for high loaded lines is shown in Table.5.39. The line loadings, the real and reactive power flow are shown in Fig.5.45.Fig.5.46 and Fig.5.47. As can be seen, the reactive power flow does not change signficantly. THe change in line loading ratio can be mostly attributed to change in real power flow.

Table 5.39: Base Case : Scenario 1 Loading Ratio Results

Generation Control	UPFC Installed	Before OPF	After OPF
All Pgen + Slack Qgen	No	0.6552	0.4507

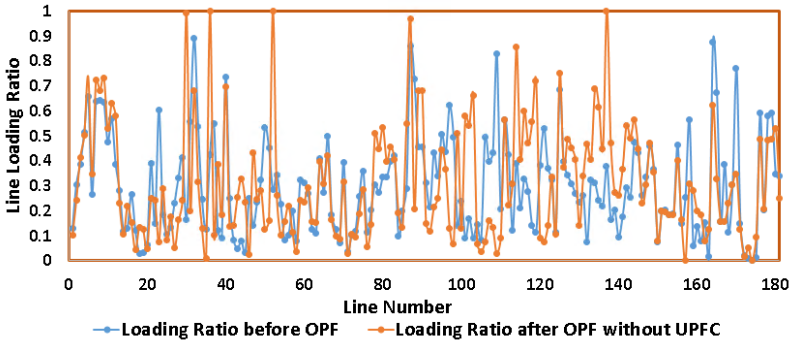

Figure 5.45: Base Case(118 Bus) Scenario 1 Line Loading Ratio

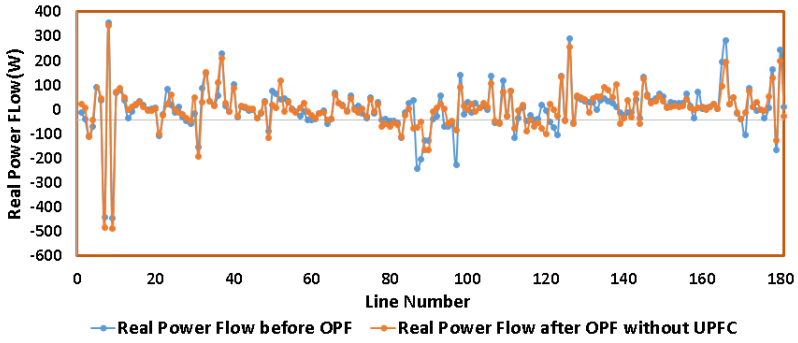

Figure 5.46: Base Case(118 Bus) Scenario 1 Real Power Flow

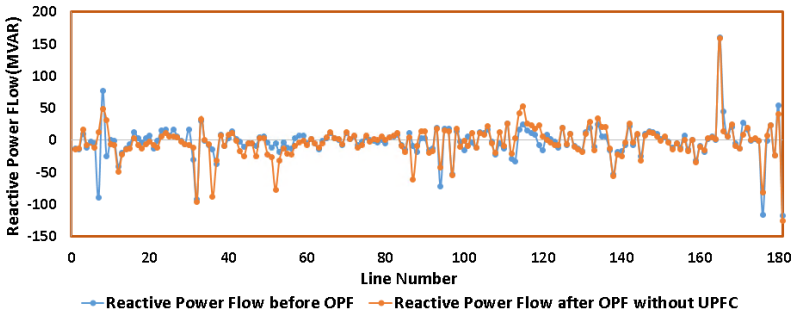

Figure 5.47: Base Case(118 Bus) Scenario 1 Reactive Power Flow

5.4.1.2 Base Case Scenario 2: All Qgen+Slack Bus Pgen

In scenario 2, all the reactive generation is allowed to vary. The change in loading ratio for high loaded lines is shown in Table.5.40. The reduction in line loading is lesser as compared to scenario 1. The line loadings, the real and reactive power flow are shown in Fig.5.48, Fig.5.49 and Fig.5.50.

Table 5.40: Base Case : Scenario 2 Loading Ratio Results

Generation Control	UPFC Installed	Before OPF	After OPF
All Qgen + Slack Pgen	No	0.6552	0.5948

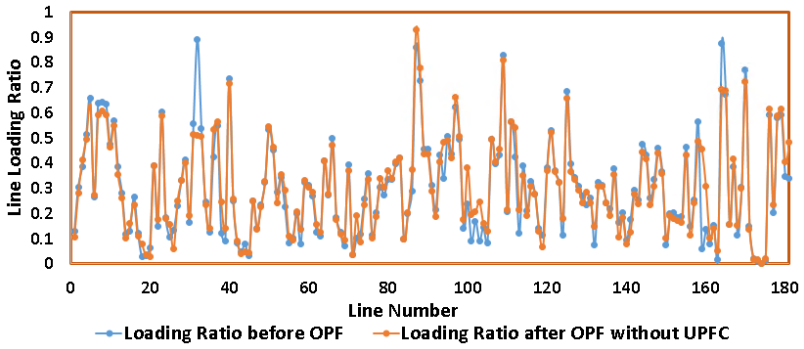

Figure 5.48: Base Case(118 Bus) Scenario 2 Line Loading Ratio

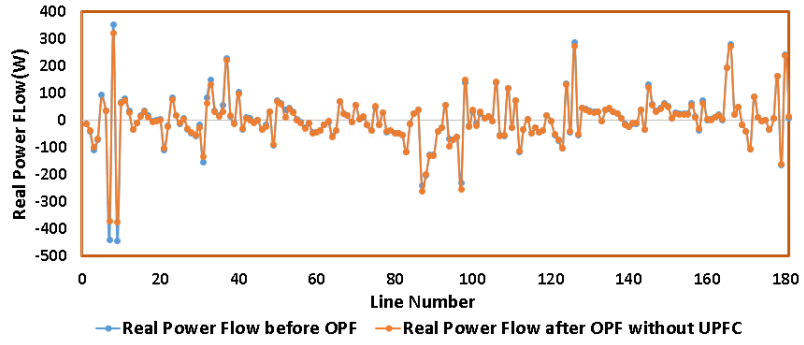

Figure 5.49: Base Case(118 Bus) Scenario 2 Real Power Flow

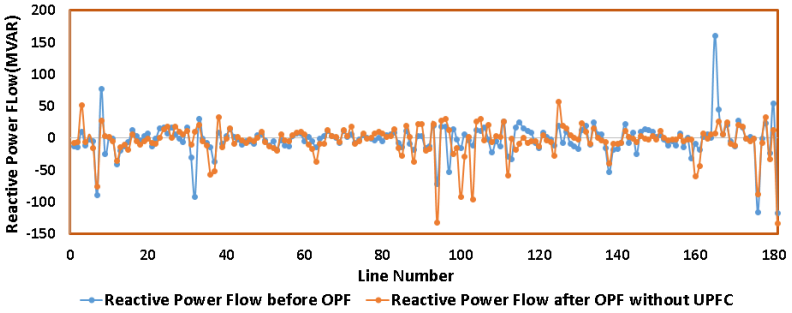

Figure 5.50: Base Case(118 Bus) Scenario 2 Reactive Power Flow

5.4.1.3 Base Case Scenario 3: All Pgen+All Qgen

In this scenario, all the real and reactive generation is allowed to vary. Since the 118 bus system is a large system, thus this scenario results in the largest reduction in line loading ratio. For larger systems, varying real and reactive generation together will give more control over line loading than varying only real generation. This is because the system is larger. The loading ratio, the real and reactive power flow are shown in Fig.5.51, Fig.5.52 and Fig.5.53.

Table 5.41: Base Case : Scenario 3 Loading Ratio Results

Generation Control	UPFC Installed	Before OPF	After OPF
All Qgen + All Pgen	No	0.6552	0.1453

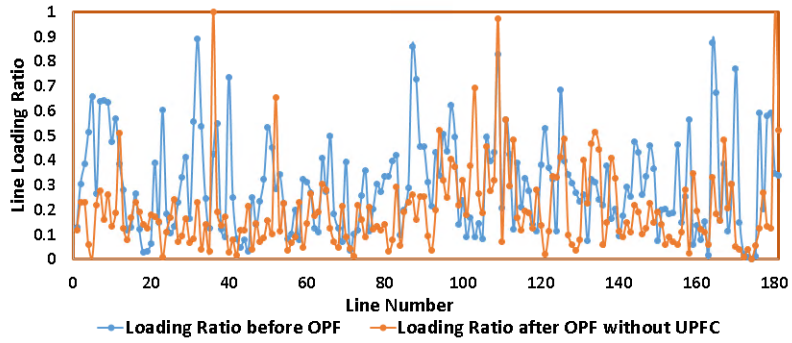

Figure 5.51: Base Case(118 Bus) Scenario 3 Line Loading Ratio

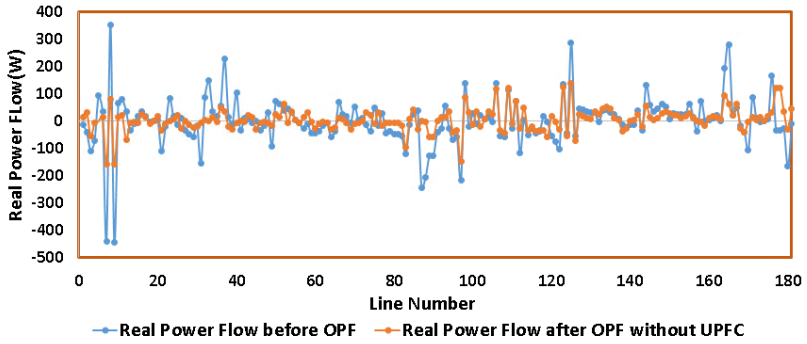

Figure 5.52: Base Case(118 Bus) Scenario 3 Real Power Flow

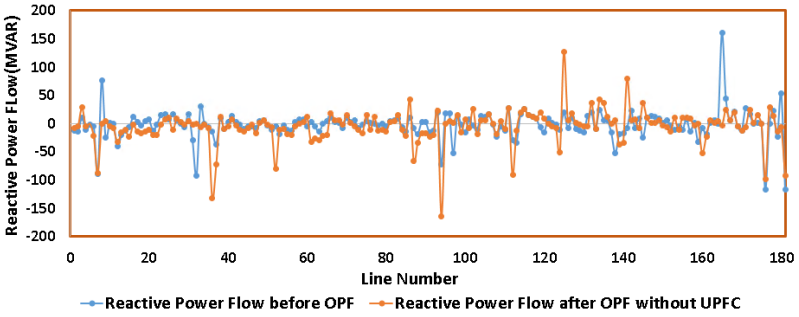

Figure 5.53: Base Case(118 Bus) Scenario 3 Reactive Power Flow

The summary of the base case results is given in Table.5.42.

Table 5.42: Summary of Base Case(118 Bus) Results

Generation Control	UPFC Installed	Before OPF	After OPF
All Pgen + Slack Qgen	No	0.6552	0.4507
All Qgen + Slack Pgen	No	0.6552	0.5948
All Qgen + All Pgen	No	0.6552	0.1453

5.4.2 Case A: UPFC Installed on Line 30-17

5.4.2.1 Case A Scenario 1: All Pgen+Slack Bus Qgen

In Case A, the UPFC is installed between buses 30 and 17. The change in line loading ratio is shown in Table.5.43. The UPFC is effective in reducing the line loading more as compared with the base case even for larger systems. Thus the addition of

the UPFC is effective. Note that for larger systems, choosing an effective location of the UPFC is very important. The choice of determining the effective location of the UPFC depends on the system topology as well as the location of the high loaded lines. The change in UPFC parameters is shown in Table.5.44. The line loading, the real and reactive power flow are shown in Fig.5.54,Fig.5.55 and Fig.5.56.

Table 5.43: Case A 118 Bus : Scenario 1 Loading Ratio Results

Generation Control	UPFC Installed	Before OPF	After OPF
All Pgen + Slack Qgen	No	0.6552	0.4507
All Pgen + Slack Qgen	Yes	0.6552	0.2784

Table 5.44: UPFC Parameters Case A 118 Bus: Scenario 1

UPFC Parameters	Before OPF	After OPF
MVA_{se}	33 MVA	155 MVA
MVA_{sh}	33 MVA	180 MVA
P_{sh}	0.4 MW	77 MW
Q_{sh}	41 MVAR	162 MVAR

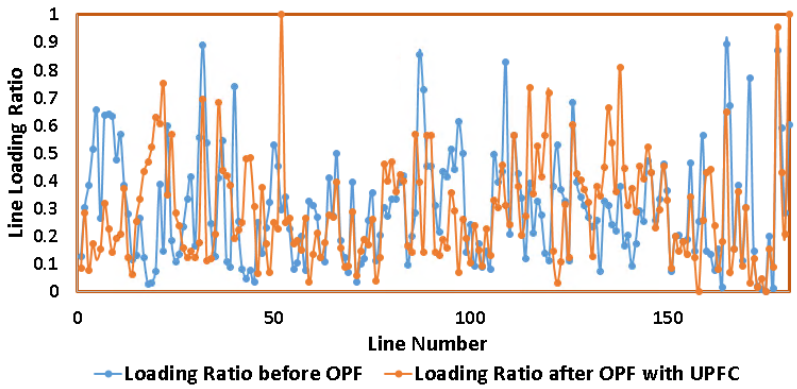

Figure 5.54: Case A(118 Bus) Scenario 1 Line Loading Ratio

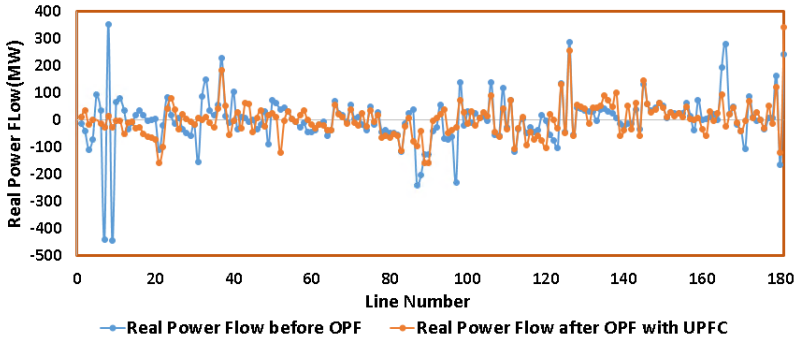

Figure 5.55: Case A(118 Bus) Scenario 1 Real Power Flow

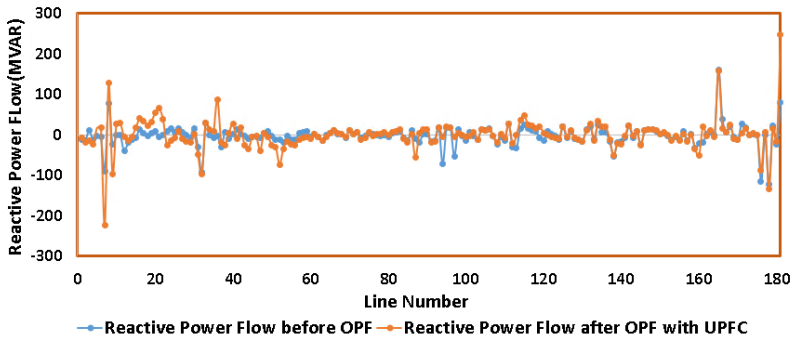

Figure 5.56: Case A(118 Bus) Scenario 1 Reactive Power Flow

5.4.2.2 Case A Scenario 2: All Qgen+Slack Bus Pgen

The change in line loading ratio is shown in Table.5.45. The UPFC is effective in reducing the line loading more as compared with the base case. Thus the addition of the UPFC is effective. The change in UPFC parameters is shown in Table.5.46. The line loading, the real and reactive power flow are shown in Fig.5.57,Fig.5.58 and Fig.5.59.

Table 5.45: Case A 118 Bus : Scenario 2 Loading Ratio Results

Generation Control	UPFC Installed	Before OPF	After OPF
All Qgen + Slack Pgen	No	0.6552	0.5948
All Qgen + Slack Pgen	Yes	0.6552	0.5762

Table 5.46: UPFC Parameters Case A 118 Bus: Scenario 2

UPFC Parameter(3-18 UPFC)	Before OPF	After OPF
MVA_{se}	33 MVA	75 MVA
MVA_{sh}	33 MVA	120 MVA
P_{sh}	0.4 MW	20 MW
Q_{sh}	41 MVAR	100 MVAR

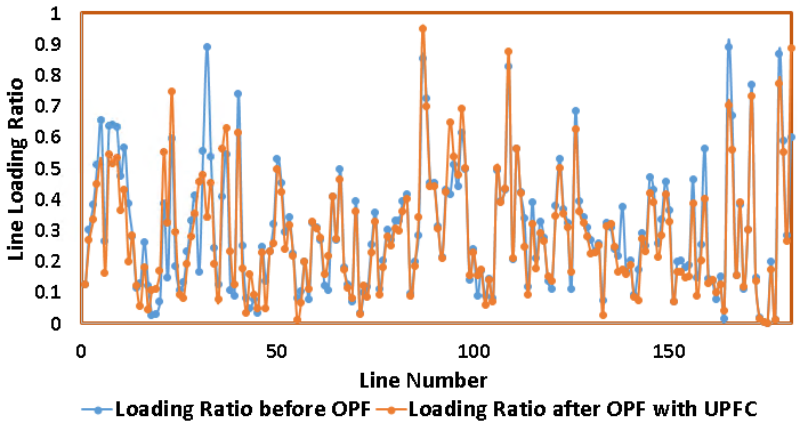

Figure 5.57: Case A(118 Bus) Scenario 2 Line Loading Ratio

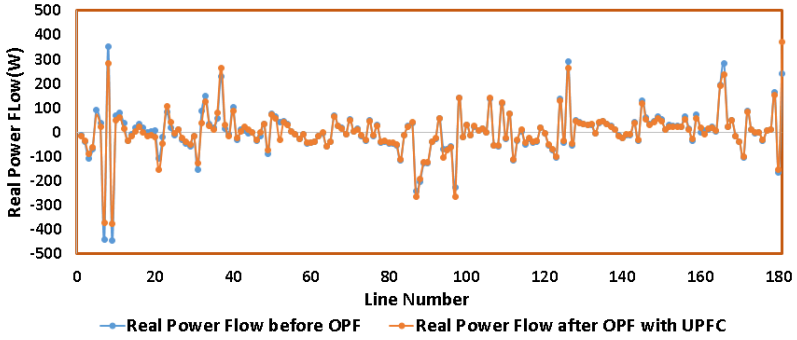

Figure 5.58: Case A(118 Bus) Scenario 2 Real Power Flow

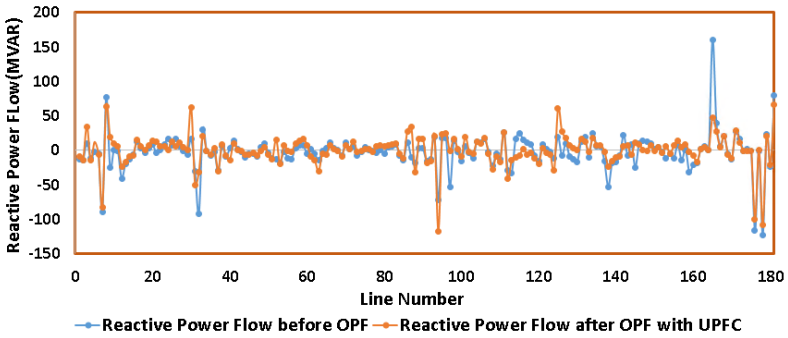

Figure 5.59: Case A(118 Bus) Scenario 2 Reactive Power Flow

5.4.2.3 Case A Scenario 3: All Qgen+All Pgen

The change in line loading ratio is shown in Table.5.47. The UPFC is not effective in reducing the line loading more as compared with the base case. This is because in this scenario, all the real and reactive generation is allowed to vary. The control over line flows given by the combination of real and reactive generation is sufficient to undermine the control over lines flows in the neighbouring lines of the UPFC location. It is important to remember that the in this system, the PV buses are located in proximity of every line as well as the number of PV buses is comparitively large which is 54 buses out of the total number of buses which is 118 buses. Thus, generation can undermine the control offered by UPFC within the region where the UPFC is installed.This will be discuused further in the subsequent section. The change in UPFC parameters is shown in Table.5.48. The line loading, the real and reactive power flow are shown in Fig.5.60,Fig.5.61 and Fig.5.62.

Table 5.47: Case A 118 Bus : Scenario 3 Loading Ratio Results

Generation Control	UPFC Installed	Before OPF	After OPF
All Qgen + All Pgen	No	0.6552	0.1453
All Qgen + All Pgen	Yes	0.6552	0.1682

Table 5.48: UPFC Parameters Case A 118 Bus: Scenario 3

UPFC Parameter	Before OPF	After OPF
MVA_{se}	33 MVA	134 MVA
MVA_{sh}	33 MVA	160 MVA
P_{sh}	0.4 MW	22 MW
Q_{sh}	41 MVAR	158 MVAR

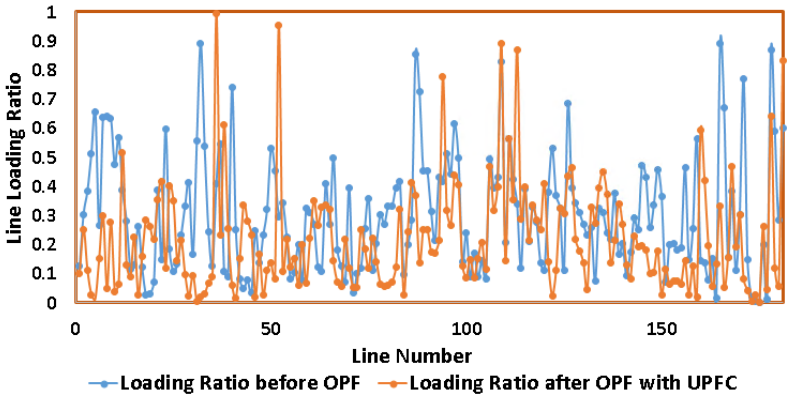

Figure 5.60: Case A(118 Bus) Scenario 3 Line Loading Ratio

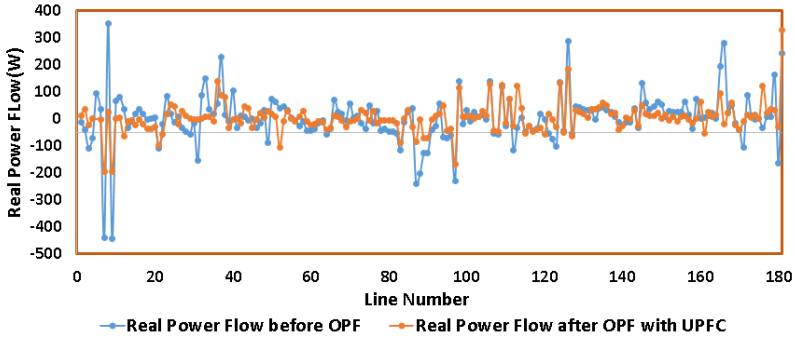

Figure 5.61: Case A(118 Bus) Scenario 3 Real Power Flow

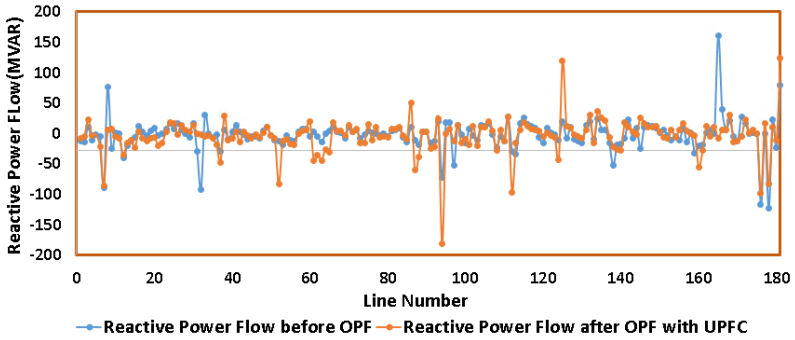

Figure 5.62: Case A(118 Bus) Scenario 3 Reactive Power Flow

A summary of Case A results is shown in Table. 5.49.

Table 5.49: Summary of Case A 118 Bus Results

Generation Control	UPFC Installed	Before OPF	After OPF
All Pgen + Slack Qgen	No	0.6552	0.4507
All Pgen + Slack Qgen	Yes	0.6552	0.2784
All Qgen + Slack Pgen	No	0.6552	0.5948
All Qgen + Slack Pgen	Yes	0.6552	0.5762
All Qgen + All Pgen	No	0.6552	0.1453
All Qgen + All Pgen	Yes	0.6552	0.1682

5.4.3 Case B: UPFC Installed on Line 65-66

5.4.3.1 Case B 118 Bus Scenario 1: All Pgen+Slack Bus Qgen

In Case B, the UPFC is installed between buses 65 and 66. The change in line loading ratio is shown in Table.5.50. The UPFC is effective in reducing the line loading more as compared with the base case. Thus the addition of the UPFC is effective. The change in UPFC parameters is shown in Table.5.51. The line loading, the real and reactive power flow are shown in Fig.5.63,Fig.5.64 and Fig.5.65.

Table 5.50: Case B 118 Bus : Scenario 1 Loading Ratio Results

Generation Control	UPFC Installed	Before OPF	After OPF
All Pgen + Slack Qgen	No	0.6552	0.4507
All Pgen + Slack Qgen	Yes	0.626	0.359

Table 5.51: UPFC Parameters Case B 118 Bus: Scenario 1

UPFC Parameters	Before OPF	After OPF
MVA_{se}	0.05 MVA	40 MVA
MVA_{sh}	122 MVA	120 MVA
P_{sh}	0.4 MW	-36 MW
Q_{sh}	-122 MVAR	-115 MVAR

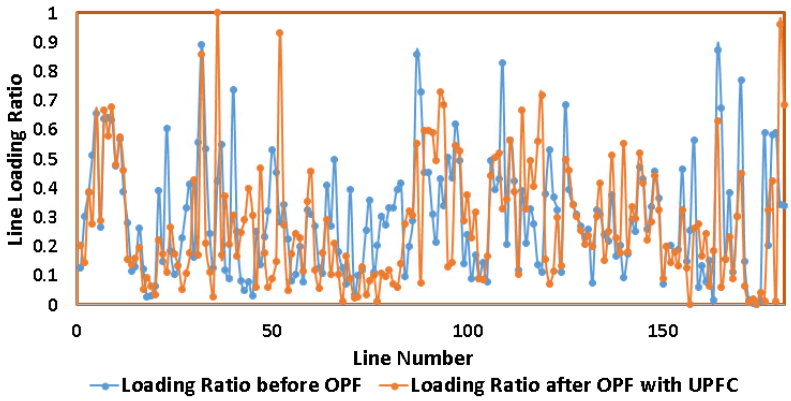

Figure 5.63: Case B(118 Bus) Scenario 1 Line Loading Ratio

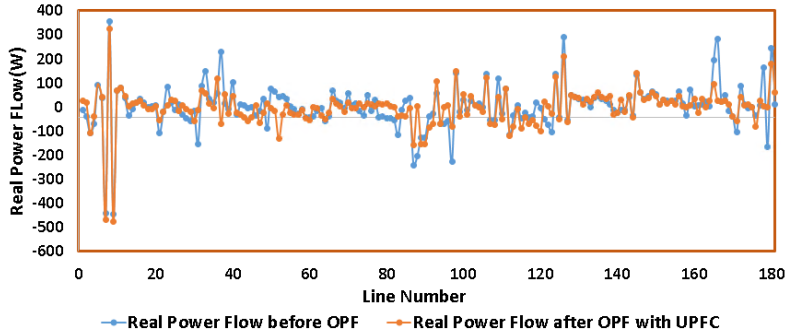

Figure 5.64: Case B(118 Bus) Scenario 1 Real Power Flow

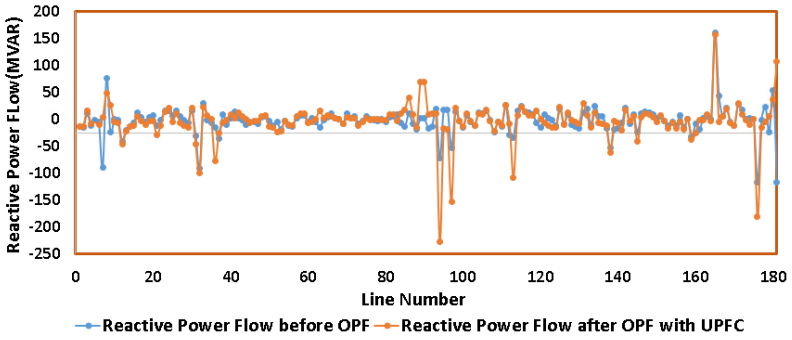

Figure 5.65: Case B(118 Bus) Scenario 1 Reactive Power Flow

5.4.3.2 Case B 118 Bus Scenario 2: All Qgen+Slack Bus Pgen

The change in line loading ratio is shown in Table.5.52. The UPFC is effective in reducing the line loading more as compared with the base case. Thus the addition of the UPFC is effective. The change in UPFC parameters is shown in Table.5.53. The line loading, the real and reactive power flow are shown in Fig.5.66,Fig.5.67 and Fig.5.68.

Table 5.52: Case B 118 Bus : Scenario 2 Loading Ratio Results

Generation Control	UPFC Installed	Before OPF	After OPF
All Qgen + Slack Pgen	No	0.6552	0.5948
All Qgen + Slack Pgen	Yes	0.6552	0.5839

Table 5.53: UPFC Parameters Case B 118 Bus: Scenario 2

UPFC Parameters	Before OPF	After OPF
MVA_{se}	0.05 MVA	30 MVA
MVA_{sh}	122 MVA	130 MVA
P_{sh}	0.4 MW	-20 MW
Q_{sh}	-122 MVAR	-127 MVAR

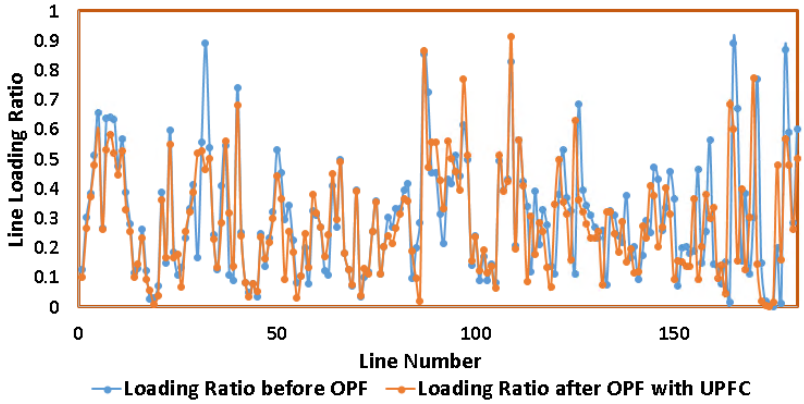

Figure 5.66: Case B(118 Bus) Scenario 2 Line Loading Ratio

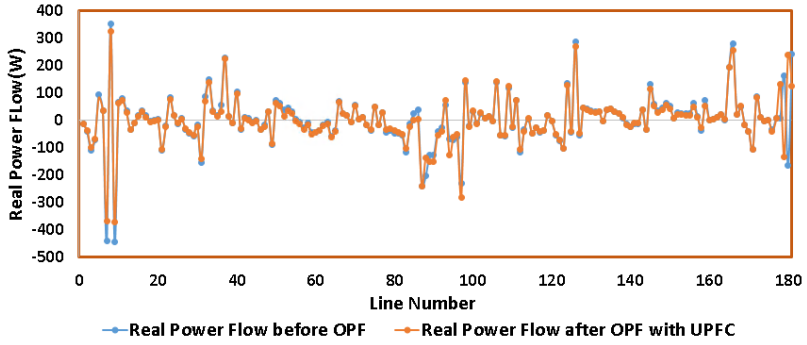

Figure 5.67: Case B(118 Bus) Scenario 2 Real Power Flow

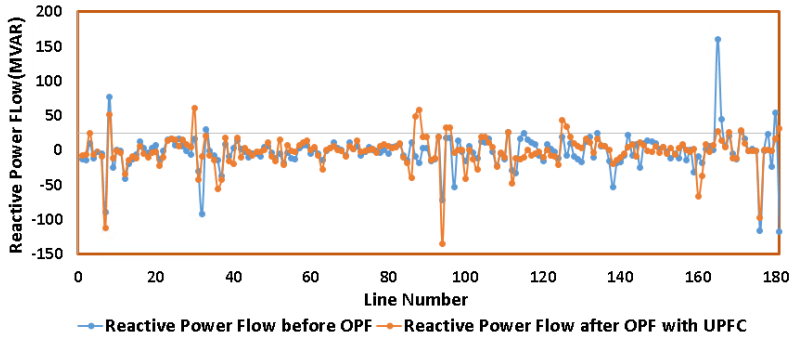

Figure 5.68: Case B(118 Bus) Scenario 2 Reactive Power Flow

5.4.3.3 Case B 118 Bus Scenario 3: All Qgen+All Pgen

The change in line loading ratio is shown in Table.5.54. The UPFC is not effective in reducing the line loading more as compared with the base case. As discussed in

the previous cases, this is because in this scenario, all the real and reactive generation is allowed to vary. The control over line flows given by the combination of real and reactive generation is sufficient to undermine the control over lines flows in the neighbouring lines of the UPFC location. The change in UPFC parameters is shown in Table.5.55. The line loading, the real and reactive power flow are shown in Fig.5.69,Fig.5.70 and Fig.5.71.

Table 5.54: Case B 118 Bus : Scenario 3 Loading Ratio Results

Generation Control	UPFC Installed	Before OPF	After OPF
All Qgen + All Pgen	No	0.6552	0.1453
All Qgen + All Pgen	Yes	0.6552	0.1452

Table 5.55: UPFC Parameters Case B 118 Bus: Scenario 3

UPFC Parameters	Before OPF	After OPF
MVA_{se}	0.05 MVA	20 MVA
MVA_{sh}	122 MVA	125 MVA
P_{sh}	0.4 MW	-25 MW
Q_{sh}	-122 MVAR	-120 MVAR

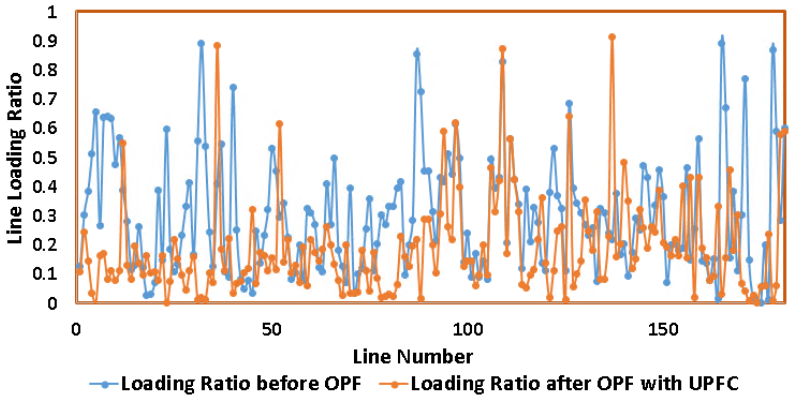

Figure 5.69: Case B(118 Bus) Scenario 3 Line Loading Ratio

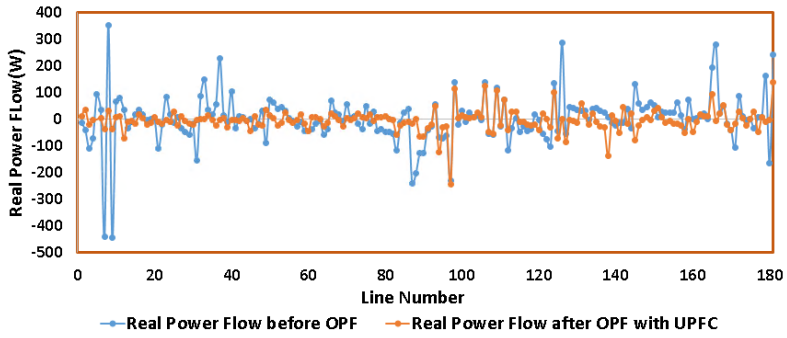

Figure 5.70: Case B(118 Bus) Scenario 3 Real Power Flow

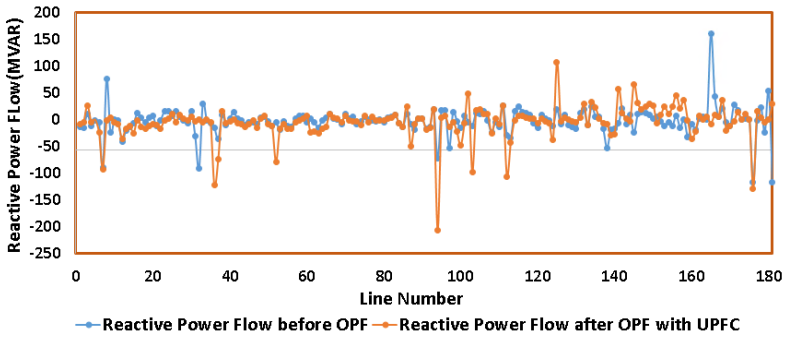

Figure 5.71: Case B(118 Bus) Scenario 3 Reactive Power Flow

A summary of Case B results is shown in Table.5.56.

Table 5.56: Summary of Case B 118 Bus Results

Generation Control	UPFC Installed	Before OPF	After OPF
All Pgen + Slack Qgen	No	0.6552	0.4507
All Pgen + Slack Qgen	Yes	0.652	0.359
All Qgen + Slack Pgen	No	0.6552	0.5948
All Qgen + Slack Pgen	Yes	0.6552	0.5839
All Qgen + All Pgen	No	0.6552	0.1453
All Qgen + All Pgen	Yes	0.6552	0.1452

5.4.4 Case C: UPFC Installed on Line 30-17 and 65-66

5.4.4.1 Case C 118 Bus Scenario 1: All Pgen+Slack Bus Qgen

In Case C, two UPFCs are installed. One of them is installed between bus 30 and 17 and the second UPFC is installed between bus 65 and 66. The change in line loading ratio is shown in Table.5.57. The UPFC is effective in reducing the line loading more as compared with the base case. Thus the addition of the UPFC is effective. Compared with Case A and Case B, where only one UPFC was installed, two UPFCs are able to provide a larger reduction in loading ratio in Case C. This suggests that given an effective location of the UPFC, they are able to provide additional control over line flows in addition to generation. The change in UPFC parameters is shown in Table.5.58. The line loading, the real and reactive power flow are shown in Fig.5.72,Fig.5.73 and Fig.5.74.

Table 5.57: Case C 118 Bus : Scenario 1 Loading Ratio Results

Generation Control	UPFC Installed	Before OPF	After OPF
All Pgen + Slack Qgen	No	0.6552	0.4507
All Pgen + Slack Qgen	Yes	0.652	0.2410

Table 5.58: UPFC Parameters 30-17 Case C 118 Bus: Scenario 1

UPFC Parameters	Before OPF	After OPF
MVA_{se}	33 MVA	150 MVA
MVA_{sh}	33 MVA	138 MVA
P_{sh}	0.4 MW	60 MW
Q_{sh}	41 MVAR	122 MVAR

Table 5.59: UPFC Parameters 65-66 Case C 118 Bus: Scenario 1

UPFC Parameters	Before OPF	After OPF
MVA_{se}	5 MVA	30 MVA
MVA_{sh}	80 MVA	92 MVA
P_{sh}	1.4 MW	-28 MW
Q_{sh}	-80 MVAR	-88 MVAR

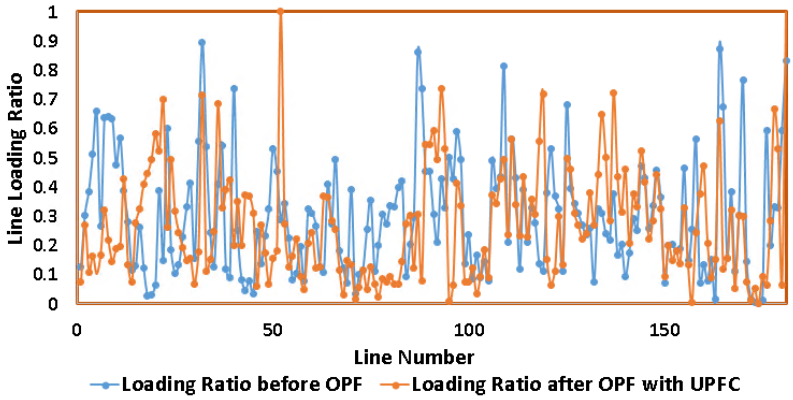

Figure 5.72: Case C(118 Bus) Scenario 1 Line Loading Ratio

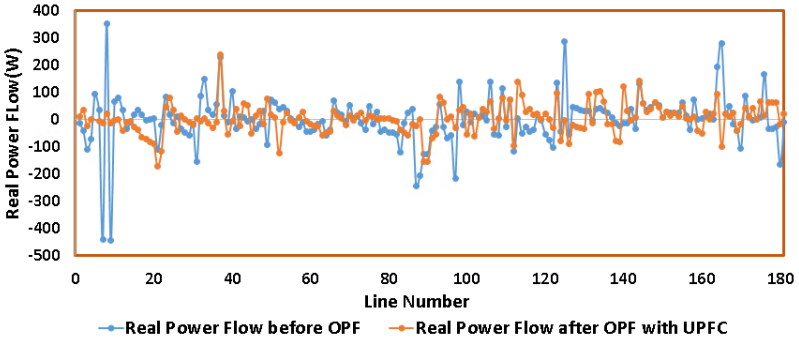

Figure 5.73: Case C(118 Bus) Scenario 1 Real Power Flow

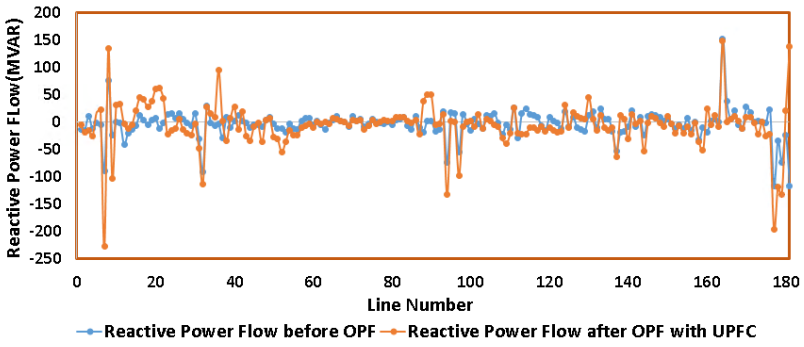

Figure 5.74: Case C(118 Bus) Scenario 1 Reactive Power Flow

5.4.4.2 Case C 118 Bus Scenario 2: All Qgen+Slack Bus Pgen

The change in line loading ratio is shown in Table.5.60. Case C is able to provide larger reduction in Scenario 2 compared with Case A and Case B thus two UPFCs are able to provide more control over line flows compared with one UPFC. The change in UPFC parameters is shown in Table.5.61 and Table.5.62. The line loading, the real and reactive power flow are shown in Fig.5.75,Fig.5.76 and Fig.5.77.

Table 5.60: Case C 118 Bus : Scenario 2 Loading Ratio Results

Generation Control	UPFC Installed	Before OPF	After OPF
All Qgen + Slack Pgen	No	0.6552	0.5948
All Qgen + Slack Pgen	Yes	0.6552	0.5642

Table 5.61: UPFC Parameters 30-17 Case C 118 Bus: Scenario 2

UPFC Parameters	Before OPF	After OPF
MVA_{se}	33 MVA	83 MVA
MVA_{sh}	33 MVA	83 MVA
P_{sh}	0.4 MW	23 MW
Q_{sh}	41 MVAR	77 MVAR

Table 5.62: UPFC Parameters 65-66 Case C 118 Bus: Scenario 2

UPFC Parameters	Before OPF	After OPF
MVA_{se}	5 MVA	18 MVA
MVA_{sh}	80 MVA	85 MVA
P_{sh}	1.4 MW	-17 MW
Q_{sh}	-80 MVAR	-81 MVAR

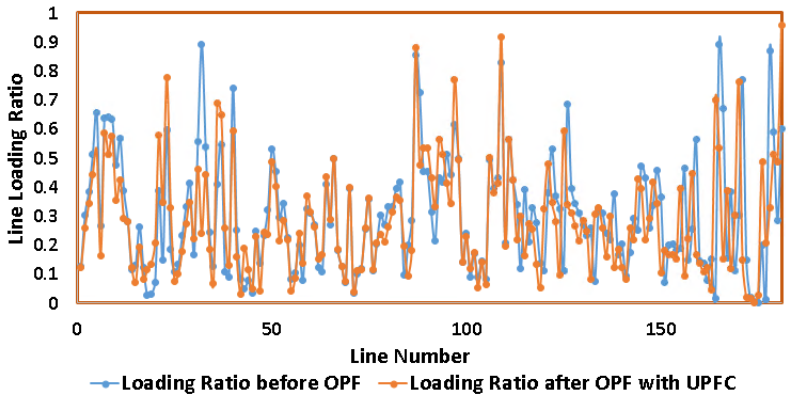

Figure 5.75: Case C(118 Bus) Scenario 2 Line Loading Ratio

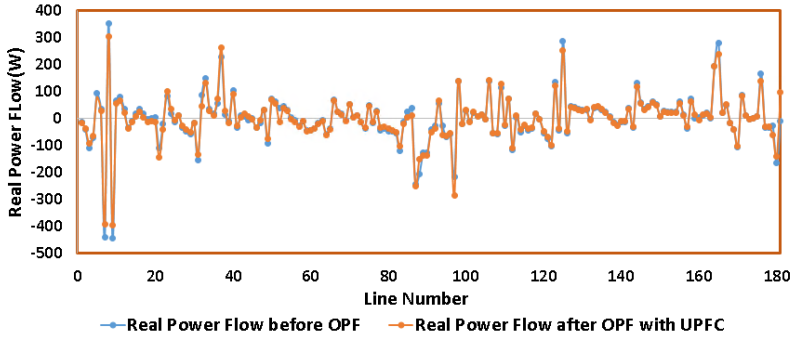

Figure 5.76: Case C(118 Bus) Scenario 2 Real Power Flow

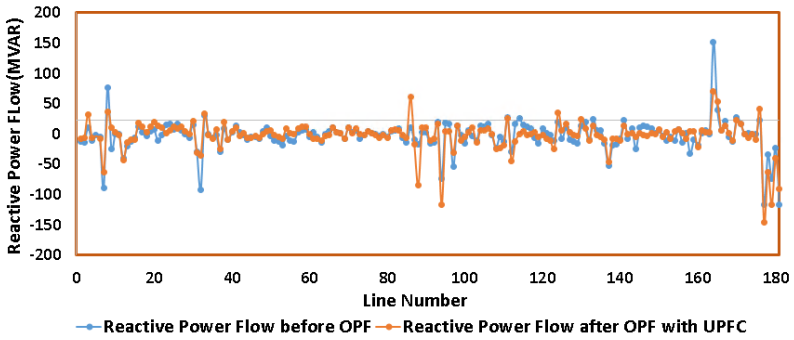

Figure 5.77: Case C(118 Bus) Scenario 2 Reactive Power Flow

5.4.4.3 Case C 118 Bus Scenario 3: All Qgen+ALL Pgen

The change in line loading ratio is shown in Table.5.63. The UPFC is not effective in reducing the line loading more as compared with the base case. As discussed in the previous cases, this is because in this scenario, all the real and reactive generation is allowed to vary. The control over line flows given by the combination of real and reactive generation is sufficient to undermine the control over lines flows in the neighbouring lines of the UPFC location. The change in UPFC parameters is shown in Table.5.64 and Table.5.65. The line loading, the real and reactive power flow are shown in Fig.5.78,Fig.5.79 and Fig.5.80.

Table 5.63: Case C 118 Bus : Scenario 3 Loading Ratio Results

Generation Control	UPFC Installed	Before OPF	After OPF
All Qgen + All Pgen	No	0.6552	0.1453
All Qgen + All Pgen	Yes	0.6552	0.1442

Table 5.64: UPFC Parameters 30-17 Case C 118 Bus: Scenario 3

UPFC Parameters	Before OPF	After OPF
MVA_{se}	33 MVA	64 MVA
MVA_{sh}	33 MVA	61 MVA
P_{sh}	0.4 MW	-6 MW
Q_{sh}	41 MVAR	61 MVAR

Table 5.65: UPFC Parameters 65-66 Case C 118 Bus: Scenario 3

UPFC Parameters	Before OPF	After OPF
MVA_{se}	5 MVA	21 MVA
MVA_{sh}	80 MVA	86 MVA
P_{sh}	1.4 MW	-21 MW
Q_{sh}	-80 MVAR	-83 MVAR

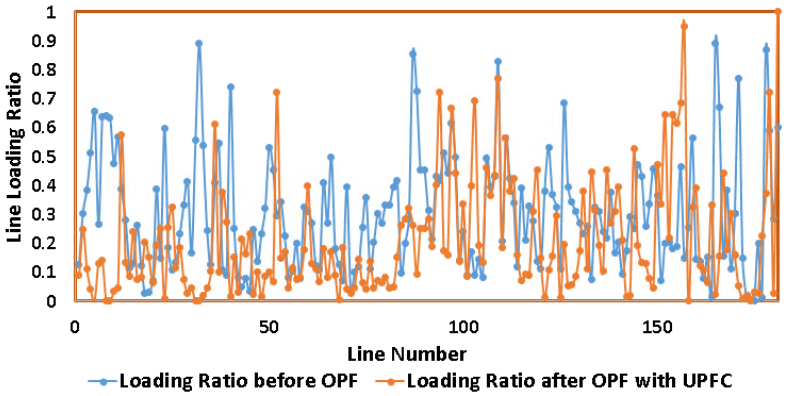

Figure 5.78: Case C(118 Bus) Scenario 3 Line Loading Ratio

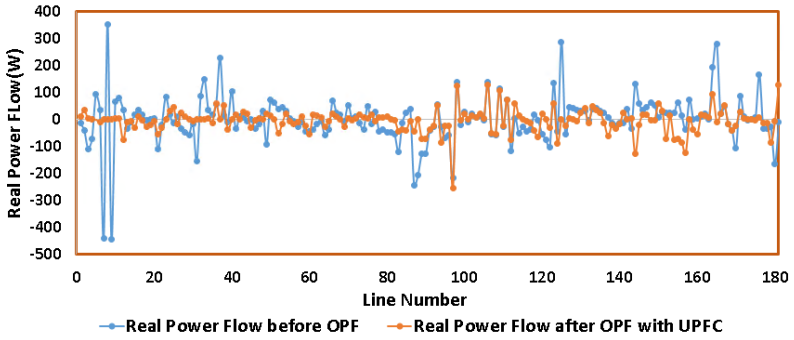

Figure 5.79: Case C(118 Bus) Scenario 3 Real Power Flow

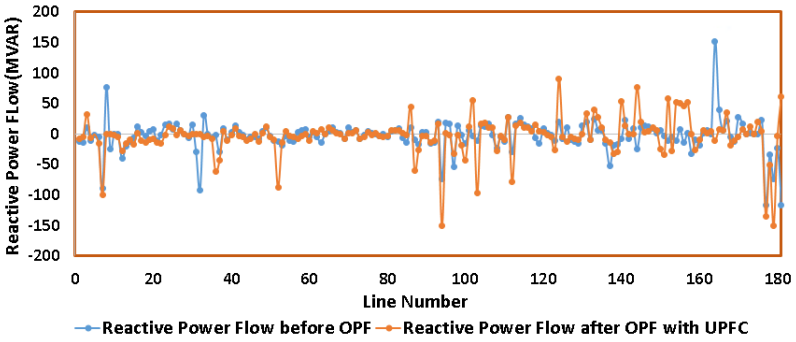

Figure 5.80: Case C(118 Bus) Scenario 3 Reactive Power Flow

A summary of the results for Case C are shown in Table.5.66.

Table 5.66: Summary of Case C 118 Bus Results

Generation Control	UPFC Installed	Before OPF	After OPF
All Pgen + Slack Qgen	No	0.6552	0.4507
All Pgen + Slack Qgen	Yes	0.652	0.2410
All Qgen + Slack Pgen	No	0.6552	0.5948
All Qgen + Slack Pgen	Yes	0.6552	0.5642
All Qgen + All Pgen	No	0.6552	0.1453
All Qgen + All Pgen	Yes	0.6552	0.1442

5.4.5 A Discussion on Control Region of UPFC 118 Bus System

The results discussed thus far for the 118 bus system show that given an effective location of the UPFC, it can provide additional control over line flows in addition to generation control. The summary of the results for the 118 bus is given in Table.5.67. For 118 bus, the UPFC is effective when either real or reactive generation is allowed to vary. It is not effective when both the real and reactive generation are allowed to vary. This is due to the topology of the 118 bus system. As can be seen in Fig.5.81, the 54 generators are evenly spread out at buses across the system. Furthermore, the high loaded lines in Fig.5.81 are also not located in a specific area of the system. This means that the high loaded lines are located within close radius of a generation bus and thus the power flow of that line can be affected by the generation located on the neighbouring PV buses. However, the UPFC can still provide advantage in addition to the control over line flows provided by generation. In the results discussed thus far, the UPFC is located either on line between buses 30-17 or 65-66 as shown in Fig.5.81. The high loaded lines located within close proximity of the two locations shown by the red rectangle can have their power flows affected by the UPFC indirectly. This location is effective as the red rectangles contain a number of high loaded lines in its reach. The effectiveness of the UPFC can be seen by All Pgen+Slack Qgen and All Qgen+Slack Pgen case. The UPFC is not effective in All Qgen+All Pgen case as the generation control is effective enough to undermine the control offered by the UPFC within its neighbouring lines.

Table 5.67: Summary of 118 Bus Results

Generation Control	UPFC Location	Before OPF	After OPF
All Pgen + Slack Qgen	No	0.6552	0.4507
All Pgen + Slack Qgen	Line 30-17	0.652	0.2784
All Pgen + Slack Qgen	Line 65-66	0.6552	0.359
All Pgen + Slack Qgen	Line 65-66 and 30-17	0.6552	0.2410
All Qgen + Slack Pgen	No	0.6552	0.5948
All Qgen + Slack Pgen	Line 30-17	0.652	0.5762
All Qgen + Slack Pgen	Line 65-66	0.6552	0.5839
All Qgen + Slack Pgen	Line 65-66 and 30-17	0.6552	0.5642
All Qgen + All Pgen	No	0.6552	0.1453
All Qgen + All Pgen	Line 30-17	0.652	0.1683
All Qgen + All Pgen	Line 65-66	0.6552	0.1452
All Qgen + All Pgen	Line 65-66 and 30-17	0.6552	0.1442

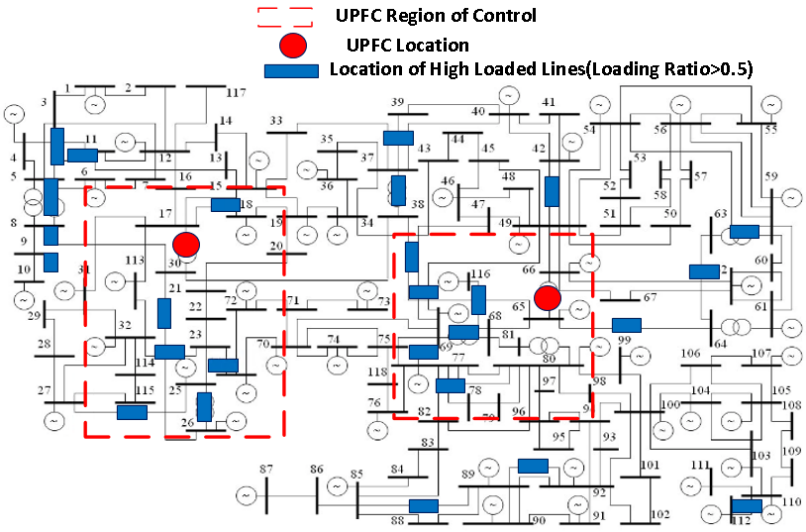

Figure 5.81: UPFC Control Region 118 Bus

5.5 A Discussion on Voltage Improvement with UPFC

5.5.1 39 Bus System

5.5.1.1 UPFC Location 16-17

The voltage profile for the 39 Bus System Case A is shown in Fig.5.82 and Fig.5.83. It can be seen that in Scenario 1 from Fig.5.82, the voltage of bus 17 is lower in the UPFC case than in the non-UPFC case. That is because it can been seen from Table.5.68 that the UPFC absorbs 70 MVAR of reactive power at the shunt voltage source located at its PV bus. In Scenario 2 voltage profile Fig.5.83, the voltage of bus 17 is higher in the UPFC case than the non-UPFC case. It can been seen from Table.5.68 that the UPFC supplies 160 MVAR of reactive power that is why the voltage of bus 17 is improved in the UPFC case.

Table 5.68: UPFC Location 16-17 Qsh

UPFC Location	16-17
Scenario 1 Qsh	70 MVAr Absorbed
Scenario 2 Qsh	160 MVAr Supplied

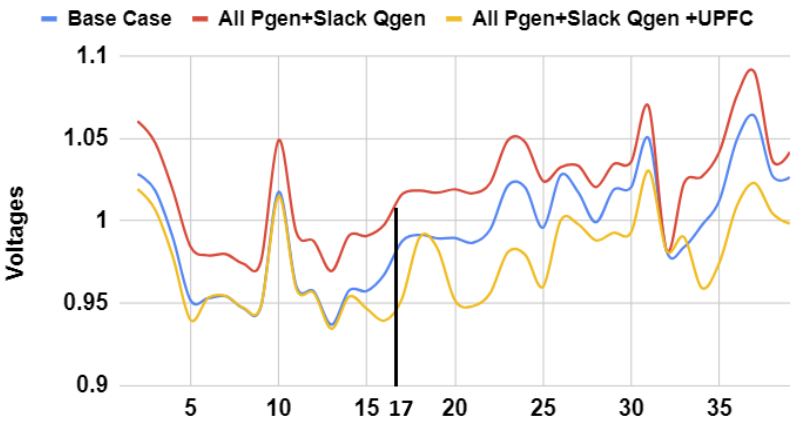

Figure 5.82: UPFC Location 16-17 Voltage Scenario 1

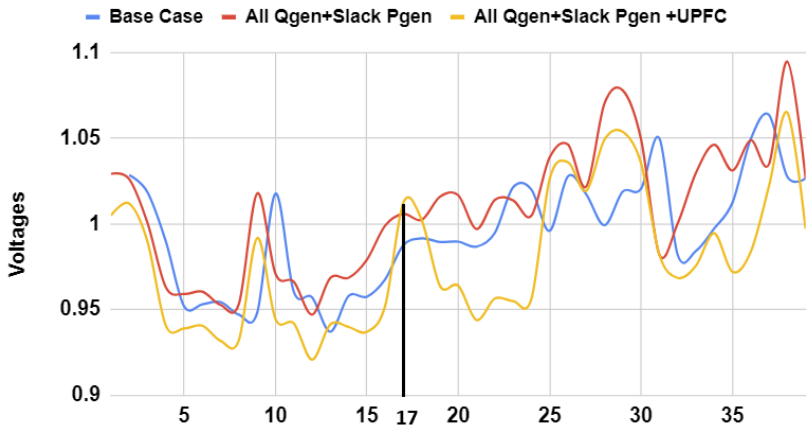

Figure 5.83: UPFC Location 16-17 Voltage Scenario 2

5.5.1.2 UPFC Location 3-18

It can be seen that in Scenario 1 from Fig.5.84, the voltage of bus 18 is lower in the UPFC case than in the non-UPFC case. That is because it can been seen from Table.5.69 that the UPFC absorbs 5 MVAr of reactive power at the shunt voltage source located at its PV bus. In Scenario 2 voltage profile Fig.UPFC Location 3-18 Voltage Scenario 2, the voltage of bus 18 is higher in the UPFC case than the non-UPFC case. It can been seen from Table.5.69 that the UPFC supplies 250 MVAR of reactive power that is why the voltage of bus 18 is improved in the UPFC case.

Table 5.69: UPFC Location 3-18 Qsh

UPFC Location	3-18
Scenario 1 Qsh	5 MVAr Absorbed
Scenario 2 Qsh	250 MVAr Supplied

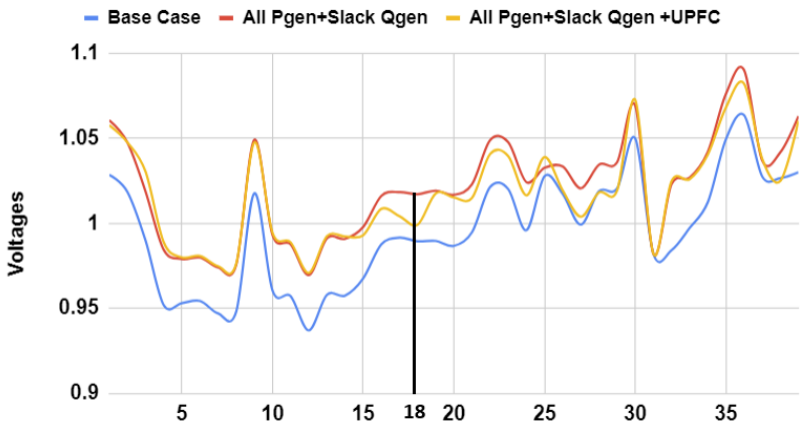

Figure 5.84: UPFC Location 3-18 Voltage Scenario 1

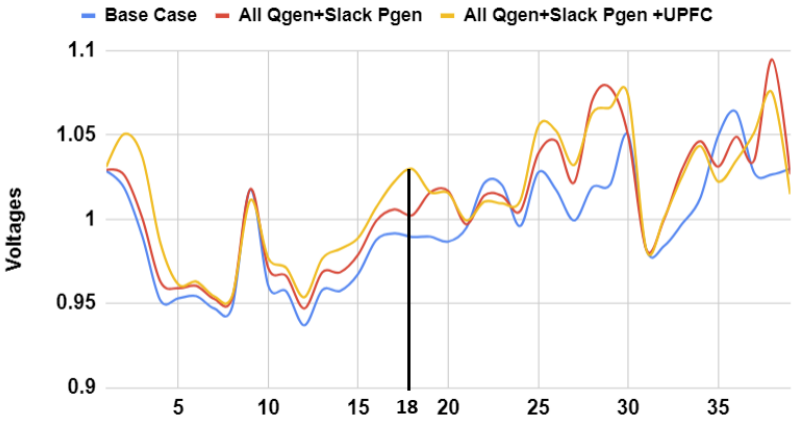

Figure 5.85: UPFC Location 3-18 Voltage Scenario 2

5.5.2 118 Bus System

It can be seen that in Scenario 1 from Fig.5.86, the voltage of bus 17 is lower in the UPFC case than in the non-UPFC case. That is because it can been seen from Table.5.70 that the UPFC absorbs 162 MVAr of reactive power at the shunt voltage source located at its PV bus. In Scenario 2 voltage profile Fig.5.87, the voltage of bus 18 is lower in the UPFC case than the non-UPFC case. It can been seen from Table.5.70 that the UPFC absorbes 100 MVAR of reactive power that is why the voltage of bus 17 is lower in the UPFC case.

Table 5.70: UPFC Location 30-17 Qsh

UPFC Location	30-17
Scenario 1 Qsh	162 MVAr Absorbed
Scenario 2 Qsh	100 MVAr Absorbed

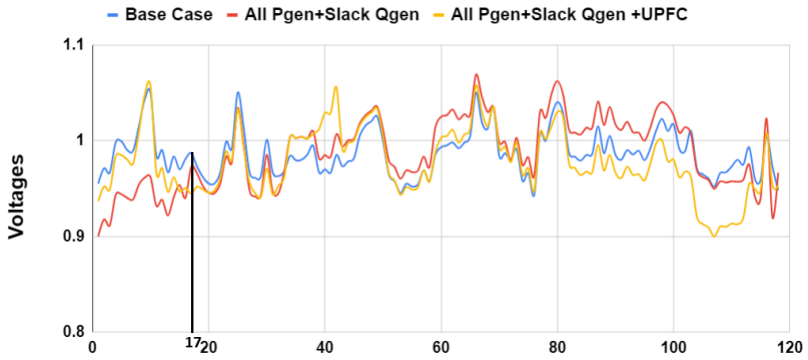

Figure 5.86: UPFC Location 30-17 Voltage Scenario 1

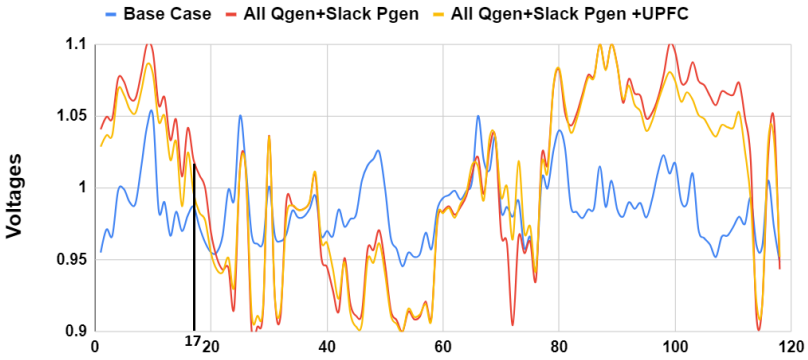

Figure 5.87: UPFC Location 30-17 Voltage Scenario 2

5.6 Comparison with TCSC Model

5.6.1 Problem incorporating TCSC in the LPOPF Model

Since the bus injection model of a TCSC is a decoupled model, thus incorporating it in a single LPOPF iteration has certain difficulties. In a decoupled model, the real and reactive power flows are modelled in seperate power flow equations. However, an approximate comparison can be made using the UPFC-based LPOPF model presented

in this chapter. The bus injection model of TCSC is shown in the Fig.5.88. It can be seen that since the TCSS only controls real power flow thus the bus injection at Bus i' can be controlled. To incorporate it with in the LPOPF model, the real and reactive power flow equations have to solved within a single iteration. However, this is not possible within the LPOPF model. Furthermore, the LPOPF model is already an approximation around the AC power flow operating point. Further error will be introduced if the power flow equations in sepertate Jacobian matrices for the real and reactive power flow equations.

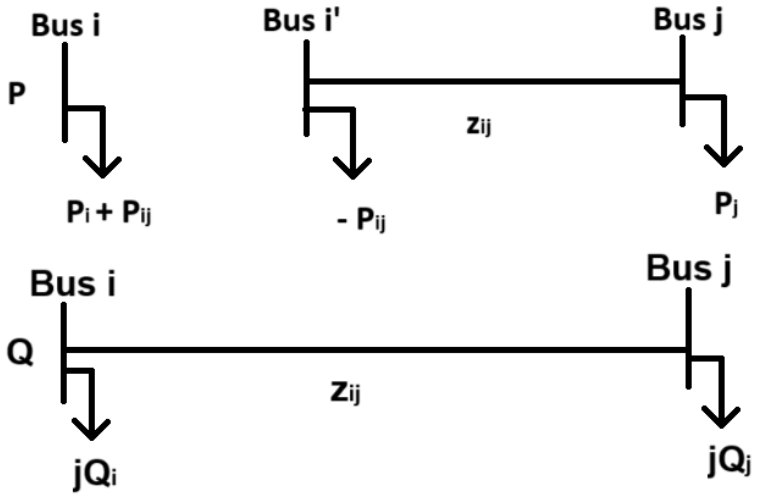

Figure 5.88: Decoupled TCSC Bus Injection Model

Moreover, another option is to the incorporate the TCSC series reactance model to model the TCSC line which is shown in Fig.5.89. The main thing to remember is that all the equations in the LPOPF must be linear or linearised with respect to the Power system state variables. Thus, with the conductance and suspectance equations given in Eq.5.2 and Eq.5.3, it can be seen that the variable TCSC reactance is located in the denominator in a squared term. Linearising this with respect to the power system state variables in the real and reactive power flow equations is not possible since this term will have higher powers(like cubed) when it is linearized.

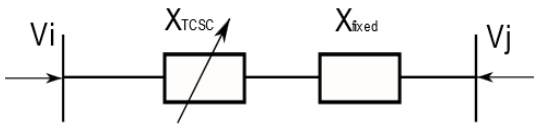

Figure 5.89: TCSC Series Reactance Model

The impedance of the line between bus i and bus j is given by Eq. 5.1.

$$z_k = r_k + j(x_k + x_{tcsc}) = \frac{1}{g_k + b_k} \tag{5.1}$$

The conductance and susceptance are given by Eq.5.2 and Eq.5.3.

$$g_{nm} = \frac{r_{nm}}{r_{nm}^2 + (x_{nm} + x_{tcsc})^2} \tag{5.2}$$

$$b_{nm} = \frac{(x_{nm} + x_{tcsc})}{r_{nm}^2 + (x_{nm} + x_{tcsc})^2} \tag{5.3}$$

The comparison between the UPFC and TCSC can be done based on the fact that UPFC can control real and reactive power flow independtly while the TCSC can only control real power flow. Even though this comparison will be approximate, but if the reactive power flow in a UPFC is fixed, then that can approximate the real power flow control provided by the TCSC.

5.6.2 All real and all reactive gen allowed to change

One case is tested where all real and reactive generation is allowed to change however two scenarios are tested. One of the scenarios is where the reactive flow in a UPFC is fixed while in the other scenario, the reactive flow in a UPFC is not fixed. From Table.5.71, it can seen that the additional gain in line loading ratio reduction is 0.009, so it is clear the real power control has larger part in line loading management. Thus, Fix UPFC Q Flow represents the real power flow control provided by TCSC approximately while Allow UPFC Q flow represents the combined impact of real

and reactive power flow control capability. Thus, this can provide an approximate comparison between TCSC and UPFC.

Table 5.71: Sample Case 1 Comparison TCSC and UPFC-All Pgen and Qgen

Description	Loading Ratio
Initial Loading Ratio before OPF	0.7245
After OPF Loading Ratio(Fix UPFC Q flow)	0.6498
After OPF Loading Ratio(Allow UPFC Q flow)	0.6408
Gain due to Additional UPFC reactive control	0.009

5.6.3 All real gen only allowed to change

In this case, only the real generation is allowed to change. It can be seen that the gain in additional reduction due to UPFC reactive control is 0.0005. This is smaller as compared to the gain in additional reduction in the case where all the real and reactive generation is allowed to change as shown in Table.5.71. This confirms that the UPFC's reactive power control capability does give additional benefit even in case where the reactive power flows have less leverage to change by fixing the reactive generation. Though this additional control may be smaller given by 0.0005 but still it is an additional gain over the control provided by TCSC only.

Table 5.72: Sample Case 2 Comparison TCSC and UPFC-All Pgen

Description	Loading Ratio
Initial Loading Ratio before OPF	0.7245
After OPF Loading Ratio(Fix UPFC Q flow)	0.6599
After OPF Loading Ratio(Allow UPFC Q flow)	0.6594
Gain due to Additional UPFC reactive control	0.0005

5.6.4 All reactive gen only allowed to change

Table 5.73: Sample Case 3 Comparison TCSC and UPFC-All Qgen

Description	Loading Ratio
Initial Loading Ratio before OPF	0.7245
After OPF Loading Ratio(Fix UPFC Q flow)	0.7187
After OPF Loading Ratio(Allow UPFC Q flow)	0.7098
Gain due to Additional UPFC reactive control	0.0089

5.7 Summary and Main Contribution

The Main contribution of this chapter is listed below:

- The LPOPF formulation proposed in this chapter co-optimizes UPFC control and real and reactive generation control to optimally manage the power flows in a power system. This has been tested out for three scenarios: only real generation control, only reactive generation control and combined real and reactive generation control. All three scenarios are simulated in presence of UPFC control. The results show that the UPFC presents additional benefit in controlling the line flows even when real and reactive generation control is present. This shows that the UPFC presents some value in its installation for different control scenarios.

A summary of the cases studied in this chapter is shown in Table.5.74 and Table.5.75. Further, it takes into account UPFC device ratings in an LPOPF format which is computationally efficient. This formulation can be made further use of in day-ahead markets where the optimal setpoints of UPFC may need to determined along with generation setpoints for reducing generation cost. However, this has not been considered in this study.

Table 5.74: Summary of the 39 Bus Cases studied for UPFC and synchronous generation control

39 Bus System			
UPFC Loc.	Control Scenario	Before OPF	After OPF
None	All Pgen+Slack Qgen	0.7289	0.6163
None	All Qgen+Slack Pgen	0.7289	0.7267
None	All Qgen+All Pgen	0.7289	0.6070
3-18	All Pgen+Slack Qgen	0.7289	0.5433
3-18	All Qgen+Slack Pgen	0.7289	0.695
3-18	All Qgen+All Pgen	0.7289	0.5416
11-12	All Pgen+Slack Qgen	0.7289	0.6044
11-12	All Qgen+Slack Pgen	0.7289	0.6997
11-12	All Qgen+All Pgen	0.7289	0.5886
16-17	All Pgen+Slack Qgen	0.7289	0.6062
16-17	All Qgen+Slack Pgen	0.7289	0.7166
16-17	All Qgen+All Pgen	0.7289	0.6085

Table 5.75: Summary of the 118 Bus Cases studied for UPFC and synchronous generation control

118 Bus System			
UPFC Loc.	Control Scenario	Before OPF	After OPF
None	All Pgen+Slack Qgen	0.6552	0.4507
None	All Qgen+Slack Pgen	0.6552	0.5948
None	All Qgen+All Pgen	0.6552	0.1453
30-17	All Pgen+Slack Qgen	0.6552	0.2784
30-17	All Qgen+Slack Pgen	0.6552	0.5762
30-17	All Qgen+All Pgen	0.6552	0.1682
65-66	All Pgen+Slack Qgen	0.6552	0.359
65-66	All Qgen+Slack Pgen	0.6552	0.5839
65-66	All Qgen+All Pgen	0.6552	0.1452
30-17,65-66	All Pgen+Slack Qgen	0.6552	0.2410
30-17,65-66	All Qgen+Slack Pgen	0.6552	0.5642
30-17,65-66	All Qgen+All Pgen	0.6552	0.1442

CHAPTER 6: OPTIMAL LOCATION OF MULTIPLE UPFC WITH OPTIMAL POWER FLOW MANAGEMENT FOR LNINE LOADING OPTIMIZATION

6.1 Introduction and Literature Review

The optimal location of FACTS device is important in regards to gaining the maximum benefit from the installed FACTs device with respect to a certain objective. The installation cost of FACTs device is relatively high thus power system operators will only be willing to invest in it if the relative benefit obtained from it outweights its capital cost. For that, various optimization techniques for locating the FACTs device in an optimal location have been studied. These methods include sensitvity based methods, population based methods, linear/non linear integer programming methods, analytic methods etc. The choice of optimization method depends on the specific problem. Often, choosing between two methods depends on finding a balance between accuracy and computational efficiency. For example mixed integer programming methods are able to find the global solution but are computationally burdensome for large scale problems. Metaheuristic methods may not always find the global optimum but are easily adaptable for continuous as well as discrete optimization problems. Population based algorithms have generally attracted attention in regards to FACTS device optimization due to its ease of computation. Among them the most popular is Particle Swarm Optimization. However, for PSO the internal parameters of the algorithm need to be tuned with respect to each respective optimization problem which may not always be a straightforward task. A list of various optimization methods is listed below:

- Classical Optimization: Mixed Integer Linear Programmin,/Mixed Integer Non-

Linear Programming .

- Evolutionary Methods:Genetic Algorithms,NSGA, Differential Evolution, Genetic Programming.
- Swarm-Based Methods:Particle Swarm Optimization, Whale optimization algorithm, Artifical Bee Algorithm,Coral Reefs Optimization,Common Scrambling Algorithm, Grasshopper Optimization Algorithm etc.
- Analytic Methods/Sensitive Index Techniques.

A recently introduced algorithm called the Teaching Learning Based Algorithm has been introduced in 2014. It is an optimization algorithm where there are no internal parameters to tune. The algorithm has the advantage that it can be used for continuous as well as discrete functions. The algorithm is easy to apply for various problems.

6.1.1 Comparison of TLBO with other algorithms

Like GA, PSO, TLBO is also a population-based technique which implements a group of solutions to proceed to the optimum solution. Many optimization methods require algorithm parameters that affect the performance of the algorithm. GA requires the crossover probability, mutation rate, and selection method; PSO requires learning factors, the variation of weight, and the maximum value of velocity. Unlike other optimization techniques TLBO does not require any algorithm parameters to be tuned, thus making the implementation of TLBO simpler. As in PSO, TLBO uses the best solution of the iteration to change the existing solution in the population, thereby increasing the convergence rate. As in GA, which uses selection, crossover and mutation, and ABC, which uses employed, onlooker and scout bees, TLBO uses two different phases, the âteacher phaseâ and the âlearner phaseâ. TLBO uses the mean value of the population to update the solution. TLBO implements greediness to accept a good solution.

6.1.2 Implementation of TLBO for optimal location of FACTs devices and Main Contributions

A summary of the studies which have used TLBO for optimal location of FACTs devices is shown in Table.6.1. Thus far, TLBO has been used for SVC and TCSC devices to improve various objective functions. To the best of authors knowledge, TLBO has not been used for UPFC devices to find the optimal combination of multiple UPFCs in order to manage the line loading of a power system.

In this study, for optimal location of UPFC, a computationally efficient algorithm,namely the teaching learning based optimization(TLBO) has been applied. This method is easy to implement relative to other population based algorithms like particle swarm optimization. The algorithm has been adapted and modified to obtain the optimal combination of UPFC placements on a power system. The discrete version of TLBO has been used which is called DTLBO. The DTBLO has been modified further in order to take into account the combinatorial optimization for the placement of 2 UPFCs. Further modifications have been made for the given DTLBO placement algorithm to improve convergence using steps used in the continuous TLBO algorithm. To the best of authors knowledge, an easy to implement algorithm such as the DTLBO has not been used previously to determine the optimal location of UPFC for line loading management.

Table 6.1: Summary of TLBO Based Algorithms

Method	**Devices**	**Description**	**Ref**
TLBO	TCSC	To minimize transmission losses and reduce total installation cost	[26]
TLBO	SVC	To reduce transmission losses	[27]

Continuation of Table 6.1			
TLBO	TCSC	To improve ATC	[28]
TLBO	SVC	To improve voltage stability of system	[29]
TLBO	SVC	To improve oscillations in an electrical network	[30]
TLBO	TCSC	Optimal Setting in N-1 Contingency Scenarios	[31]
TLBO	TCSC	To maximize ATC and minimize power losses using TLBO	[28]
TLBO	TCSC/SVC	Optimal Sizing of FACTs devices	[32]
TLBO/PSO	TCSC	Optimal Sizing of FACTs devices	[33]

Table 6.2: Summary of UPFC Allocation Methods

Design Variables	**Method**	**Number of UPFCs**	**Objective Function**	**Ref**
Location+Size	Sensitivity Index	single	min power loss	[34]
Location	fuzzy-based logic	single	Max Voltage stability	[35]
Location+Settings	Sensitivity-Based Approach	single	Max Social Welfare	[36]

Continuation of Table 6.2

Location	sensitivity-based screening technique	single	Min operational cost	[37]
Location+Settings	Sensitivity-based technique	single	Min Gen cost	[38]
Location+Size	Sensitivity-based technique	single	Min Congestion cost	[39]
Number+Location + Settings	Non Linear Optimal Power Flow	Multiple	Min operational cost	[40]
Location+Size Settings	Particle-Swarm Optimization	Single	Min total system cost	[41]
Number+Location Size/Settings	Sensitivity-Based Marginal Pricing	Multiple	Max Social Welfare	[42]
Location+Settings	Genetic Algorithm	Single	Max Damping Ratio	[43]
Location+Size	Newton Raphson CPF	Single	Max Loading margin	[44]

Continuation of Table 6.2

Location+Settings	Artificial Bees Colony	Single	Improve Stability	[45]
Location+Settings	Hybrid Imperialist Competitive Algorithm-Pattern Search	Single	Improve Voltage Stability Margin	[46]
Location+Settings	sensitivity based approach	multiple	Improve Load Curtailment	[47]
Location+Settings	**DTLBO**	**1 or 2 UPFCs**	**Reduce Congestion on High Loaded Lines**	

6.2 Proposed Formulation

6.2.1 Teaching Learning Based Optimization

Teaching Learning Based Optimization is a heuristic algorithm. It is based on the concept of teaching and learning process in a class. TLBO is generally composed of two phases however additional phases can be introduced to speed up convergence. The two phases are the teacher phase and learner phase.

- Teacher Phase: In the teacher phase, the learners learn from the teacher. The teacher is the person who has the most knowledge and by learning from that

person, the rest of the population who are the students can improve their knowledge and increase the results of the class from previous average to the teachers' level. Assume Xi is a matrix consisting of decision variables that is the learner, Mi is the average of the class and $Xibest$ is the best learner that is called teacher at iteration i. The difference between teachers' level and the average of the class is expressed as:

$$DifferenceMean_i = r_i(X_i^{best} - T_F M_i) \tag{6.1}$$

where r_i between 0 and 1, $DifferenceMean_i$ is the difference between mean and teacher, and T_F is the teaching factor. The value of T_F can be either 1 or 2 and is obtained randomly as follows:

$$T_F = round(1 + r_i) \tag{6.2}$$

where r_i is a random number between 0 and 1. Each learner is updated according to the following equation:

$$X_{new,i} = X_{old,i} + DifferenceMean_i \tag{6.3}$$

If $f(X_{new}) < f(X_{old}), X_{new}$ is accepted, otherwise $X_{new} = X_{old}$.

- Learner Phase: In the last part of algorithm, the learners increase their knowledge through interation among themselves. For enhancing the learners knowledge, each learner interacts randomly with other learners. This part is presented as follows:

  where r_i is a random number between 0 and 1. Npop is the number of population. X_{new} is accepted if $f(X_i) < f_(X_j)$, otherwise $X_{new,i} = X_{old,i}$.

Algorithm 7 Learner Phase

for $i = 1, , Npop \ldots$ **do**
  Select another learnerX_j randomly such that i is not equal to j.
  if $f(X_i) < f_(X_j)$ **then**
    $X_{new,i} = X_{old,i} + r_i(X_i - X_j)$
  else
    $X_{new,i} = X_{old,i} + r_i(X_j - X_i)$
  end if
end for

- Mutation Phase: This phase can be understood as a modification of the Learner Phase. This phase improves the performance of the algorithm to search for global optimum. It avoids premature convergence to the local optima of the objective function. This phase is repeated for all students. In each iteration(from i=1 to the total number of individuals) a new mutant vector or modified student is generated as:

$$X_{mut} = X_{rand1} + r(X_{rand2} - X_{rand3}) \tag{6.4}$$

$X_{rand1}, X_{rand2} and X_{rand3}$ are three students randomly selected for learner i. The three random numbers rand1,rand2 and rand3 should be three random numbers not equal to each other. r is a random number in the range between 0 and 1. The following equation is implemented:

$$X_{new} = X_{mut} if r1 > r2 \tag{6.5}$$

$$X_{new} = X_i otherwise \tag{6.6}$$

r1 and r2 are two random numbers in the range [0,1].X_i is the ith individual from the population and X_{mut} is the mutated vector which has been generated for X_i. The new indivudal X_{new} is accepted if it is better than the original individual X_i.

6.2.2 Discrete Teaching Learning Based Optimization

Orginial TLBO is a continuous optimization algorithm. However, choosing the optimal location of the upfc is a discrete problem. To make the continuous TLBO adapt to the choosing the optimal location of the UPFC, a discrete TLBO formulation can be used. This method does not have any control parameter and can converge to global optimum. The main the discretisation of DTLBO is to provide mapping from the continous space to discrete space. The continuous space is defined as a continuous number between 0 and 1. The discrete number in case of the optimal location of the UPFC will be the branch number(e.g. the 45th branch of the system). It must be noted that the discrete mapping needs to cover all the branches of the system. Thus the following formulation is used to show the mapping between continuous space and discrete space:

$$\alpha = 1 + N \times C \tag{6.7}$$

$$\beta = min(floor(\alpha), N) \tag{6.8}$$

In the above equations, α maps from continuous space [0,1] to discrete space [1,N+1] where N=number of branches. β maps from [1,N+1] to [1,N]. For example:

$$\begin{aligned} C &= 0.2 \\ \alpha &= 1 + N \times C \\ \alpha &= 1 + 186 \times 0.2 = 38.2 \\ \beta &= min(floor(38.2), 186) = 38 \end{aligned} \tag{6.9}$$

N is the number of branches in the system which in the above equation is defined as 186 for the 118 bus system. For every discrete serch space, C is equal to [0,1]. In other words, DTLBO searches in continuous space of C and for every member in C, a member in D is assigned.

In regards to choosing the optimal location for multiple UPFCs, there have to be

two continuous spaces both of which will lie between [0,1] but have to be distinct since two UPFCs can not be installed on the same location. For example, for two UPFCs, there will be C1 and C2. The equations above will map C1 and C2 to discrete space D1 and D2. They will denote the two branch numbers of the system.

Table 6.3: Mapping Range

Continuous Space	Discrete Space
[0,1]	[1,N]

Table 6.4: Mapping from Continuous space to Discrete Space

Continuous space	Discrete Space	Branch Number
C1	D1	N_1
C2	D2	N_2

The pseudocode of the algorithm is shown in Algorithm .8. Note that the function evaluation for each location in the DTLBO algorithm is carried out using Algorithm .9.

6.3 Results for 39 Bus

6.3.1 1 UPFC Case

The algorithm is applied on the 39 bus system. The parameters of the DTLBO algorithm are shown in Table.6.5 where 10 generations are run for this case. The convergence plots for all 10 generations are shown in Figure.6.1. The optimal location for the UPFC is the Line connceting bus 10 and 13 with a reduction in objective cost of around 0.035. However, it can be seen from the convergence plots that the DTLBO does not guarantee global optimum. To add to that,for finding the optimal location of the UPFC, the DTLBO may not be able to find it because it is a discrete version of the TLBO. The TLBO in the first place does not guarantee global optimum but

Algorithm 8 DTLBO Algorithm

```
while Number of Generations < Genmax do
    Generate the Population Randomly of Size Npop in Continuous space.
    Map the population from Continuous space to Discrete Space.
    Evaluate the cost function of each student.*
    while Iterations < Max Iterations do
        while i < Population Size do
            Run the Teacher Phase.*
            Run the Learner Phase.*
            Run the Mutation Phase*
            Delete Duplicate Solutions.
        end while
    end while
end while
Choose the Best Solution as the Optimal Location.
*The cost function for the members in a population in every phase is evaluated
using LPOPF algorithm.
```

is preferred only because it is easier to implement. For the purpose of our study, if the DTLBO is able to find the global optimum or a solution in close proximity to the global optimum, then the application of DTLBO for finding the optimal location of the UPFC does provide advantages in terms of simplicity of implementation. This can be seen from Table.6.7 where it can be seen that the DTLBO finds the global optimum solution 80 percent of the generations which is sufficient for practical purposes. The optimal location of the UPFC is shown in Fig.6.2 where it is compatible with the location of the high loaded lines shown in Fig.6.3.

Table 6.5: 39 Bus System-1 UPFC Case

Number of Generations	10
Number of Iterations	15
Population Size	5
Best Location	Line connecting Bus 10 and 13

Algorithm 9 Proposed LPOPF Algorithm

Initialize network parameters.
Initialize the UPFC Operating Point.
Run ACPF.
Find which lines have Loading Ratio more than 0.5. Calculate the Objective Function Loading Ratio.
while do$(iter) \leq (Maxiterations)$
Calculate the Objective Function Start Point.
Calculate the Sensitivity/partial derivatives.
Set up the LPOPF equations in matrix form.
Solve the LPOPF.
Obtain the New Operating Point. $(P_{des}, Q_{des}, V_{des}, P_{gen}, Q_{gen}, V_{pv})$.
Input the New Operating Point in ACPF. $(P_{des}, Q_{des}, V_{des}, P_{gen}, Q_{gen}, V_{pv})$.
Run ACPF.
The solution of the ACPF is obtained.
Calculate the new $V_{se}, \delta_{se}, V_{sh}, \delta_{sh}$.
Calculate Sigma.

if $Sigma \geq 0.1$ **then**
Increase the maximum change in control Variables.
else if $Sigma \leq 0$ **then**
Reduce the maximum change in Control Variables.
else if $(objectivestartpoint - objectivelinearproj) \leq 0$ **then**
Reduce the maximum change in Control Variables.
end if

if $Sigma \geq 0.1$ and $(objectivestartpoint - objectivelinearproj) \geq 0$ and $(LineLimitsnotexceedinginACPFsolution) \equiv 0$ **then**
The new operating point is feasible and the objective function cost reduction is stored.
else
The new operating point is not feasible. The objective function cost change is not stored.
end if

if $(Tol = (objectivestartpoint - objectivenewpoint)) \leq (1e-5)$ and (Operating Point is feasible) **then**
The LPOPF has Converged.
else
Continue with the next iteration.
end if
end while

Table 6.6: 39 Bus 1 UPFC Case: Optimal Location for each Generation

Generation No.	**Reduction in Objective Cost**	**UPFC Optimal Location 1**
1	0.034	Line 10-13
2	0.034	Line 10-13
3	0.02	Line 2-3
4	0.022	Line 17-18
5	0.034	Line 10-13
6	0.034	Line 10-13
7	0.034	Line 10-13
8	0.034	Line 10-13
9	0.034	Line 10-13
10	0.034	Line 10-13

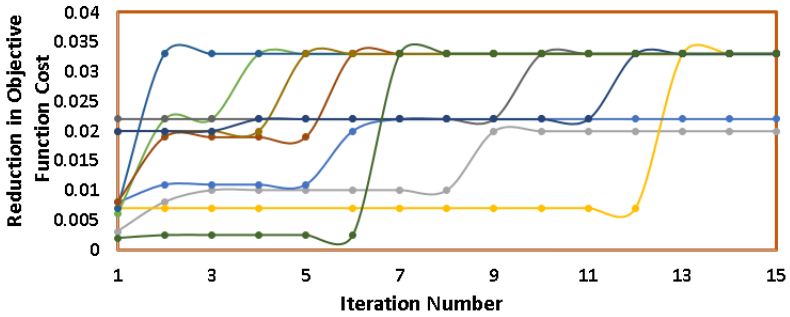

Figure 6.1: 39 Bus 1 UPFC Convergence Plot(10 Generations)

tabularx

Table 6.7: 39 Bus System-1 UPFC Case Convergence Rate

Solution Rank	Solution Obtained	Convergence Rate	Optimal Location
1	0.034	80 %	Line 10-13
2	0.022	10 %	Line Line 17-18
3	0.02	10 %	Line 2-3

Table 6.8: 39 Bus System-1 UPFC Case Convergence Summary

Solution Rank	Obtained Solution
Best Solution	0.034
Worst Solution	0.02
Mean Solution	0.032

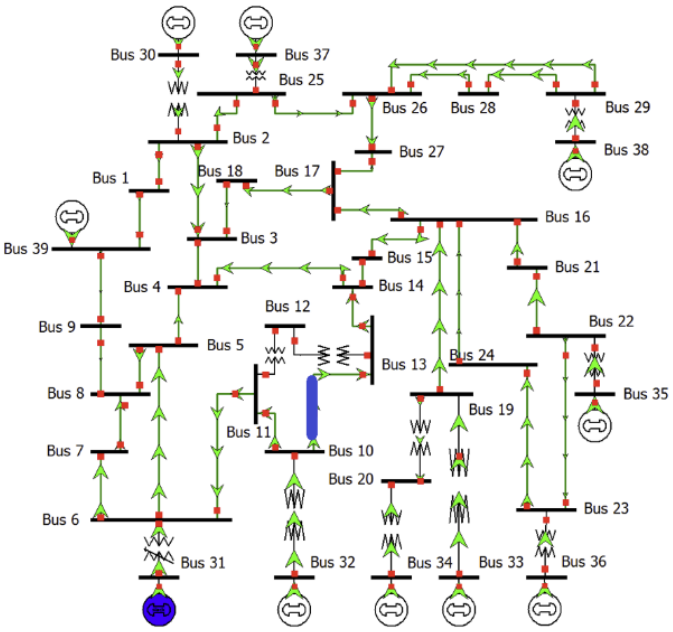

Figure 6.2: 39 Bus 1 UPFC Case Optimal Locations

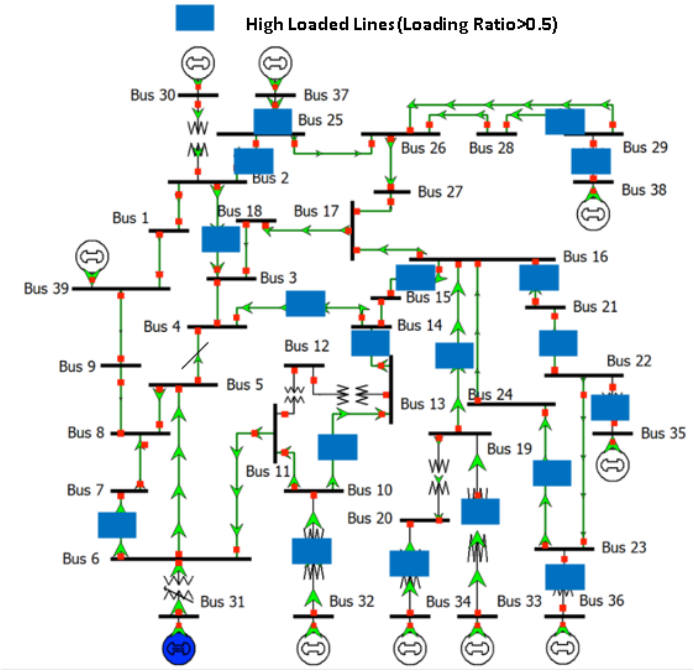

Figure 6.3: 39 Bus System High Loaded Lines

6.3.2 2 UPFC Case

The Algorithm is then applied on the 39 bus system for the combination of optimal location of 2 UPFCs. The parameters of the algoroithm are shown in Table.6.9. The population size is increased from 5 to 10 compared with the 1 UPFC case to improve convergence to global optimum. The larger the population size, the more chances are that the solution obtained will be the global optimum. It must be emphasized that the computational time also increases with a larger population size thus there exists a trade-off between convergence rate to global optimum and computational time.

The convergence plots for all 15 generations are shown in Fig.6.4. The combination of optimal location is one UPFC installed on Line 10-13 and second UPFC installed on Line 3-18 which is shown in Fig.6.5. It can be seen from Table.6.12 that this combination is achieved only once in Generation No.6 where the reduction in objective function cost is 0.0942. The second best solution is combination of UPFCs on Line 17-18 and Line 10-13. The third best solution is combination of UPFCs on Line 10-

13 and Line 16-21. It is to be kept in mind that in the combination problem with 2 UPFCs, there is added complexity compared with the 1 UPFC case.

The convergence rate of combinatorial optimization using DTLBO is dependent on a number of factors and is not deterministic in nature. The convergence to global optimum for the case of 2 UPFCs is less than that for 1 UPFC case as can be seen by comparing Table.6.10 and Table.6.7. In case of optimizing for combination of 2 UPFCs, the continuous space(C1 and C2) for each respective location(Loc 1 and Loc 2) moves independently of each other through the iterations by learning from other students. Thus achieving the optimal combination is harder compared with the 1 UPFC case. In the one UPFC case, the movement of a student(C1) towards the global optimum is easier as it can move independently on its own by learning from other students without any hindrance of a partner location. However, overall it can be seen that the solution ranks from 1 to 4 have a cumulative convergence of 53 percent and all of them are above the mean. Thus, the proposed DTLBO algorithm performs well in terms of rate of convergence.

Table 6.9: 39 Bus System-2 UPFC Case

Number of Generations	15
Number of Iterations	20
Population Size	10
Best Location for 1st UPFC	Line connecting Bus 10 and 13
Best Location for 2nd UPFC	Line connecting Bus 3 and 18

Table 6.12: 39 Bus 2 UPFC Case: Optimal Location for each Generation

Generation	**Reduction in Objective Cost**	**UPFC Optimal Location 1**	**UPFC Optimal Location 2**
1	0.0934	Line 17-18	Line 10-13
2	0.0807	Line 3-18	Line 10-11
3	0.0920	Line 10-13	Line 16-21
4	0.0627	Line 4-14	Line 10-13
5	0.0772	Line 28-29	Line 10-13
6	0.0942	Line 10-13	Line 3-18
7	0.0920	Line 10-13	Line 16-21
8	0.0497	Line 6-11	Line 3-18
9	0.0622	Line 4-14	Line 15-16
10	0.0614	Line 4-14	Line 13-14
11	0.0851	Line 10-13	Line 3-18
12	0.092	Line 10-13	Line 16-21
13	0.092	Line 10-13	Line 16-21
14	0.0913	Line 10-13	Line 2-3
15	0.0913	Line 10-13	Line 2-3

Table 6.10: 39 Bus System-2 UPFC Case Convergence Rate

Solution Rank	Solution	Convergence Rate	Optimal Location
1	0.0942	6.7 %	Line 10-13/Line 3-18
2	0.0934	6.7 %	Line 10-13/Line 17-18
3	0.092	27 %	Line 10-13/Line 16-21
4	0.0913	13 %	Line 10-13/Line 2-3

Table 6.11: 39 Bus System-2 UPFC Case Convergence Summary

Solution Rank	Obtained Solution
Best Solution	0.0942
Worst Solution	0.0497
Mean Solution	0.0811

tabularx

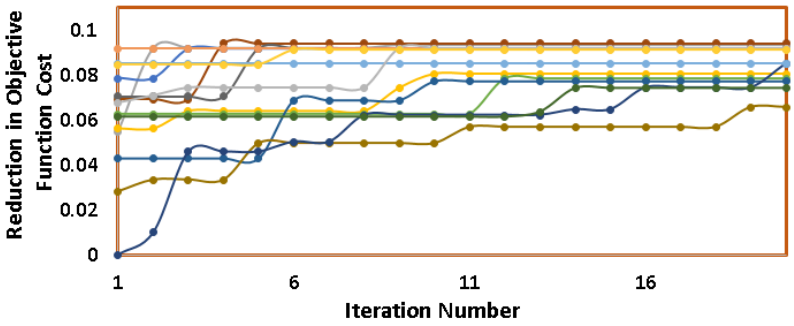

Figure 6.4: 39 Bus 2 UPFC Convergence Plot(15 Generations)

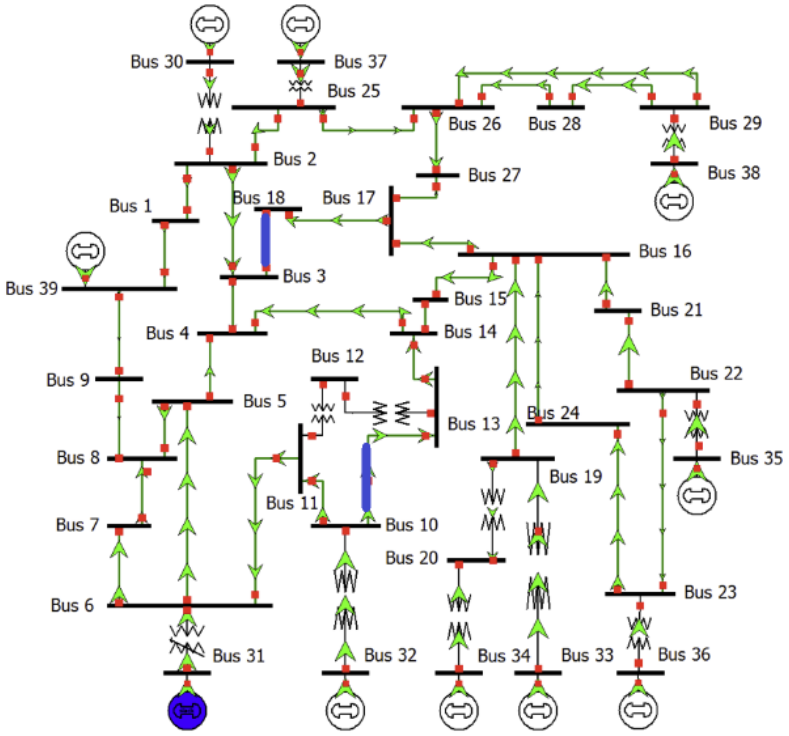

Figure 6.5: 39 Bus 2 UPFC Case Optimal Locations

6.4 Results for 118 Bus

6.4.1 1 UPFC Case

The proposed DLTBO algorithm is applied on the 118 Bus system. The parameters of the algorithm are shown in Table.6.13. The optimal location is the line connecting bus 17 and bus 18. The convergence rate of the solution ranks from 1 to 4 is shown in Table.6.14. As can be seen, the convergence for the global optimum is 60

percent which is satisfactory convergence rate for a population based algorithm. The convergence plots for all 10 generations are shown in Fig.6.6 and the detail of each generation is shown in Table.6.16. As was discussed earlier, the convergence for the 1 UPFC case is higher compared with the 2 UPFC case.

Table 6.13: 118 Bus System-1 UPFC Case

Number of Generations	10
Number of Iterations	15
Population Size	5
Best Location for UPFC	Line connecting Bus 17 and 18

Table 6.14: 118 Bus System-1 UPFC Case Convergence Rate

Solution Rank	Solution	Convergence Rate	Optimal Location
1	0.0324	60 %	Line Line 17-18
2	0.0222	20 %	Line 69-77
3	0.0192	10 %	Line 85-89
4	0.0083	10 %	Line 5-11

Table 6.15: 118 Bus System-1 UPFC Case Convergence Summary

Solution Rank	Obtained Solution
Best Solution	0.0324
Worst Solution	0.0083
Mean Solution	0.0266

tabularx

Table 6.16: 118 Bus 1 UPFC Case: Optimal Location for each Generation

Generation No.	**Reduction in Objective Cost**	**UPFC Optimal Location**
1	0.0324	Line 17-18
2	0.0324	Line 17-18
3	0.0324	Line 17-18
4	0.0222	Line 69-77
5	0.0324	Line 17-18
6	0.0083	Line 5-11
7	0.0192	Line 85-89
8	0.0222	Line 69-77
9	0.0324	Line 17-18
10	0.0324	Line 17-18

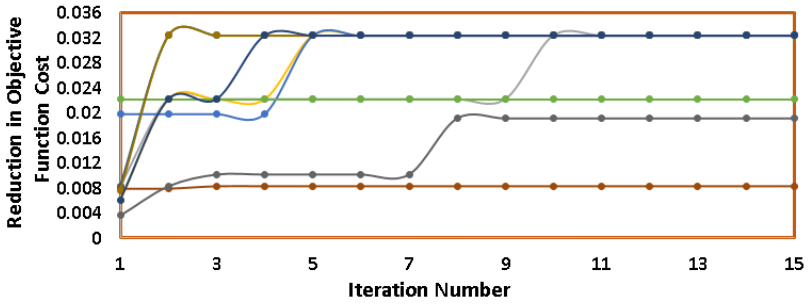

Figure 6.6: 118 Bus 1 UPFC Convergence Plot(10 Generations)

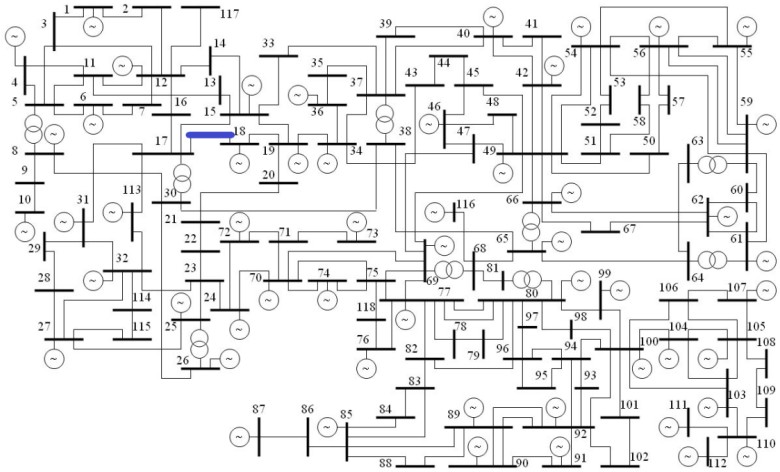

Figure 6.7: 118 Bus 1 UPFC Case Optimal Locations

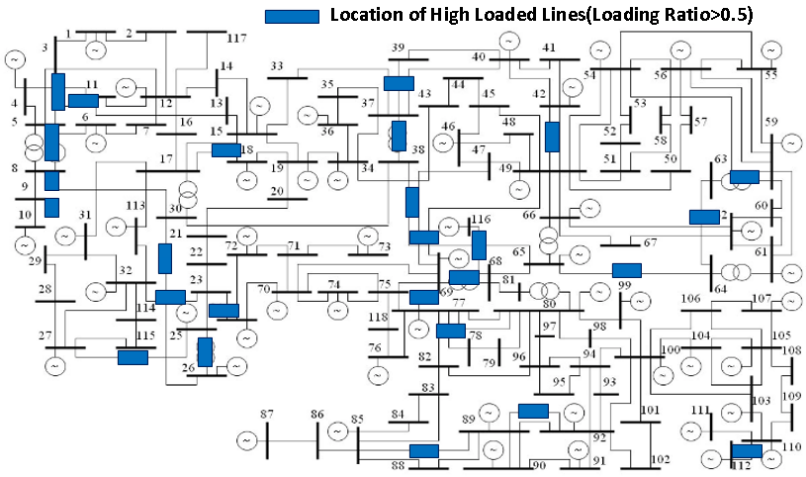

Figure 6.8: 118 Bus System High Loaded Lines

6.4.2 2 UPFC Case

The algorithm is tested for a combination of 2 UPFCs on the 118 bus system. The parameters and results of the algorithm are shown in Table.6.17. The optimal location for the 2 UPFCs are the lines connecting bus 17 and bus 18 and the lines connecting buses 69 and 77. It can be seen that the optimal location for the 2nd UPFC is an additional location in addition to the 1 UPFC case where the optimal location was the line connecting bus 17 and bus 18. This pattern is similar to the 39 bus system.

It can be seen from Table.6.17 that the population size used for the 2 UPFC case is 20 versus 5 for the 1 UPFC case while the number of iterations for the 2 UPFC case is 50 versus 15 for the 1 UPFC case. The reason for this is that since the 118 bus system is a large scale system with the number of 2 UPFC combinations equal to 17,205 versus the number of 1 UPFC combinations which is equal to 186 as it is equal to the number of branches. The search space for the DTLBO needs to be expanded for the 2 UPFC case to increase chances to reach global optimum. However, for the purpose of this study, the aim is to show that the algorithm can be applied for the specific problem and that global convergence is achievable by searching the sufficient solution space. The determination of the minimum number of generations,iterations

and population size to achieve the global optimum solution in every generation is another relevant topic which is out of the scope of this chapter.

The convergence rates for the best 4 solutions are shown in Table.6.18. It can be seen that the 60 percent of the solutions(which include the highest 3 solutions) achieve an objective cost which is better than the mean(0.0425). Furthermore, it can also be seen that the solution rank 1,2 and 4 comprise a UPFC location on line connecting bus 17 and bus 18. Thus the second UPFC location will be in addition to the 1 UPFC case optimal location. However, it must be enphasized that this may not hold for 3 UPFC case for the 118 Bus system or for larger systems compared with the 118 bus system. The 3 UPFC case for the 118 bus system has not been tried in the study as the computational time required to go through the iterations for a single generation is too large in MATLAB specific environment. The following improvements are suggested to reduce the computational time/burden for finding the optimal location of 3 or more UPFCs:

- The computational speed of the LPOPF algorithm can be improved to reduce the time for objective cost calculation further for each student in the DTLBO algorithm.

- The search space could be reduced to a specific set of possible lines for UPFC installation to reduce the computational time for the overall DTLBO algorithm. The set of possible lines for UPFC installation can be shortlisted based on the topology of the system.

Table 6.17: 118 Bus System-2 UPFC Case

Number of Generations	10
Number of Iterations	50
Population Size	20
Best Location for 1st UPFC	Line connecting Bus 17 and 18
Best Location for 2nd UPFC	Line connecting Bus 69 and 77

Table 6.18: 118 Bus System-2 UPFC Case Convergence Rate

Solution Rank	Solution	Convergence Rate	Optimal Location
1	0.0457	20 %	Line 69-77/Line 17-18
2	0.0439	20 %	Line 64-65/Line 17-18
3	0.0434	20 %	Line 69-77/Line 85-89
4	0.0404	10 %	Line 23-25/Line 17-18

Table 6.19: 118 Bus System-2 UPFC Case Convergence Summary

Solution Rank	Obtained Solution
Best Solution	0.0457
Worst Solution	0.0356
Mean Solution	0.0425

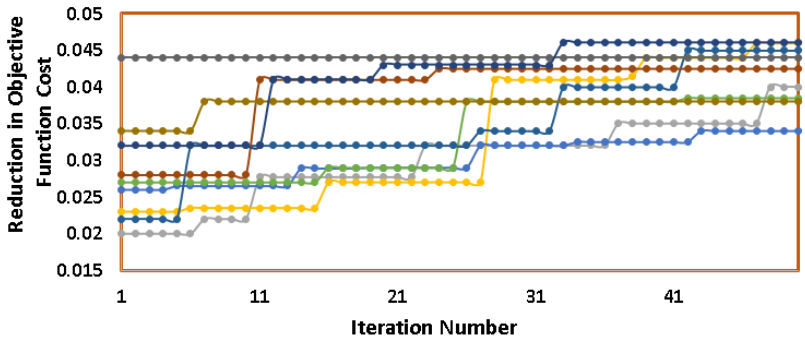

Figure 6.9: 118 Bus 2 UPFC Convergence Plot(10 Generations)

Table 6.20: 118 Bus 2 UPFC Case: Optimal Location for each Generation

Generation No.	**Reduction in Objective Cost**	**UPFC Optimal Location 1**	**UPFC Optimal Location 2**
1	0.0439	Line 64-65	Line 17-18
2	0.0439	Line 64-65	Line 17-18
3	0.0398	Line 69-77	Line 63-59
4	0.0457	Line 69-77	Line 17-18
5	0.0404	Line 23-25	Line 17-18
6	0.0429	Line 63-59	Line 23-32
7	0.0434	Line 85-89	Line 69-77
8	0.0434	Line 69-77	Line 85-89
9	0.0356	Line 26-25	Line 4-11
10	0.0457	Line 69-77	Line 17-18

tabularx

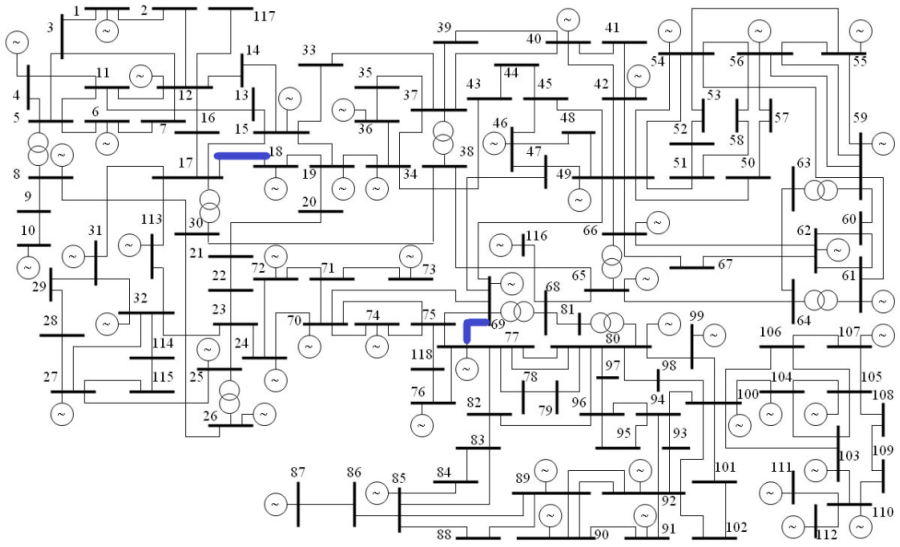

Figure 6.10: 118 Bus 2 UPFC Case Optimal Locations

6.5 Summary and Main Contribution

The Main contribution of this chapter is listed below:

- The Discrete Teaching Learning based optimization algorithm presented in this chapter is able to suggest optimal locations of the UPFC for optimal management of power flows in a power system. This algorithm is easy to implement and gives a sufficiently high convergence rate(greater than 50 percent) to the

global optimum or above mean solution though it does not guarantee convergence to the global optimum at all times. The algorithm is tested for 1 UPFC as well as combination of 2 UPFCs as well. It is seen that the location of the 2nd UPFC is an addition to the location of the 1st UPFC most of the times further clarifying the advantage of this algorithm. The algorithm is effectively used for the 39 Bus system and the 118 Bus system.

A summary of the results for the DTLBO algorithm is shown in Table.6.21. As can be seen the DTLBO algorithm is able to find the optimal locations for the two systems with an above 50 percent convergence rate for the above mean solutions. The convergence rate for the global optimum solution is above 50 percent for the 1 UPFC cases but is 7 percent and 20 percent for the 2 UPFC cases for the 39 and 118 Bus system respectively. The results must be considered keeping in mind that the it is a discrete version of the TLBO with combinatorial optimization. Overall, the proposed DTLBO algorithm is able to find the optimal locations of the UPFC with sufficient convergence rate.

Table 6.21: Summary of the Cases studied

39 Bus System			
No. Of UPFCs	Convergence Rate(Global Optimum)	Convergence Rate(Above Mean)	Optimal Locations
1	80%	80%	Line Line 17-18
2	6.7%	53%	Line 10-13/Line 3-18
118 Bus System			
No. Of UPFCs	Convergence Rate(Global Optimum)	Convergence Rate(Above Mean)	Optimal Locations
1	60%	60%	Line 17-18
2	20%	60%	Line 17-18/Line 69-77

CHAPTER 7: OPTIMAL RATING OF UPFC FOR LINE LOADING MANAGEMENT

7.1 Introduction

In the previous sections, it was determined that the UPFC can be beneficial in managing the line flows for a power system using an improved LPOPF algorithm. However, in the previous sections, the installation cost of a UPFC as well as the congestion cost was not taken into account. It may not always be the case that the power system planners are willing to invest in as many number of UPFCs or as large a rated UPFC as possible to gain greater control over the line flows in a power system. Thus, there must be a weighted consideration of the costs associated with the a higher rated UPFC as well as the benefit obtained from increased control over the line flows in a power system.

7.2 Literature Review

Operation uncertainties of the load demand are important to consider. Moreover, this is important with regards to renewable energy penetration as well. With the increased usage of renewable energy, the UPFC sizing and location as well needs to incorporate various power system uncertainties. A list of reference which incorporate load variations is shown in Table.7.1 with respect to optimal siting and sizing of various FACTs devices. It can be seen that very few references have incorporated load variations more than 5 in number. In this study, multiple load variations are also considered with regards to UPFC optimal rating. Accounting for these probabilities will help in ensuring that the resulting solutions are more realistic and practical and can provide a better performance under a range of operating conditions and

uncertainties.

Table 7.1: Summary of Load Variations for Optimal Sizing of FACTs Devices

No of Load Variations	**Number of Refs**	Ref
0	29 References	[48], [45], [49], [50], [50], [51], [52], [53], [54], [55], [33], [56], [57], [58], [59], [60], [61], [62], [63], [64], [65], [66], [67], [68], [69], [70], [71], [72]
1	5 References	[73], [74], [75], [76], [77]
2	6 References	[78], [79], [80], [81], [82], [59]
3	3 References	[83], [84], [85]
4	3 References	[86], [87], [88]
5	2 References	[89], [90]

7.3 Main Contribution

The main contribution of this chapter is listed below:

- The proposed algorithm finds the minimum rating required to achieve a significant control over line loading in three control scenarios: Only upfc set point is allowed to change, all real generation and only slack bus reactive generation setpoints as well as upfc setpoints can change and all reactive generation and only slack bus real generation setpoints as well as upfc setpoints can change. Moreover, a cost benefit analysis is carried out to show the tradeoff between optimal rating and degree of control over line loading of the power system.

- Load Variations are considered in the finding the optimal sizing of UPFC to give a more realistic solution for a given location. Furthermore, it should be

emphasized that since demand is not constant, a wide range of load variations should be considered to find a solution which will prove the effectiveness of the UPFC Location for various scenarios.

7.4 Formulation

The formulation of the proposed algorithm is shown below:

Algorithm 10 Optimal Rating of UPFC Algorithm

for Scenario A,B and C **do**
  Set UPFC rating as 300 MVA for both shunt and series voltage sources.
  while UPFC Rating > 0 and Additional reduction in line loading is not achieved **do**
    Evaluate the cost function using the LPOPF algorithm.
    Set the UPFC Rating to the next lowest step.
  end while
end for
Find the minimum rating required to achieve the desirable level of control common to Scenario A,B and C. In our case, it is the minimum level of control.

The formulation of the proposed algorithm considering the cost of the UPFC is shown below:

Algorithm 11 Optimal Rating of UPFC considering Cost of UPFC

for Scenario A,B and C **do**
  Set UPFC rating as 300 MVA for both shunt and series voltage sources.
  while UPFC Rating > 0 and Additional reduction in line loading is not achieved **do**
    Evaluate the cost function using the LPOPF algorithm.
    Set the UPFC Rating to the next lowest step.
  end while
end for
Find the cost of each UPFC rating.
Plot the Cost-Benfit plots for each scenario.
The optimal rating of the UPFC is selected based on the largest gradient or closeness to the origin.

7.5 Results for a 39 Bus System

For the 39 Bus System, the ratings of the UPFC were varied from a minimum range to a maximum range and the line loading ratio was obtained for each case. Three

cases were tested, each of them with a UPFC installed at a different location.

Table 7.2: Description of Scenarios

Scenario A	Only UPFC Case
Scenario B	All Pgen+ Slack Qgen Case
Scenario C	All Qgen+ Slack Pgen Case

7.6 Results for a 39 Bus System

The ratings were tested for 3 different locations for Scenario A,B and C.

7.6.1 UPFC installed on Line 16-17

In this case, the UPFC is installed on Line 16-17. As can be seen, for Scenario A(Only UPFC Scenario), the UPFC is able to reduce the line loading from 0.663 to 0.651 even with an MVAse and MVAsh rating of 50 MVA and 50 MVA respectively. The same is the case for Scenario B(All Pgen+Slack Qgen Case) where the UPFC is able to reduce line loading from 0.728 to 0.6643. For Scenario C (All Qgen+Slack Pgen Scenario), the UPFC reduces line loading ratio from 0.728 to 0.7169. Thus, if the purpose of the operator is to reduce the cost of the installed UPFC as much as possible, then the optimal rating of the UPFC will be 50 MVA for both the series and shunt sources.

It can be further seen from Table.7.4 that the MVAse settings for the UPFC are consistently higher for each row compared with the Table.7.5 case. This is because the in All Pgen+Slack Qgen case, there is much more leverage for the real power flow to be managed thus the series source acts to manage the real power flow which is seen by a higher MVAse setting for each row. For example, if you compare the 300 MVAse max and 300 MVAsh max cases for Table.7.4 and Table.7.5, then in All Pgen+Slack Qgen case, the UPFC MVAse is 200 MVA while in Table.7.5, the UPFC MVAse setting is 80 MVA. The vice versa is the case for MVAsh where it has a setting

of 60 MVA in Table.7.4 while it has a setting of 200 MVA in Table.7.5.

In order to determine the optimal rating, all three scenarios must be tested as the objective is to reduce the line loading on heavily congested lines. In real power systems, the generator settings can be changed to allow to relieve overload if it does not increase the generation cost by a significant percentage. Again, it must be emphasized that the objective of this chapter is not to put a cost on the trade-off between a higher rated UPFC and the additional control gained for the line loading, but to showcase a qualitative discussion of how this algorithm can be used to determine the rating of a UPFC device based on the operator's objectives.

Table 7.3: Only UPFC Scenario(Line 16-17)

Only UPFC Case							
MVAse(max)	MVAsh(max)	Psh(max)	Before	After	MVAse	MVAsh	Qsh
300	300	100	0.663	0.6465	72	50	-40
200	200	100	0.663	0.6465	72	50	-40
100	100	50	0.663	0.6465	72	50	-40
50	50	25	0.663	0.651	47	30	26
40	40	25	0.663	0.663	-	-	-

Table 7.4: All Pgen+Slack Qgen Scenario(Line 16-17)

All Pgen+Slack Qgen Case							
MVAse(max)	MVAsh(max)	Psh(max)	Before	After	MVAse	MVAsh	Qsh
300	300	100	0.728	0.6153	200	60	50
200	200	100	0.728	0.6147	200	80	78
100	100	50	0.728	0.6298	100	70	60
50	50	25	0.728	0.6643	50	10	20
40	40	25	0.728	0.728	-	-	-

Table 7.5: All Qgen+Slack Pgen Scenario(Line 16-17)

All Qgen+Slack Pgen Case							
MVAse(max)	MVAsh(max)	Psh(max)	Before	After	MVAse	MVAsh	Qsh
300	300	100	0.728	0.7121	80	200	-200
200	200	100	0.728	0.7121	82	200	-200
100	100	50	0.728	0.7144	72	100	-100
50	50	25	0.728	0.7169	57	35	-34
40	40	25	0.728	0.728	-	-	-

For the sake of showing the cost-benefit analysis of the above settings, a cost is put on the congestion congestion and the UPFC rating. The cost of the UPFC is

$$C_{upfc} = 0.00003S^2 - 0.2691S + 188.2 USDollars/KVAR \tag{7.1}$$

S is the operating range of the UPFC device in MVAR.

As can be seen from Table.7.6 that the power system operator can make a different choice depending on the what the preference of the operator is. There is a cost associated with the congestion in a power system thus the operator can choose to install a UPFC rated 300 MVA with 3 times more cost as compared to the 50 MVA or settle for 50 MVA rated UPFC with a smaller degree of control over line flows. The tradeoff can also be seen in Fig.7.1 between the three ratings of the UPFC. Briefly speaking, the 100 MVA UPFC provides a middle ground in terms of cost as well as the degree of line loading control. The line loading ratio after OPF is 0.6298 which is not a large drop from the 0.6153 value for the 300 MVA case while the cost is reduced by almost 50 percent compared with the 300 MVA Case. For the 50 MVA UPFC, the line loading control is reduced by a great degree so the additional reduction in cost compared with 100 MVA case may not be too beneficial.

Table 7.6: Cost-Benefit Analysis of UPFC(All Pgen+Slack Qgen Case)

MVAse	MVAsh	Cost of UPFC(USD)	Before	After
300	300	3.3 $\times 10^7$	0.728	0.6153
100	100	1.6 $\times 10^7$	0.728	0.6298
50	50	0.87 $\times 10^7$	0.728	0.6643

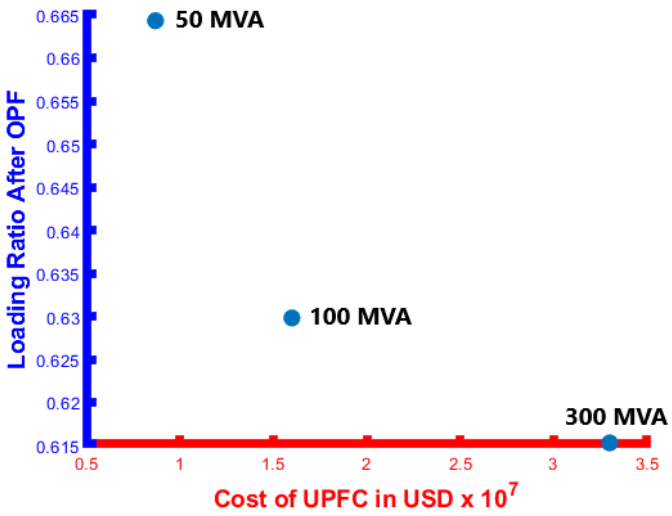

Figure 7.1: Cost-Benefit Plot

7.6.2 UPFC installed on Line 3-4

The second location where the UPFC is installed is Line 3-4. The results for the loading ratio for the three scenarios for different ratings are shown in Table.7.7, Table.7.8 and Table.7.9. It can be seen that a minimum UPFC rating of 100 MVA for the series and shunt converters are able to obtain a feasible solution for the three scenarios. A rating of 50 MVA is not able to give a feasible solution with a lower line loading ratio for the only UPFC and All Qgen+Slack Pgen Scenario.

As was discussed for the previous location, for the All Pgen+Slack Qgen scenario, the UPFC MVAse settings are higher on average compared with the Only UPFC scenario for the same reasons as was discussed previously.

Table 7.7: Only UPFC Scenario(Line 3-4)

Only UPFC Case							
MVAse(max)	MVAsh(max)	Psh(max)	Before	After	MVAse	MVAsh	Qsh
300	300	100	0.663	0.6506	40	80	80
200	200	100	0.663	0.6506	40	80	80
100	100	50	0.663	0.6624	20	70	70
50	50	25	0.663	0.663	-	-	-

Table 7.8: All Pgen+Slack Qgen Scenario(Line 3-4)

All Pgen+Slack Qgen Case							
MVAse(max)	MVAsh(max)	Psh(max)	Before	After	MVAse	MVAsh	Qsh
300	300	100	0.728	0.6159	160	63	-60
200	200	100	0.728	0.6159	160	61	-63
100	100	50	0.728	0.6324	65	91	-88
50	50	25	0.728	0.6466	50	33	-32
40	40	25	0.728	0.65	40	13	-14
30	30	25	0.728	0.728	-	-	-

Table 7.9: All Qgen+Slack Pgen Scenario(Line 3-4)

All Qgen+Slack Pgen Case							
MVAse(max)	MVAsh(max)	Psh(max)	Before	After	MVAse	MVAsh	Qsh
300	300	100	0.728	0.667	154	56	-52
200	200	100	0.728	0.667	154	56	-52
100	100	50	0.728	0.653	100	60	-50
50	50	25	0.728	0.728	-	-	-

Furthermore, a cost-benefit analysis can be performed for this UPFC location as well shown in Table.7.10 and is shown in Fig.7.2. It can be seen that a higher rated UPFC MVA of 300 MVA is no more useful than a 200 MVA rated UPFC. Further,

like the previous location, the UPFC rating of 100 MVA provides a good trade-off between the cost of UPFC and the degree of control over line loading. However, you can also see that the operator might prefer to install a 200MVA rated UPFC as the cost increase is not too much compared with the additional control gained over the line loading.

Table 7.10: Cost-Benefit Analysis of UPFC Location 3-4(All Pgen+Slack Qgen Case)

MVAse	MVAsh	Cost of UPFC(USD)	Before	After
300	300	3.3 $\times 10^7$	0.728	0.6159
200	200	2.3 $\times 10^7$	0.728	0.6159
100	100	1.6 $\times 10^7$	0.728	0.6298
50	50	0.87 $\times 10^7$	0.728	0.6466

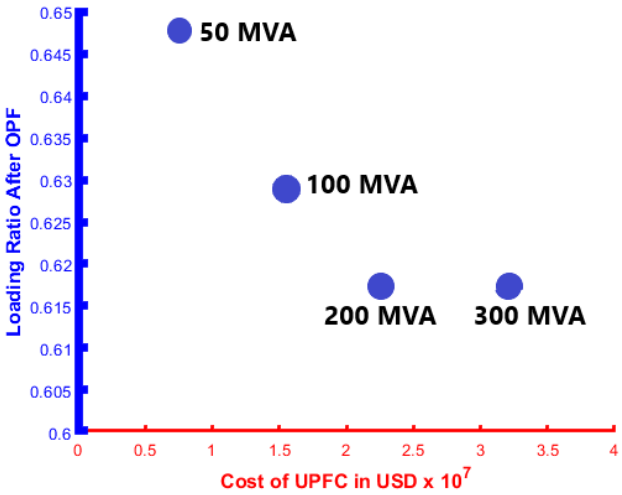

Figure 7.2: Cost-Benefit Plot Line 3-4

If the loading is increased, the cost-benefit plot may look different as shown in Fig.7.3. It can be seen that for higher loading 103 percent, the same rating of UPFC has higher loading ratio after OPF. Furthermore, it can be seen that for a loading of 103 percent, the increase in cost from 100 to 200 MVA may not be justified for the additional gain in reduction as compared for the 100 percent loading scenario.

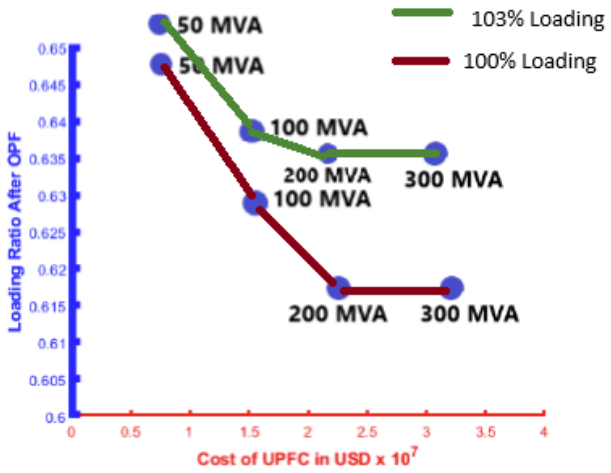

Figure 7.3: Cost-Benefit Plot Line 3-4 Vary Loading

7.6.3 UPFC installed on Line 11-12

Another UPFC location is tried between buses 11 and 12. It can be seen from Table.7.11, Table.7.12 and Table.7.13 that the minimum rating ruquired to gain control over the line loading is different for all three scenarios. The overall minimum rating required is 100 MVA for all three scenarios.

Table 7.11: Only UPFC Scenario(Line 11-12)

Only UPFC Case							
MVAse(max)	MVAsh(max)	Psh(max)	Before	After	MVAse	MVAsh	Qsh
300	300	100	0.663	0.6491	72	16	19
200	200	100	0.663	0.6491	72	16	19
100	100	50	0.663	0.6491	72	16	19
50	50	25	0.663	0.663	-	-	-

Table 7.12: All Pgen+Slack Qgen Scenario(Line 11-12)

All Pgen+Slack Qgen Case							
MVAse(max)	MVAsh(max)	Psh(max)	Before	After	MVAse	MVAsh	Qsh
300	300	100	0.728	0.6024	110	5	0.96
200	200	100	0.728	0.6024	100	5	0.86
100	100	50	0.728	0.6153	99	12	12
50	50	25	0.728	0.629	50	8	-5
40	40	25	0.728	0.6327	43	11	10
30	30	25	0.728	0.6383	30	6	-2
20	20	15	0.728	0.728	-	-	-

Table 7.13: All Qgen+Slack Pgen Scenario(Line 11-12)

All Qgen+Slack Pgen Case							
MVAse(max)	MVAsh(max)	Psh(max)	Before	After	MVAse	MVAsh	Qsh
300	300	100	0.728	0.6806	182	268	-265
200	200	100	0.728	0.685	182	200	-200
100	100	50	0.728	0.6993	100	100	-100
50	50	25	0.728	0.705	50	50	-50
40	40	25	0.728	0.728	-	-	-

Table 7.14: Cost-Benefit Analysis of UPFC Location 11-12(All Pgen+Slack Qgen Case)

MVAse	MVAsh	Cost of UPFC(USD)	Before	After
300	300	3.3 $\times 10^7$	0.728	0.6024
200	200	2.3 $\times 10^7$	0.728	0.6024
100	100	1.6 $\times 10^7$	0.728	0.6153
50	50	0.87 $\times 10^7$	0.728	0.629

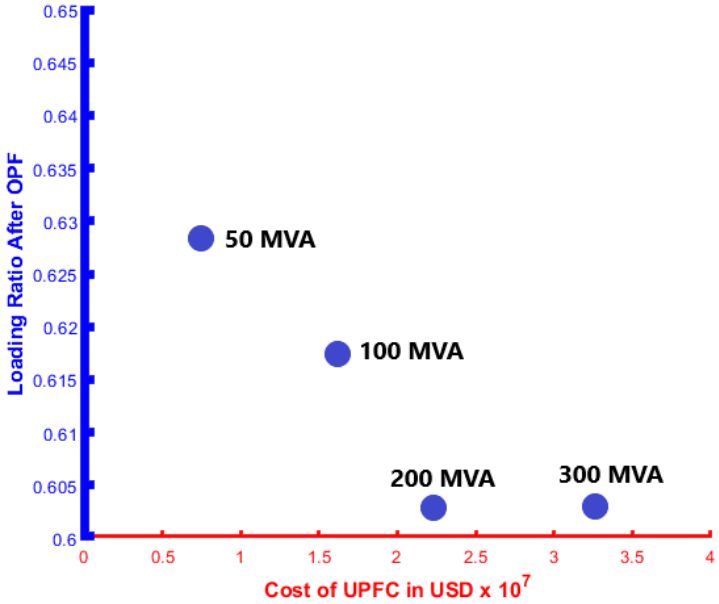

Figure 7.4: Cost-Benefit Plot Line 11-12

In the figure.7.5, the cost benefit plot is plotted with respect to different loading levels. It can be seen that for 104 percent loading level, the 100 MVA rated UPFC is not able to give an improved control as compared to the 50 MVA rated UPFC. For 100 and 103 percent loading levels, the 100 MVA rated UPFC is able to give an improved control as compared to the 50 MVA rated UPFC. Furthermore, the 200 MVA rated UPFC also gives additional control as compared to the 100 MVA rated UPFC. However, overall, based on the cost-benefit tradeoff, the 100 MVA rated UPFC may prove to be a good option considering different loading levels.

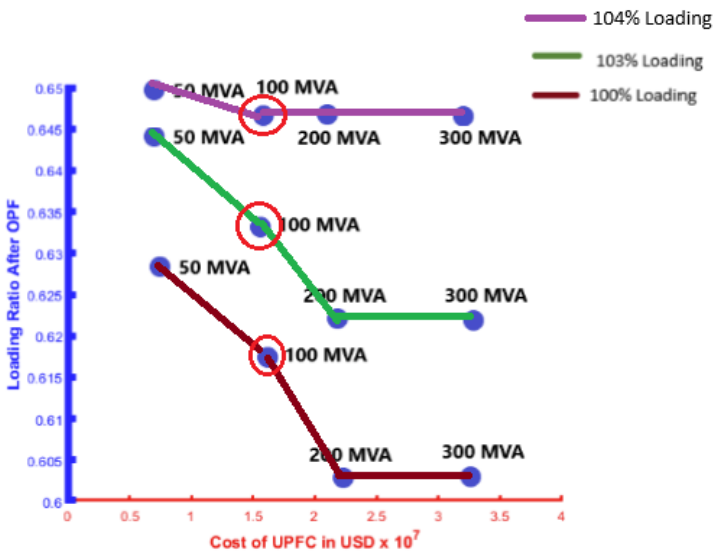

Figure 7.5: Cost-Benefit Plot Line 11-12 Vary Loading

7.7 Optimal Rating of UPFC considering Load Variations

The optimal rating of the UPFC has been tested for various loading levels. The loading levels are varied with respect by trying different combinations of loading variations at combinations of buses. This is done randomly and the optimal rating is tested out using using Scenario A,B and C as discussed in the previous section. As compared to the previous section, where the optimal rating is determined using the minimal rating, in this section, the optimal rating is determined using the maximum control over line loading ratio. The total number of runs of load variations run are around 100. A sample of random load variations are shown in table below:

Table 7.15: Sample of Load Variations

Sample 1	Sample 2	Sample 3	Sample 4
Bus 1/-20%	Bus 11/-1%	Bus 10/-4%	Bus 6/+0.4%
Bus 2/+10%	Bus 24/+2%	Bus 4/+7%	Bus 1/+1%
Bus 5/+30%	Bus 27/+3%	Bus 8/+3%	Bus 23/+3%
Bus 10/-20%	Bus 31/+7%	Bus 36/+2%	Bus 22/+1.4%

7.7.1 Case 1:UPFC Installed on Line 4-14

The UPFC is installed on Line 4-14. It can be seen from Fig.7.6, Fig.7.7 and Fig.7.8 that the MVASe,MVASh and Vse ratings vary with different loading levels. Generally, the higher the UPFC rating, the higher the reduction in line loading ratio achieved. However, the operator must decide as how to how large the UPFC must be sized because the cost needs to be considered as well. For example, one operator may prefer to size the UPFC according to the largest reduction in line loading achieved while the other operator may prefer to size the UPFC to cover at least the average reduction in line loading ratio. SO it is the operator's decision as to what his/her preference is. In this section, we have decided to find the optimal rating of UPFC so that most of the load variations are taken into account.

For example, for Fig.7.6, the load variation scenarios that are ignored are shown in the red rectangle. The load scenarios variations which will most likely most cover all scenarios are bounded by the black rectangle. Among those scenarios, the mean MVAse rating is around 50 MVA. Thus, the optimal MVAse rating is 50 MVA considering load variations. Furthermore, in Fig.7.7, the variation in ratings of MVAsh with respect to reduction in loading ratios is shown. It can be seen that scenarios in red rectangle are ignored as they lie as outliers. Most of the loading variation can be covered by an optimal rating of around 120 MVA for MVAsh. Furthermore, in Fig.7.8, the Vse optimal rating is around 0.2 as it covers most load variations. The load variations in the red rectangle are ignored even though the highes reduction in loading ratio occurs where the reduction in loading ratio is the highest.

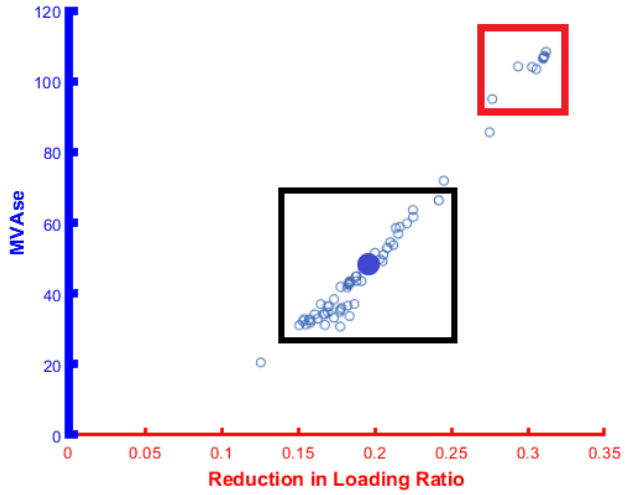

Figure 7.6: Variation of MVAse with Loading Levels Case 1

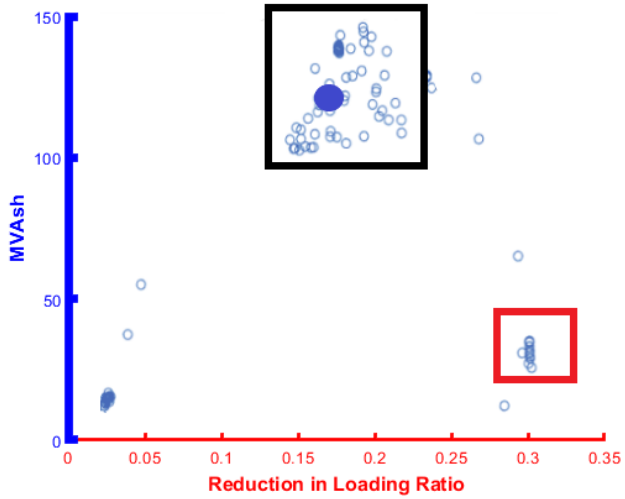

Figure 7.7: Variation of MVAsh with Loading Levels Case 1

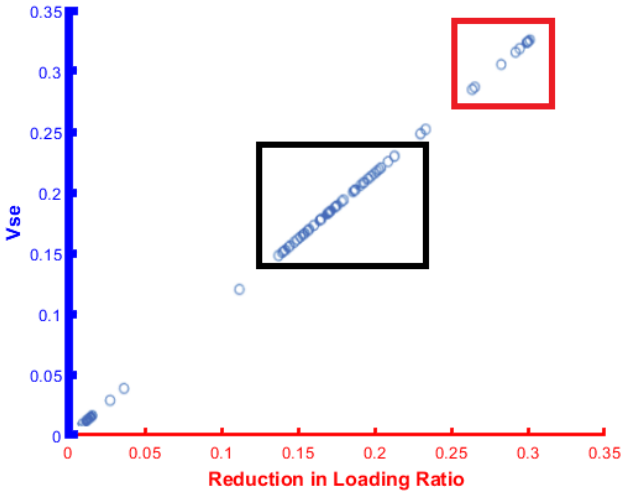

Figure 7.8: Variation of Vse with Loading Levels Case 1

Table 7.16: Summary of Optimal Rating for Location 4-14

Rating	Value
MVAsh	125 MVA
MVAse	50 MVA
Vse	0.2 V

7.7.2 Case 2:UPFC Installed on Line 17-18

The variation of Vse,MvAse and MVAsh with respect to different loading levels is shown in Fig.7.9,Fig.7.10 and Fig.7.11. It can be seen that most load variations lie within close proximity.Thus unlike Case 1,where the load variations caused some amount of variation in UPFC rating as well. In case 2, the reduction in loading ratio is less than Case 1.Thus the location of Case 2 is less optimal as compared to Case 1.This also leads us to the point that whatever the load variation, the UPFC ratings remain the same. Thus, increasing the sizing of the UPFC is not beneficial for this location since it is not an optimal location. If there is no variation in the loading ratio reduction by varying the sizing of the UPFC then that means the location of the UPFC is not optimal.

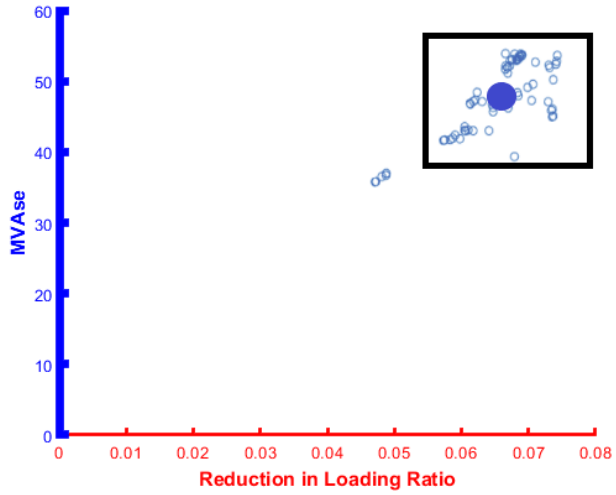

Figure 7.9: Variation of MVAse with Loading Levels Case 2

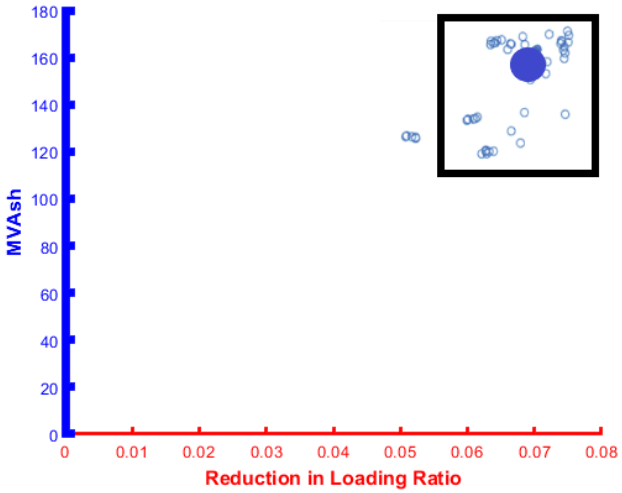

Figure 7.10: Variation of MVAsh with Loading Levels Case 2

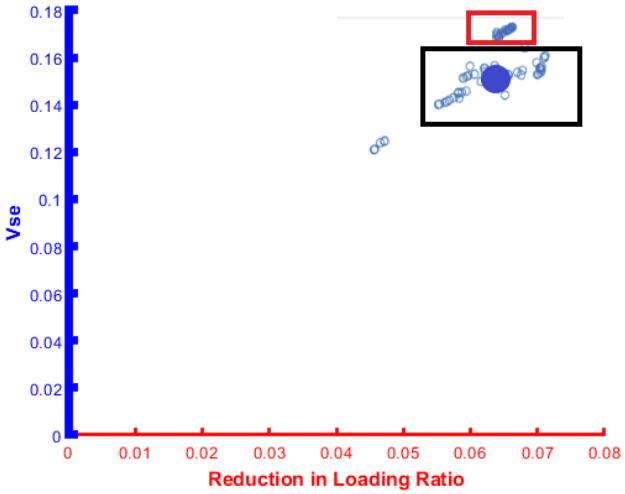

Figure 7.11: Variation of Vse with Loading Levels Case 2

Table 7.17: Summary of Optimal Rating for Location 17-18

Rating	Value
MVAsh	160 MVA
MVAse	55 MVA
Vse	0.15 V

7.7.3 Case 3:UPFC Installed on Line 3-18

In Case 3, the UPFC is installed on Line 3-18. The variation of Vse,Mvase and Mvash with respect to load variations is shown in Fig.7.12,Fig.7.13 and Fig.7.14. It can be seen that for different load variations, the UPFC sizing varies to a considerable degree.The main point to emphasize is that the higher the UPFC sizing, the higher the reduction in line loading achieved. THus it is a better location for UPFC installation. Table.7.18 shows the optimal rating of the UPFC for location 3-18 considering different load scenarios.

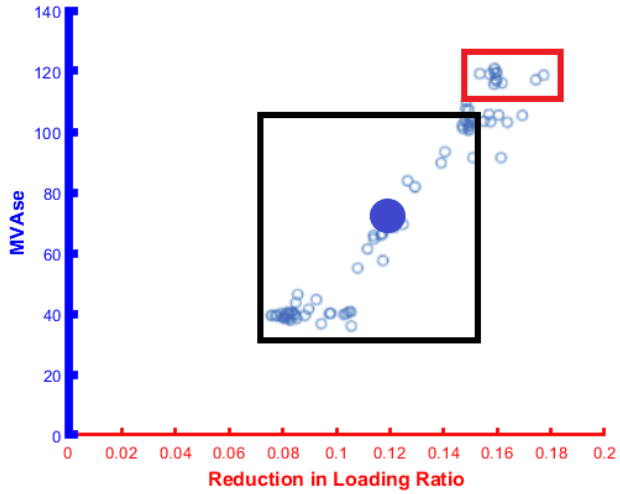

Figure 7.12: Variation of MVAse with Loading Levels Case 3

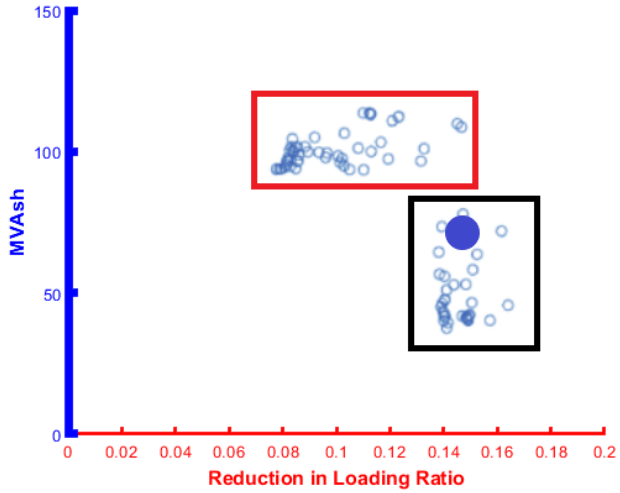

Figure 7.13: Variation of MVAsh with Loading Levels Case 3

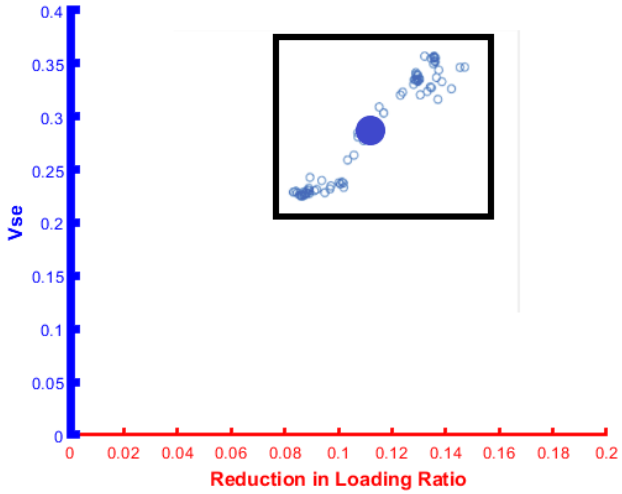

Figure 7.14: Variation of Vse with Loading Levels Case 3

Table 7.18: Summary of Optimal Rating for Location 3-18

Rating	Value
MVAsh	70 MVA
MVAse	80 MVA
Vse	0.3 V

7.7.4 Case 4:UPFC Installed on Line 11-12

In case 4, a UPFC is installed on Line 11-12. The reduction in loading ratio for most load scenarios is on average 0.12. THe variation in UPFC sizing does not affect the reduction in loading ratios by a considerable degree.Thus,this location of the UPFC may not be optimal for all load variations. This is shown in Fig.7.15,Fig.7.16 and Fig.7.17.

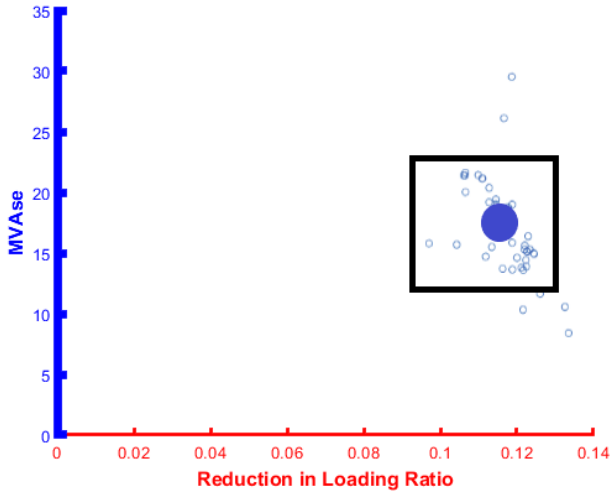

Figure 7.15: Variation of MVAse with Loading Levels Case 4

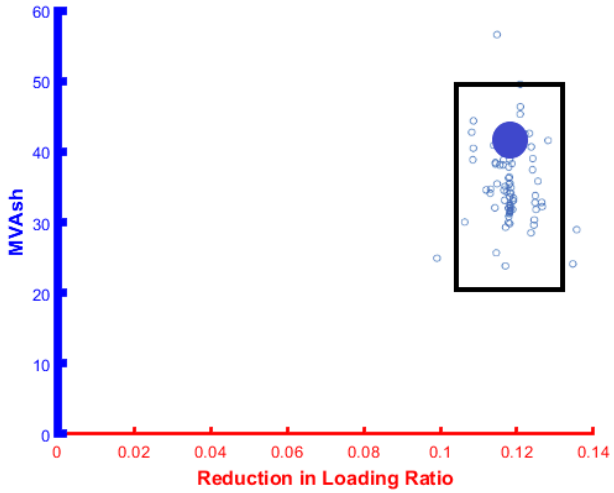

Figure 7.16: Variation of MVAsh with Loading Levels Case 4

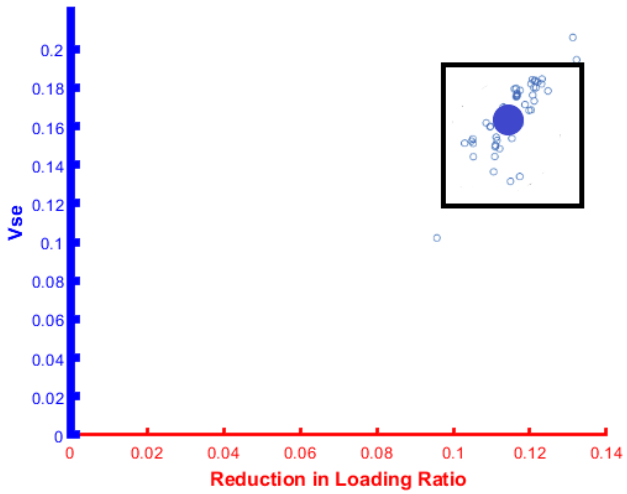

Figure 7.17: Variation of Vse with Loading Levels Case 4

Table 7.19: Summary of Optimal Rating for Location 11-12

Rating	Value
MVAsh	40 MVA
MVAse	17 MVA
Vse	0.16 V

7.7.5 Summary of the Optimal Rating with respect to Load Variation

Table.7.20 shows the summary of the optimal ratins obtained for different load variations. It can be seen that the Location 4-14 gives the maximum average reduction. THe optimal rating obtained for Location 4-14 is given by 50 MVA for MVAse, 125 MVA for MVAsh and 0.2V for Vse. However, it can be seen that Location 11-12 gives an average reduction 0.12 with a lower optimal rating. The operator may prefer to install a lower sized UPFC at a different location with a lower average reduction in loading ratio compared with a higher average reduction in loading ratio with a higher sized UPFC. Furthermore, in this section for load variations, the optimal rating is determined to be the maximum rating obtained for gaining reduction in line loading.

This is done in order to give the maximum leverage for managing the line flows for various load variations.

Table 7.20: Summary of Optimal Rating for Various Load Variations

Location	Average Reduction	MVAse	MVAsh	Vse
11-12	0.12	17MVA	40MVA	0.16V
3-18	0.12	80MVA	70MVA	0.3V
17-18	0.07	55MVA	160MVA	0.15V
4-14	0.2	50MVA	125MVA	0.2V

7.8 Summary and Main Contribution

The main contribution of this chapter is listed below:

- The formulation proposed in this chapter is used to find the optimal rating of a UPFC for optimal power flow management. UPFC has a high installation cost and thus the optimal sizing of the UPFC needs to be determined which can give you a sufficient degree of control over the line loading in a power system required by the power system operator. The sizing of the UPFC is obtained over three generation control scenarios: only UPFC control, only real generation control and only reactive generation control. A minimum rating is obtained across these three control scenarios and a cost-benefit analysis is performed to obtain a trade-off between the UPFC sizing and the degree of control over the line loading in a power system. The results show that it is important to find out the optimal rating of a UPFC for different control scenarios as the optimal rating differs with respect to different control scenarios and morevoer, it is not always beneficial to size the UPFC at a higher rating as beyond a certain rating, the higher sized UPFC will give you no additional benefit over lower sized UPFCs.

- Monte-Carlo simulation has been applied for finding out the optimal rating con-

sidering different load variations. This is important to consider since a UPFC installed in a power system has to operate for various power system operating states. THus the preliminary analysis should include all various probable scenarios. THe results show that given that load variations are taken into account, some locations of the UPFC give you better overall control over line loadings with a lower rated UPFC compared to other locations which may give you less control over line loadings with a higher rated UPFC. Thus, the optimal location of the UPFC may also not be the same as expected if various load variations are accounted for.

CHAPTER 8: CONCLUSIONS AND FUTURE FUTURE WORK

Possible future work that can be further explored with regards to the topic of this dissertation are listed below:

- Optimal Power flow management incorporating the TCSC in an LPOPF model can be further explored. However, approximations will have to be made since the bus injection model of the TCSC is a decoupled model. A possible way to do this can be to solve for the LPOPF using only real power flow equations and then input the solution from the LPOPF into an AC power flow model with the real and reactive power flow equations combined within the same iteration.

- Furthermore, to provide more value to the work, the loading ratio defined in the dissertation should be presented in terms of money value in dollars per hour cost. This is because the loading ratio directly affects congestion cost so reducing or increasing the loading ratio in a transmission system directly affects congestion costs in the transmission system. This will require much effort as the congestion costs do not remain the same while solving for an LPOPF. THe highest locational marginal price can be used as an estimate of the congetion present in the system. If the loading ratio is reduced, then is the highest locational marginal prive reduced in the system or not.

- Multiple UPFCs can be added to the model in the dissertation. The maximum number of UPFCs that has been tested out is 2. This model can be scaled to larger systems such as the 179 bus system which will require a larger number of UPFCs. However, it must be remembered that the LPOPF has to maintain its accuracy for each iteration of the LPOPF. With a larger number of UPFCs,

the coordination required among multiple UPFCs to work towards achieving an optimal solution will require modifications to the algorithm presented in the dissertation. With multiple UPFCs, there may be cases where the control of one UPFC may contradict the control of another UPFC and the solution may be worse after the LPOPF versus before the OPF.

- Moreover, the addition of voltage index to the objective function can be further explored. This is because the UPFC can provide reactive support. Thus, for different loading levels, specially at higher loading levels, the voltage at some buses may drop. Thus, the UPFC can provide voltage support to those buses as well.

- The optimal rating of a UPFC can be further explored in terms of future scenarios as well. THis is because a UPFC once installed can not be resized nor installed at another location. It is assumed that it is a fixed device. Thus, the optimal rating of a UPFC should consider future scenarios such as load increases, additional renewable energy deployment, future changes in generation costs etc.

REFERENCES

[1] W. Shao and V. Vittal, "Lp-based opf for corrective facts control to relieve overloads and voltage violations," *IEEE Transactions on Power Systems*, vol. 21, no. 4, pp. 1832–1839, 2006.

[2] M. Sahraei-Ardakani and K. W. Hedman, "A fast lp approach for enhanced utilization of variable impedance based facts devices," *IEEE Transactions on Power Systems*, vol. 31, no. 3, pp. 2204–2213, 2015.

[3] M. Sahraei-Ardakani and K. W. Hedman, "Computationally efficient adjustment of facts set points in dc optimal power flow with shift factor structure," *IEEE Transactions on Power Systems*, vol. 32, no. 3, pp. 1733–1740, 2016.

[4] K. M. Rogers and T. J. Overbye, "Power flow control with distributed flexible ac transmission system (d-facts) devices," in *41st North American power symposium*, pp. 1–6, IEEE, 2009.

[5] K. Rogers and T. J. Overbye, "Some applications of distributed flexible ac transmission system (d-facts) devices in power systems," in *2008 40th North American Power Symposium*, pp. 1–8, IEEE, 2008.

[6] K. W. Cheung and J. Wu, "An iterative approach to facts set point optimization in day-ahead generation scheduling," in *2019 IEEE PES Asia-Pacific Power and Energy Engineering Conference (APPEEC)*, pp. 1–6, IEEE, 2019.

[7] T. Ding, R. Bo, F. Li, and H. Sun, "Optimal power flow with the consideration of flexible transmission line impedance," *IEEE Transactions on Power Systems*, vol. 31, no. 2, pp. 1655–1656, 2015.

[8] A. Brissette, D. Maksimović, and Y. Levron, "Distributed series static compensator deployment using a linearized transmission system model," *IEEE Transactions on Power Delivery*, vol. 30, no. 3, pp. 1269–1277, 2014.

[9] H. Li, F. Li, P. Zhang, and X. Zhao, "Optimal utilization of transmission capacity to reduce congestion with distributed facts," in *2009 IEEE Bucharest PowerTech*, pp. 1–5, IEEE, 2009.

[10] A. Nikoobakht, J. Aghaei, M. Parvania, and M. Sahraei-Ardakani, "Contribution of facts devices in power systems security using milp-based opf," *IET Generation, Transmission & Distribution*, vol. 12, no. 15, pp. 3744–3755, 2018.

[11] I. Ullah, W. Gawlik, and P. Palensky, "Analysis of power network for line reactance variation to improve total transmission capacity," *Energies*, vol. 9, no. 11, p. 936, 2016.

[12] Y. Sang, M. Sahraei-Ardakani, and M. Parvania, "Stochastic transmission impedance control for enhanced wind energy integration," *IEEE Transactions on Sustainable Energy*, vol. 9, no. 3, pp. 1108–1117, 2017.

[13] M. N. Nazir, S. Omran, and R. Broadwater, "Feasibility of dsr applications in transmission grid operationâcontrol of power flow and imbalanced voltage," *Electric Power Systems Research*, vol. 131, pp. 187–194, 2016.

[14] S. Omran, R. Broadwater, J. Hambrick, and M. Dilek, "Dsr design fundamentals: Power flow control," in *2014 IEEE PES General Meeting| Conference & Exposition*, pp. 1–5, IEEE, 2014.

[15] K. Rahimi, H. Jain, R. Broadwater, and J. Hambrick, "Application of distributed series reactors in voltage balancing," in *2015 IEEE Power & Energy Society General Meeting*, pp. 1–5, IEEE, 2015.

[16] M. Sahraei-Ardakani and K. W. Hedman, "Day-ahead corrective adjustment of facts reactance: A linear programming approach," *IEEE Transactions on Power Systems*, vol. 31, no. 4, pp. 2867–2875, 2015.

[17] M. Dorostkar-Ghamsari, M. Fotuhi-Firuzabad, F. Aminifar, A. Safdarian, and M. Lehtonen, "Optimal distributed static series compensator placement for enhancing power system loadability and reliability," *IET Generation, Transmission & Distribution*, vol. 9, no. 11, pp. 1043–1050, 2015.

[18] Y. Sang and M. Sahraei-Ardakani, "Effective power flow control via distributed facts considering future uncertainties," *Electric Power Systems Research*, vol. 168, pp. 127–136, 2019.

[19] X.-P. Zhang, "Advanced modeling of the multicontrol functional static synchronous series compensator (sssc) in newton power flow," *IEEE Transactions on Power Systems*, vol. 18, no. 4, pp. 1410–1416, 2003.

[20] G. Radman and R. S. Raje, "Power flow model/calculation for power systems with multiple facts controllers," *Electric power systems research*, vol. 77, no. 12, pp. 1521–1531, 2007.

[21] D. J. Gotham and G. Heydt, "Power flow control and power flow studies for systems with facts devices," *IEEE Transactions on power systems*, vol. 13, no. 1, pp. 60–65, 1998.

[22] A. Nasri, A. J. Conejo, S. J. Kazempour, and M. Ghandhari, "Minimizing wind power spillage using an opf with facts devices," *IEEE Transactions on Power Systems*, vol. 29, no. 5, pp. 2150–2159, 2014.

[23] X.-P. Zhang and E. Handschin, "Optimal power flow control by converter based facts controllers," 2001.

[24] A. Rajabi-Ghahnavieh, M. Fotuhi-Firuzabad, and M. Othman, "Optimal unified power flow controller application to enhance total transfer capability," *IET Generation, Transmission & Distribution*, vol. 9, no. 4, pp. 358–368, 2015.

[25] M. Noroozian, L. Angquist, M. Ghandhari, and G. Andersson, "Use of upfc for optimal power flow control," *IEEE Transactions on Power delivery*, vol. 12, no. 4, pp. 1629–1634, 1997.

[26] R. V. Rao and R. V. Rao, *Teaching-learning-based optimization algorithm*. Springer, 2016.

[27] R. Agrawal, S. Bharadwaj, and D. Kothari, "Optimal location and sizing of svc considering transmission loss and installation cost using tlbo," in *2015 Annual IEEE India Conference (INDICON)*, pp. 1–6, IEEE, 2015.

[28] A. Gautam, Ibraheem, G. Sharma, P. N. Bokoro, and M. F. Ahmer, "Available transfer capability enhancement in deregulated power system through tlbo optimised tcsc," *Energies*, vol. 15, no. 12, p. 4448, 2022.

[29] R. Verma and A. Rathore, "Optimal placement of facts device considering voltage stability and losses using teaching learning based optimization," *Journal of The Institution of Engineers (India): Series B*, vol. 102, no. 4, pp. 771–776, 2021.

[30] Y. WELHAZI, T. GUESMI, and H. H. ABDALLAH, "Coordinated tuning of svc and psss in power system using teaching learning based algorithm," in *2019 10th International Renewable Energy Congress (IREC)*, pp. 1–6, IEEE, 2019.

[31] A. Rezaee Jordehi, "Optimal setting of tcscs in power systems using teaching–learning-based optimisation algorithm," *Neural Computing and Applications*, vol. 26, pp. 1249–1256, 2015.

[32] M. H. Sulaiman and Z. Mustaffa, "Optimal placement and sizing of facts devices for optimal power flow using metaheuristic optimizers," *Results in Control and Optimization*, vol. 8, p. 100145, 2022.

[33] R. Agrawal, S. Bharadwaj, and D. Kothari, "Population based evolutionary optimization techniques for optimal allocation and sizing of thyristor controlled series capacitor," *Journal of electrical systems and information technology*, vol. 5, no. 3, pp. 484–501, 2018.

[34] K. Verma, S. Singh, and H. Gupta, "Location of unified power flow controller for congestion management," *Electric power systems research*, vol. 58, no. 2, pp. 89–96, 2001.

[35] K. Visakha, D. Thukaram, and L. Jenkins, "Application of upfc for system security improvement under normal and network contingencies," *Electric Power Systems Research*, vol. 70, no. 1, pp. 46–55, 2004.

[36] K. Verma and H. Gupta, "Impact on real and reactive power pricing in open power market using unified power flow controller," *IEEE Transactions on Power Systems*, vol. 21, no. 1, pp. 365–371, 2006.

[37] S. An, J. Condren, and T. W. Gedra, "An ideal transformer upfc model, opf first-order sensitivities, and application to screening for optimal upfc locations," *IEEE Transactions on Power Systems*, vol. 22, no. 1, pp. 68–75, 2007.

[38] J. Singh, S. Singh, and S. Srivastava, "Optimal placement of unified power flow controller based on system loading distribution factors," *Electric Power Components and Systems*, vol. 37, no. 4, pp. 441–463, 2009.

[39] B. Chong, X.-P. Zhang, K. Godfrey, L. Yao, and M. Bazargan, "Optimal location of unified power flow controller for congestion management," *European transactions on electrical power*, vol. 20, no. 5, pp. 600–610, 2010.

[40] A. L. Ara, A. Kazemi, and S. N. Niaki, "Modelling of optimal unified power flow controller (oupfc) for optimal steady-state performance of power systems," *Energy conversion and Management*, vol. 52, no. 2, pp. 1325–1333, 2011.

[41] S. Hajforoosh, S. Nabavi, and M. Masoum, "Coordinated aggregated-based particle swarm optimisation algorithm for congestion management in restructured power market by placement and sizing of unified power flow controller," *IET Science, Measurement & Technology*, vol. 6, no. 4, pp. 267–278, 2012.

[42] P. Tiwari and Y. Sood, "Efficient and optimal approach for location and parameter setting of multiple unified power flow controllers for a deregulated power sector," *IET generation, transmission & distribution*, vol. 6, no. 10, pp. 958–967, 2012.

[43] L. H. Hassan, M. Moghavvemi, H. A. Almurib, and O. Steinmayer, "Application of genetic algorithm in optimization of unified power flow controller parameters and its location in the power system network," *International Journal of Electrical Power & Energy Systems*, vol. 46, pp. 89–97, 2013.

[44] S.-H. Lee, J.-H. Liu, and C.-C. Chu, "Modelling and locating unified power-flow controllers for static voltage stability enhancements," *International Transactions on Electrical Energy Systems*, vol. 24, no. 11, pp. 1524–1540, 2014.

[45] B. V. Kumar and N. Srikanth, "Optimal location and sizing of unified power flow controller (upfc) to improve dynamic stability: A hybrid technique," *International Journal of Electrical Power & Energy Systems*, vol. 64, pp. 429–438, 2015.

[46] M. Moazzami, M. J. Morshed, and A. Fekih, "A new optimal unified power flow controller placement and load shedding coordination approach using the hybrid imperialist competitive algorithm-pattern search method for voltage collapse prevention in power system," *International journal of electrical power & energy systems*, vol. 79, pp. 263–274, 2016.

[47] J. G. Singh, H. W. Qazi, and M. Ghandhari, "Load curtailment minimization by optimal placement of unified power flow controller," *International Transactions on Electrical Energy Systems*, vol. 26, no. 10, pp. 2272–2284, 2016.

[48] B. V. Kumar and N. Srikanth, "A hybrid approach for optimal location and capacity of upfc to improve the dynamic stability of the power system," *Applied Soft Computing*, vol. 52, pp. 974–986, 2017.

[49] G. N. Kumar and M. S. Kalavathi, "Cat swarm optimization for optimal placement of multiple upfcâs in voltage stability enhancement under contingency," *International Journal of Electrical Power & Energy Systems*, vol. 57, pp. 97–104, 2014.

[50] M. Packiasudha, S. Suja, and J. Jerome, "A new cumulative gravitational search algorithm for optimal placement of fact device to minimize system loss in the deregulated electrical power environment," *International Journal of Electrical Power & Energy Systems*, vol. 84, pp. 34–46, 2017.

[51] V. S. Rao and R. S. Rao, "Optimal placement of statcom using two stage algorithm for enhancing power system static security," *Energy Procedia*, vol. 117, pp. 575–582, 2017.

[52] S. Alamelu, S. Baskar, C. Babulal, and S. Jeyadevi, "Optimal siting and sizing of upfc using evolutionary algorithms," *International Journal of Electrical Power & Energy Systems*, vol. 69, pp. 222–231, 2015.

[53] K. Pandiarajan and C. Babulal, "Fuzzy harmony search algorithm based optimal power flow for power system security enhancement," *International Journal of Electrical Power & Energy Systems*, vol. 78, pp. 72–79, 2016.

[54] A. R. Jordehi, "Brainstorm optimisation algorithm (bsoa): An efficient algorithm for finding optimal location and setting of facts devices in electric power systems," *International Journal of Electrical Power & Energy Systems*, vol. 69, pp. 48–57, 2015.

[55] K. Balamurugan, R. Muralisachithanandam, and V. Dharmalingam, "Performance comparison of evolutionary programming and differential evolution approaches for social welfare maximization by placement of multi type facts devices in pool electricity market," *International Journal of Electrical Power & Energy Systems*, vol. 67, pp. 517–528, 2015.

[56] S. Dutta, S. Paul, and P. K. Roy, "Optimal allocation of svc and tcsc using quasi-oppositional chemical reaction optimization for solving multi-objective orpd problem," *Journal of Electrical Systems and Information Technology*, vol. 5, no. 1, pp. 83–98, 2018.

[57] R. Sirjani, "Optimal placement and sizing of pv-statcom in power systems using empirical data and adaptive particle swarm optimization," *Sustainability*, vol. 10, no. 3, p. 727, 2018.

[58] K. Balamurugan, R. Muralisachithanandam, V. Dharmalingam, and R. Srikanth, "Optimal choice and location of multi type facts devices in deregulated electricity

market using evolutionary programming method," *Int J Electr Electron Sci Eng*, vol. 7, pp. 96–102, 2013.

[59] K. Balamurugan and K. Muthukumar, "Differential evolution algorithm for contingency analysis-based optimal location of facts controllers in deregulated electricity market," *Soft computing*, vol. 23, pp. 163–179, 2019.

[60] T. Kang, J. Yao, T. Duong, S. Yang, and X. Zhu, "A hybrid approach for power system security enhancement via optimal installation of flexible ac transmission system (facts) devices," *Energies*, vol. 10, no. 9, p. 1305, 2017.

[61] S. M. Nabavi, K. Khafafi, A. Sakhavati, and S. Nahi, "Optimal location and sizing of sssc using genetic algorithm in deregulated power market," *International Journal of Computer Applications*, vol. 22, no. 4, pp. 37–41, 2011.

[62] M. Ebeed, S. Kamel, and L. S. Nasrat, "Optimal siting and sizing of sssc using improved harmony search algorithm considering non-smooth cost functions," in *2017 Nineteenth International Middle East Power Systems Conference (MEPCON)*, pp. 1286–1291, IEEE, 2017.

[63] I. Ali, "Optimal location of sssc based on pso to improve voltage profile and reduce iraqi grid system losses," *Engineering and Technology Journal*, vol. 35, no. 4 Part A, pp. 372–380, 2017.

[64] S. Dawn, P. K. Tiwari, and A. K. Goswami, "An approach for long term economic operations of competitive power market by optimal combined scheduling of wind turbines and facts controllers," *Energy*, vol. 181, pp. 709–723, 2019.

[65] M. B. Shafik, H. Chen, G. I. Rashed, and R. A. El-Sehiemy, "Adaptive multi objective parallel seeker optimization algorithm for incorporating tcsc devices into optimal power flow framework," *IEEE Access*, vol. 7, pp. 36934–36947, 2019.

[66] E. A. Belati, C. F. Nascimento, H. de Faria, E. H. Watanabe, and A. Padilha-Feltrin, "Allocation of static var compensator in electric power systems considering different load levels," *Journal of Control, Automation and Electrical Systems*, vol. 30, pp. 1–8, 2019.

[67] K. Venkatraman, B. Paramasivam, and I. Chidambaram, "Optimal allocation of tcsc devices for the enhancement of atc in deregulated power system using flower pollination algorithm," *J. Eng. Sci. Technol*, vol. 13, no. 9, pp. 2857–71, 2018.

[68] A. Sharma and S. K. Jain, "Gravitational search assisted algorithm for tcsc placement for congestion control in deregulated power system," *Electric Power Systems Research*, vol. 174, p. 105874, 2019.

[69] E. R. Sanseverino, Q. Tran, L. R. Roose, S. T. Sadoyama, T. Tran, B. Doan, and N. Nguyen, "Optimal placements of svc devices in low voltage grids with high penetration of pv systems," in *2018 9th IEEE International Symposium on*

Power Electronics for Distributed Generation Systems (PEDG), pp. 1–6, IEEE, 2018.

[70] S. Rezaeian Marjani, V. Talavat, and S. Galvani, "Optimal allocation of d-statcom and reconfiguration in radial distribution network using mopso algorithm in topsis framework," *International Transactions on Electrical Energy Systems*, vol. 29, no. 2, p. e2723, 2019.

[71] A. K. Dwivedi and S. Vadhera, "Reactive power sustainability and voltage stability with different facts devices using psat," in *2019 6th international conference on signal processing and integrated networks (SPIN)*, pp. 248–253, IEEE, 2019.

[72] U. Musa, G. Bakare, A. Mati, A. Mohammed, and A. Umar, "Radial distribution network enhancement with d-statcom using bacterial foraging algorithm," *Arid Zone Journal of Engineering, Technology and Environment*, vol. 14, no. 2, pp. 249–260, 2018.

[73] S. R. Inkollu and V. R. Kota, "Optimal setting of facts devices for voltage stability improvement using pso adaptive gsa hybrid algorithm," *Engineering science and technology, an international journal*, vol. 19, no. 3, pp. 1166–1176, 2016.

[74] A. Elmitwally and A. Eladl, "Planning of multi-type facts devices in restructured power systems with wind generation," *International Journal of Electrical Power & Energy Systems*, vol. 77, pp. 33–42, 2016.

[75] S. Dutta, P. K. Roy, and D. Nandi, "Optimal location of upfc controller in transmission network using hybrid chemical reaction optimization algorithm," *International Journal of Electrical Power & Energy Systems*, vol. 64, pp. 194–211, 2015.

[76] S. A. Jumaat and I. Musirin, "σ-multi-objective evolutionary particle swarm optimization approach for transmission loss and cost minimization with svc installation," *Journal of Fundamental and Applied Sciences*, vol. 10, no. 3S, pp. 715–728, 2018.

[77] T. Kumar and R. Satyanarayana, "Enhancing power system security: A multi-objective optimal approach to identify the location and size of svc," *IUP Journal of Electrical and Electronics Engineering*, vol. 11, no. 1, pp. 45–58, 2018.

[78] S. A. Taher and M. K. Amooshahi, "New approach for optimal upfc placement using hybrid immune algorithm in electric power systems," *International Journal of Electrical Power & Energy Systems*, vol. 43, no. 1, pp. 899–909, 2012.

[79] S. A. Taher and M. K. Amooshahi, "Optimal placement of upfc in power systems using immune algorithm," *Simulation Modelling Practice and Theory*, vol. 19, no. 5, pp. 1399–1412, 2011.

[80] A. Mishra *et al.*, "Congestion management of deregulated power systems by optimal setting of interline power flow controller using gravitational search algorithm," *Journal of Electrical Systems and Information Technology*, vol. 4, no. 1, pp. 198–212, 2017.

[81] B. Bhattacharyya and S. Kumar, "Loadability enhancement with facts devices using gravitational search algorithm," *International Journal of Electrical Power & Energy Systems*, vol. 78, pp. 470–479, 2016.

[82] S. Chansareewittaya, "Optimal power flow for enhance ttc with optimal number of svc by using improved hybrid tssa," *ECTI Transactions on Computer and Information Technology (ECTI-CIT)*, vol. 13, no. 1, pp. 37–48, 2019.

[83] K. Kavitha and R. Neela, "Optimal allocation of multi-type facts devices and its effect in enhancing system security using bbo, wipso & pso," *Journal of Electrical Systems and Information Technology*, vol. 5, no. 3, pp. 777–793, 2018.

[84] S. S. Reddy, "Determination of optimal location and size of static var compensator in a hybrid wind and solar power system," *International Journal of Applied Engineering Research*, vol. 11, no. 23, pp. 11494–11500, 2016.

[85] M. K. M. Zamani, I. Musirin, S. A. S. Mustaffa, and S. I. Suliman, "Optimal svc allocation via symbiotic organisms search for voltage security improvement," *TELKOMNIKA (Telecommunication Computing Electronics and Control)*, vol. 17, no. 3, pp. 1267–1274, 2019.

[86] E. Ghahremani and I. Kamwa, "Optimal placement of multiple-type facts devices to maximize power system loadability using a generic graphical user interface," *IEEE transactions on power systems*, vol. 28, no. 2, pp. 764–778, 2012.

[87] M. Shafik, G. Rashed, R. A. El-Sehiemy, and H. Chen, "Optimal sizing and sitting of tcsc devices for multi-objective operation of power systems using adaptive seeker optimization algorithm," in *2018 IEEE region ten symposium (tensymp)*, pp. 231–236, IEEE, 2018.

[88] J. Jamnani and M. Pandya, "Coordination of svc and tcsc for management of power flow by particle swarm optimization," *Energy Procedia*, vol. 156, pp. 321–326, 2019.

[89] K. Kavitha and R. Neela, "Comparison of bbo, wipso & pso techniques for the optimal placement of facts devices to enhance system security," *Procedia Technology*, vol. 25, pp. 824–837, 2016.

[90] A. R. Jordehi, "Optimal allocation of facts devices for static security enhancement in power systems via imperialistic competitive algorithm (ica)," *Applied Soft Computing*, vol. 48, pp. 317–328, 2016.